SALINITY AND TIDES IN ALLUVIAL ESTUARIES

By Hubert H.G. Savenije

Delft University of Technology
Water Resources Section
P.O.Box 5048
2600 GA, Delft, The Netherlands

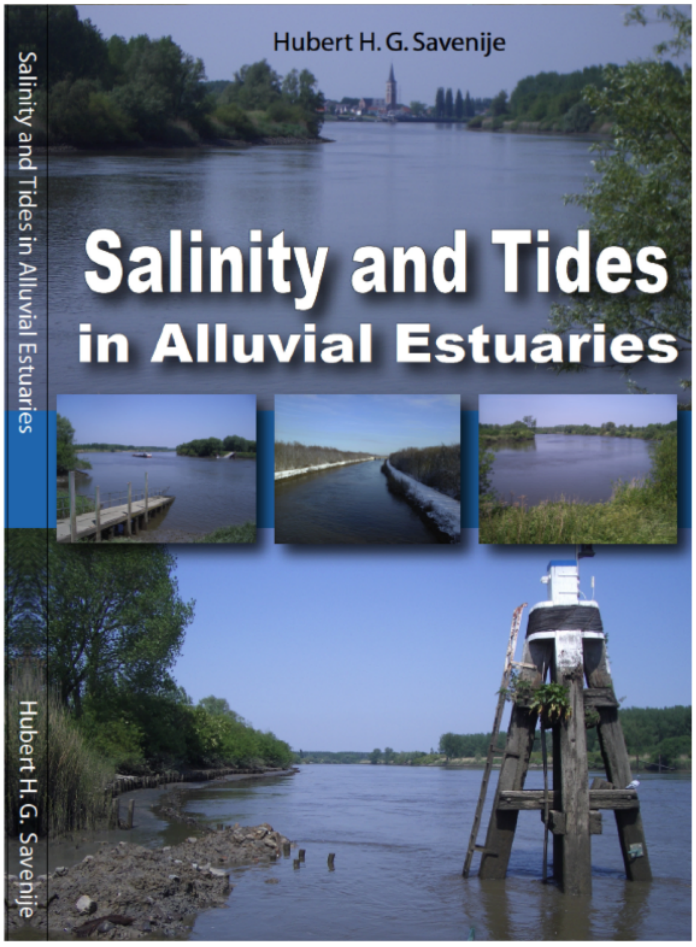

Second Completely Revised Edition
2012
Version 2.6

Contents

Preface

This is the open access version of the fully revised second edition (2012) of "Salinity and Tides in Alluvial Estuaries", first published by Elsevier Publications in 2005. This open access edition has been fully updated, using the latest insights in the field of estuary hydrodynamics. It is freely available at www.salinityandtides.com. This web site also links to a wide range of applications in 27 estuaries and includes valuable data and information that other researches may want to use.

As it is, this remains the only book on alluvial estuaries that presents an integrated theory on estuary shape, estuary hydrodynamics, mixing and salt intrusion. Traditional publications focus on sub-disciplines: the hydrodynamics, the mixing (e.g. Fischer et al., 1979), the salinity, or the morphology, but seldom are these fields considered as interdependent. Although the literature on tidal hydrodynamics is vast, most concentrates on flow in prismatic (i.e. constant cross-section) channels, or, if a variable topography is used, then authors make use of 2-D or 3-D simulations using an imposed bathymetry.

By this fragmented approach we miss opportunities. An estuary system and its component parts work as a single physical entity, where potential and kinetic energy is dissipated through the interaction between water, sediment and salinity. This interaction leads to clear patterns in the morphology, the hydrodynamics and the salinity, many of which can be surprisingly simple and even predictable. It was this realisation that inspired me to write this book.

An estuary is the transition between a river and a sea. There are two main drivers: the river that discharges fresh water into the estuary and the sea that fills the estuary with salty water, on the rhythm of the tide. The salinity of the estuary water is the result of the balance between two opposing fluxes: a tide-driven saltwater flux that penetrates the estuary through mixing, and a freshwater flux that flushes the saltwater back. Both fluxes strongly depend on the topography: the salt water flux because the amount of water entering the estuary depends on the surface area of the estuary; and the fresh water flux, because the cross-sectional area of the estuary determines the efficiency of the fresh water flow to push back the salt.

So, the topography is crucial. It provides the most important boundary condition for tidal hydraulics, mixing and salt intrusion. One of the innovations of this book is that, throughout, it works with the natural topography of alluvial estuaries. This natural topography is one with converging banks following an exponential function. Both the width and the cross-sectional area obey exponential functions. Moreover, in coastal plain estuaries, the depth is constant and there is no bottom slope. Estuaries in coastal areas with a strong relief are generally too short for this type of estuary to develop. They form a special category of alluvial estuaries where standing waves occur and where the depth decreases in the upstream direction. These estuaries have been described by others (e.g. by Wright et al., 1973; Prandle, 2003). The topography of alluvial estuaries, whether short or long, can be characterised by a single parameter: the convergence length: the length scale of the exponential function. This length scale is a key parameter for understanding tidal and mixing processes. In classical literature on tidal hydraulics, tidal mixing and salt intrusion, this parameter has been overlooked more often than not, leading to incomplete, or even flawed, dimensional analysis. The reason probably lies in the fact that the early literature was based on laboratory experiments in prismatic channels. This book is unique in that it systematically integrates these natural topographies with tidal movement, mixing and salt intrusion.

Mixing in estuaries is driven by both the tide and the density gradient. The density gradient induces vertical mixing, while the tide mainly causes horizontal mixing through tidal trapping

and residual circulation (and to a minor extent turbulent mixing). It is recognised that residual circulation is a dominant mechanism, particularly near the mouth of the estuary, but it is poorly understood. Several mixing mechanisms have been well documented in the literature, such as the vertical density-driven circulation and turbulence-driven mixing, but, until now, no consistent theory exists for residual circulation. This book demonstrates that residual circulation is strongly related to an estuary's topography, and particularly to its width, which in alluvial estuaries is predictable. The book therefore provides an integrated mixing theory and a practical computational approach for the prediction of salt intrusion and tidal propagation in alluvial estuaries.

The result is a book that tries to build a bridge between science and engineering. It is useful both for students, practitioners or scientists from related fields (such as environmentalists, ecologists, or geographers) who require relatively simple analytical equations to describe estuary behaviour. It deals with the theoretical background in detail, but also provides simple guidelines and examples for practical applications. It provides tools with which human interference in estuary dynamics can be described and predicted, resulting from, for instance: upstream fresh water abstraction, dredging or sea level rise. In describing the interactions between tide, topography, water quality and river discharge, it provides useful information for hydraulic engineers, morphologists, ecologists and people concerned with water quality in alluvial estuaries.

This book is based on years of fieldwork and research in different parts of the world and involves the work of many people, many of them former students (I acknowledge them below). I am grateful to all these people who have contributed to the results and will hopefully continue to do so, because there still is much to discover.

Delft,
Hubert H.G. Savenije

Acknowledgements:

In preparing and updating this book, I made use of contributions from my former MSc and PhD students, who worked with me on different subjects of this book. In particular I would like to thank Nicolas Zimmermann, who helped me with analytical solutions of the damping equation, Twan Horrevoets who did his MSc work on the influence of river discharge on the damping equation, Susan Graas and Mark Hegnauer who did field work in the Pungue river and helped me to refine the geometry of the Pungue, Niels Schuurmans who made a numerical model of the Schelde, Nguyen Anh Duc who applied the theory in the Mekong delta and helped me derive the theory on tide-driven mixing, Huayang Cai who helped me in advancing the analytical solutions of the tidal equations, Jacqueline Isabella Gisen who expanded our data base of application to the Malaysian estuaries and helped me with further developing the equations that link the geometry to hydrological drivers. Finally I have to thank my fellow researchers Erfeng Zhang who applied the analytical theory to the Yangtse estuary, and last but not least Marco Toffolon who is a champion in mathematical analysis and who has made crucial contributions to the analytical theory in this book.

A final word of thank I have for Marieke Hilhorst who gave me substantial editorial support. To her and to all my fellow researchers and former students I owe a lot, not only for their invaluable contributions, but also for their friendship and camaraderie.

Notation

The following symbols are used in this book:

a	Cross-sectional convergence length [L]
A	Cross-sectional area [L^2]
$\widehat{A}$	Amplitude of the cross sectional area [L^2]
A_f	Cross-sectional area of the flood channel [L^2]
A_0	Cross-sectional area at the estuary mouth [L^2]
b	Convergence length of the stream width [L]
B	Stream width [L]
B_L	Width at which there are no ebb and flood channels [L]
B_S	Storage width [L]
B_0	Width at the estuary mouth [L]
c	Wave celerity [L/T]
c_i	x-dependendent coefficient equal to the ratio between dispersion coefficient and the fresh water velocity [-]
c_0	Classical wave celerity [L/T]
C_c	Convergence term (in Chapter 3) [-]
C	Coefficient of Chézy [$L^{0.5}$/T]
d_s	Sediment transport factor [$L^{(2-n)}T^{(n-1)}$]
D	Longitudinal dispersion [L^2/T]
D_c	Damping term (in Chapter 3) [-]
D_{ef}	Longitudinal dispersion due to residual circulation in ebb and flood channels [L^2/T]
D_g	Longitudinal dispersion due to gravitational circulation [L^2/T]
D_{SS}	Steady state dispersion [L^2/T]
D_t	Tide driven dispersion [L^2/T]
D_{50}	Diameter of the bed material that is exceeded by 50% of the sample weight [L]
e_p	Pumping efficiency: relative difference of the tidal velocity amplitude between flood and ebb currents [-]
E	Tidal excursion [L]
E_0	Tidal excursion at the estuary mouth [L]
E_d	Dissipated energy [ML^2T^{-2}]
E_m	Potential energy per tidal period [ML^2T^{-2}]
E_t	Kinetic energy per tidal period [ML^2T^{-2}]
f	Friction factor [-]
f'	Adjusted friction factor [-]
f_D	Darcy-Weisbach friction factor
F	Force per unit mass (in Chapter 2) [$MT^{-2}L^{-2}$]
F	Mass flux (in Chapter 5) [M/T]
$\mathbf{F}$	Froude number (U/c_0) or Tidal Froude number (v/c) [-]
F_c	Celerity damping function [-]
F_d	Densimetric Froude number (v/c) [-]
F_e	Salt flux in the ebb channel [M/T]
F_f	Salt flux in the flood channel [M/T]
g	Acceleration due to gravity [L/T^2]
h	Stream depth [L]

$\overline{h}$	Tidal average stream depth [L]
h_0	Depth at the estuary mouth, or constant tidal average stream depth [L]
H	Tidal range [L]
H'	Slack tidal range [L]
i	Side slope [-]
I	Water level slope [-]
I_r	Density slope [-]
I_b	Bottom slope [-]
I_R	Residual depth gradient [-]
k	Tidal wave number [L^{-1}]
k_s	Coefficient of proportionality in Lacey's equation [$T^{0.5}L^{-0.5}$]
K	Manning's coefficient (in Chapter 2-3) [$L^(1/3)T^(-1)$]]
K	Dimensionless Van den Burgh's coefficient (in Chapter 4-5) [-]
L_T	Length of the tidal intrusion [L]
L	Salt intrusion length [L]
L_{ef}	Length of a ebb-flood channel loop [L]
L_T	Length of tidal intrusion [L]
M	Moment per unit volume driven by gravitational circulation [$ML^{-1}T^{-2}$]
n	exponent [-] or Manning's roughness coefficient [$L^(-1/3)T$]
N	Canter-Cremers Estuary number [-]
N_E	Estuary-type number [-]
N_R	Estuarine Richardson number [-]
N_P	Prandle's estuary number [-]
N_i	Dimensionless numbers (i=1,2,3,4,5,P,Q,D) (in Chapter 5) [-]
O	Surface area of the estuary [L^2]
P	Wetted perimeter [L]
P_t	Flood volume [L^3]
q	Coefficient of the advective term (in Chapter 5) [L/T]
Q	Discharge [L^3/T]
Q_b	Bankfull discharge [L^3/T]
Q_f	The freshet or fresh water flushing [L^3/T]
Q_p	Tidal peak discharge [L^3/T]
Q_r	The river discharge [L^3/T]
Q_s	Sediment discharge [L^3/T]
Q_t	Tidal discharge [L^3/T]
Q_0	Dry season fresh water discharge [L^3/T]
r	Net rainfall (the difference between rainfall and evaporation) [L/T]
r_S	storage width ratio [-]
r_0	Net rainfall rate during the dry season [L/T]
R	Friction term (in Chapter 2) [-]
R_c	Friction term (in Chapter 3) [-]
R'	Resistance term [T^{-1}]
R_D	Dronkers' friction term [-]
R_L	Lorentz linearised friction factor (in Chapter 2) [T^{-1}]
R_L	Lorentz linearised friction factor (in Chapter 3) [-]
R_s	Source term [L^2/T]
s	Salinity [M/L^3]
S	Distance travelled by a water particle (in Chapter 2) [L]
S	Steady state salinity (in Chapter 5) [M/L^3]
S_f	Fresh water salinity [M/L^3]
t	Time [T]
T	Tidal period [T]
T_f	Particle travel time [T]
T_K	Time scale for the system response [T]
T_Q	Time scale of the discharge reduction [T]
T_S	Time scale for the system response (steady state) [T]

U	Mean cross-sectional flow velocity [L/T]
U_b	Velocity of the bankfull discharge [L^3/T]
U_f	Velocity of the fresh water discharge [L/T]
U_S	Stokes drift velocity [L/T]
v	Flow velocity (averaged over the cross-section) [L/T]
V	velocity of the moving particle [L/T]
x	Distance [L]
y	Dimensionless tidal range H/H_0 [-]
z	Vertical ordinate [L]
Z	Water level [L]
Z_b	Bottom elevation [L]
α	Mixing coefficient (in Chapter 5) [L-1]
α_S	Shape factor [-]
α_L	Coefficient for the length of an ebb-flood interaction cell [-]
β	Ideal dimensionless amplitude [L]
β	Dispersion reduction rate (in Chapter 5) [-]
β_c	Asymptotic ideal dimensionless amplitude [-]
β_L	Coefficient for the length of an ebb-flood interaction cell [-]
γ	The shape number [-]
Δ	Error term (in Chapter 2-3) [-]
Δ_S	Relative sediment density (in Chapter 2) [-]
δ_h	relative depth gradient [L^{-1}]
δ_H	Damping rate of tidal range [L^{-1}]
δ_U	Damping rate of tidal velocity amplitude [L^{-1}]
δ	The damping number (in Chapter 3) [-]
ε	Phase lag between HW and HWS, or LW and LWS [-]
η	Tidal amplitude [L]
η_0	Tidal amplitude at estuary mouth [L]
λ_0	Length of the tidal wave [L]
λ	The celerity number (in Chapter 3) [-]
μ	The velocity number (in Chapter 3) [-]
π	Real number=3.1414.. representing 180 degrees [-]
ξ	Dimensionless argument (representing a moving observer in the x-t plane) [-]
ρ	Density of the water [ML^{-3}]
σ	Dimensionless salinity [-]
υ	Tidal velocity amplitude [L/T]
ϕ	Angle or phase lag [-]
φ	Relative influence of river discharge: U_f/υ [-]
Φ	Harmonic function of the tidal velocity [-]
χ	The friction number [-]
Ψ	Harmonic function of the water level [-]
ω	Angular velocity [T^{-1}]

Abbreviations and subscripts:

LWS	Low water slack
HWS	High water slack
LW	Low water
HW	High water
TA	Tidal average

Operators:

Δ	Finite difference
d	Lagrangean difference

Chapter 1

INTRODUCTION: DESCRIPTION AND CLASSIFICATION OF ALLUVIAL ESTUARIES

1.1 What is an estuary?

The simplest definition of an estuary is "Where the river meets the sea". Dionne (1963) defined it very nicely as: ".. an inlet of the sea reaching into the river valley as far as the upper limit of tidal rise..". A unnecessarily lengthy and unfortunately erroneous definition, which is very commonly heard, is attributed to Pritchard (1967): "An estuary is a semi-enclosed coastal body of water which has free connection to the open sea and within which seawater is measurably diluted with fresh water derived from land drainage". This definition is clearly wrong since a water body that receives water from land drainage cannot be closed at the upstream end. It is open-ended on both sides. In fact, alluvial estuaries – the topic of this book – have very special characteristics purely stemming from the fact that they have an open, and very dynamic, fluvial boundary at the upstream end.

What is special about alluvial estuaries and what makes them different from non-alluvial and man-made estuaries? This chapter presents a classification of estuaries and related types of salt intrusion. It then describes the characteristics, peculiarities and resulting behaviour of alluvial estuaries.

The shape of an alluvial estuary is similar all over the world. The width reduces in upstream direction as an exponential function. In coastal plain estuaries there is no significant bottom slope, but in estuaries with strong relief, the depth may decrease exponentially. As a result, in both types of alluvial estuaries, the cross-sectional area varies exponentially, and so does the flood volume, also called "tidal prism" (the volume of water that enters the estuary on the tide). Morphological equilibrium and entropy considerations (such as minimum stream power) are the cause of this typical shape. There is a similarity between the exponential reduction of the width of an estuary (in the upstream direction) and the exponential increase of the drainage area of a catchment (in the downstream direction) described in Rodriguez-Iturbe and Rinaldo (2001).

The constant depth and exponentially varying width correspond with the shape of an "ideal estuary" as described by Pillsbury (1939) and Langbein (1963), a topography that can be observed in coastal plain estuaries all over the world. The shape of an alluvial estuary is characterised by the ratio of the depth of flow (h) to the convergence length (b), the length scale of the exponential function. Although there is empirical evidence (examples of a wide range of estuaries will be provided) and mathematical proof of this fact, acceptance of this phenomenon is still low among scientists used to working with a different schematization of topography (most authors assume a bottom slope and many use a constant width). In 1.2, a classification of estuaries is presented that takes into account tidal range, river flow, type of salt intrusion, estuary topography and relief.

The topography is key to estuary processes. The fact that water flows as it does is strongly influenced by the medium through which it flows. In principle, the non-linear hydraulic equations (the St. Venant equations) can demonstrate irregular and unpredictable behaviour, but in alluvial estuaries we seldom observe this. Instead we observe a number of surprisingly simple "laws":

1 . The tidal excursion (the distance a water particle travels during a tidal cycle) is near constant along a coastal plain estuary. This is related to the morphological equilibrium (Savenije, 1989).

2 . There are simple analytical relations for estuary topography (h/b), wave celerity (c) and phase lag (ε) between high water and the subsequent moment of slack water that can be derived from the equation for conservation of mass (Savenije, 1992b, 1993b).

3 . We also see that tidal amplification of the tidal wave follows a simple linear function, whereas tidal damping is partly linear and partly exponential, based on the equation for conservation of momentum (Savenije, 1998, 2001b; Horrevoets et al., 2004). Although this equation is more complex than "Green's Law", it is still surprisingly simple.

4 . We see that in coastal plain estuaries of 'infinite' length, the estuary depth tends asymptotically to the 'ideal' depth: the depth of an ideal estuary, where no amplification or damping occurs (Cai et al., 2012b).

5 . The propagation of the tidal flood wave is influenced by tidal damping (and vice versa). This interaction can also be described by a simple analytical equation (Savenije and Veling, 2005).

6 . The set of relatively simple analytical equations can be solved explicitly without the need for a numerical model (Savenije et al., 2008).

7 . We observe that salt intrusion is well mixed or partially mixed at the time when it matters. In tidal estuaries, the salt wedge, which most people think is the dominant salt intrusion mechanism, either does not occur at all, or only occurs during high river floods, when people are (rightly) more worried about flood protection (Savenije, 1992a).

8 . Mixing of salt and fresh water, although a complex process that results from many different mixing mechanisms, can be described by a surprisingly simple formula, originally coined by Van der Burgh (1972).

9 . Salt intrusion can be described by an analytical equation that can be applied to new situations with a minimum of calibration. In fact, the equation is predictable in that it can be applied outside the range of calibration; e.g. to analyse the effect of river discharge, interventions in the estuary by dredging, sea level rise, etc. (Savenije, 1993a,c).

These phenomena are briefly introduced in this chapter, and more fully described and derived from the basic equations in subsequent chapters.

1.2 Importance of estuaries to mankind

An estuary is the transition between two distinct water bodies: a river and a sea. One of the few things that a river and a sea have in common is that they contain water, and therefore provide an aquatic environment. There are, however, many differences: a river transports and does not retain water, whereas a sea primarily stores water; river water is fresh, whereas sea water is saline; a river has more or less parallel banks and a bottom slope in the direction of flow, whereas a sea is virtually unlimited and has no bottom slope in the direction of flow; in a sea the tidal waves - perpendicular to the coast - are primarily standing waves, whereas in a river the flood waves are primarily progressive (for definitions, see Chapter 2). This list is not exhaustive.

An estuary, on the other hand, has characteristics of both a river and a sea (see Table 1.1). Typical riverine characteristics of an estuary are that it has banks, flowing water, sediment transport, occasional floods, and - in the upper parts - fresh water. Its typical marine characteristics are the presence of tides and saline water. But the most typical feature of an estuary is that it is the transition between a river and a sea, with its own hydraulic, morphologic and biologic characteristics such as: tidal waves of a mixed type, a funnel shape, and a brackish environment, quite different from other water bodies. Rivers carry nutrients to the nutrient poor oceanic environment. The estuary is the region where these two environments interact, serving as a crucial

feeding and breeding ground for many life forms. Because of these typical characteristics and the related unique habitats, the estuarine environment plays an important role in the life cycle of numerous species. The flora and fauna of estuaries are extremely rich and the area of influence through the migration of species is large. The importance of estuaries to the global environment is not easily overestimated.

Table 1.1: Characteristics of an estuary compared to a river and a sea.

	Sea	**Estuary**	**River**
Shape	Basin	Funnel	Prismatic
Main hydraulic function	Storage	Storage and transport	Transport of water and sediments
Flow direction	No dominant direction	Dual direction	Single downstream direction
Bottom slope	No slope	No slope	Downward slope
Salinity	Salt	Brackish	Fresh
Wave type	Standing	Mixed	Progressive
Ecosystem	Nutrient poor, marine	High biomass productivity, high biodiversity	Nutrient rich, riverine

To people estuaries have always been important, both as a source of food and as a transport link between river and sea. In addition, lands bordering estuaries generally have excellent potential for agriculture: soils are fertile, the land is flat, and fresh water is, in principle, available. That's why most densely populated areas of the world are situated in coastal areas near estuaries. However, estuaries are also fragile. An estuary is a sediment sink, accumulating sediments stemming both from the river and the sea. As a result, the residence time of pollutants, attached to the sediments, is high. Given the high value of the estuarine ecosystem, the intense human use of the coastal zone and the high susceptibility to pollution, it is imperative that estuarine environments are protected. However, in some areas, human development has interfered with the water resource system, leading to serious deterioration of invaluable ecosystems. As concern grows about these developments, management for the sustainable use of the estuary water resources is receiving increasing attention.

This book aims to supply insight into the dominant hydraulic and hydrologic processes that determine the estuarine environment, and in doing so provide a tool for improving the sustainable management of the water resources of estuaries. Using the formulas derived, one can determine and predict the impact that interventions in the estuary system (such as dredging or fresh water withdrawal) have on the tidal range, the tidal propagation, the mixing processes and the salt intrusion (e.g. Cai et al., 2012a). The formulas can be used to determine the amount of fresh water that needs to be released to counterbalance saltwater intrusion and to compute the longitudinal distribution of the salinity as a function of geometric, hydraulic and hydrological parameters (e.g. Zhang et al., 2011; Nguyen et al., 2008a).

Knowledge of the physical phenomena that determine the process of tidal flow, tidal mixing and salt intrusion are important as they influence the environment of an estuary and its water resources potential in many ways. Interventions in the estuary topography can have drastic impacts on the hydraulic behaviour of an estuary, which may cause dramatic, and often irreversible, ecological change. Upstream developments, such as river regulation by dams and fresh water withdrawal, have a direct impact on the salinity distribution in the estuary, sometimes leading to hypersalinity (Savenije and Pagés, 1992). Changes in the salinity distribution impact on water quality, water utilisation and agricultural development in the coastal area, and the aquatic environment in general.

The importance of estuaries to mankind cannot be easily overstated. We are witnessing a period of rapid development and change, at a pace unprecedented in history. Our thirst for further development lies at the heart of most of our environmental problems. The global processes of development have unleashed forces that are difficult to contain. At the same time, our knowledge of natural systems is growing fast and the technology at our disposal and the

related computational capacity is increasing by the day. This book aims to contribute to the sustainable development of coastal zones by enhancing our insight and understanding of the processes at play in the estuarine environment, in the hope that the next generation of scientists, engineers and water managers will find the inspiration and the means to use the estuary resources wisely and conserve what is most fragile and valuable.

1.3 Classification of estuaries

In understanding how an estuary is classified, it is important to define the **main drivers** that affect its character. These are:

- **The tide**, which is generated by interactions in the planetary system, particularly between the Earth, the sun and the moon. It acts as a periodic function consisting of multiple components, depending on the frequencies of the Earth's rotation, the orbits of the Earth and the moon and other planetary processes at longer time scales. The dominant periods are in the order of 12.3 (semi-diurnal) and 24 (diurnal) hours. The tide is the main supplier of energy and salt water to the estuary system. The tide is responsible for the harmonic pumping of water into and out of the estuary with an erosive power that is neutralised only if the banks converge at an exponential rate.

- **The (flood) discharge of the river**, which provides fresh water and sediments to the estuary system. During a flood, river sediments settle as soon the fresh water enters the estuary, the banks begin to widen, the cross-section increases and, therefore, the velocity of the fresh water reduces. These sediments can only be transported downstream by the residual downstream energy of the flow, which is a combination of the harmonic tidal flow and the downward river flow. If the banks are parallel, the downstream transport process is faster. This is why estuaries with a high flood discharge tend to have modest bank convergence (near parallel banks).

- **The waves**, which have a stochastic nature, depending on meteorological conditions. Waves can have a dominant influence on the formation of the estuary mouth. The amount of energy supplied by waves, particularly during extreme events, can be substantial. However, in contrast to tidal energy, which dissipates along the entire estuary axis, wave energy dissipation is concentrated near the mouth of the estuary.

- **Lateral (littoral) sediment transport** along the coast can be responsible for the formation of spits and bars. If the littoral transport is strong in relation to the erosive power of the tide and of the river discharge, then this can lead to estuaries that are (temporarily) closed off from the sea by an ephemeral bar. Such an estuary is called a "blind" estuary.

- **The density difference**, which is responsible for a residual inward current along the bottom, transporting marine sediments into the estuary. In general, the fine sediments transported by the river as 'wash load' deposit once they come into contact with saline water, through a mechanism called flocculation. Together with the upstream transport of marine sediments, this leads to turbidity peaks and mud or sand bar formation at the upstream limit of the salt intrusion.

- **The climate**, which determines the rate of evaporation, the rainfall on the estuary, the hydrological regime of the streams feeding the estuary, the temperature of the water and the radiation on which the aquatic ecosystem thrives. It also determines whether mangroves and sea grass can grow, which are important agents in the stability of the banks and mud flats.

Of these drivers, tide and river floods are the two most important in determining estuary shape. However, it is the combination of all these drivers that leads to the wide range of estuary shapes and behaviours, each with a different aquatic environment. Several ways to classify estuaries are described below, according to: a) shape, b) tidal influence, c) river influence, d) geology and e) salinity.

a) Classification by shape.
In estuaries, the following characteristic shapes can be distinguished:

- **Prismatic**: The banks of the estuary are parallel. This is a type of estuary that only exists in a man-made environment where the banks are artificially fixed. Examples are shipping channels that are regularly dredged and where the banks are stabilised. In an estuary where the flood volume reduces in the upstream direction, and consequently the flow velocity amplitude reduces as well, no morphological stability is possible. A constant cross-section can only be maintained through dredging, such as in the Rotterdam Waterway.

- **Delta**: A near prismatic estuary where the tidal influence is small compared to the amount of river water feeding the delta. Deltas occur in seas with a relatively small tidal range and on rivers with a high sediment load (e.g. the Mississippi, the Nile, the Mekong).

- **Funnel or trumpet shape**: The banks converge in the upstream direction. This is the natural shape of an alluvial estuary, where the tidal energy is equally spread along the estuary axis (e.g. the Maputo, the Pungue, the Schelde).

- **Rias, fjords and sounds**: Fjords are the result of glaciers that eroded the underlying rock, after which the valley was submerged by sea level rise. In North America and New Zealand, these fjords are also called sounds. Drowned river valleys (also called by the Portuguese name 'ria') stem from the irregular topography of a watershed drowned by sea level rise, where the feeding rivers carry too little sediment to keep up with the seas level rise. This type of estuary generally has irregular banks with several side channels and embayments.

- **Bays**: These are semi-enclosed bodies that do not have a significant input from a river. The distinction between a bay and a drowned valley is often not easy to make.

A good description of several of these estuaries is provided by (Dyer, 1997, pp.7-12).

b) Classification by tidal influence.
The most general classification used is by Davies (1964), who distinguishes micro-, meso-, macro- and hyper-tidal estuaries on the basis of their tidal range (see section 2.1.1). This assumes that tidal range is a good indicator for the amount of tidal energy dissipated in the estuary, which is responsible for the erosive power of the tide and hence the shape of the estuary. Nichols and Biggs (1985) introduced the term of a 'synchronous estuary' where the amount of tidal energy per unit width is constant along the estuary axis, and the tidal amplitude is constant. However, this term is erroneous since 'synchronicity' suggests that water levels in the estuary are reached at the same time (which happened in estuaries experiencing a standing wave), but that is not what the authors meant. We call such an estuary an 'ideal estuary', following the definition by Langbein (1963). An ideal estuary is one of three types of tidal classification used in this book:

- **Ideal** estuary: An estuary where, as the tidal wave travels upstream, the amount of energy per unit width lost by friction is exactly equal to the amount of energy gained by convergence of the banks. In an ideal estuary the tidal range is constant along the estuary axis.

- **Amplified** estuary: An estuary where the tidal range increases in upstream direction because convergence is stronger than friction. Clearly this process cannot continue indefinitely, implying that at some point along the estuary the friction should become more pronounced, leading to a reduction of tidal amplification and subsequently to tidal damping. The process of damping is enhanced by the river discharge, which increases the friction.

- **Damped** estuary: An estuary where friction outweighs bank convergence. Tidal damping occurs in estuaries with a small convergence length or in drowned river values with a narrow opening.

c) Classification by river influence
If we classify by river influence, we can distinguish two extreme cases, the riverine and the marine estuary:

- **Riverine** estuary: This estuary is dominated by the river flow, both its discharge and sediment supply. The water is fresh and it behaves like a river: parallel banks, regular bank overtopping if not protected by dikes, a sandy bottom and sandy banks. The tide propagates as a progressive wave.
- **Marine** estuary: This estuary is dominated by the sea. The water is completely saline. There is no significant fresh water and sediment input from the landward side. The banks are often muddy. The ecosystem is primarily marine. The tide propagates as a standing wave.

There is obviously a clear link between this classification and the classification by shape (a). Riverine estuaries are prismatic or delta estuaries, whereas marine estuaries are bays.

d) Classification by geology
An estuary has been shaped within a geological setting, which reflects its geological history. Since an estuary is a transition from a river to the sea, the geology is at least partially alluvial. Depending on the degree to which an estuary is alluvial or not, we distinguish three types:

- **Fixed bed** estuary: An estuary with a fixed bed is a remnant of a different geological era. Alluvial estuaries are very young in geological terms, whereas fixed bed estuaries stem from an older geological period. Fjords are the remnants of glaciers that were active during the ice ages, and rias are remnants of drowned river basins where the river does not generate sufficient water and sediment to keep up with the rate of sea level rise.
- **'Short' alluvial** estuary: An estuary that is generally situated in a submerged valley (ria) or fjord. These estuaries are alluvial in the sense that the water flows in its own sediments, but they have not yet reached a stage of morphological equilibrium. The geological formation process (e.g. sea level rise or tectonic dip) is too fast, or the supply of sediments is too small, for the sedimentation to keep up. These estuaries have not been able to develop an equilibrium length, often because they are too short and the topography is too steep, resulting in standing waves. An example is the Ord River described by Wright et al. (1973). Van der Wegen et al. (2008) used a 3-D morphological model to generate the natural shape of an alluvial estuary, without imposing a river discharge. It led to a short coastal plain estuary with an exponentially varying cross-section and an almost linear bottom slope. The length of these estuaries is typically a quarter of the tidal wave length.
- **'Long' alluvial** or **coastal plain** estuary: A fully alluvial estuary consisting of sediments that have been deposited by the two water bodies that feed it: the river and the sea. Within these sediments, the estuary has shaped its own bed in a way that spreads the energy available for erosion and deposition equally along its length, resulting in minimum stream power. The coastal plain is long enough for the alluvial estuary to develop fully. It has an exponentially varying cross-section and almost no bottom slope.

e) Classification by salinity

We can also classify the estuary according to its salinity profile. Because the salinity profile depends on the estuary's shape and is the result of the main drivers, we can use it to infer information on estuary geometry and dominant drivers.

- **Positive** or **normal** estuaries: These are estuaries where the salinity decreases gradually in the upstream direction, from sea salinity to river water salinity. These estuaries are the dominant type in temperate and wet tropical climates. Because there is a significant river input, these estuaries are generally alluvial. In Section 1.4.4 we further divide this type of estuary into three sub-types - the recession shape, the bell shape and the dome shape - each the result of the estuary's geometry.

- **Negative** or **hypersaline** estuaries: These estuaries have a salinity that increases upstream because they are shallow, evaporation exceeds rainfall and the amount of fresh water input from the river is too small to compensate for the difference. These estuaries occur in arid and semi-arid climates and are characterised by the occurrence of salt flats (salinas). Because of the low fresh water discharge, and subsequently the low sediment input, these estuaries are often not fully alluvial; they are more commonly rias. Hypersaline estuaries have a very peculiar ecosystem often dominated by pink algae. Ample attention is given to these estuaries in Chapter 4.

1.4 Classification by estuary numbers

In Section 1.3, the two dominant drivers of estuary shape are the tide and the river discharge. The simplest dimensionless number that characterises this ratio is the Estuary number N, which in the Dutch literature is called the Canter-Cremers [1] number, equal to the ratio between the amount of fresh and saline water entering the estuary during a tidal period. The first volume is the product of the fresh water discharge Q_f and the tidal period T, the latter is the flood volume P_t, also called the tidal prism:

$$N = \frac{Q_f T}{P_t} \tag{1.1}$$

Another important estuary number is the Estuarine Richardson[2] number, which is defined as the ratio of potential energy provided to the estuary by the river discharge through buoyancy of fresh water and the kinetic energy provided by the tide during a tidal period:

$$N_R = \frac{\Delta\rho}{\rho}\frac{gh}{v^2}\frac{Q_f T}{P_t} \tag{1.2}$$

This estuary number accounts for more driving factors than the Canter-Cremers number. It incorporates the effect of the relative density difference between fresh water and sea water and of the Froude[3] number, which is the ratio between the amplitude of the tidal velocity v and the celerity of a frictionless finite amplitude wave ($c_0 = \sqrt{gh}$):

$$F = \frac{v}{c_0} \tag{1.3}$$

If the Estuarine Richardson number is high, there is enough energy available in the river discharge to maintain a sharp interface and subsequently stratification occurs; if it is low, there is enough energy available in the tidal currents to mix the river water with saline water and the estuary is well mixed. These estuary numbers, which are key in the classification of estuaries, are derived and presented in more detail in Chapter 2.

In Table 1.2, a combined overview of the different estuary types is presented, together with their main characteristics related to tide, river influence, geology, salinity and estuary number. Table 1.2 shows that the tidal wave type and the type of the salinity intrusion are very different in these estuaries. Some of the characteristics are not always obvious. For instance, in fjords, which generally do not drain large catchments (otherwise they would already have become alluvial) and hence do not have a very high river discharge, stratification generally does occur. This is because they generally are very deep and, as a result, have a relatively low tidal velocity amplitude

[1] J.J. Canter-Cremers (1879-1925) was a Dutch hydraulic engineer working for the Ministry of Public Works on the propagation of storm surges and tides in river branches. He laid the foundation for Dutch research on tidal propagation in estuaries, essential for the prestigious "Delta-Works" constructed in the branches of the Rhine, Schelde and Meuse deltas during the 20th century.

[2] Lewis Fry Richardson (1881-1953) was a British scientist with a very broad background, holding degrees in physics, mathematics, chemistry, biology and psychology. His field of work was equally broad. His earliest publications are on meteorology, while his latest work is on the psychology of war and peace. In hydraulic engineering he is known for his theory on fluid convective stability, leading to the Richardson number, and for his law on turbulent diffusion.

[3] William Froude (1810-1879) was a British engineer who established the important scaling law for scale models, which he developed for testing scale models of ship hulls. The Froude number is an essential scaling law in physical model tests.

(and tidal excursion), leading to a high Estuarine Richardson number. In prismatic channels, stratification can also occur if there is sufficient river discharge.

Table 1.2: Estuary classification in relation to the aspects: tide, river influence, geology, salinity and estuary number.

Shape	**Tidal wave type**	**River influence**	**Geology**	**Salinity**	**Estuarine Richardson number**
Bay	Standing wave	No river discharge	-	Sea salinity	Zero
Ria	Mixed wave	Small river discharge	Drowned drainage system	High salinity, often hypersaline	Small
Fjord	Mixed wave	Modest river discharge	Drowned glacier valley	Partially mixed to stratified	High
Funnel	Mixed wave; large tidal range	Seasonal discharge	Alluvial in coastal plain	Well mixed	Low
Delta	Mixed wave; small tidal range	Seasonal discharge	Alluvial in coastal plain	Partially mixed	Medium
Infinite prismatic channel	Progressive wave	Seasonal discharge	Man-made	Partially mixed to stratified	High

1.5 Alluvial estuaries and their characteristics

Alluvial estuaries are estuaries that have movable beds, consisting of sediments of both riverine and marine origin, in which there is a measurable influence of fresh water inflow. The water moving in the estuary can either erode the estuary bed (by deepening or widening) or it can deposit sediments and, in doing so, make the estuary narrower or shallower. Hence, the shape of an alluvial estuary is directly related to the hydraulics of the estuary, or as Wright et al. (1973) put it: "the simultaneous co-adjustment of both process and form has yielded an equilibrium situation". This equilibrium is a dynamic equilibrium between deposition and erosion, where at some point in time erosion is dominant, and at another point in time deposition dominates. This happens at different time scales: the short intra-tidal time scale where the tidal velocity accelerates and decelerates within the tidal period; at the inter-tidal time scale, between spring and neap tide, as a result of the difference in the available tidal energy; and at a seasonal or annual time scale, as a result of river discharge variation. The residual current that results from the river discharge gradually, and slowly, transports sediments downstream. However, during floods, it deposits sediments because the transport capacity of flow reduces as the estuary widens and the flow decelerates.

So, in an alluvial estuary, water movement depends on the topography, and the topography in turn depends on the erosive power of the hydraulics. The interdependence between hydraulics and topography is important because it permits us to derive hydraulic information from the estuary shape, and to derive geometric information from the hydraulics. This is probably why predictive equations, such as those presented in Section 2.1.2, appear to work (e.g. Gisen et al., 20xx).

Pethick (1984), elaborating on the differences between alluvial estuaries and rivers, stated that: "in its simplest form" the major difference is "that the tidal flow of the estuary, unlike the flow of a river is not going anywhere". In a river water flows because upstream rainfall generated a discharge that seeks a way downstream, while the water in an estuary flows just because the

estuary is there. For estuary water to flow, it requires an opening in the coastline, with a storage area behind it. Its flow is entirely governed by the shape of the estuary. A further difference between alluvial estuaries and rivers is that the amount of flow entering and leaving the estuary depends on the channel size, while in a river the discharge does not depend on the channel size; rather it depends on the rainfall that has fallen in the upstream catchment.

In an estuary with fixed beds (e.g. fjords), the estuary shape is not affected by the flow (although the flow is affected by the shape). In such estuaries no sediment is supplied from a feeding river and, if there is no continental shelf, there is also no supply of sediment from the sea. In estuaries with fixed beds, there is no interdependence between hydraulics and shape and it is therefore not possible to derive universal relations between shape and hydraulics in these estuaries (see Table 1.3).

Table 1.3: Interaction between shape and flow in estuaries and rivers.

	Shape determines discharge	**Shape does not determine discharge**
Discharge determines shape	Alluvial estuaries	Alluvial rivers
Discharge does not determine shape	Fjords and Rias	Canals and non-alluvial rivers

1.5.1 The shape of alluvial estuaries

Alluvial estuaries have converging banks that can be described by an exponential function. The equations describing estuary shape and hydraulics are presented in Chapter 2. This section discusses the shape in more general terms. Figure 1.1 shows a top view of a typical estuary. The origin of the longitudinal axis of the estuary is located at the mouth, which is the point where the estuary meets the ocean. The exact position of this point is often difficult to determine, but it can generally be found by connecting the adjacent shorelines by a fluid line. A good rule of thumb is to identify the point where the primarily one-dimensional flow pattern of the estuary changes into two-dimensional flow, or the point where the ebb and flood currents that fill and empty the estuary are fanning-out into the ocean.

Figure 1.1 shows two important horizontal length scales of the estuary: the width B, which is a function of x; and the tidal excursion E, which in alluvial estuaries appears to be near constant. The tidal excursion is the distance that a water particle travels on the tide. It moves inland during the flood tide and moves out again during ebb. The tidal excursion is in fact the horizontal tidal range, which is the integral over time of the tidal velocity between the two moments of slack: low water slack (LWS) and high water slack (HWS). The typical length of the tidal excursion for a diurnal tide is 10 km. In the widest part of the estuary the ratio of E/B can be small, particularly in strongly funnel-shaped estuaries, but in the upper part of the estuary this ratio is generally large.

Figure 1.2 shows a longitudinal cross-cut of the estuary. What strikes us is that the estuary bottom is horizontal. It is in agreement with Pethick (1984) observation that the tidal flow is not going anywhere. It is logical that, where there is no resultant direction of flow, there also is no resultant bottom slope. In reality, the depth of the estuary fluctuates as the flow meanders through the channel, deep in the bends and shallow in the crossings, but on average, in 'long' alluvial estuaries, there is no bottom slope, contrary to what most people believe. The bottom slope only begins where the estuary gradually changes into the river and the river discharge Q_f becomes dominant over the tidal currents. In 'short' estuaries, however, where the relief is steep, there is a clear bottom gradient, which is generally linear. This phenomenon is discussed further in Section 2.2.

The longitudinal cross-section also shows two important vertical length scales. The (vertical) tidal range H and the depth of flow h. The ratio of tidal range to depth is an important tidal characteristic. If this ratio is small, then the non-linear hydraulic equations may be linearised

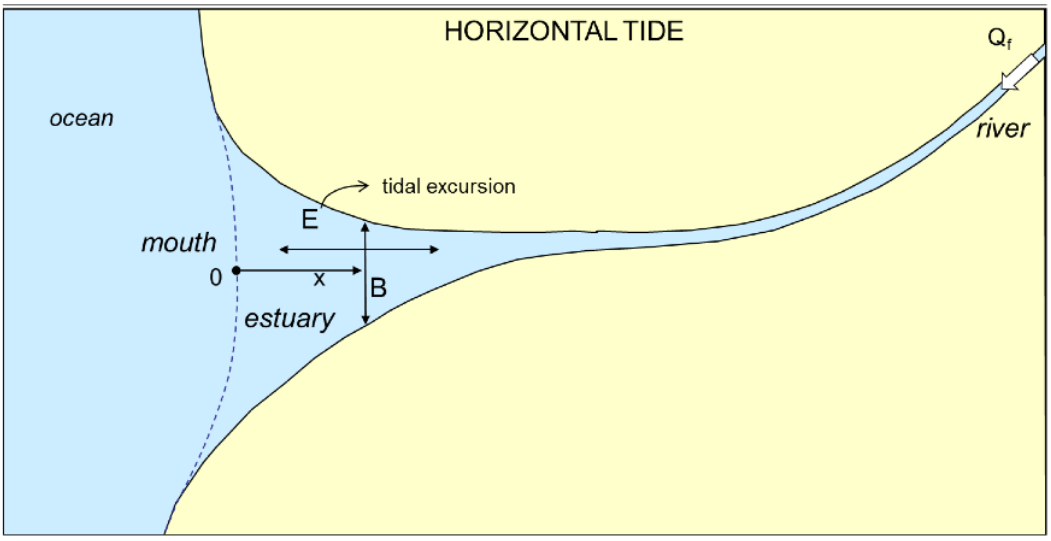

Figure 1.1: Definition sketch of an estuary: view from the top.

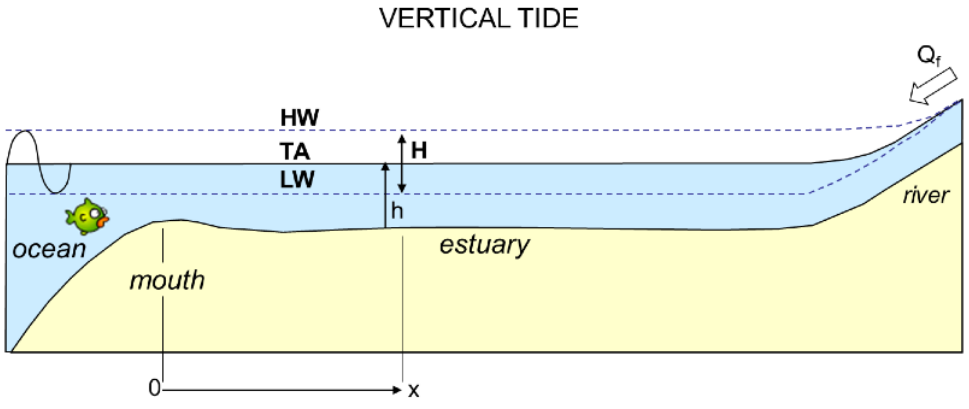

Figure 1.2: Definition sketch of an estuary: longitudinal cross section.

and relatively simple solutions of the hydraulic equations are possible. If this ratio is large, however, second order effects in the non-linear hydraulic equations become dominant and simple solutions are no longer possible.

Figure 1.2 shows two envelopes: one for high water (HW) and one for low water (LW). At all times, the water levels in the estuary remain between these envelopes. The mean water level (TA) is essentially horizontal[1] and links up with the backwater curve of the river. We see that also the two envelopes converge to the water level of the river, which is sloped. In the river, the water level slope is the same for high and low flows, but during floods the river influence reaches further. Being a schematic picture, these processes are somewhat exaggerated.

1.5.2 Dominant mixing processes

There are two main drivers for mixing in estuaries: the potential energy resulting from the density difference between the fresh and salt water; and the kinetic and potential energy provided by the tide. The tide drives the tidal currents and the density difference causes an imbalance in hydrostatic pressure that drives gravitational circulation, which is further discussed in Section 2.1.4. These two drivers generate four mixing mechanisms:

1 . **Turbulent mixing**, or shear mixing: In a river cross-section there is a balance between the driving forces (essentially components of the gravity force), friction and acceleration (Newton's 2^{nd} law, see Section 2.1.1). Although gravity and acceleration work on all water particles, friction only works along the bottom and banks of the estuary. The friction force is transported to all other particles through a shear stress that is transferred by turbulence. As a result the flow velocity in a cross-section is generally highest at the largest distance from the bottom and the banks. The turbulence that is associated with this shear stress causes mixing of water, much as in a regular river. Turbulent mixing has been intensively studied and described by hydraulic engineers. It is reasonably well understood, but this knowledge is of much less importance in estuaries. The other three mechanisms described below are much more efficient in mixing salt and fresh water.

2 . **Gravitational mixing**: Gravitational mixing stems from the fact that the hydrostatic pressure on the sea-side and on the river-side do not make equilibrium. Because sea water is denser than river water, the pressure on the ocean-side would be higher at equal depth than on the river-side. To compensate for the density difference, the water level at the limit of the salt intrusion is set up slightly above sea level (about 10 cm if the estuary is 8 m deep). Although on average the hydrostatic forces cancel out, the pressures are not equal over the depth. Near the surface the resultant pressure is directed towards the sea, while near the bottom it is directed upstream. As a result there is a residual circulation that carries relatively saline water upstream along the bottom and relatively fresh water downstream along the surface. The vertical salinity gradient that stems from this is an important cause of saline and fresh water mixing, particularly in the part of the estuary where the salinity gradient is steep. Besides vertical gravitational circulation, there is also lateral circulation as a result of the lateral differences in salinity over the cross-section. This phenomenon has also been amply studied, both in laboratories and in the field, and analytical equations have been derived to describe this mixing process. For more details on gravitational circulation, see Section 2.1.4.

3 . **'Trapping'**: Tidal trapping arises from the irregularity of the banks of an estuary. If there are tidal inlets, or tidal flats, then the water that fills these water bodies on the incoming tide is generally released with different density. There is a phase lag between the filling and emptying of tidal flats and the flow in the main channel, which results in density differences. In irregular channels, tidal trapping can be an important mixing mechanism, particularly in large estuaries with tidal flats. The tidal excursion is the dominant mixing length scale of tidal trapping, since this is the maximum distance over which a water particle can travel. The larger the salinity gradient is, the more important is this mixing mechanism.

[1] The mean water level is not exactly horizontal. There is a residual slope caused by the density gradient, the river discharge and the non-linearity of the momentum balance equation. For details see Chapters 2 and 3.

4 . **'Tidal pumping'** or mixing by residual currents: This mechanism is the least studied, yet it is very important (as was also observed by Fischer et al. (1979)). It is the dominant mechanism particularly near the mouth of a wide estuary. The most important difference from gravitational circulation and trapping is that tidal pumping does not depend on the salinity gradient; rather, it is proportional to the estuary's width. Few researchers have dedicated analytical effort to this mixing mechanism; instead their efforts have been concentrated on the middle reach of an estuary where gravitational circulation is dominant. Section 4.4 gives special attention to this type of mixing.

These mixing mechanisms are dealt with in detail in Chapter 4, and a predictive theory is presented that allows them to be integrated into one analytical equation: the modified Van der Burgh equation, developed by Savenije (1992b) after Van der Burgh (1972).

1.5.3 How the tide propagates

In an alluvial estuary, the tide propagates as a wave of a mixed character that has elements of both a standing and a progressive wave. A progressive wave is much like the wave that the bow of a boat generates, or that we feel when swimming in the surf. At the maximum elevation, the water moves into the direction of the wave; at the lowest elevation the velocity is backward, opposite to the direction of the wave; at the average water level, the movement is vertical. The highest flow velocity occurs at maximum elevation. In a progressive wave, the phase lag between the water elevation and the velocity is zero.

Flood waves in rivers are also progressive waves. At maximum elevation, the discharge is also at its maximum; at lowest elevation the discharge is at its minimum. Purely progressive waves occur in frictionless channels of infinite length and with a constant cross-section. For a progressive wave to occur in a channel, the channel should have a constant cross-section and be very long.

A standing wave is different. A standing wave is like a wave we can create in a tub by rocking it. After we have rocked the tub, the water in the tub continues to rock back and forth. In the tub, the maximum and minimum water levels are reached all at the same time. The water just swings back and forth like a swing. At the extremes the velocity is zero and changes direction. Here we see a phase lag between elevation and velocity of $\pi/2$. Standing waves occur in harbours, bays and, in general, in semi-enclosed basins that are connected to the sea.

Alluvial estuaries are none of the above. In alluvial estuaries, waves are of a mixed type: a mixture between a progressive and a standing wave with a phase lag between zero and $\pi/2$. The value of the phase lag depends on the channel geometry and the friction. In Section 2.3 an equation for the phase lag is derived.

If we make a longitudinal cross-section along the estuary we can draw the envelopes of HW and LW, as in Figure 1.2. If we could observe the instantaneous water levels in the estuary, then we would obtain an instantaneous tidal wave as shown schematically in Figure 1.3. This wave is contained between the envelopes. A full tidal wave seldom fits within the length of an estuary (except in very long estuaries, such as the Gambia), and the slope of the river is somewhat exaggerated. In Figure 1.4, some more instantaneous tidal waves are drawn between the HW and LW envelopes. The figure suggests that the tidal range is constant as we move upstream. While this happens in an 'ideal' estuary, it is not always the case in other estuary types. Some estuaries have a tidal wave that is damped, while others experience tidal amplification. In the latter case, the tidal range is only damped as the river influence becomes dominant over the tide (e.g. in the Schelde Estuary).

As the river discharge gains influence, the flow velocities are modified. Without river discharge, the moment of high water slack (HWS) occurs some time after high water (HW), whereby the incoming current stops, changes direction and subsequently starts to ebb. The reverse happens some time after low water (LW). At low water slack (LWS) the ebb current halts, changes direction and the flood flow starts. If there is substantial river discharge, then the moments of slack are shifted: the occurrence of LWS is delayed and HWS occurs earlier. Figure 1.5 provides a schematic illustration of this. We see that there is superposition of the river discharge over the tidal flows and, as a result of the river discharge, the ebb current becomes larger and the flood

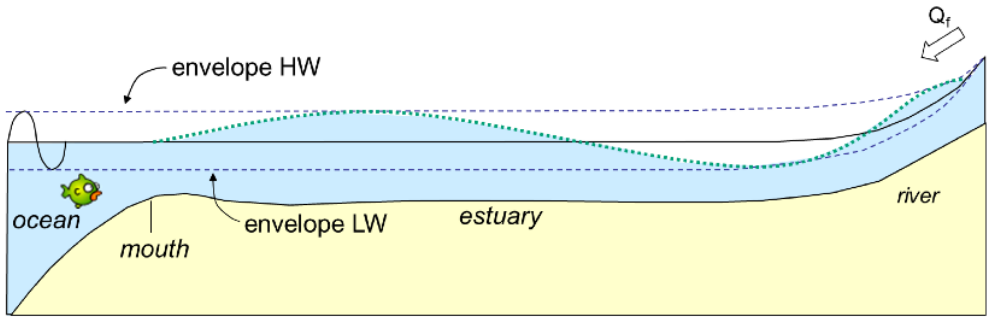

Figure 1.3: Longitudinal cross section showing an instantaneous tidal wave.

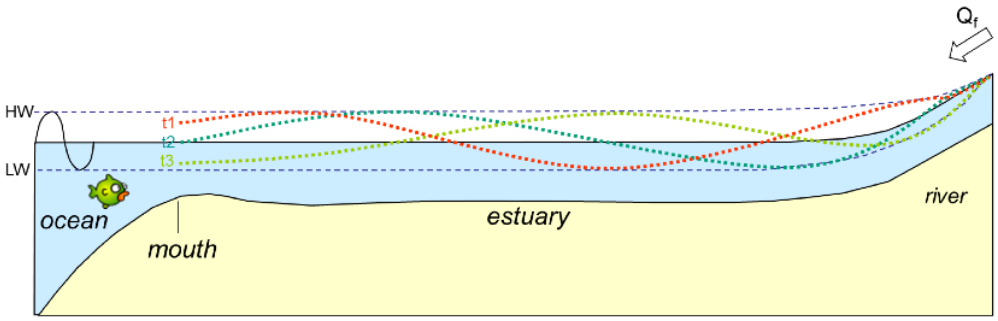

Figure 1.4: Instantaneous water levels contained between envelopes of HW and LW.

current is reduced (the top graph), until the point where there is only one moment of slack and no longer a change of flow direction (the middle graph). Further upstream (the lower graph) there is still a tidal wave, but the flow is perminently downstream.

We can calculate the fresh flow velocity Q_f/A that identifies the point where there is only one slack. We should realise that the fresh water discharge can be considered constant along the estuary axis, but that the cross-sectional area varies, increasing towards the estuary mouth. So the fresh water velocity increases in upstream direction.

Let the tidal velocity be given by a pure sinus:

$$V = v \sin \omega t \tag{1.4}$$

and let $\Delta\varepsilon$ (expressed in radians) be the change in the moment of slack (earlier for HWS and later for LWS) as a result of the river discharge. We then define the dimensionless river discharge as:

$$\varphi = \frac{Q_f}{Av} \tag{1.5}$$

It can then easily be seen from Figure 1.5 that:

$$\Delta\varepsilon = \arcsin \varphi \tag{1.6}$$

and that the point where only one slack occurs corresponds with the location where the cross-sectional area is such that: $\varphi = 1$. This point is indicated by a P in Figure 1.6

In Figure 1.6 we also see the envelopes of the water levels at HWS and LWS. The difference between these two envelopes is indicated by H', the slack tidal range. The figure also shows the point P, where the two slacks coincide - upstream from P the flow no longer changes direction. The dashed part between the envelopes for HWS and LWS is equal to the tidal prism P_t, as we shall see in Section 2.3.2.

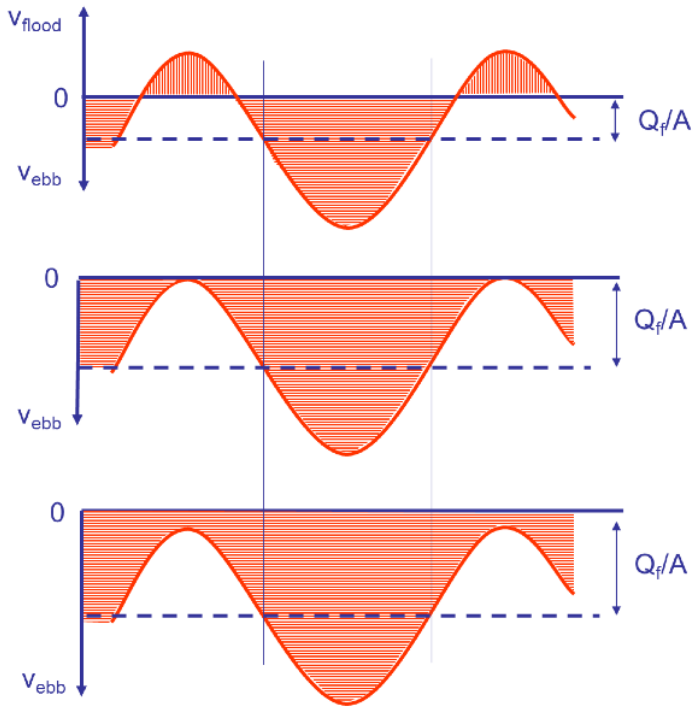

Figure 1.5: The influence of river discharge. On the vertical axis is the flow velocity of the current, which is affected by the strength of the river flow velocity Q_f/A. The velocity of the flood flow is in the positive direction; the ebb flow is negative.

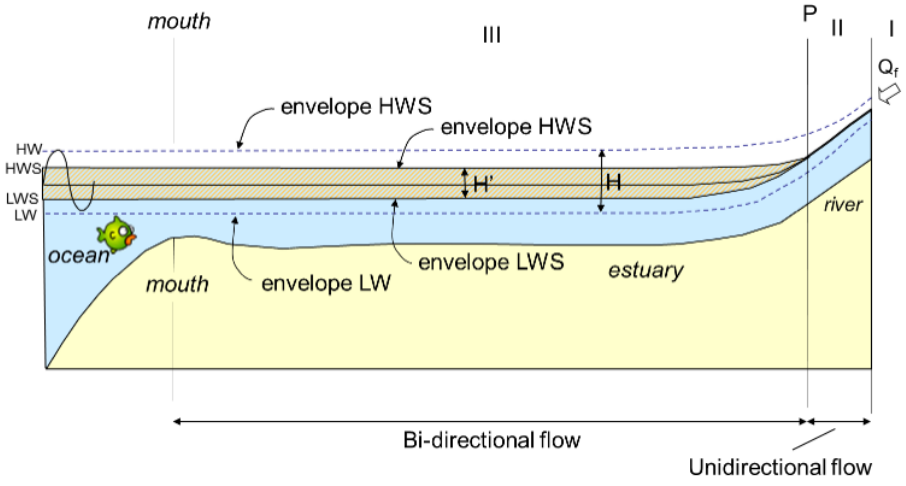

Figure 1.6: The tidal prism contained between the envelopes of HWS and LWS.

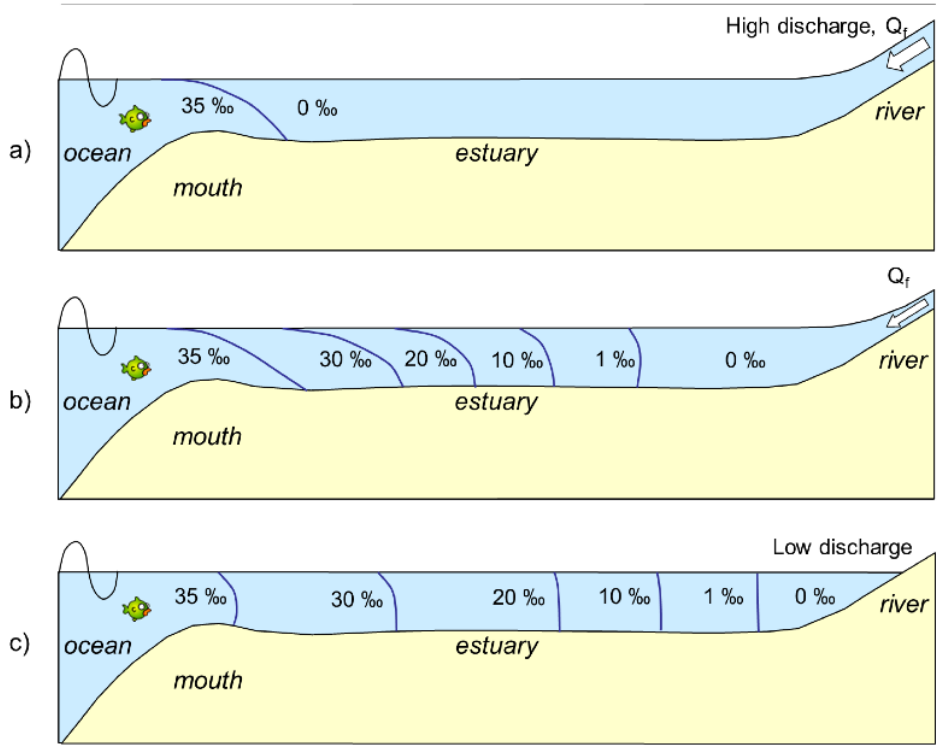

Figure 1.7: Longitudinal distribution of the salinity for a stratified estuary (a), a partially mixed estuary (b), and a well-mixed estuary (c).

1.5.4 How the salt intrudes

The salt intrusion mechanism is generally divided into three types:

a) the stratified type, or the saline wedge type,

b) the partially mixed type,

c) the well mixed type.

Figure 1.7 illustrates the three types. A stratified estuary occurs when the fresh water discharge in an estuary is large compared to the tidal flows (a large Canter-Cremers number and a large Estuarine Richardson number). A well mixed estuary occurs when the fresh water discharge is small compared to the tidal flows (a small Canter-Cremers number, and a small Estuarine Richardson number). Figure 1.8 shows a schematic of the corresponding vertical salinity gradients: a sudden increase of the salinity over the depth in a stratified estuary; a smooth gradient in a partially mixed estuary; and the absence of a gradient in a well mixed estuary.

What is seldom seen in figures of this type is the relative length of the salt intrusion. For instance, the sketch presented in (Fischer et al., 1979, figure 7.1) gives a wrong impression: it suggests that in stratified, partially mixed and well mixed estuaries, the intrusion length reaches equally far and that it can occur at the same river discharge. It also suggests a bottom slope. In contrast, Figure 1.7 clearly indicates that a saline wedge only occurs close to the mouth and during a period of high river discharge (when the Canter- Cremers number is large). The well mixed estuary occurs during low flow, resulting in a much deeper salt intrusion.

During the dry season, when water availability is lowest, water requirements are highest. At these times, when the problems of maintaining an acceptable water quality are most pronounced, the salt intrusion is generally of the mixed type. As the water consumption increases, the salt intrusion becomes even more strongly mixed as the Canter-Cremers number reduces further. For water managers aiming for the optimum use of available water resources, the critical case to considered for design is therefore the well mixed type, when salt intrusion is at its maximum. In alluvial estuaries, the saline wedge only occurs during periods of high river discharge; a time at which we are hardly interested in salt intrusion, but rather in flood protection (in man-made estuaries with a constant width this may be different due to the associated high Estuarine Richardson number). The relatively high attention given to stratified salt intrusion by hydraulic engineers, is therefore often more related to their professional interest than with a societal need.

This book is limited to estuaries of the partial to well mixed type, both with regard to the hydraulics (Chapters 2 and 3) and the mixing (Chapter 4) or salt intrusion (Chapter 5). The gradually varying density can be well incorporated in the analytical solutions for tidal hydraulics and salt intrusion.

The distinction between the partially mixed and the well mixed type is arbitrary. The salt intrusion is generally regarded as well mixed when the stratification (the difference between the salinity at the water surface and the salinity near the bottom divided by their average) is less than 10%. This is no objective criterion. Near the sea, there is more stratification than further upstream. In practice, however, the arbitrary value of 10% is not so important. Until a stratification of 20% to 30% is reached, no serious drawbacks have been encountered in applying well mixed theory.

Figure 1.9 shows a longitudinal cross-cut over a saline wedge. It shows that the water level increases slightly in the upstream direction due to the density gradient. As a result, there is a resultant downstream fresh water flow in the upper layer and a resultant upstream flow in the salt layer. We can see that there is a sharp interface, but that along the interface there is entrainment of saline water by the fresh water that flows over it. In fact, the slope of the saline wedge is maintained by a shear stress exercised by the fresh water discharge. This shear stress, and the related turbulent mixing, is responsible for the downward salt transport that counterbalances the upstream salt transport over the bottom.

Figure 1.10 shows the longitudinal distribution of the salinity along a well mixed estuary. It shows different intrusion lines for HWS (the maximum salt intrusion), LWS (the minimum salt intrusion), and for the tidal average (TA) situation. The horizontal distance between the HWS

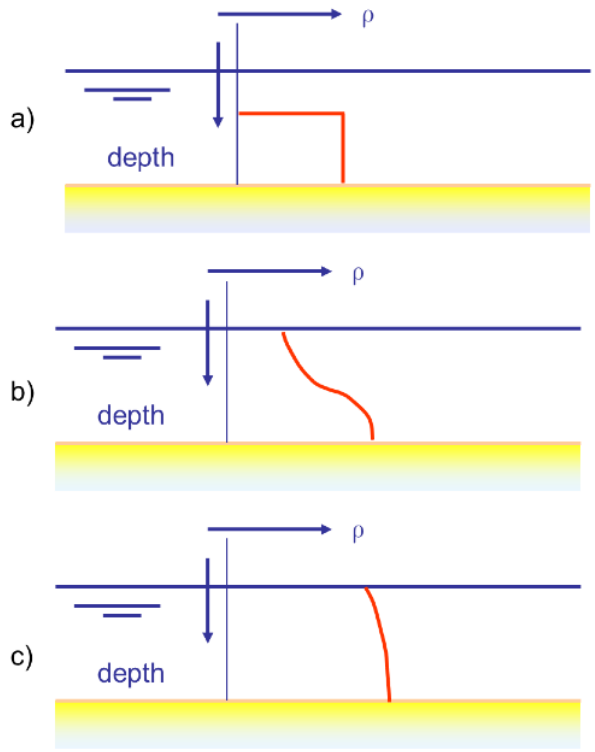

Figure 1.8: Variation of the salinity over the depth in a stratified (a), partially mixed (b), and well-mixed estuary (c).

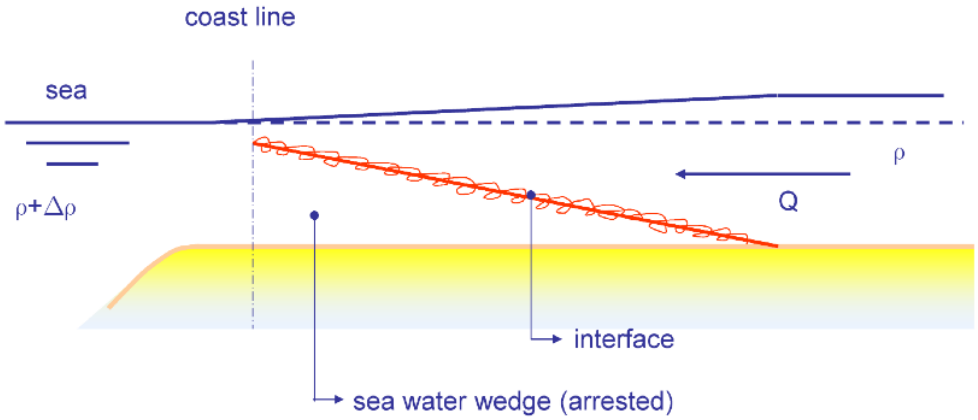

Figure 1.9: A longitudinal cross section over a saline wedge.

and LWS curve is the tidal excursion. We see that the salinity moves up and down the estuary following the water particles that travel between HWS and LWS. The horizontal translation of the curves demonstrates a constant tidal excursion along the estuary.

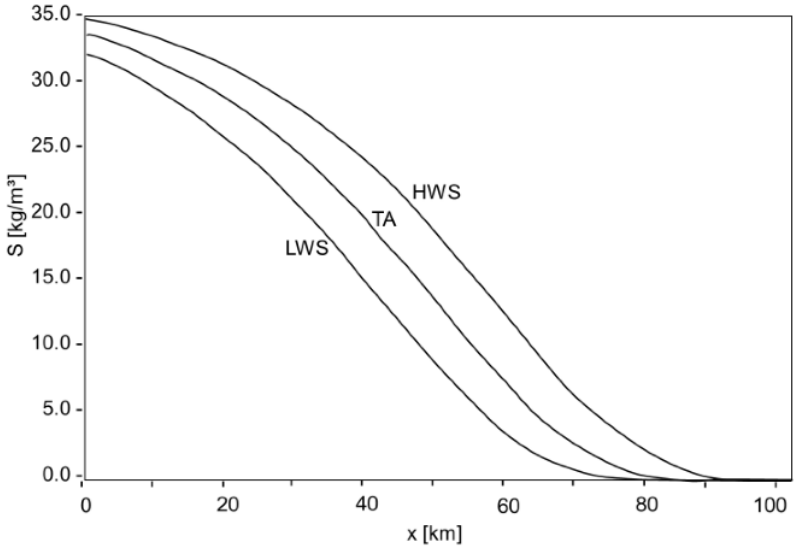

Figure 1.10: The longitudinal salinity distribution in a well-mixed estuary at high water slack (HWS), low water slack (LWS) and tidal average (TA) condition.

Finally, Figure 1.11 shows the different shapes of well mixed salt intrusion curves that can be distinguished:

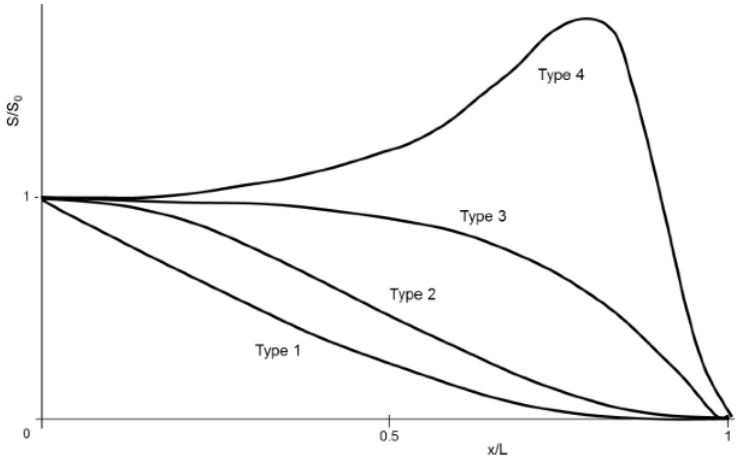

Figure 1.11: Different shapes of well-mixed salt intrusion curves.

1 . **Recession** shape, which occurs in narrow estuaries with a near-prismatic shape and a high river discharge. This type is more common in deltas and shipping channels, but is also dominant in riverine estuaries such as: the Corantijn (Suriname), the Chao Phya (Thailand), the Limpopo (Mozambique), the Solo (Indonesia), and the Rotterdam Waterway (Netherlands).

2 . **Bell** shape, which occurs in estuaries that have a trumpet shape, i.e. a long convergence length in the upstream part, but a short convergence length near the mouth. There are several estuaries that have a strong widening near the estuary mouth, possibly related with littoral processes. Examples are: the Mae Klong (Thailand), the Incomati (Mozambique), and the Maputo (Mozambique).

3 . **Dome** shape, which occurs in strong funnel-shaped estuaries (with a short convergence length). Examples are: the Schelde (Netherlands), the Thames (England), the Pungue (Mozambique), and the Delaware (United States of America).

4 . **Humpback** shape, which is a negative or hypersaline estuary, mentioned above. The driver for hypersalinity is evaporation. If evaporation exceeds rainfall and fresh water inflow, and if the estuary is shallow, it can become hypersaline. Estuaries with dome-shaped salt intrusion are most susceptible to hypersalinity. Hypersalinity often occurs in shallow rias in semi-arid areas, which have large water bodies compared to the amount of fresh water input. Examples are: the Saloum (Senegal) and the Casamance (Senegal) (see section 5.7).

These shapes are very much determined by the topography of the estuary. Topography is a key driver of both tidal hydraulics and mixing in estuaries, and as a result of salt intrusion. This interaction of estuary processes with topography is a key feature of this book.

The different types of salt intrusion curves are discussed in more detail in Chapter 4, which analyses the physical processes that generate these shapes.

1.6 What will follow

The following chapters deal in detail with the issues of tidal hydraulics, mixing processes and salt intrusion in alluvial estuaries. Chapters 2 and 3 cover the theory of tidal hydraulics. Chapter 2 concentrates on the effect of estuary shape on estuary hydraulics and uses the water balance equation to derive three analytical equations. Chapter 3 brings in the conservation of momentum equation, and derives two more analytical equations for tidal damping and wave celerity. As a result, a set of five new analytical equations is presented that follow from the combination of the general hydraulic equations with the typical topography of alluvial estuaries. These are equations for:

1) the phase lag between HW and HWS

2) the relation between estuary geometry and the tidal range

3) the ratio between the Froude number and the tidal amplitude to depth ratio, named the "scaling equation"

4) tidal damping and amplification

5) the wave celerity.

All these equations are more general versions of the classical equations commonly used to date. They have in common that they consider the effect of friction and channel convergence, as well as the fact that tidal waves are neither progressive waves nor standing waves, but waves of a mixed character with a phase lag between zero and $\pi/2$. Subsequently we show that the set of equations obtained can be solved explicitly and that the solution compares well with other analytical approaches, as well as with numerical benchmark cases (see Section 3.3-3.4).

Chapter 4 provides a theory for mixing in alluvial estuaries, building on the work done to date, and introducing a theory on one of the most important mixing mechanisms of funnel-shaped estuaries: residual circulation by "tidal pumping". It shows that Van der Burgh's method is a very convenient approach for combining into one equation the effect of the three main mixing mechanisms: tidal pumping, trapping and gravitational circulation.

Based on the previous chapters, Chapter 5 presents a one-dimensional steady state and non-steady state model for salt intrusion in estuaries. The resulting equations are surprisingly simple

and have yielded very good results in a wide range of estuaries studied worldwide. The method is predictive in that it can be extrapolated to discharge regimes outside the range of calibration and can be applied to new estuaries without the explicit need for further calibration. The unsteady model allows the application to estuaries that do not reach an equilibrium situation in the dry season, or that may become hypersaline. This makes the model a very useful tool to assess the consequences of upstream withdrawals, and particularly to assess the risk of estuaries becoming hypersaline.

Combined, the chapters present a complete theory of tidal hydraulics, tidal mixing and salt intrusion to assist both researchers and water managers in studying the behaviour of alluvial estuaries in a rapidly changing environment.

Chapter 2

TIDE AND ESTUARY SHAPE

This chapter covers the theory of tidal hydraulics, specifically dealing with equations that describe the relation between an estuary's shape and its hydraulics.

As with all open channel flow, tidal hydraulics in an estuary can be described by the St. Venant equations: a set of two non-linear partial differential equations that govern the movement of water through a medium. What makes tidal hydraulics in alluvial estuaries special is the medium through which the water flows. As we saw in the previous chapter, in coastal plains this medium has a particular shape, similar to the shape of an ideal estuary. Although this knowledge is far from new, in practice only few people make use of it-modern computational power allows us to make 3-dimensional computations that no longer require geometric simplification. However, merely applying computer models without using the knowledge and insight provided by analytical equations may cause numerical blindness. Analytical solutions not only provide insight into the processes at play, more importantly, they provide a means to verify or disprove the computer models.

This chapter describes the hydraulic equations of alluvial estuaries where there is a close interaction between geometry and flow, mutually influencing each other through continuous feedback. As a result, a regular topography appears in which the hydraulics obey surprisingly simple analytical equations. By combining the conservation of mass and momentum equations with the topography of an alluvial estuary, a number of analytical equations are derived for: 1) tidal propagation; 2) tidal damping; 3) tidal amplification; 4) wave celerity; 5) phase lag; and 6) the influence of river flow on tidal damping. In section 2.3, integrating the conservation of mass equation leads to the Geometry-Tide equation (a relation between topographical and tidal length scales) and an expression for wave celerity and phase lag (the Phase Lag equation). Combining these two equations yields the Scaling equation. These equations are derived through Lagrangean[1] analysis, which is a mathematical approach more natural to estuary hydraulics and salt intrusion since the reference system moves with the water. This chapter deals with the relation between hydraulic parameters and estuary shape and focuses on the conservation of mass equation. The next chapter looks into the tidal dynamics. It builds further on the equations we derive here and combines them with the equation of motion, providing derivations for tidal damping (or amplification), tidal wave propagation, and their dependence on river discharge.

Although this text introduces the equations for conservation of mass and momentum sequentially, we should realise that they are inseparable and can't be considered in isolation. In the first chapter we assumed that the Lagrangean velocity can be described by a sine function. As this provided an implicit linear solution for the coupled set of equations, this can only be an approximation given their non-linearity. In this chapter, we shall check the validity of this assumption by confronting the analytical equations with observations in a range of real estuaries.

[1] Joseph-Louis Lagrange (1736-1813), a French mathematician and mathematical physicist, was one of the greatest mathematicians of the eighteenth century. His work, Mécanique Analytique (1788), was a mathematical masterpiece. Lagrange succeeded Euler as the director of the Berlin Academy. The term 'Lagrangean' means: using a reference frame that moves with the water particle, or unit volume. Commonly it is mispelled, ending with -ian, but this is wrong. As with Shakespeare, Boole and Europe, which also end with an 'e', the correct spelling for the adjective is -ean.

2.1 Hydraulic equations

In hydraulics, waves are always the result of the combination of two hydraulic equations: the conservation of mass and the conservation of momentum equation - the latter is introduced in the next section. Further down, in section 2.3, we'll derive analytical equations based on the mass balance equation alone. While this may seem to contradict the earlier statement, that the equations cannot be considered in isolation, it is not. In the derivations of these equations we assume that the tide varies according to sinusoidal functions. This is an implicit solution of the coupled set of equations. In fact, the sinusoidal function is only a correct solution if the set of equations is linear (as we shall demonstrate in section 2.2.2). Obviously, this is not usually the case - it is only correct if the tidal amplitude to depth ratio is very small. However, we shall see that the use of an approximately correct sinusoidal function will allow us to explore the behaviour of the non-linear system of equations. So we retain the non-linear terms in the equations, but we make use of a linear solution to explore analytical solutions. The solutions obtained in this and the following chapter are therefore quasi-linear, as opposed to derivations where the equations have been fully linearised beforehand.

2.1.1 Basic equations

Alluvial estuaries have a dynamic equilibrium between erosion and the deposition of sediments that are picked up, transported and deposited by water. In turn, the water movement strongly depends on the geometry it has created. This close interaction between the dynamics of water and sediment is an important characteristic of alluvial estuaries, as discussed in the previous chapter. The movement of water and sediment is generally described by a set of four 1 dimensional equations: the conservation of momentum and mass for water, the conservation of mass for sediment and an empirical formula that relates sediment transport to flow parameters (see e.g. Jansen et al., 1979):

$$\frac{\partial Q}{\partial t} + \alpha_S \frac{\partial (Q^2/A)}{\partial x} + gA\frac{\partial h}{\partial x} + gA\frac{\partial Z_b}{\partial x} + gA\frac{h}{2\rho}\frac{\partial \rho}{\partial x} + gA\frac{U|U|}{C^2 h} = 0 \tag{2.1}$$

$$r_S \frac{\partial A}{\partial t} + \frac{\partial Q}{\partial x} = R_s \tag{2.2}$$

$$B\frac{\partial Z_b}{\partial t} + \frac{\partial Q_s}{\partial x} = 0 \tag{2.3}$$

$$Q_s = Bd_s U^n \tag{2.4}$$

where:

$Q = Q(x,t)$ is the discharge in m^3/s;
α_s is a shape factor (assumed constant) to account for the spatial variation of the flow velocity over the cross-section ($\alpha_s > 1$);
$A = A(x,t)$ is the cross-sectional area of the flow in m^2;
$h = h(x,t)$ is the mean cross-sectional depth of flow in m;
$Z_b = Z_b(x,t)$ is the mean cross-sectional bottom elevation in m;

— g is the acceleration due to gravity in $\mathrm{m/s}^2$;
— $\rho = \rho(x,t)$ is the density of the fluid in $\mathrm{kg/m}^3$;
— $U = U(x,t)$ is the mean cross-sectional flow velocity in m/s;
— $C = C(x)$ is the coefficient of Chézy in $\mathrm{m}^{0.5}/\mathrm{s}$;
— $B = B(x,t)$ is the stream width of the channel in m;
— $B_S = B_S(x,t)$ is the storage width of the channel in m;
— $r_S = r_S(x)$ is the cross-sectional storage ratio, or the storage width ratio (if the width is much larger than the depth) ($r_S > 1$);
— R_s is a source term accounts for rainfall, evaporation or lateral inflow in m^2/s;

— $Q_s = Q_s(x,t)$ is the sediment discharge in terms of sediment volume (including pores) in m^3/s;
— n is an exponent;
— $d_s = d_s(x)$ is a parameter with the dimension $m^{(2-n)}s^{(n-1)}$ that depends on sediment characteristics and channel roughness.

Throughout this book, since the most important boundary condition lies at the estuary mouth, the positive x-direction chosen is the upstream direction with the origin at the sea or ocean boundary. The first two equations are generally known as the St. Venant equations (named after A.J.C. Barré de Saint-Venant[2]).

The first equation, (2.1), is the equation for conservation of momentum, derived from Newton's[3] second law of motion, which states that the acceleration of an object is equal to the balance of forces, in this case the component of gravity in the direction of flow and friction. The first term in (2.1) is the Eulerian[4] acceleration term, while the second term is the convective acceleration term. The coefficient α_S accounts for the shape of the channel. The more irregular a cross-section and the more the variation in flow velocity over the cross-section, the larger α_S is. It is larger than unity, but generally smaller than 2. In a regularly shaped, single channel, alluvial stream, α_S is usually close to unity (Jansen et al., 1979). In estuaries where there are no floodplains that discharge considerable parts of the flow, α_S is normally close to one.

The third, fourth and fifth terms jointly represent gravity, exercised through the water pressure gradient. These terms are the gradient of the water depth, the bottom slope and the density gradient. The density term is often disregarded, but it can play an important role in the brackish part of an estuary. For the derivation of this term, the assumption has been made that the density is merely a function of x and t and that there is no vertical salinity gradient (i.e. the estuary is well mixed). The fourth term will be discussed in detail in section 2.1.4.

The last term of (2.1) is the friction term, based on the formula of Chézy[5]. In this term, the depth h is used instead of the hydraulic radius. This assumption is justified if the estuary is wide in relation to its depth ($B \gg h$). In alluvial estuaries this is always the case. Since Chézy's coefficient is not independent of the depth, the formula of Manning[6] is considered more appropriate to describe the resistance term R:

$$R = \frac{U\,|U|}{C^2 h} = \frac{U\,|U|}{K^2 h^{4/3}} \tag{2.5}$$

where K is Manning's coefficient, generally indicated by its inverse value n ($K = 1/n$).

The second St. Venant equation, (2.2), is the conservation of mass equation, or the equation of continuity. In this equation there is a balance between the first term, indicating the rate of increase of the volume over time, and the second term, indicating net inflow of water over the stretch considered. The sum of these terms should equal the source term, which accounts for lateral input of water from drainage, rainfall or evaporation (negative). In this chapter, the

[2]In 1843, seven years after the death of Claude Navier (1785-1836), the Frenchman Adhémar Jean Claude Barré de Saint-Venant (1797-1886) rederived Navier's equations for a viscous flow. In this paper he was the first to properly identify the coefficient of viscosity. He further identified viscous stresses acting within the fluid as a result of friction. George Stokes (1819-1903), like Saint-Venant, also derived the Navier-Stokes equations but he published the results two years after Saint-Venant (after: J. J. O'Connor and E. F. Robertson).

[3]Isaac Newton (1643-1727) published his single greatest work, the *Philosophiae Naturalis Principia Mathematica*, in 1686. It contains his famous laws of motion, and the law of universal gravitation.

[4]Leonhard Euler (1707-1783), a Swiss mathematician and student of Bernoulli, may be considered as the founding father of modern mathematics (introducing among other things, the exponential function, complex calculus and the notation $f = f(x)$). His *Introducio in analysia infinitorum* (1748) provided the foundations of mathematical analysis. The term 'Eulerian' is used for a reference frame that is fixed on the river or estuary bank, in contrast to a Lagrangean reference frame that moves with the water.

[5]In 1776 the French engineer, Antoine de Chézy (1718-1798), published his well-known formula, which he had been using for some time, where the flow velocity is proportional to the root of the product of the hydraulic radius and the slope.

[6]In 1891, Robert Manning (1816-1897), an Irish engineer, published his well-known formula, building on the work of De Chézy (among others). Although he tried to make his coefficient dimensionless, he did not succeed. After the introduction of $\sqrt{g}$, there still remained a length to the power 1/6 to account for. This was done in 1923 by the Swiss hydraulic engineer, Albert Strickler (1887-1963), who related the roughness to the 1/6th power of the ratio between effective roughness depth and water depth. As a result, the Manning formula is often called the Manning-Strickler formula.

source term can be disregarded where it relates to tidal hydraulics, since lateral inflow generally has a marginal influence on tidal parameters such as velocity and depth. In Chapter 4, however, the source term can play a key role in the salt balance equation, particularly when an estuary turns hypersaline.

In the second equation we see the appearance of the cross-sectional storage ratio. This ratio needs to be included because the cross-sectional areas used in the two St. Venant equations are not the same. In the equation of motion, the cross-sectional area represents the water that is in motion (the part that flows under the influence of gravity and friction). In the second equation it is the whole part of the water body where water is stored. This also includes stagnant water that does not take part in the equation of motion. In order to combine these two equations we have to use a relation between the active cross-sectional area A and the total area A_S, which is the cross-sectional storage ratio r_S. This ratio is always larger than unity, or equal to unity if there is no dead storage. If the width is large compared to the depth, we can generally simplify this ratio to the proportion of the total width of the channel B_S in relation to the active width of the stream B (see below). Particularly close to the mouth of an estuary, where there are mudflats, this ratio can be significant. It is mostly not significant in the upper part of an estuary. If an estuary has a lot of dead-end side channels, then the ratio can be much larger. In all practical cases $r_S < 1.2$.

The third equation is the conservation of mass equation of the sediment (or, rather, the conservation of volume). It represents the balance between sediment deposition over time and the increase of sediment transported over the reach being considered. If the transport capacity increases then erosion occurs; otherwise deposition occurs. Erosion balances deposition when the sediment transport capacity is constant with x. The fourth equation is the sediment transport equation. It appears in several forms in the literature. The most widespread formula, well appreciated for its wide applicability in alluvial rivers as well as for its simplicity, is the formula of Engelund and Hansen (1967), where the exponent n equals 5 and the parameter d_s is defined by:

$$d_s = \frac{0.05}{D_{50}\,\Delta_S^2\,C^3\,\sqrt{g}} \tag{2.6}$$

where D_{50} is the diameter of the bed material that is exceeded by 50% of the sample by weight and Δ_S is the relative density of submerged sediment (generally $\Delta_S = (2600-1000)/1000 = 1.6$).

In addition, the following geometric relationships define A, r_S and Q as:

$$A = hB \tag{2.7}$$

$$Q = UA \tag{2.8}$$

$$r_S = \frac{B_S}{B} \tag{2.9}$$

Finally there is an equation for the density gradient, which is not reproduced here. In Chapter 4, a relation will be presented that allows the determination of ρ as a function of space and time. For the following analysis it is assumed that the water density gradient is either known through measurements, or can be computed by an appropriate salt intrusion model. Assuming that α_s, r_S, ρ, C, g, n, Δ, D_{50} and hence d_s are known, the list of dependent variables consists of the following seven parameters:

- The mean cross-sectional flow velocity $U(x,t)$
- The mean cross-sectional depth of flow $h(x,t)$
- The mean cross-sectional bottom elevation $Z_b(x,t)$
- The channel width $B(x,t)$
- The cross-sectional area $A(x,t)$
- The discharge $Q(x,t)$

- The sediment discharge $Q_s(x,t)$

We therefore have six equations ((2.1)-(2.4) and (2.7)-(2.8)), with seven dependent variables. Consequently, one more equation is required, besides boundary conditions, to solve the set of equations for the seven dependent variables - we need something to relate geometric parameters to flow parameters. All conventional hydraulic models are based on the above equations, which can only be solved if the geometry of the channel (in particular, its width) is fixed. With the present models we are not yet able to predict what the shape of a channel will be when we provide a certain discharge at the upstream boundary of a freely erodable slope. New research, documented by Rodriguez-Iturbe and Rinaldo (1997), used concepts such as self-organisation, minimum stream power and entropy to find this missing relation, but as yet the solution has not been found.

As a result, in computational hydraulics, instead of a seventh equation the width is imposed as a function of distance x and water level elevation ($Z = Z_b + h$). For a freely varying width, however, a 'seventh equation' is needed. Van der Wegen et al. (2008), for instance, use a wetting function where the banks either erode or accrete depending on the local flow conditions. Such an algorithm is a closure relation replacing the seventh equation.

2.1.2 The seventh equation

Although several efforts have been made to relate the width B to flow parameters, no unequivocal physically-based method has yet been developed (to the disappointment of many researchers). For alluvial channels, Lacey, in 1930, formulated a theory based on earlier work by Kennedy (1894) and Lindley (1919), which became known as "regime" theory. It which was based on the assumption that an alluvial channel adjusts its width, depth and slope in accordance with the amount of water and the amount and kind of sediment supplied (Stevens and Nordin, 1987). Lacey's theory is almost entirely empirical and supplies simple power expressions that relate stream depth, width, slope and velocity to the discharge. Regime theory has been relatively successful in India and Pakistan in the design of stable irrigation channels under natural regimes. On the other hand, regime theory has been widely criticised mainly because of its lack of physical basis, its empirical character and the scanty and incomplete database used for its derivation (Stevens and Nordin, 1987). Investigations by Stevens (1989) on stream width however indicated that, although there still is no satisfactory physical backing, there is also no reason to reject the empirical relation between stream width and discharge (see also: Rodriguez-Iturbe and Rinaldo, 1997, pp. 12-15).

Recent work by Eaton and Church (2007) and by Eaton et al. (2010) confirm that Lacey's equation is correct for the "downstream hydraulic geometry". This is to distinguish it from the geometry "at the station", where water levels are below the spilling level, within the banks-in this case, Manning's equation (or the rating curve) applies. In the downstream approach we assume 'bankfull discharge'[7], under which conditions Lacey's formula performs remarkably well in a wide range of natural channels.

For his stream width formula, Lacey made use of the wetted perimeter P instead of the surface (or bottom) width B. The wetted perimeter is the length of the wetted cross-sectional profile over which shear stress is exercised, which is a better measure for the width in the friction term than the surface or bottom width. The wetted perimeter is somewhat larger than the width (in a rectangular profile $P = B + 2h$), but in alluvial streams where the width is generally much larger than the depth ($B \gg h$), the wetted perimeter is approximately equal to the stream width ($P \approx B$). Lacey found a surprisingly simple proportionality between the wetted perimeter and the root of the bankfull discharge:

$$B \approx P = k_s \, {Q_b}^{0.5} \tag{2.10}$$

where k_s, in metric units, equals 4.8 ($\mathrm{s}^{-0.5}\mathrm{m}^{0.5}$). Savenije (2003), making use of Lane (1955) stable channel theory, suggested that this coefficient of proportionality depends on the flow velocity at bankfull discharge U_b and the natural angle of repose ϕ of the bed material:

[7] 'Bankfull discharge' is the discharge at which the river starts spilling over the natural levees. It is the discharge above which the river can deposit sediments on its banks. Regular overtopping is necessary for the river to maintain its bed.

$$k_s = \sqrt{\frac{\pi^2}{2U_b \tan\phi}} \tag{2.11}$$

Leopold and Maddock (1953), who extended the regime concept to American rivers, confirmed that the width is proportional to the square root of the bankfull discharge. Blench (1952) arrived at the same conclusion and gave an expression for Lacey's coefficient k_s, which he related to the bed material and tractive force acting on the sides of the river bed. Later studies in American streams by Simons and Albertson (1960) showed similar results:

$$B = k_s {Q_b}^{0.51} \tag{2.12}$$

albeit that the exponent was slightly increased. The coefficient of proportionality k_s appeared to vary with the soil properties of the banks. The value of k_s varied between 3.1 for banks with coarse non-cohesive material, to 6.3 for sandy banks (in metric units), which is in general agreement with (2.11). The former value is lower than the latter because sandy banks are easier to erode. Lacey (1963), in the paper's discussion, maintained that an exponent of 0.5 is correct.

In estuaries, empirical studies of cross-sectional dimensions have yielded similar relations between tidal discharge and cross-sectional area. O'Brien (1931) presented a relation between the cross-sectional area of the estuary mouth and the tidal flood volume P_t (the amount of sea water that enters the estuary on the flood tide), which, in its turn, is approximately proportional to the peak of the tidal discharge Q_p:

$$A \propto {P_t}^{0.85} \propto {Q_p}^{0.85} \tag{2.13}$$

In later studies, described by Bruun and Gerritsen (1960), other equations of the type of (2.13) were derived based on the stable channel theory of Lane (1955) and Bretting (1958). Bretting's formula for estuaries reads:

$$A \propto {Q_p}^{0.9} \tag{2.14}$$

Using Manning's equation, the "within the banks" case, one can easily demonstrate that the power of the discharge should be 0.8:

$$A \propto Q^{0.8} \tag{2.15}$$

Savenije (2003), who considered bankfull flow as a singularity where Manning's equation no longer applies (because the water slope is forced by the overtopping levees and not by the balance between friction and gravity), found the exponents for B and h both to be equal to 0.5, leading to a direct proportionality between A and Q_b, and a bankfull velocity U_b that is independent of Q. This result is close to (2.14). In fact, Bruun and Gerritsen (1960) showed that in the tidal inlets between the islands along the Dutch coast, there was a direct proportionality between Q_p and A at a rate of a tidal peak velocity v=1 m/s (see Fig. 2.1). Although Bruun and Gerritsen (1960) use an exponent of 0.9, an exponent of 1 with a peak velocity of 1 m/s is as feasible (see Fig. 2.1). However, the fact that the exponent of Bruun and Gerritsen(0.9) lies between 1 and 0.8 (between a value for bankfull ("downstream") and within-bank "at the cross-section") discharge respectively) indicates that bankfull discharge (where the banks just overtop) is not often achieved in estuaries.

The good correspondence between these equations for both estuaries and rivers suggests that estuaries do not substantially differ from alluvial rivers in their morphology. The main difference being, that in a river the bankfull discharge determines the channel shape, whereas in an estuary this is the peak spring-tidal discharge, which (according to Pethick (1984)) also corresponds to bankfull flow. The latter is based on the experience that Q_p just overtops the banks. Another important difference lies in the fact that in an estuary the water level is governed by the backwater effect of the ocean, whereas in a river the water level fully depends on the discharge from upstream.

In general, close to the sea, the bank slope of an estuary is very small due to the fine grain sizes and the relatively high shear stress exercised by alternating tidal flows with a peak velocity in

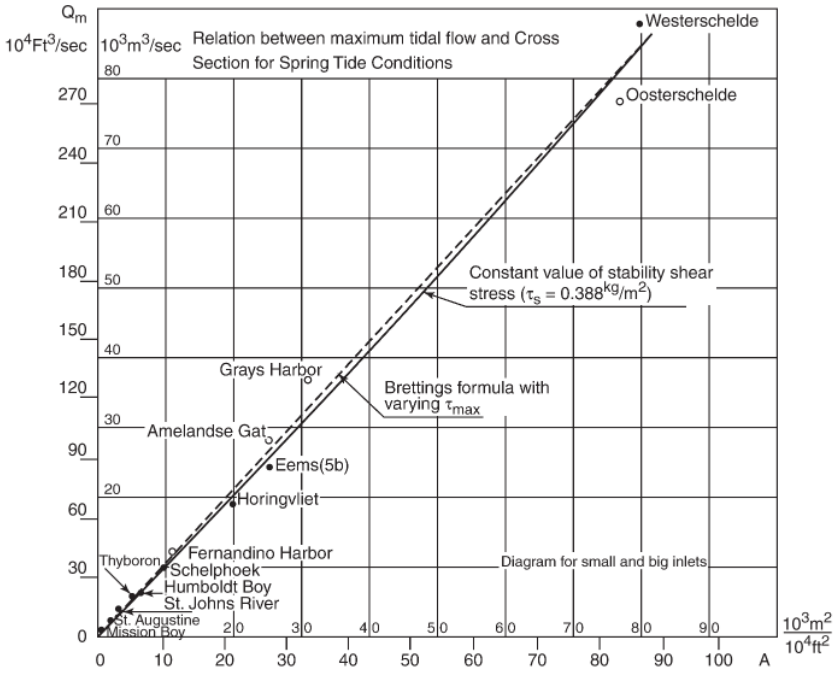

Figure 2.1: Relationship between peak tidal discharge Q_p and cross-sectional area of the tidal inlet A as reported by Bruun and Gerritsen (1960).

the order of 1.0 m/s. If erosion occurs near the toe of the bank, then erosion propagates sideways to maintain a stable slope. This widening process often takes place through bank failure. Since side slopes are small, widening is several times more than deepening. The widening, in turn, reduces the stream's flow velocity and thus its sediment transport capacity, leading to a new equilibrium. Therefore, an increase in transport capacity of the stream eventually leads to a new equilibrium with a wider channel.

The widening of an estuary through bank failure is rapid. The opposite process is slower. Building up a bank by sedimentation, starting from its toe, may take months if not years. Hence the dynamic equilibrium that is reached as a balance between erosion and sedimentation lies nearer to the maximum eroded profile than to the minimum (silted up) profile. Thus the width of a stream mainly reflects the situation of its maximum eroding capacity. In a river, the width is determined by the bankfull flow, in an estuary by the peak spring-tidal discharge.

Observations in excavated tidal canals in Indonesia (at Karang Agung, in the Banyuasin estuary, South Sumatra, where the author carried out field surveys in 1989) illustrate this process. An initially prismatic (constant cross-section) excavated dead-end canal is seriously eroded at the mouth as high tidal flows enter and leave the canal. The mouth grows deeper, after which the banks collapse. At the upstream dead end of the canal, where tidal velocities are almost non-existent, sedimentation occurs. The canal thus gradually acquires a funnel shape.

In the mouth of an estuary two different media interact: the ocean, in which the movement of water and sediment has a three-dimensional character; and the estuary, where the motion is primarily one-dimensional (see Ippen and Harleman, 1966). This interaction often leads to the formation of a shallow area or bar. This shallow reach urges the estuary to become wide and influences the depth of its upstream reaches.

It is beyond the scope of this book to go into details regarding the morphological processes that determine channel development. D'Alpaos et al. (2005) have done pioneering work in this field. Rather, we make use of the particular exponential shape of alluvial estuaries that is further discussed in section 2.2. Equations describing the exponential variation of width and cross-sectional area are essential to the approach followed here, and serve the purpose of the

"seventh equation". But before we do that, we shall see how the St. Venant's equations can be written as functions of tidal velocity and depth.

2.1.3 The 1-dimensional equations for depth and velocity

Intermezzo 2.1: Substitution of (2.15) and (2.16) in (2.1) yields:

$$A\frac{\partial U}{\partial t}+\left(2\alpha_S-\frac{1}{r_S}\right)U\frac{\partial Q}{\partial x}-\alpha_S U^2\frac{\partial A}{\partial x}+gA\frac{\partial\left(h+Z_b\right)}{\partial x}+gA\frac{h}{2\rho}\frac{\partial\rho}{\partial x}+gA\frac{U|U|}{C^2\,h}=0$$

Since $Q=Q(U,B,h)$, elaboration of $\partial Q/\partial x$ yields:

$$A\frac{\partial U}{\partial t}+\left(2\alpha_S-\frac{1}{r_S}\right)U\left(A\frac{\partial U}{\partial x}+U\frac{\partial A}{\partial x}\right)-\alpha_S U^2\frac{\partial A}{\partial x}+gA\frac{\partial\left(h+Z_b\right)}{\partial x}-gAI_r+gA\frac{U|U|}{C^2\,h}=0$$

where I_r is the water level residual slope resulting from the density gradient. Defined in this way, I_r has a positive value leading to a water level rise in upstream direction. Rearrangement yields:

$$\frac{\partial U}{\partial t}+\left(2\alpha_S-\frac{1}{r_S}\right)U\frac{\partial U}{\partial x}+\left(\alpha_S-\frac{1}{r_S}\right)\frac{U^2}{A}\frac{\partial A}{\partial x}+g\frac{\partial h}{\partial x}+g\frac{\partial Z_b}{\partial x}-gI_r+g\frac{U|U|}{C^2\,h}=0$$

After introduction of the Froude number, $\mathbf{F}{=}U/\sqrt{gh}$, this equation can be modified into:

$$\frac{\partial U}{\partial t}+\left(2\alpha_S-\frac{1}{r_S}\right)U\frac{\partial U}{\partial x}+\ \mathbf{F}^2\left(\alpha_S-\frac{1}{r_S}\right)g\frac{h}{A}\frac{\partial A}{\partial x}+g\frac{\partial h}{\partial x}+gI_b-gI_r+g\frac{U|U|}{C^2\,h}=0$$

where I_b is the bottom slope, which has a positive value if the estuary shallows in upstream direction. I_b and I_r therefore counteract if the estuary is shallowing in upstream direction.

In the following sections the only dependent variables used in the equations for conservation of momentum and mass of water are U, Z_b, h and B. The main state variables of interest are the flow parameters: the velocity (U) and the water level ($Z=Z_b+h$). In Fig. 2.2, the parameters used in the following derivations are shown in a definition sketch. To obtain the St. Venant equations expressed in these variables, the variables A and Q have to be eliminated from (2.1) and (2.2).

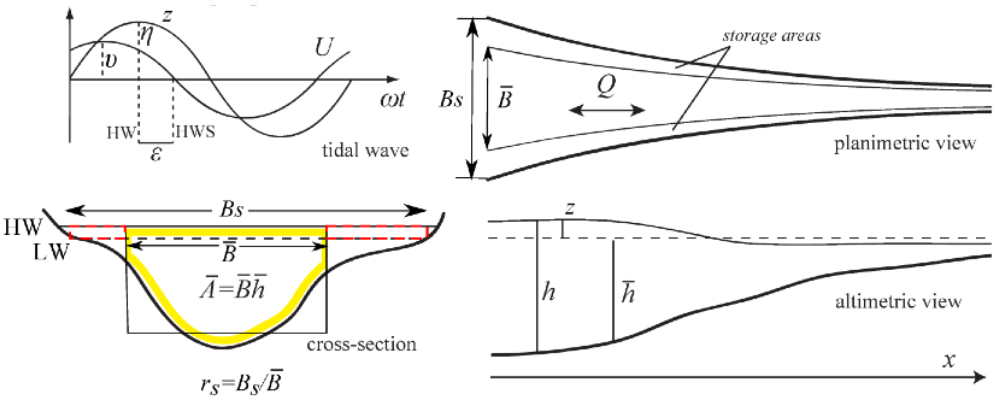

Figure 2.2: Sketch and notation.

The momentum equation

(2.1) is the 1-dimensional equation of conservation of momentum for water integrated over the cross-section. To eliminate the discharge Q and the cross-sectional area A from the equation, use is made of (2.2), (2.7) and (2.8). The following steps are taken:

$$\frac{\partial Q}{\partial t}=A\frac{\partial U}{\partial t}+U\frac{\partial A}{\partial t}=A\frac{\partial U}{\partial t}-\frac{U}{r_S}\frac{\partial Q}{\partial x}\tag{2.16}$$

$$\alpha_S \frac{\partial \left(Q^2/A\right)}{\partial x} = \alpha_S \left(2U\frac{\partial Q}{\partial x} - U^2\frac{\partial A}{\partial x}\right) \tag{2.17}$$

Substitution of (2.16) and (2.17) in (2.1) leads to (for details see Intermezzo 2.1):

$$\frac{\partial U}{\partial t} + \left(2\alpha_S - \frac{1}{r_S}\right)U\frac{\partial U}{\partial x} + \mathbf{F}^2\left(\alpha_S - \frac{1}{r_S}\right)g\frac{h}{A}\frac{\partial A}{\partial x} + g\frac{\partial h}{\partial x} + g\left(I_b - I_r\right) + g\frac{U|U|}{C^2\,h} = 0 \tag{2.18}$$

where $\mathbf{F}$ is the Froude number: $\mathbf{F}$=U/$\sqrt{gh}$ $= U/c_0$, c_0 is the celerity of propagation of a frictionless progressive wave, I_b is the bottom slope and I_r is the residual slope due to the density gradient. The Froude number in alluvial streams is smaller than unity and generally much smaller: in the order of 0.1. Knowing that $\alpha_S \approx 1$, $r_S \approx 1$ and that $\mathbf{F}^2 \ll 1$, the term containing $\mathbf{F}^2(\alpha_s - 1/r_S)$ is at least two orders of magnitude smaller than the fourth term and may be disregarded. Hence, (2.18) may be simplified into:

$$\frac{\partial U}{\partial t} + \left(2\alpha_S - \frac{1}{r_S}\right)U\frac{\partial U}{\partial x} + g\frac{\partial h}{\partial x} + g\left(I_b - I_r\right) + g\frac{U|U|}{C^2\,h} = 0 \tag{2.19}$$

Scaling the momentum equation

To assess the order of magnitude of the terms in (2.19) it is useful to define a set of dimensionless numbers:

$$U^* = \frac{U}{\upsilon}$$

$$h^* = \frac{h}{\overline{h}}$$

$$x^* = \frac{x}{\lambda_0}$$

$$t^* = \frac{t}{T}$$

where υ is the amplitude of the tidal velocity, T is the tidal period, $|lambda_0$ is the length of the tidal wave (note that $|lambda_0 = c_0 T$) and $\overline{h}$ is the tidal average depth. (2.19) then becomes:

$$\frac{\upsilon}{T}\frac{\partial U^*}{\partial t^*} + \left(2\alpha_S - \frac{1}{r_S}\right)\frac{\upsilon^2}{|lambda_0}U^*\frac{\partial U^*}{\partial x^*} + g\frac{\overline{h}}{|lambda_0}\frac{\partial h^*}{\partial x^*} + g\left(I_b - I_r\right) + g\frac{\upsilon^2}{\overline{h}}\frac{U^*|U^*|}{C^2\,h^*} = 0 \tag{2.20}$$

and with $|lambda_0 = c_0 T$, $c_0 = \sqrt{gh}$, and with the tidal Froude number $\mathbf{F} = \upsilon/c_0$:

$$\frac{\partial U^*}{\partial t^*} + \mathbf{F}U^*\frac{\partial U^*}{\partial x^*} + 2\left(\alpha_S - \frac{r_S + 1}{2r_S}\right)\mathbf{F}U^*\frac{\partial U^*}{\partial x^*} + \frac{1}{\mathbf{F}}\frac{\partial h^*}{\partial x^*} + \frac{gT}{\upsilon}\left(I_b - I_r\right) + \frac{gT\upsilon}{C^2\overline{h}}\frac{U^*|U^*|}{h^*} = 0 \tag{2.21}$$

All scaled variables in (2.21) now have an order of magnitude of 1 and the relative importance of the terms are determined by their dimensionless coefficients. Thus we can see from (2.21) that, since $\mathbf{F} << 1$, the second term (the advective term) is small compared to the fourth term (the depth gradient term). As a result, the advective term is often neglected. However, we are not going to do so. Although on average the second term is small, this may not be true at certain moments during the tidal cycle when the dimensionless velocity gradient can be larger than unity. Therefore we retain the term, unless there are specific reasons not to do so. What we can do, however, is neglect the third term representing the higher order effect of α_S and r_S on the advective term. Since in alluvial estuaries both α_S and r_S are close to unity, the third term is an order of magnitude smaller than the second term and, as a result, may be disregarded. We only disregard the higher order effect on the advection term, but not the term itself. Thus (2.19) becomes:

$$\frac{\partial U}{\partial t} + U\frac{\partial U}{\partial x} + g\frac{\partial h}{\partial x} + g\left(I_b - I_r\right) + g\frac{U|U|}{C^2\,h} = 0 \tag{2.22}$$

The conservation of mass equation
The conservation of mass equation for water, (2.2), is dealt with in a similar way by making use of (2.7) and (2.8):

$$r_S\left(h\frac{\partial B}{\partial t}+B\frac{\partial h}{\partial t}\right)+UB\frac{\partial h}{\partial x}+hB\frac{\partial U}{\partial x}+hU\frac{\partial B}{\partial x}=0 \tag{2.23}$$

In geometric terms, at a fixed location, the width B is a sole function of h. Hence the first term can be written as:

$$h\frac{\partial B}{\partial t}=h\frac{\mathrm{d}B}{\mathrm{d}h}\frac{\partial h}{\partial t} \tag{2.24}$$

If we assume a trapezoidal cross-sectional shape with a side-slope i, then (2.23) can be written as:

$$r_S\left(1+\frac{2h}{iB}\right)\frac{\partial h}{\partial t}+U\frac{\partial h}{\partial x}+h\frac{\partial U}{\partial x}+\frac{hU}{B}\frac{\partial B}{\partial x}=0 \tag{2.25}$$

In estuaries, the variation of the cross-sectional area over time is mainly caused by variation in the water level and much less by the variation in width ($B \gg h$). Consequently, the term h/iB is normally small with respect to unity. Therefore, in the first term of (2.21), the effect of side slope is disregarded, or considered part of the storage width ratio.

$$r_S\frac{\partial h}{\partial t}+U\frac{\partial h}{\partial x}+h\frac{\partial U}{\partial x}+\frac{hU}{B}\frac{\partial B}{\partial x}=0 \tag{2.26}$$

(2.26) is written in terms of the water depth. It is also possible to write the same equation in terms of the water level variation $Z = h - \bar{h}$ (Savenije et al., 2008). If, for a small amplitude wave, we assume that the depth convergence is small compared to the width convergence, then (2.26) can be written as:

$$r_S\frac{\partial Z}{\partial t}+U\frac{\partial Z}{\partial x}+h\frac{\partial U}{\partial x}+\frac{hU}{\bar{A}}\frac{\partial \bar{A}}{\partial x}=0 \tag{2.27}$$

which has the advantage that the depth convergence, important in estuaries where there is a bottom slope, is implicitly taken into account by the convergence of the tidal average cross-sectional area $\overline{A}$:

Assuming that values for C and r_S can be determined independently through measurements, (2.22) and (2.26) form a set of two equations with four unknowns: U, h, I_b and B (or $\overline{A}$ if we use (2.27)) from which A and Q have been eliminated. Therefore, if we want to solve these equations, we still require two geometric relations to determine the width (or the cross-sectional area) and the bottom slope. This is done in section 2.2.

2.1.4 The effect of density differences and tide

Until this point, the derivations made could apply to any channel of varying shape, whether it is a river, a canal, a lagoon or an estuary, as long as it can be described as a 1-dimensional system. Here, the typical hydraulic characteristics are presented for a tidal estuary with salt intrusion of the well-mixed type. These characteristics are twofold:

- The effect of density differences
- The tidal movement

The density effect

In the downstream part of an estuary, in the period of the year when the upstream fresh discharge is small, the tidal flows dominate the fresh water flow with the consequence that the water in that part of the estuary turns saline. If the fresh water discharge from upstream is small, the mixing in the estuary is generally good and the salinity decreases gradually from the estuary

mouth in an upstream direction. In the above equations, the residual slope I_r has been used to account for the effect of the density gradient $\partial\rho/\partial x$ on the momentum balance; see (2.22). In the Intermezzo 2.2, the expression for this density term is derived from the water pressure force, resulting in:

$$\frac{\partial U}{\partial t} + U\frac{\partial U}{\partial x} + g\frac{\partial h}{\partial x} + \frac{gh}{2\rho}\frac{\partial \rho}{\partial x} + g\frac{\partial Z_b}{\partial x} + g\frac{U|U|}{C^2\,h} = 0 \tag{2.28}$$

Intermezzo 2.2: The force per unit mass of water F exercised by the water pressure is defined as:

$$F(x,z) = -\frac{1}{\rho}\frac{\partial\left(\rho g(h - Z_b - z)\right)}{\partial x}$$

where z is the vertical ordinate. The force can be split up into three components (Van Os and Abraham, 1990):

$$F(x,z) = -g\frac{\partial\left(h + Z_b\right)}{\partial x} - \frac{gh}{2\rho}\frac{\partial\rho}{\partial x} - \frac{g}{\rho}\left(\frac{h}{2} + Z_b - z\right)\frac{\partial\rho}{\partial x}$$

The separation in three terms has been done in a way that only the third term is z-dependent. At the water surface, where $z = Z_b + h$, the third term is equally large as the second term, but of the opposed sign; at the bottom, the third term equals the second term. The second term is independent of z, because in a well-mixed estuary it is assumed that $\partial\rho/\partial x$ is not z-dependent. Integration over the depth from Z_b to $Z_b + h$ and division by the depth h yields the depth average water pressure force per unit mass:

$$F(x) = -g\frac{\partial\left(h + Z_b\right)}{\partial x} - \frac{gh}{2\rho}\frac{\partial\rho}{\partial x} - \frac{g}{\rho h}\frac{\partial\rho}{\partial x}\int_{Z_b}^{Z_b+h}(h/2 + Z_b - z)\mathrm{d}z$$

The first term represents the water level slope. The second term is a density driven force which points upstream (in a positive estuary). The last term equals zero, as - in this term - the pressure varies linearly from a downstream-directed pressure at the surface to an equal but opposed upstream-directed pressure at the bottom. Hence the second term is the effective upstream-directed pressure as a result of the density gradient. This does not mean that the third term is unimportant. In some cases it has a dominant effect on salinity intrusion through gravitational circulation. As a result of a net upstream water pressure near the bottom, and a net downstream water pressure near the surface (see Fig. 2.3), there exists a time-average upstream flow near the bottom and a net downstream flow near the surface.

Compared to the other terms in the cross-sectional average conservation of momentum equation, the density term is small. Scaling of the terms in (2.28) leads to the conclusion that the ratio of the third and fourth term is of the order $h\Delta\rho/(2\eta\rho)$, where η is the tidal amplitude and $\Delta\rho$ is the density difference of ocean and river water. In open sea estuaries, this ratio is about (1025-1000)/2000 $h/\eta = 0.0125\ h/\eta$. Even though h/η is supposed to be less than unity, this is still a small number. However, the third term (the water slope) alternates (with the tide) between a positive and negative value, whereas the fourth term always exercises a pressure in an upstream direction (in a normal, "positive", estuary). This pressure is counteracted by a residual water level slope amounting to 1.25% of the estuary depth over the salt intrusion length L - the distance from the mouth to the point where the estuary water is fresh. If, for example, the estuary depth is 8 m, then the water level rise amounts to 0.1 m over the salt intrusion length L. In formula, this yields the following expression for the residual slope I_r:

$$I_r \approx \frac{\Delta\rho}{2\rho}\frac{\overline{h}}{L} = 0.0125\frac{\overline{h}}{L} \tag{2.29}$$

The same relation is obtained by equating the shadowed areas in Fig. 2.3: $\rho h\Delta h{=}\Delta\rho h^2/2$. A water level rise is required to balance the hydrostatic forces. The two forces F_1 and F_2 that make equilibrium in the horizontal plane per unit width over the salt intrusion length L are:

$$F_1 = \frac{1}{2}\rho_1 g h_1^2 \tag{2.30}$$

and

$$F_2 = \frac{1}{2}\rho_2 g h_2^2 \tag{2.31}$$

where the subscripts 1 and 2 indicate the upstream and downstream ends of the salt intrusion length L. Since $(\rho_2 = \rho + \Delta\rho) > (\rho_1 = \rho)$, there can only be equilibrium if $h_1 > h_2$. However,

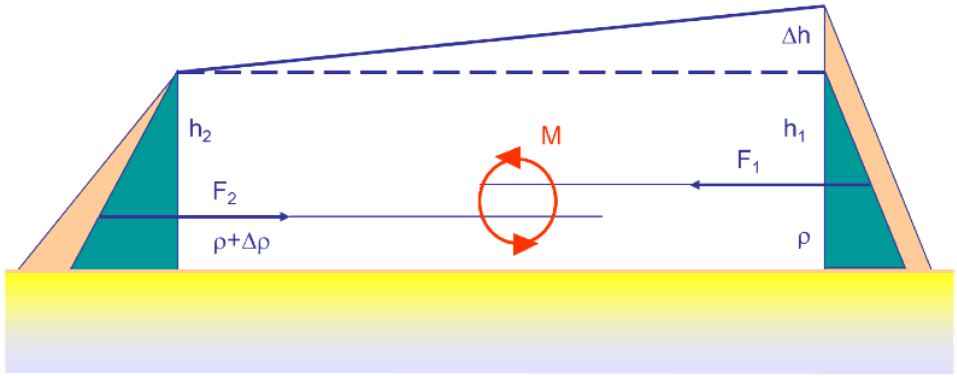

Figure 2.3: Resultant hydrostatic forces driving vertical net circulation.

the two forces, although equal and opposite, exert a momentum that drives the gravitational circulation described in Intermezzo 2.2. Since the arm of the momentum is $\Delta h/3$, the moment M, exercised per unit volume of water per unit width (L h), equals:

$$M = \frac{\frac{1}{3}\frac{h}{2\rho}\frac{\partial \rho}{\partial x} L \frac{1}{2}\rho g h^2}{Lh} = \frac{1}{12}\frac{\partial \rho}{\partial x} g h^2 \tag{2.32}$$

This moment drives the vertical mixing process, called gravitational circulation, which is further discussed in section 4.2.

Tidal characteristics

A second characteristic of the lower part of an estuary is that both the water level fluctuations and the velocity of the water are tidally dominated and that U and h vary according to periodic functions. In the mouth of an estuary the water level rises and falls periodically. This cyclic rise and fall produces a tidal wave of primarily 1-dimensional character which travels up the estuary. The period T of a tidal wave is generally so long that the wavelength λ_0=Tc_0 (c_0 is the celerity of a wave in an ideal estuary (see section 2.2.2)) is usually much larger than the length of the estuary considered. In 'short' estuaries, where a standing wave occurs, the estuary length is typically $1/4\lambda_0$. In 'long' coastal plain estuaries the estuary length is longer, around $1/2$ λ_0, but generally less than λ_0 (see Table 2.2). To show that exceptions prove the rule, the tidal influence in the Gambia Estuary reaches a distance of 500 km, which is larger than the tidal wave length. These long tidal waves have the important characteristic that the associated displacement of the water is essentially horizontal and parallel to the estuary banks (Ippen and Harleman, 1966).

Tidal waves in alluvial estuaries generally have an amplitude which is small compared to the depth. The tidal excursion E, the distance which a water particle travels between low water slack (LWS) and high water slack (HWS), is generally substantially larger than the estuary width but small in relation to the estuary length. If this is not the case, then the estuary is so wide that it loses its 1 dimensional character and should rather be considered as a lagoon, a bay or a part of the estuary mouth. This brings us to the following inequalities:

$$\eta < h \ll B < E \ll \lambda_0 \tag{2.33}$$

The volume of water entering the estuary between LWS and HWS is known as the flood volume P_t, which in the literature is often referred to as the tidal prism:

$$P_t = \int_{LWS}^{HWS} Q(0,t)\mathrm{d}t \approx A_0 E_0 \tag{2.34}$$

The product of the tidal excursion E_0 and the cross-sectional area A_0 at the estuary mouth appears to be a good approximation for the tidal prism (see section 2.3). For the analysis of

mixing of fresh water and saline water the ratio between the amount of fresh water and salt water entering the estuary is important. This ratio, in the Dutch literature referred to as Canter Cremers' estuary number N, is defined as:

$$N = \frac{Q_f T}{P_t} \tag{2.35}$$

where Q_f is the fresh river discharge which enters the estuary during the tidal period T.

A more significant estuary number is the Estuarine Richardson number N_R (Fischer et al., 1979) which represents the balance between, on the one hand, the potential energy per tidal period needed for mixing against buoyancy (or the potential energy gained by making fresh water saline): $E_m{=}\Delta h \rho g Q_f T{=}\ 0.5\ \Delta \rho h g Q_f T$, and, on the other hand, the kinetic energy per tidal period supplied by the tidal current for realising the mixing $E_t = 0.5 \rho A_0 E_0 \upsilon_0^2$, where υ_0 is the amplitude of the tidal flow velocity at the estuary mouth:

$$N_R = \frac{E_m}{E_t} = \frac{\Delta\rho}{\rho}\frac{ghQ_f T}{A_0 E_0 \upsilon_0^2} = \frac{\Delta\rho}{\rho}\frac{ghQ_f T}{P_t \upsilon_0^2} \tag{2.36}$$

Hence $N_R{=}N/F_d$, where F_d is the densimetric Froude number defined as $F_d{=}(\rho/\Delta\rho)\upsilon_0^2/(gh)$. Fischer et al. (1979) wrote: "If N_R is very large, we expect the estuary to be strongly stratified and the flow to be dominated by density currents. If N_R is very small, we expect the estuary to be well mixed, and we might be able to neglect density effects. Observations of real estuaries suggest that, very approximately, the transition from a well mixed to a strongly stratified estuary occurs in the range $0.08{<}\ N_R\ {<}0.8$ ".

Harleman (1974) used a similar estuary number, which is the reciprocal value of N_R. Prandle (1985) has a number similar to Harleman & Thatcher, which he also based on energy considerations, but used the ratio of the energy dissipated by friction over the salt intrusion length $E_d = 4/(3\pi)(g/C_2)\rho\upsilon^3 LBT$ to the potential energy E_m gained by mixing. This yields Prandle's estuary number N_P:

$$N_P = \frac{8}{3}\frac{g}{C^2}\frac{L}{h}\frac{1}{N_R} \tag{2.37}$$

In addition to the Estuarine Richardson number, it accounts for friction and the salt intrusion length to depth ratio. In particular, the inclusion of the salt intrusion length makes this number a strong indicator for stratification. Both a large L/h ratio and a small value of N_R correspond with a well-mixed estuary; so a large value of N_P corresponds with a well-mixed estuary and a small value implies stratification. However, because both the friction and the intrusion length are difficult to determine a priori, this is not a very useful estuary number to predict stratification.

The tidal wave

With respect to their wave celerity c, three types of tidal waves can be distinguished:

1. Standing wave
2. Progressive wave
3. Mixed wave

The wave celerity is the speed with which the tidal wave propagates into the estuary. The wave celerity is also called the "phase speed", indicating how the phase of the wave changes along the estuary. It is measured by observing the time that, for instance, high water (HW) or low water (LW) takes to cover a certain distance along the estuary.

For a **standing wave**, HW (or LW) is reached everywhere at the same time in the estuary, indicating an 'infinite' wave celerity. A purely standing wave requires either a short estuary with a length equal to the resonance length $\lambda_0/4$, or a semi-enclosed body (a bay) which acts as a storage basin. Since an alluvial estuary gradually changes into a river, a standing wave seldom occurs in a fully developed alluvial estuary. They are however common in fjords and rias. A standing wave can also occur if a closing structure blocks the progression of the wave, but then it occurs only in the vicinity of the structure since the reflected wave, moving in downstream

direction, quickly loses energy due to friction and widening of the channel (see also Jay, 1991). A standing wave reaches extreme water levels simultaneously along the estuary. Consequently, the wave celerity c tends to infinity (as extreme water levels occur everywhere at the same time, it appears as if the celerity is infinitely large). In addition, HWS coincides with HW, and LWS coincides with LW. The phase lag ϕ between the fluctuation of the water level Z and the flow velocity U is $\pi/2$ (see Fig. 2.4). In Fig. 2.4, the positive direction of flow is in the upstream direction.

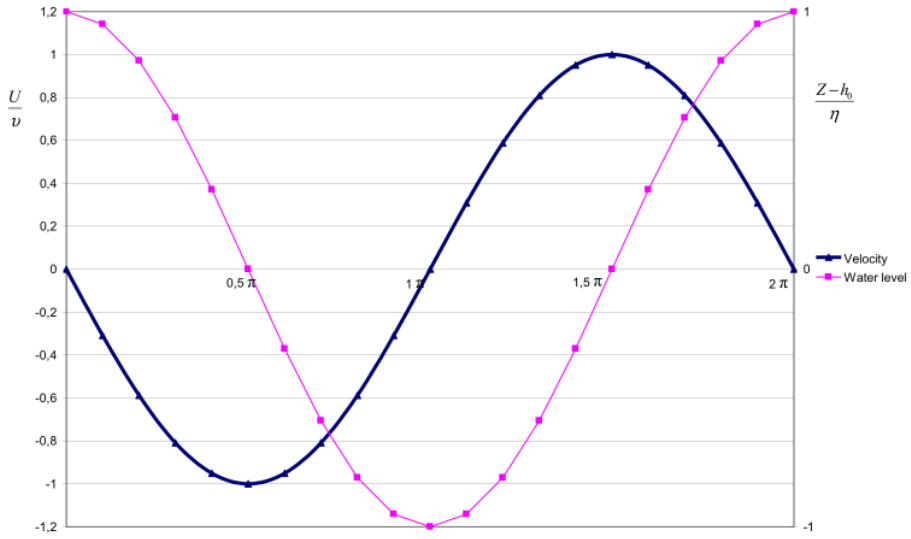

Figure 2.4: A standing wave.

A purely **progressive wave** only occurs in a frictionless channel of constant cross-section and infinite length. Progressive waves occur in rivers or in deep man-made (shipping) channels of constant cross-section. Alluvial estuaries clearly do not belong to this category. A progressive wave has no phase difference between water level and stream velocity - they are exactly in phase (i.e. high water occurs at the same time as the maximum flow velocity). The phase lag ϕ between water level and flow velocity is zero and the wave celerity $c = c_0 = \sqrt{gh}$ (see Fig. 2.5).

Alluvial estuaries experience tidal wave of the **mixed** type, with a phase lag ϕ between 0 and $\pi/2$ (see Fig. 2.6). This means that in an alluvial estuary HWS occurs after HW and before mean tidal level; and LWS occurs after LW and before mean tidal level. The determining factor for this phase lag is the shape (the convergence and depth) of the estuary.

Several researchers limited their study of tidal wave propagation to channels of constant cross-section of infinite length (e.g. Ippen, 1966b; Van Rijn, 1990). In some cases, this led to incorrect conclusions, which proved persistent. Van Rijn (1990) states that bottom friction and river discharge are responsible for the phase lag between horizontal movement (current velocities) and vertical movement (water levels). However, the effect of the river discharge, as we have seen, is not a phase lag, but a vertical shift of the velocity-time graph, which causes HWS to occur earlier and LWS to occur later (see Fig 1.5). The second cause mentioned (friction), only has an indirect and often minor effect on the phase lag. Later in this chapter we see that the phase lag is closely linked to the wave celerity and the convergence of the banks (see Eq. (2.85). The wave celerity is indeed related to friction, but the sensitivity to friction is very small if the wave is amplified or if the tidal range is constant (ideal estuary). The most important factor determining the phase lag is the shape of the estuary, which, depending on the convergence of the banks, causes the tidal wave to gain energy per unit width as it travels upstream. The relationship for the phase lag as a function of bank convergence and wave celerity is derived in section 2.3.

Here we introduce the phase lag ε between HW and HWS (see Fig. 2.6), or between LW and LWS, which is related to ϕ as: $\varepsilon + \phi = \pi/2$. This implies that cos($\varepsilon$)=sin($\phi$) and sin($\varepsilon$)=cos($\phi$).

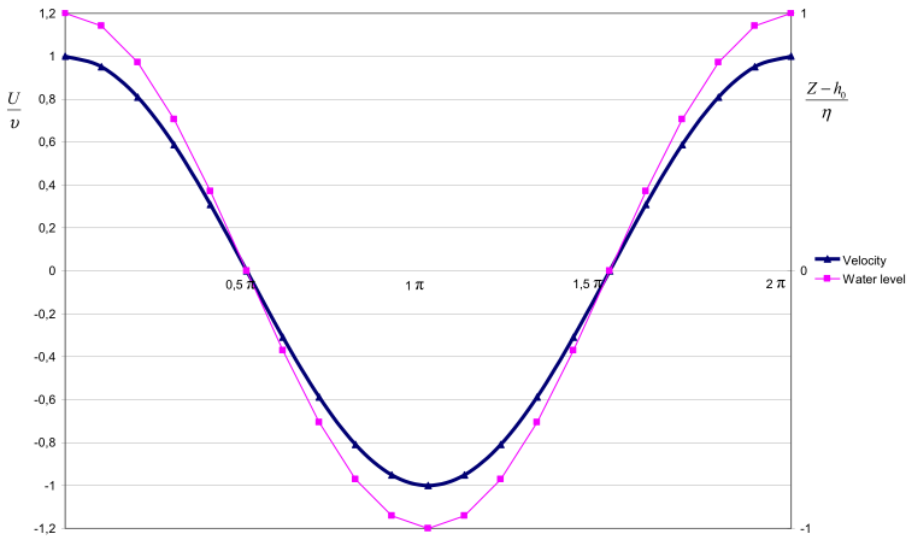

Figure 2.5: A progressive wave.

The phase lag ε, although disregarded by many authors, is a very important parameter in tidal hydraulics, characterising the hydraulics of an estuary. It is closely related to estuary shape. The phase lag is primarily a function of the ratio between bank convergence and tidal wave length (see section 2.3). In alluvial estuaries, this phase lag is always between zero and $\pi/2$, but typically in the order of 0.3, resulting in a time lag between HW and HWS of around 30-45 minutes for a semi-diurnal tide. We also define the dimensionless Wave-type number: N_E=sin(ε)=cos(ϕ), which defines the wave-type in an estuary. The Wave-type number is always between zero and unity. If it is close to unity the wave is a progressive wave and the estuary is a frictionless prismatic channel. If it is close to zero, the wave is a standing wave and the estuary is either short or looks like a tidal embayment. Because estuary shape is so important in tidal hydraulics, the next section will elaborate on the topography of alluvial estuaries.

2.2 The shape of alluvial estuaries

2.2.1 Classification of estuary shape

Until recently, most researchers limited their research on tidal hydraulics and salt intrusion to prismatic (constant width) channels. As we have seen, this is a serious shortcoming, which moreover misses out on the mathematical opportunity that exponentially-shaped water bodies have to offer. Throughout this book, we use exponential functions to describe the longitudinal variation of the cross-section and width. The rate of convergence is determined by a length scale: the convergence length. This schematisation also allows for prismatic channels. A channel with constant cross-section is a special type of exponential estuary with an infinitely long convergence length.

While researchers probably used prismatic channels for mathematical convenience, there were also practical reasons. Many tests were done on the basis of laboratory experiments, and laboratory flumes are generally prismatic. Moreover, several real-life problems that early researchers had to analyse concerned man-made shipping access channels, such as the Rotterdam Waterway, which has a constant cross-section. A vast amount of literature on salt water intrusion deals with prismatic channels. Until 1992, virtually all formulas that existed to determine the salt intrusion length had been derived for prismatic channels. As shown in Chapter 4, these equations perform very poorly in natural estuaries.

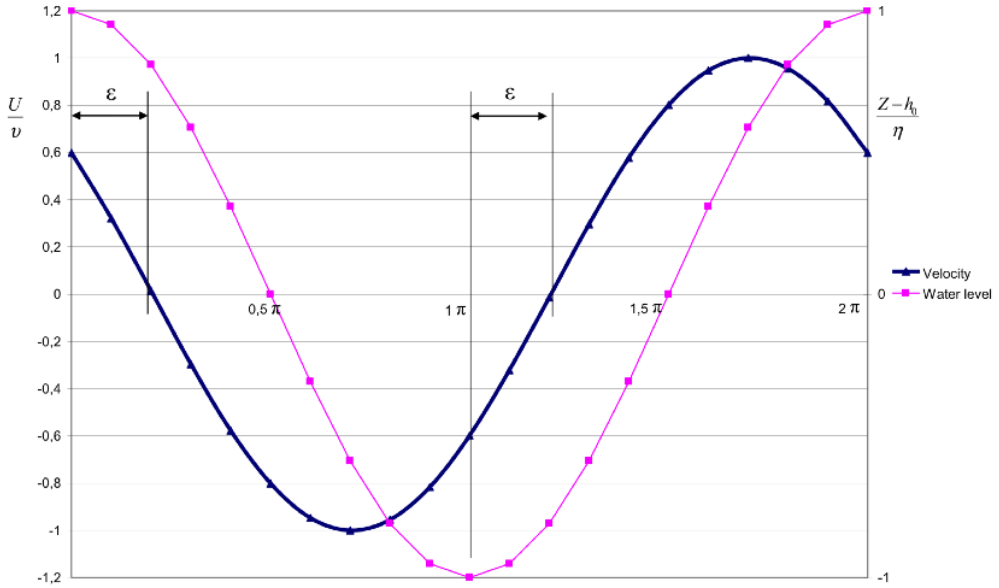

Figure 2.6: A wave of the mixed type showing the phase lag between HW and HWS, and between LW and LWS.

Only a few estuaries can be adequately described by a prismatic channel. Therefore, throughout this book, we describe the cross-sectional area as an exponential function of the distance along the estuary axis:

$$A = A_0 \exp\left(-\frac{x}{a}\right) \tag{2.38}$$

where the x-axis point in the upstream direction and A_0 is the cross-sectional area at x=0. The parameter a is defined as the cross-sectional convergence length (a is the distance from the mouth at which the tangent through the point (0, A_0) intersects with the x-axis). Similarly, the assumption that the width varies exponentially yields the equation:

$$B = B_0 \exp\left(-\frac{x}{b}\right) \tag{2.39}$$

where B_0 is the width at the estuary mouth and the coefficient b is the width convergence length. Combination of (2.38) with (2.39) leads to an expression for the depth:

$$h = h_0 \exp\left(\frac{x\,(a-b)}{ab}\right) \tag{2.40}$$

It follows from (2.40) that, if a is larger than b, the depth increases exponentially; if a is less than b, the depth decreases exponentially. If a is much larger than b, an unrealistic situation of exponentially increasing depth is obtained, which in natural channels never occurs. As we shall see further on, in real estuaries the convergence lengths do not differ much. In the special case where the two convergence lengths are equal, a=b, the depth is constant along the estuary: h=h_0. This shape corresponds with an ideal estuary, for which a mathematical justification is provided in section 2.2.2.

For illustration purposes, Fig. 2.7 shows a sketch of two estuaries: The Schelde in Belgium and The Netherlands, and the Incomati in Mozambique. Figs. 2.8 and 2.9 show the geometry of these estuaries of which measurements of A, B, and h are available, plotted on a semi-log scale. Further examples of a variety of estuaries are provided in the annexed topographical data base. In the Incomati, the individual marks of the depth are based on scattered point observations where soundings were made during salt measurements. They do not reflect the average depth.

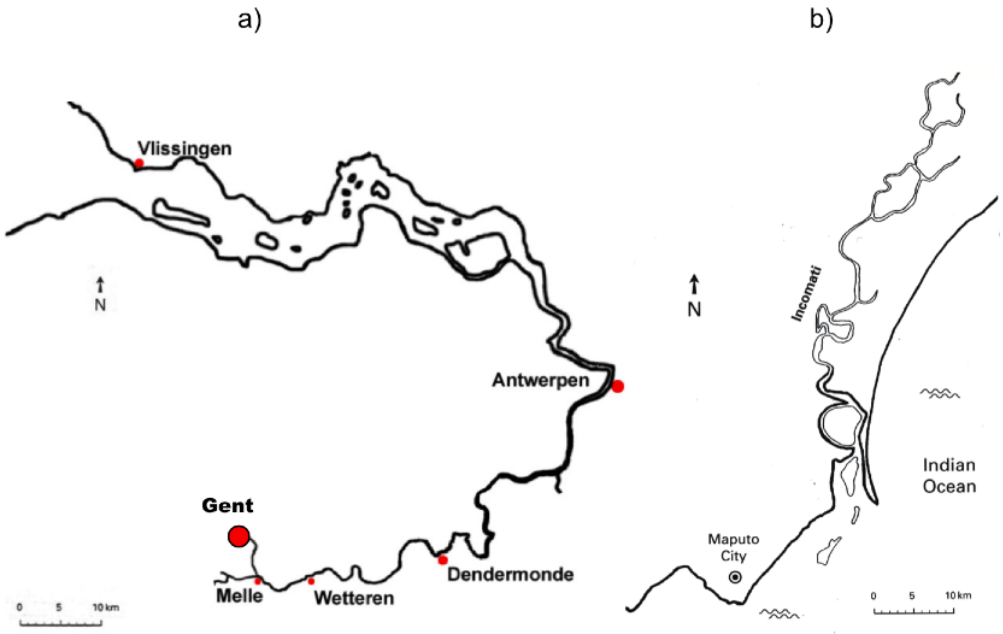

Figure 2.7: Sketch of the Schelde (a) and Incomati (b) estuaries.

The observations of the cross-sectional area are the result of a complete echo-sounding. It can be clearly seen that the trends in cross-sectional area and the width conform very neatly to (2.38) and (2.39). The geometry of the Incomati has an inflection point 14 km from its mouth, while the Schelde becomes more shallow at 110 km when several tributaries branch off. In spite of these irregularities, the geometry can be described very well by (2.38)-(2.40). Also, it appears that a and b are almost, or exactly equal. The question is: what are the factors determining estuary shape?

Factors affecting estuary shape

The shape of estuaries depends on several factors such as:

Tidal movement -both the vertical and horizontal displacements. The main variable determining the downstream boundary condition for tidal movement is the tidal range H, a good indicator for the strength of the tidal movement.

River floods The morphologic activity of the river can strongly influence the estuary shape; if river floods are large then the estuary gets a more riverine character and a more prismatic shape. A good indicator for a river flood is the bankfull discharge Q_b.

Wave action The shape of the mouth of an estuary can depend strongly on wave action. The existence and shape of spits, bars or barrier islands depends on the predominant direction of wave attack and on the magnitude of the waves.

Storm action Storms can change the configuration of the estuary mouth considerably. The permanence of changes inflicted by a storm depends on the amount of sediment supplied by both the littoral zone and the river itself.

Sediment properties Estuaries with coarse sediments generally have a strong riverine character and tend to be more prismatic. Estuaries with very fine sediments generally have mud flats, have a marine character and are more funnel shaped. Clearly the occurrence of coarse riverine sediments is linked to the occurrence of large river floods.

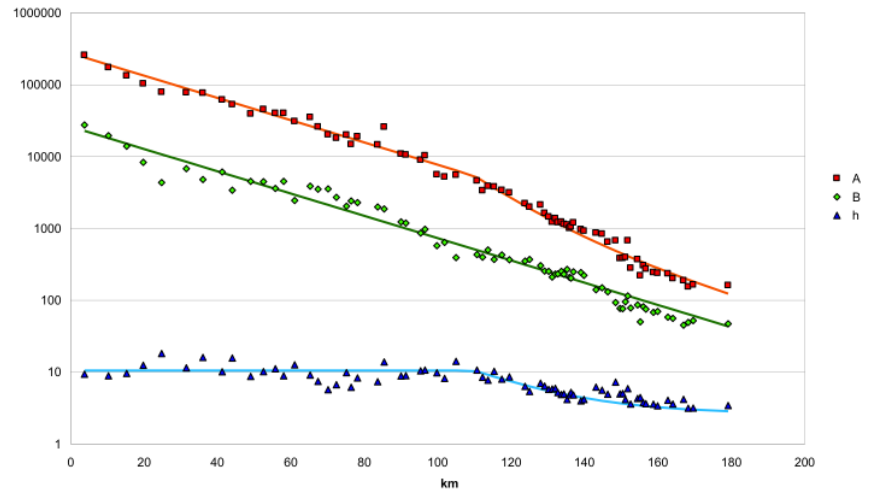

Figure 2.8: Semi-logarithmic plot of the geometry of the Schelde estuary: A is the cross-sectional area in m^2, B is the width in m, h is the cross-sectional average depth in m.

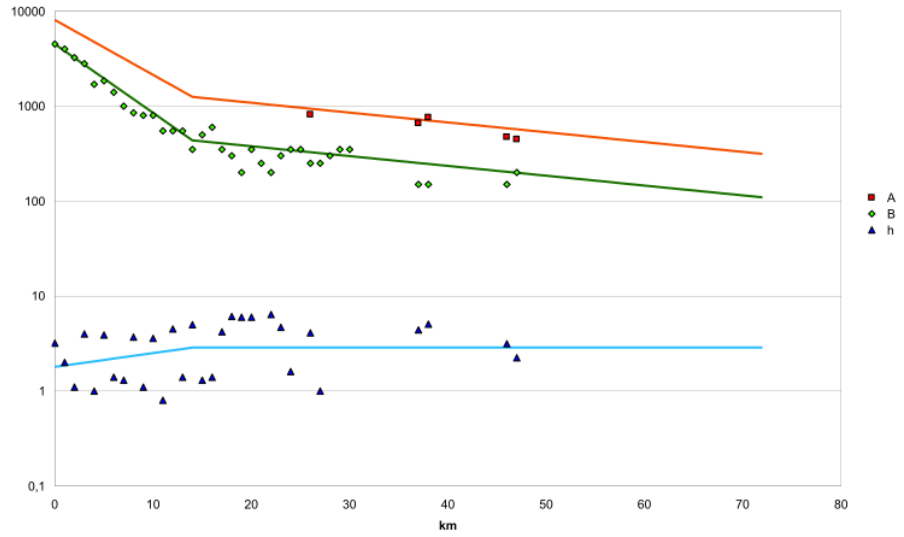

Figure 2.9: Semi-logarithmic plot of the geometry of the Incomati estuary: A is the crosssectional area in m^2, B is the width in m, h is the cross-sectional average depth in m.

Of these factors, the tidal range is the easiest variable to determine. Moreover, Hayes (1975) (who followed the classification proposed by Davies (1964)) stated that: "the tidal range had the broadest effect in determining large-scale differences in morphology of sand accumulation" and that a classification of estuaries could best be based on the tidal range.

Pethick (1984), although recognising the importance of upland flows, also followed the classification of Davies (1964) based on the tidal range, which is summarised as micro-, meso- and macro-tidal estuaries:

Micro-tidal estuaries

When the tidal range is less than 2 m, the estuarine processes are dominated by both the upland discharge and the wave and storm action from the sea. The sediments carried by the upland discharge sustain the formation of a delta, whereas the waves produce spits, barrier islands and a bar-built estuary. The convergence of the tidal channel is small (the convergence lengths a and b are long).

Meso-tidal estuaries

Estuaries with a tidal range between 2 and 4 m experience such strong tidal action that a marine delta can no longer be shaped. Instead, two shallow reaches are formed upstream and downstream of the estuary mouth, and are called the flood-tide and the ebb-tide delta respectively.

Macro-tidal estuaries

In macro-tidal estuaries the tidal range is over 4 m. The tide produces strong tidal currents which may extend for hundreds of kilometres inland. They do not possess ebb-tide or flood-tide deltas but have a pronounced funnel shape with a strong convergence (the convergence lengths are short).

Although this classification has the advantage of simplicity and is probably adequate for a physical geographer (it allows the classification of the mouth of the estuary), it is not sufficiently accurate for the engineer interested in estuarine morphology.

Estuaries, according to Dyer (1973), are sediment traps. The sediment supplied by the river floods is deposited in the estuary as soon as the channel becomes wider and the flow velocities decrease. In addition, the gravitational circulation sketched in Fig. 2.3 continuously supplies fine marine sediments which move upstream near the estuary bottom to be eventually deposited at the limit of the salt intrusion. Only the river floods are able to flush out the sediments which have accumulated over the year.

Wright et al. (1975), who studied the morphology of Western Australia's Ord estuary, a typical macro-tidal estuary, formulated it thus: "In a channel of uniform cross-section, the upstream increase in tidal asymmetry and accompanying flood-dominated bed load transport would, in the absence of significant riverine flow, lead to an upstream accumulation of sediment to clog the channel; only during a river flood would this sediment be flushed". Hence, a substantial river flow is required to maintain a channel with a long convergence length.

In a prismatic channel, the tidal flow velocities increase in a downstream direction. Consequently, erosion dominates at the downstream end of such an estuary. If the river discharge and its sediment load are small, this erosion is not replenished by riverine sediments. In such a case, the estuary expands to form a funnel shape. If, on the other hand, the upland discharge and sediment load are large, then the channel is only stable if the convergence length is long. If the convergence length was short, the channel would soon fill up with riverine sediments. Consequently, a high upland discharge induces a channel with a long convergence length. A large tidal range, however, induces a channel with a short convergence length, in agreement with the classification of Pethick (1984). Hence it is the proportion between these two actions which determines estuary shape.

Table 2.1 presents a number of characteristics related to estuary shape with a qualification of how they behave in channels that are predominantly funnel shaped or prismatic. If the pro-

portion of upland flood discharge to tidal range is small, the estuary has a predominantly funnel shape; if the proportion is large the estuary is predominantly prismatic. A better classification

Table 2.1: Characteristics of funnel-shaped and prismatic estuaries.

Shape	Bay shape	Funnel shape	Prismatic shape
Character	Marine	Estuarine	Riverine
Convergence length (a)	0	Short	∞
HW-HWS phase lag (ε)	0	$0 < \varepsilon < \pi/2$	$\pi/2$
Wave type	Standing	Mixed	Progressive
Salt intrusion	Saline	Well-mixed	Stratified
$Q_b T/P_t$	0	Small	Large

would be based on the proportion of the river flood discharge to the tidal range; or, to make it dimensionless, the ratio of a river flood volume entering the estuary during a tidal period to the flood volume P_t, the volume of ocean water entering the estuary during a tidal period. This ratio is a Canter Cremers number for an upland flood discharge. The upland discharge to be used in the classification is the characteristic annual flood discharge. In regime theory, the flood discharge that determines the shape of an alluvial channel is the bankfull discharge Q_b. For the purpose of classification this discharge is a good selection, not because it is better than any other criterion, but because it is objective and relatively easy to determine. Riggs (1974), making use of investigations by Leopold et al. (1964), stated that bankfull stage has a return period of 1.5 years. Personal observations confirm this statement, which may be explained by the fact that natural river banks need regular replenishment with bed material for the river to maintain its course.

If a satisfactory relation can be found between $Q_b T/P_t$ and estuary shape, then that would be a better means for classification than the one proposed by Davies (1964) and Pethick (1984).

2.2.2 Assumptions about the shape of alluvial estuary in coastal plains

The assumptions of an ideal estuary

During the many boat surveys carried out by the author during the 1980s in Mozambican and Asian estuaries (Limpopo, Pungue, Maputo, Incomati, Pungue, Lalang, Tha Chin, Chao Phya), it appeared that these estuaries, although quite different in hydrology and geometry, had certain geometric characteristics in common.

First, it became clear that, contrary to expectation, the mean depth of the estuaries did not significantly change when moving upstream from the estuary mouth. Although the depth sometimes fluctuated strongly from place to place (deep in bends and shallow in a straight stretch), there did not appear to be an upward or downward bottom slope. This indicated that the depth of flow h was more or less constant with distance.

A second phenomenon observed was that the amplitude of the tidal flow velocity v (i.e. the maximum flow velocity) did not vary much between the mouth and a point near the limit of the salt intrusion, 50 to 100 km upstream. Even more remarkably, this velocity did not differ much from estuary to estuary, regardless of whether the tidal range was large (such as in the Pungue) or small (as in the Limpopo). In both estuaries the amplitude of the flow velocity was in the order of 1 m/s during spring tide. The absence of a gradient in the velocity amplitude implies a constant tidal excursion E along the estuary axis. The fact that the peak velocity is similar in different estuaries is the result of similar physical characteristics of alluvial estuaries (discussed earlier in section 2.1.1) having an almost direct proportionality between Q and A (e.g. Bruun and Gerritsen (1960)).

In addition, although most estuaries experience some degree of tidal damping or amplification, it appeared that the gradient of the tidal range H was modest or, in other words, that the tidal

range remained fairly constant along these estuaries, at least in the tidal dominated part of the estuary.

It should be noted that these are all coastal plain estuaries unaffected by steep topography. In estuaries where the coastal plain is short, with a steep underlying topography, another type of estuary occurs, which we shall describe in section 2.2.3.

The experiences gained during these surveys formed the inspiration to develop a salt intrusion model (Savenije, 1986) based on the following assumptions regarding the shape and hydraulics of an alluvial estuary:

$$\frac{\partial h}{\partial x} \approx 0 \tag{2.41}$$

$$\frac{1}{B}\frac{\partial B}{\partial x} = -\frac{1}{b} \tag{2.42}$$

$$\frac{\partial H}{\partial x} \approx 0 \tag{2.43}$$

$$\frac{\partial E}{\partial x} \approx 0 \tag{2.44}$$

It should be observed that these are all partial derivatives with respect to the distance along the estuary axis. The width and the depth vary over the tidal period (intra-tidal) and the tidal range H, and the tidal excursion E vary from day-to-day as the tidal wave changes from neap tide to spring tide (inter-tidal). As a result, H and E are functions of time. However, for a certain tidal wave that travels up an estuary they are merely functions of space.

(2.41) and (2.42) agree with (2.38) -(2.40) if $a = b$. These equations correspond to an "ideal estuary" as described theoretically by Pillsbury (1939, 1956), which in addition to the above geometric conditions requires a constant Chézy coefficient. Apparently a funnel shaped estuary, with the width obeying an exponential function, is best suited to preserve a constant tidal range and, therefore, to maintain a constant amount of wave energy per unit volume of water. The contracting width tends to increase the tidal range, whereas the friction tends to reduce the tidal range. Dyer (1973) formulates it thus: "As an estuary narrows towards the head, the tidal range tends to increase upstream because of the convergence, but decrease because of friction". In an ideal estuary (according to Langbein, 1963) the convergence of the estuary banks is just sufficient to balance the damping of the tidal range due to friction.

A constant amount of energy per unit volume of water implies that energy dissipation by friction is balanced by energy gained through convergence. Since in an exponentially shaped estuary the latter is constant, the amount of energy spent per unit volume of water is also constant. The latter is a condition for morphological stability that is also used to describe river channel networks. Rodriguez-Iturbe & Rinaldo (1997; p267) use the criterion of "equal energy expenditure per unit volume" to describe and simulate natural topographies. An ideal estuary is the coastal version of a self-organised river network, the difference lying mainly in the forcing boundary condition. An estuary is forced by the tidal variation at the downstream boundary, while a river is forced by the river discharge at the upstream boundary. A brief theoretical justification of an ideal estuary follows.

Theoretical justification for the ideal estuary

It can be shown that the (2.41)-(2.44) are a consistent solution of the general St.Venant equations (as formulated in (2.22) and (2.26)), under the following assumptions.

1. Since the Froude number is small, the non-linear convergence term of (2.22) is much smaller than $g\partial h/\partial x$, and may therefore be disregarded.

2. The tidal amplitude to depth ratio is small and the resistance term $U|U|/(C^2h)$ of (2.22) may therefore be linearised.

3. The velocity of the fresh water discharge u_f is negligible when compared to the tidal velocity amplitude v.

4. In the downstream part of the estuary, the mean tidal water level Z_0 is independent of x (implying that the residual slope I_r in (2.22) can be disregarded as well).
5. The storage width ratio in (2.26) is close to unity.
6. The water movement (both velocity and water level) can be described by a combination of harmonics.
7. The damping of both the tidal range and the amplitude of the tidal velocity is small. Hence the relative variation of H and E with x is small or negligible.

The first six assumptions are not very restrictive and are, in fact, often made in alluvial estuaries (although we shall use less restrictive assumptions in section 2.3 and Chapter 3). The last assumption (#7) assumes that the tidal amplitude η and the tidal velocity amplitude v are both near constant. This assumption may not by made in estuaries that are forced by the topography to be short (see section 2.2.3). In short estuaries $a \neq b$. In coastal plain estuaries, however, particularly in the downstream marine-dominated area, the tidal range and the velocity amplitude are not significantly damped or amplified. In the following we prove that the assumption of an undamped (small amplitude) tidal wave leads to the topography of an ideal estuary.

Assumptions (1) and (2) imply that use can be made of the linearized St. Venant equations:

$$\frac{\partial U}{\partial t} + g\frac{\partial Z}{\partial x} + R_L U = 0 \tag{2.45}$$

$$B\frac{\partial Z}{\partial t} + Bh\frac{\partial U}{\partial x} + U\frac{\partial Bh}{\partial x} = 0 \tag{2.46}$$

(2.45) follows from (2.22), where $Z = h + Z_b$ is the water level and R_L is Lorentz's[1] linearised friction factor:

$$R_L = \frac{8}{3\pi}\frac{g}{C^2}\frac{v}{\bar{h}} \tag{2.47}$$

In (2.46) a substitution has been made of $\partial Z/\partial t = \partial h/\partial t$, since the bottom slope does not vary at the time-scale considered.

If we take into account assumptions (3)-(7), then the velocity U and the water level Z can be written as undamped functions of the variable ξ (Savenije (1986), after a personal communication by Kranenburg, 1985) with constant amplitudes η and v:

$$U = v\Phi\left(\xi - \varepsilon\right) \tag{2.48}$$

$$Z = \eta\Psi\left(\xi\right) + \bar{h} \tag{2.49}$$

$$\xi = \omega t - \phi\left(x\right) + \xi_0 \tag{2.50}$$

where ε is the phase lag between HW and HWS, ω is the angle velocity ($\omega = 2\pi/T$) and $\phi(x)$ is the phase shift resulting from wave propagation. The functions Φ and Ψ are periodic functions with unit amplitude. Substitution of (2.48), (2.49) and (2.50) in (2.45) and (2.46), and some rearrangement yields:

$$v\frac{\mathrm{d}\Phi}{\mathrm{d}\xi}\frac{\partial \xi}{\partial t} + g\eta\frac{\mathrm{d}\Psi}{\mathrm{d}\xi}\frac{\partial \xi}{\partial x} + R_L v\Phi = 0 \tag{2.51}$$

$$vBh\frac{\mathrm{d}\Phi}{\mathrm{d}\xi}\frac{\partial \xi}{\partial x} + B\eta\frac{\mathrm{d}\Psi}{\mathrm{d}\xi}\frac{\partial \xi}{\partial t} + \frac{\mathrm{d}Bh}{\mathrm{d}x}v\Phi = 0 \tag{2.52}$$

Further elaboration yields:

$$\omega\left(v\frac{\mathrm{d}\Phi}{\mathrm{d}\xi}\right) - g\frac{\mathrm{d}\phi}{\mathrm{d}x}\left(\eta\frac{\mathrm{d}\Psi}{\mathrm{d}\xi}\right) + R_L\left(v\Phi\right) = 0 \tag{2.53}$$

[1] While the Nobel prize winner H.A. Lorentz is not normally associated with hydraulic engineering, he pioneered the numerical approach in hydraulic engineering after his retirement, when he took up the job of predicting the effect of the closure of the Zuiderzee (the main inland sea of The Netherlands) on the tidal variations in the semi-enclosed Waddenzee.

$$-Bh\frac{\mathrm{d}\phi}{\mathrm{d}x}\left(v\frac{\mathrm{d}\Phi}{\mathrm{d}\xi}\right)+B\omega\left(\eta\frac{\mathrm{d}\Psi}{\mathrm{d}\xi}\right)+\frac{\mathrm{d}Bh}{\mathrm{d}x}\left(v\Phi\right)=0 \tag{2.54}$$

The solution only suffices if Φ and Ψ are solely dependent on ξ and there is therefore a proportionality between the coefficients of the terms of each equation (all coefficients are constant or proportional to each other):

$$\omega \propto g\frac{\mathrm{d}\phi}{\mathrm{d}x} \propto R_L \tag{2.55}$$

and:

$$Bh\frac{\mathrm{d}\phi}{\mathrm{d}x} \propto B\omega \propto \frac{\mathrm{d}Bh}{\mathrm{d}x} \tag{2.56}$$

As a result of this proportionality, R_L is a constant, $\mathrm{d}\phi/\mathrm{d}x$ is a constant (ϕ=$\omega x/c$), $h = h_0$ is a constant (confirming (2.41)), and B=B_0 $\exp(-x/b)$ (confirming (2.42)). The condition that $\mathrm{d}\phi/\mathrm{d}x$ is a constant implies that an observer travelling with the wave celerity (x=ct and ξ= ξ_0) sees no change in both U and Z: U=$U(\xi_0)$ and Z=$Z(\xi_0)$.

Moreover, the function Ψ is given by the downstream boundary condition. This implies that there are two equations with only one unknown function Φ. Hence the equations are dependent and there should be proportionality between the equations. Making use of the results from (2.56) yields:

$$\frac{\omega c}{-h\omega}=\frac{-g\omega}{\omega c}=\frac{-R_L b}{h} \tag{2.57}$$

This leads to the classical equation for the tidal wave propagation $c^2 = gh$ and also to the relation between convergence and friction: $b = c/R_L$. The first equation is the same as the classical equation for the frictionless tidal wave in a prismatic channel, which apparently also applies to an ideal estuary, but which does not apply in estuaries where there is some degree of tidal damping or amplification. The second relation is the condition for an ideal estuary, where the energy gained by convergence is balanced by the energy lost through friction. These two equations are special cases of the general solution derived from the non-linearised equations, applicable to damped or amplified tidal waves, and presented in section 3.2.

Assumption #7, expressed in (2.43) and (2.44) , leads through the use of the linearised St. Venant equations to (2.41) and (2.42) , under the condition that $b = c/R_L$. Or, in other words, assumption #7 is only justified if the friction and the depth are constant with x, the width varies exponentially and the friction is compensated by convergence. Section 3.2 shows, also for the non-linear St. Venant equations, that if friction and convergence balance out ($b = c/R_L$), there is indeed no tidal damping and c=$\sqrt{gh}$.

Several other authors have made use of similar geometric conditions as in (2.41)-(2.44). For example: Ketchum (1951) derived a theory based on a horizontal estuary bed; Abbott (1960) used a horizontal bed for the Thames; Hunt (1964) used a constant depth and an exponentially varying width for the Thames; Harleman (1966), in Ippen (1966a), used a constant depth and an exponential width variation for the Delaware.

McDowell and O'Connor (1977), elaborating on the concept of ideal estuaries developed by Pillsbury (1939), stated that since an ideal estuary implies that a unique relationship exists between maximum tidal discharges and channel cross-sectional area at all points along the estuary, this unique relationship might also exist between different estuaries of similar bed material. They analysed the relation between the size of tidal inlets and the maximum tidal flow in much the same way as Bretting (1958) and Bruun and Gerritsen (1960) did.

In the following empirical assessment of the applicability of the shape of an ideal estuary, it will be demonstrated that, although the assumptions required for an ideal estuary do not fully apply in most estuaries, the geometry of coastal plain estuaries generally can be described by (2.41) and (2.42) and that, even if there is some bottom slope, (2.38) always applies.

Empirical illustrations

We have already seen two examples of how real-life alluvial estuaries correspond with the shape of an ideal estuary. In Table 2.2, more examples of estuaries are given. The topographical data base provides more details of more estuaries. Table 2.2 provides values for a number of typical parameters that characterise alluvial estuaries. Besides data on shape (B, A and h),

there is information on the normal spring tidal range (H), the classical wave celerity (c_0), the tidal amplification/damping (δ_H) and the tidal intrusion length (L_T)

Table 2.2: Characteristic values of alluvial estuaries.

Estuaries	A_o (m^2)	A'_o (m^2)	B_o (m)	h (m)	a (km)	b (km)	H (m)	c_o (m/s)	δ_H ($10^{-6}m^{-1}$)	λ_0 (km)	L_T (km)	λ_0/L_T
Mae Klong	1400		250	5.2	102	155	2.0	7.1	-4.2	317	120	0.38
Limpopo	1710	1340	222	7.0	50	18	1.1	8.3	0.0	368	150	0.41
Lalang	2550		371	10.6	217	96	2.7	10.2	-1.0	453	200	0.44
Tha Chin	3000	1380	3600	5.3	87	87	2.6	3.0	-9.4	133	120	0.37
Sinnamary	3500	1210	2100	3.8	39	13	2.9	6.1	-5	271		
Chao Phya	4300		600	7.2	109	109	2.5	7.0	-3.6	311	120	0.32
Ord	7900		3200	4.0	22.1	15.2	5.9	6.3	0.0	278	65	0.23
Incomati	8100	1750	4500	2.9	42	42	1.4	3.6	-13.0	160	100	0.42
Pungue	28000		6512	3.8	21	21	6.7	6.1	-8.5	271	120	0.44
Maputo	40000	6460	9000	3.6	16	16	3.4	5.9	1.0	264	100	0.38
Thames	58500		7480	7.1	23	23	4.3	8.3	2.3	371	110	0.30
Corantijn	69000	34600	30000	6.5	64	48	2.3	8.0	-1.7	355	120	0.34
Gambia	84400	27200	9687	8.7	121	121	1.2	9.2	-1.0	410	500	1.22
Schelde	150000		15207	10.0	26	28	3.7	13.0	3.8	577	200	0.45
Delaware	255000		37655	6.6	41	42	1.5	8.0	1.7	357	200	0.56

In some estuaries the longitudinal profile is split in two parts (mostly when there is a clear trumpet shape near to the estuary mouth). In those cases the logarithmic relation for A or B consists of two branches. For these estuaries a value of A'_0 is presented, which corresponds to the value that would have been obtained if the upstream branch were extended towards the estuary mouth. The observed rate of damping δ_H, is defined as:

$$\delta_H = \frac{1}{H}\frac{\partial H}{\partial x} = \frac{1}{\eta}\frac{\partial \eta}{\partial x} \tag{2.58}$$

Since the tidal range is about twice the tidal amplitude, the damping of the tidal range is the same as the damping of the tidal amplitude. Some estuaries with a positive value of δ_H are amplified (e.g. the Thames, Delaware and Schelde), whereas the ones with negative values are damped (e.g. the Incomati, Pungue and Tha Chin). Remarkably, many have hardly any damping (the Limpopo, the Lalang, the Maputo, the Gambia). These are close to ideal estuaries.

2.2.3 Assumptions about estuary shape in short estuaries

Many alluvial estuaries are not coastal plain estuaries, but are forced by the underlying topography to be short. This occurs when the slope of the land is too steep for a long coastal plain to develop. There are many of these estuaries in Great Britain, Australia and the USA, although these countries also have several coastal plain estuaries (e.g. Thames, Delaware, Mississippi). Mountainous islands generally have short estuaries as well (such as in New Zealand). Prandle (2003), for instance, mainly describes this type of estuary and therefore uses a different geometry than that presented in this book. The paper by Wright et al. (1973) is one of the few that specifically deals with short estuaries and also compares them to a coastal plain estuary. The interesting thing is that Wright et al. compare two branches of the same estuary system, the Ord and King rivers, which both are part of the Cambridge Gulf in the north of Western Australia. Another example of such a system is the Banyuasin-Lalang system on Sumatra, Indonesia. Here the Banyasin is a short estuary and its main tributary, the Lalang, a coastal plain estuary. The Ord is a typical short estuary that fits the classification of Wright et al. (1973), namely:

1 a strong funnel shape with a cross-sectional area that obeys (2.38);

2 the length of the tidal intrusion is finite, forced by the topography, and equal to $\lambda/4$;

3 a standing wave occurs, whereby the amplitude of the wave obeys:

$$\eta(x) = \eta_0 \cos\left(2\pi \frac{x}{\lambda_0}\right) \tag{2.59}$$

where η_0 is the tidal amplitude at the estuary mouth.

4 there is no tidal damping or amplification on top of this, since there is a balance between friction and convergence.

5 both the depth and the width reduce exponentially

The fourth item is motivated by the entropy principle, whereby there is uniform dissipation of energy, as discussed in the previous section for coastal plain estuaries. To prove the validity of (2.59), Wright et al. applied Green's law and field observations (However, Green (1837) assumed frictionless flow and a progressive wave).

Several short estuaries, with a relatively small river discharge in relation to the tidal flood volume, appear to fit in this category. It will be shown in section 3.1 that the assumption of a purely standing wave is at par with an un-amplified tidal wave. In fact, a completely standing wave implies zero friction, thereby introducing tidal amplification. The stronger the funnel shape, the greater the amplification. An amplified wave also amplifies the velocity amplitude. However, the velocity amplitude at the head of the estuary should be zero, and at its maximum near the mouth of the estuary. So short estuaries with a standing wave are forced to a length of $\lambda_0/4$ (or $3\lambda_0/4$), with a velocity node at the head of the estuary.

The condition of zero friction to produce a purely standing wave is not very workable in reality. There will always be friction and so the wave will not be a purely standing wave. This is also observed by Wright et al. (1973), who noticed that, although the wave (seemingly) travels very fast at almost infinite speed (HW and LW occurring everywhere at the same time and slack occurring almost at the same time as HW and LW), there is a discernible time lag between the occurrence of HW along the Ord estuary, and even more so at LW. As a result the wave does not completely behave as a standing wave (although ε is close to zero) - there is friction, and there is a modest bottom level gradient (the convergence length of the depth is almost twice as large as the width convergence length, making the width convergence twice as pronounced as the shallowing).

Therefore, although the theory is a bit more complex than described by Wright et al. (1973), their schematisation is quite workable. We also see here that the exponential shape used for coastal plain estuaries, particularly (2.38), may also be applied to short estuaries.

2.3 Relating tide to shape

2.3.1 Why look for relations between tide and shape?

Although ideal estuaries have a simple topography determined by: B_0, b and $\overline{h}$, the latter parameter is not always easy to determine. The width at the estuary mouth and the width convergence length can be readily measured from a map or aerial photograph, but the tidal average depth is much more complicated. With an echo sounder or a drop-weight, we can sound the depth at different locations. Determining the cross-sectional average depth along an estuary however is a lot of work. And there are other important tidal parameters that are not easy to measure, such as the tidal excursion E and the flood volume P_t.

To determine the estuary depth, an extensive hydrometric survey is required of cross-sectional areas at a number of locations. For reasonable accuracy, a minimum of 10 cross-sections over the salt intrusion length is required. The tidal excursion can be measured directly by using floats, but such a method is cumbersome. It requires a full tidal cycle and has a relatively low accuracy due to wind effects and the non-uniform velocity distribution over the cross-section. Also, floats tend to get stuck in the estuary bends. The flood volume is very difficult to measure directly, requiring an extensive discharge measurement at the mouth of the estuary during a full tidal cycle. So let us see if we can derive analytical equations for this purpose, on the basis of the geometry of an ideal estuary.

2.3.2 Intuitive derivation

Let us start with the flood volume P_t, which is the integral of the tidal discharge between LWS and HWS at x=0:

$$P_t = \int_{LWS}^{HWS} Q\,(0,t)\,\mathrm{d}t \tag{2.60}$$

where $Q(0,t)$ is the discharge at the estuary mouth. Since this integral is difficult to determine

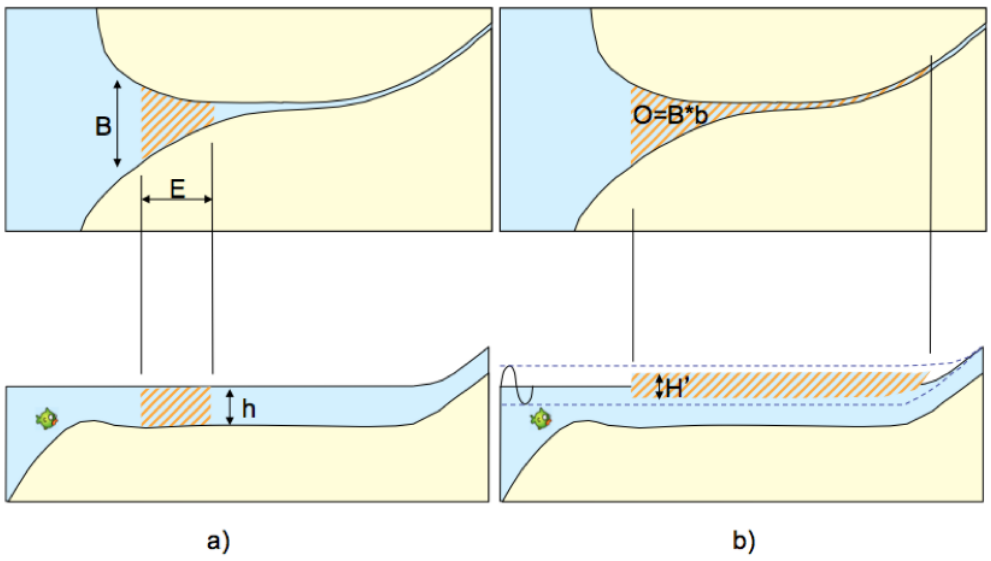

Figure 2.10: Definition sketch for the dial flood volume: (a) as the product of B, h, and E; and (b) as the product of the surface area O and H', the tidal range between slacks.

through direct measurement, it is approximated in two ways. The first is by computing the flood volume as the tidal prism enclosed between the envelopes of HWS and LWS; the second, by equating it to the product of the tidal excursion with the cross-sectional area of the estuary mouth (see Fig. 2.10). The first approach yields:

$$P_t \approx \int_0^{\infty} H' B \mathrm{d}x \tag{2.61}$$

where $H'(x)$ is the range between HWS and LWS as a function of the distance - i.e. the difference between the envelopes of the water levels occurring at HWS and LWS along the estuary. Here it is assumed that these levels are reached almost instantaneously along the estuary, implying that the wave length is large compared to the length of the estuary. In addition (for this derivation only) it is assumed that the tidal range is damped exponentially:

$$H = H_0 \exp\left(\delta_H x\right) \tag{2.62}$$

This is the integral of (2.58) for a constant rate of amplification/damping, where H_0 is the tidal range at the estuary mouth and δ_H is the longitudinal rate of amplification/damping of the tidal range (if δ_H <0, the wave is damped). The relation between H and H' can be seen simply from Fig. 2.6 and reads:

$$H' = H\cos(\varepsilon) \tag{2.63}$$

where ε is the phase lag between HW and HWS, which is considered constant along the estuary axis. Hence (2.61) becomes:

$$P_t \approx H_0 B_0 \cos(\varepsilon) \int_0^{\infty} \exp\left[\left(\delta_H - \frac{1}{b}\right) x\right] \mathrm{d}x = \frac{H_0 B_0 b}{1-\delta_H b}\cos(\varepsilon) = \frac{H_0 O}{1-\delta_H b}\cos(\varepsilon) \tag{2.64}$$

where O is the surface area of the estuary. This is the product of the surface area O and H', taking into account tidal damping. If the wave is damped, then the flood volume is smaller; if there is amplification than the flood volume is larger. There is an additional error made by assuming that the surface area does not vary significantly between HWS and LWS. In view of the many assumptions made, this approach does not seem very accurate. However, Savenije (1992a, 1993a) using simulations of a hydraulic model, showed that the equation is accurate for a wide range of estuary shapes (depth ranging between 4 and 10 m; convergence length ranging between 10 and 100 km; tidal range ranging between 1.2 and 6 m).

The second approach yields:

$$P_t = \int_{LWS}^{HWS} A_0 U(0,t) \mathrm{d}t \approx A_0 E_0 \tag{2.65}$$

where E_0 is the tidal excursion at the estuary mouth. The assumptions made here are: 1) that the cross-sectional area does not vary significantly with time; and 2) that the integral over time of the Eulerian velocity U between low water slack (LWS) and high water slack (HWS) is approximately equal to the tidal excursion E, whereas E is the integral between LWS and HWS of the Lagrangean velocity V of a moving water particle. The first assumption is acceptable in deep estuaries, the second is only acceptable if the Froude number is small. To support this equation, Savenije (1992b, 1993a) demonstrated with numerical model simulations that it is indeed accurate as long as the tidal range to depth ratio is smaller than unity, implying that the Froude number is small.

Equating (2.64) and (2.65) yields:

$$\frac{H_0 b}{(1-\delta_H b)} \cos(\varepsilon) = h_0 E_0 \tag{2.66}$$

Essentially, this equation is the conservation of mass equation, where we have equated the volume change in the estuary between HWS and LWS to the amount of sea water entering the estuary during the same period.

Although a lot of assumptions were made in deriving this intuitive equation, it is still a very interesting equation, providing a relationship between two parameters that we find difficult to measure directly: h_0, and E_0. In the following, we derive an expression for the tidal excursion on the basis of a Lagrangean analysis, where we follow the water particle as it flows between LWS and HWS. Subsequently this Lagrangean analysis is also an adequate tool to develop (2.66) more strictly.

2.3.3 Lagrangean analysis of a water particle

In a Lagrangean approach, the reference frame moves with the velocity of the water particle. The following equations apply:

$$V = \frac{\mathrm{d}x}{\mathrm{d}t} \tag{2.67}$$

$$S = \int_0^t V \mathrm{d}t \tag{2.68}$$

and hence:

$$x = x_0 + S \tag{2.69}$$

where $V = V(x,t)$ is the velocity of the moving particle and $S(x,t)$ is the distance travelled by the particle from a starting point x_0. Analysis of model simulations showed that the velocity variation in a Lagrangean reference frame was surprisingly regular and that it could be described as a simple harmonic (Savenije, 1992a). This is not so surprising. The forces working on the (moving) water particle are cyclic, hence the reaction is also cyclic; much like a person on a swing. Although the harmonic assumption in the Lagrangean reference frame makes complete sense, most authors apply harmonic functions in the Eulerian reference frame. However, this

causes an unnecessary error, associated to the Stokes drift (see section 2.4). While the non-linearity of the friction generates higher harmonics and distortion of the tidal wave, this is the same in both the Lagrangean and Eulerian reference frame.

If we now assume that the water particle moves according to a simple harmonic, starting at x_0 at LWS ($t = 0$), then the velocity can be described by:

$$V(x,t) = v(x)\sin(\omega t) \tag{2.70}$$

$$\omega = \frac{2\pi}{T} \tag{2.71}$$

where ω is the harmonic constant. For the time being it is assumed that the influence of the fresh water discharge on the tidal velocities in the saline area is negligible. If there is a substantial fresh water discharge, then this has to be taken into account. We shall analyse this effect in sections 2.5 and 3.3.

In (2.70), the effect of damping is present through the x-dependency of v. In contrast to what was assumed in the previous section, the damping of the velocity amplitude is not necessarily exponential, meaning that the damping rate of the tidal velocity δ_U is not necessarily constant with x. Similar to the definition of the damping/amplification of the tidal range in (2.58), the damping/amplification of the tidal velocity amplitude is defined as:

$$\delta_U = \frac{1}{v}\frac{\partial v}{\partial x} \tag{2.72}$$

where δ_U is the longitudinal relative rate of amplification of the velocity amplitude (which is negative in the case of damping). In the following derivations this damping is not neglected, but considered to be small over the distance travelled by the water particle ($|\delta_U E| \ll 1$).

The distance travelled by the water particle is found by substitution of (2.70) in (2.68) (for details see Intermezzo 2.3):

$$S = \frac{v}{\omega}\left(1 - \cos(\omega t)\right) \tag{2.73}$$

The tidal excursion E (the distance travelled between LWS and HWS) is obtained by substitution of $t = T/2$:

$$E = S(T/2) = \frac{vT}{\pi} = \frac{2v}{\omega} \tag{2.74}$$

which is a useful equation for the calculation of the tidal excursion. We saw in Figure 2.1 that the tidal velocity amplitude at spring tide in alluvial estuaries is remarkably similar all over the world: about 1 m/s. This offers the opportunity to estimate the order of magnitude of the tidal excursion even in ungauged situations. Consequently, for a semi-diurnal tide, the tidal excursion is about 14 km near spring tide. Savenije (1992b, 1993a) confronted with a wide range of model simulations, demonstrated that this equation underestimates the real value by 8%.

Intermezzo 2.3: The integral of the Lagrangean velocity is the distance travelled S:

$$S = \int_0^t v\sin(\omega t)\mathrm{d}t = -\int_0^t \frac{v}{\omega}\mathrm{d}\cos(\omega t) = -\frac{v}{\omega}\cos(\omega t)\Big|_0^t + \frac{1}{\omega}\int_0^t \cos(\omega t)\mathrm{d}v$$

Since $\mathrm{d}v = \partial v/\partial x\,(V\mathrm{d}t) = v\delta_U V\mathrm{d}t = v^2\delta_U \sin(\omega t)\mathrm{d}t$, the second integral reads:

$$\frac{1}{\omega}\int_0^t \cos(\omega t)\mathrm{d}v = \frac{v^2\delta_U}{\omega}\int_0^t \cos(\omega t)\sin(\omega t)\mathrm{d}t = -\frac{v^2\delta_U}{4\omega^2}\cos(2\omega t)\Big|_0^t$$

Hence:

$$S = \frac{v}{\omega}\left(1 - \cos(\omega t) + \frac{v\delta_U}{4\omega}(1 - \cos(2\omega t))\right) = \frac{v}{\omega}\left(1 - \cos(\omega t) + \frac{E\delta_U}{8}(1 - \cos(2\omega t))\right)$$

Since $|\delta E| \ll 1$ in alluvial estuaries, the latter term may be disregarded. Similarly, differentiation of V with respect to t yields:

$$\frac{dV}{dt} = \omega v\cos(\omega t) + \frac{\mathrm{d}v}{\mathrm{d}t}\sin(\omega t)$$

The last term is further elaborated, realising that $\partial v/\partial t$=0:

$$\frac{\mathrm{d}v}{\mathrm{d}t}\sin(\omega t) = \frac{\partial v}{\partial x}V\sin(\omega t) = \delta_U v^2 \sin^2(\omega t) = \omega v \frac{E\delta_U}{2}\sin^2(\omega t)$$

Hence:

$$\frac{\mathrm{d}V}{\mathrm{d}t} = \omega v \left(\cos(\omega t) + \frac{E\delta_U}{2}\sin^2(\omega t)\right) \approx \omega v \cos(\omega t)$$

as the term containing $\delta_U E/2$ may be disregarded. Note that in these derivations δ_U may still be a function of x.

If we assume that the Lagrangean velocity of a water particle is a pure sinus, then the harmonics are distorted in the Eulerian reference frame. Through the introduction of the argument ξ (similar to (2.50)), the above equations can be transformed into a Eulerian reference frame:

$$\xi = \omega t - \frac{\omega\,(x - x_0 - S)}{c} \tag{2.75}$$

yielding:

$$U = v\,\sin\,(\xi) \tag{2.76}$$

where $U = U(x,t)$ is the velocity of flow at a certain location at a certain time and c is the tidal wave celerity. If we move with the water particle, then $x = x_0 + S$, $\xi = \omega t$ and $U = V$. At $x = x_0 + E$, a time lag of E/c occurs between HWS of the moving particle and HWS observed at $x = x_0$ (see Fig. 2.11). This time lag, which is only observed in the Eulerian reference frame, is not a time lag the water particle experiences. It is purely an artefact of Eulerian referencing where we continuously 'look' at a different water particle. This phenomenon is related to the Stokes drift discussed in section 2.4. Using (2.75) and (2.76), the Eulerian continuity equation

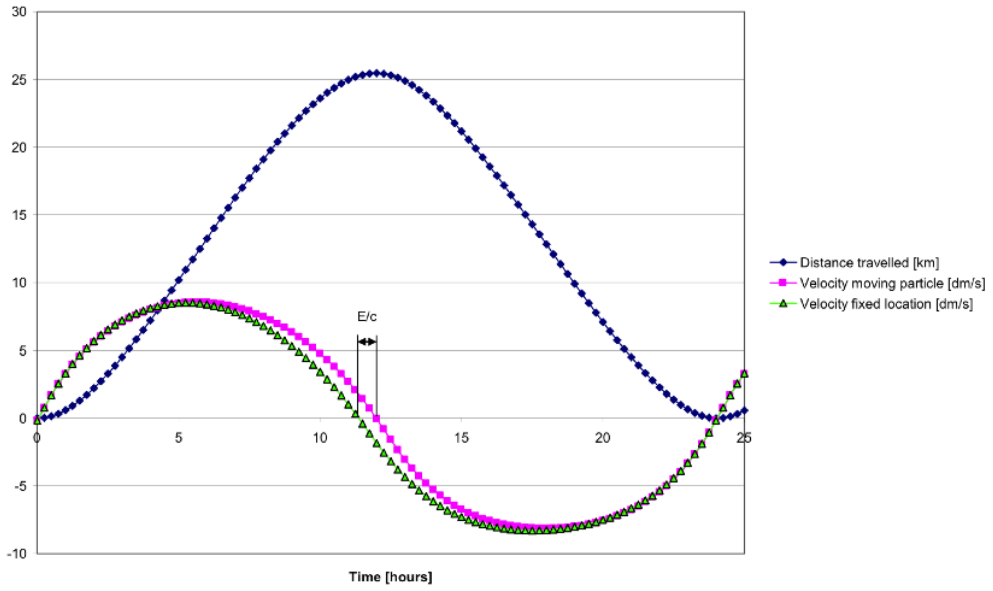

Figure 2.11: Velocity (dm/s) and distance traveled (km) by a water particle.

for one-dimensional flow, (2.26), can be transformed to the Lagrangean reference frame, where it can be solved analytically. Combination of (2.26) with (2.39) yields:

$$r_S \frac{\partial h}{\partial t} + U\frac{\partial h}{\partial x} + h\frac{\partial U}{\partial x} - \frac{hU}{b} = 0 \tag{2.77}$$

Partial differentiation of (2.76) with respect to x for a moving particle where $x{=}x_0{+}S$, and combination of the result with (2.72) and (2.75), yields a Lagrangean expression for the partial derivative of U with respect to x:

$$\frac{\partial U}{\partial x} = -\frac{1}{c}\frac{\mathrm{d}V}{\mathrm{d}t} + \delta_U V \tag{2.78}$$

the details of which are explained in Intermezzo 2.4:

Intermezzo 2.4:

$$\frac{\partial U}{\partial x} = \frac{\partial v}{\partial x}\sin\xi + v\cos\xi\frac{\partial \xi}{\partial x} = \delta_U V + \frac{1}{\omega}\frac{\mathrm{d}V}{\mathrm{d}t}\frac{\partial \xi}{\partial x}$$

$$\frac{\partial \xi}{\partial x} = -\frac{\omega}{c}\left(1 - \frac{\partial S}{\partial x}\right) = -\frac{\omega}{c}\left(1 - \frac{\partial v}{\partial x}\frac{1}{\omega}\left(1-\cos(\omega t)\right)\right) = -\frac{\omega}{c}\left(1-\delta_U S\right)$$

Substitution of $\partial\xi/\partial x$ and $\mathrm{d}V/\mathrm{d}t$ (from Intermezzo 2.3) in the equation for $\partial U/\partial x$ yields:

$$\frac{\partial U}{\partial x} = \delta_U V - \frac{1}{c}\frac{\mathrm{d}V}{\mathrm{d}t}(1-\delta_U S)$$

(2.78) is obtained under the assumption that $|\delta_U S| < |\delta_U E| \ll 1$. In section 2.5 this term is retained to assess its impact, but we also see that the effect of this damping term is negligible (an order Froude smaller than the first damping term). Note that in this derivation δ may still be a function of x.

For higher order computations it maybe useful to also have the second spatial derivative of U. This reads under the same condition that $|\delta_U S| < |\delta_U E| \ll 1$:

$$\frac{\partial^2 U}{\partial x^2} = 2\frac{\partial v}{\partial x}\cos\xi\frac{\partial \xi}{\partial x} - v\sin\xi\left(\frac{\partial \xi}{\partial x}\right)^2 = -2\frac{\delta_U}{c}\frac{\mathrm{d}V}{\mathrm{d}t} - \frac{\omega^2}{c^2}V$$

Moreover, the variation of the water depth with time for a moving water particle is defined by:

$$\frac{\mathrm{d}h}{\mathrm{d}t} = \frac{\partial h}{\partial t} + V\frac{\partial h}{\partial x} \tag{2.79}$$

Substitution of (2.78) and (2.79) into (2.77) yields the continuity equation for a moving volume of water ($U = V$) in a Lagrangean reference frame. We can further assume that: 1) r_S is close to unity; and 2) the Froude number is small. As a result, the second term of (2.79) is much smaller than the first. Therefore the introduction of the storage width ratio in the second term of the water balance equation creates only a third order error. Hence:

$$r_S\frac{\mathrm{d}h}{\mathrm{d}t} = +\frac{h}{c}\frac{\mathrm{d}V}{\mathrm{d}t} + hV\frac{(1-\delta_U b)}{b} \tag{2.80}$$

Elaboration of (2.80) yields:

$$r_S\frac{\mathrm{d}h}{h} = \frac{(1-\delta_U b)}{b}\mathrm{d}x + \frac{1}{c}\mathrm{d}V \tag{2.81}$$

The first term of the right hand member is a conservation of mass term leading to depth gain as a result of bank convergence and deceleration due to damping, which the moving particle experiences. The second term is a conservation of mass term that a drives water level variation due to the velocity variation. Integration between LWS ($t{=}0$) and t yields:

$$r_S\ln(h) = r_S\ln(h_{LWS}) + S\frac{(1-\delta_U b)}{b} + \frac{V}{c} \tag{2.82}$$

When plotted against the distance travelled, this is an exponential function of an inclined ellipse (see Fig. 2.12). The drawn curve through the heart of the inclined ellipse represents the first term on the right hand side. If damping is small and $b \to \infty$ this term is zero (as in a prismatic channel with no damping) and the inclination of the ellipse disappears. In this case, the velocity and water depth of the moving particle are in phase, creating an undamped progressive wave. This is in agreement with other analytical methods where a progressive wave occurs in a channel of constant cross-section, of infinite length, and without friction.

In the derivation of (2.82) it appears that the factor $(1-\delta_U b)$ has been assumed constant with x. This is obviously only correct if either the damping/amplification is modest ($|\delta_U b| \ll 1$),

or if the damping is constant with x (exponential damping or amplification). In the intermezzo 2.5 we demonstrate that (2.82) is indeed correct if damping/amplification is modest, irrespective of the damping equation used.

Intermezzo 2.5: Rearrangement of Eq. (2.81) and using $\delta_U = \delta_H$ yields:

$$r_S \frac{\mathrm{d}h}{h} = \frac{1}{b}\mathrm{d}x + \frac{1}{c}\mathrm{d}V - \delta_U \mathrm{d}x = \frac{\mathrm{d}x}{b} + \frac{\mathrm{d}V}{c} - \frac{\mathrm{d}v}{v} = \frac{\mathrm{d}x}{b} + \frac{\mathrm{d}V}{c} - \frac{\mathrm{d}H}{H}$$

Integration from LWS to a certain point in time yields:

$$r_S \ln\left(\frac{h}{h_{LWS}}\right) = \frac{S}{b} + \frac{V}{c} - (\ln H - \ln H_{LWS})$$

We can make use of the function $f(x) = \ln H - \ln H_{LWS}$ and use the first order Taylor approximation:

$$f(x) \approx (x - x_{LWS}) \frac{\mathrm{d}}{\mathrm{d}x}(\ln H) + ... = S \frac{1}{H}\frac{\mathrm{d}H}{\mathrm{d}x} + ... = S\delta + ...$$

As long as $S\delta < 1$, this is valid for every damping function, which does not have to be exponential with constant δ. As a result, the general solution of the equation is:

$$r_S \ln\left(\frac{h}{h_{LWS}}\right) = \frac{S}{b} + \frac{V}{c} - S\delta$$

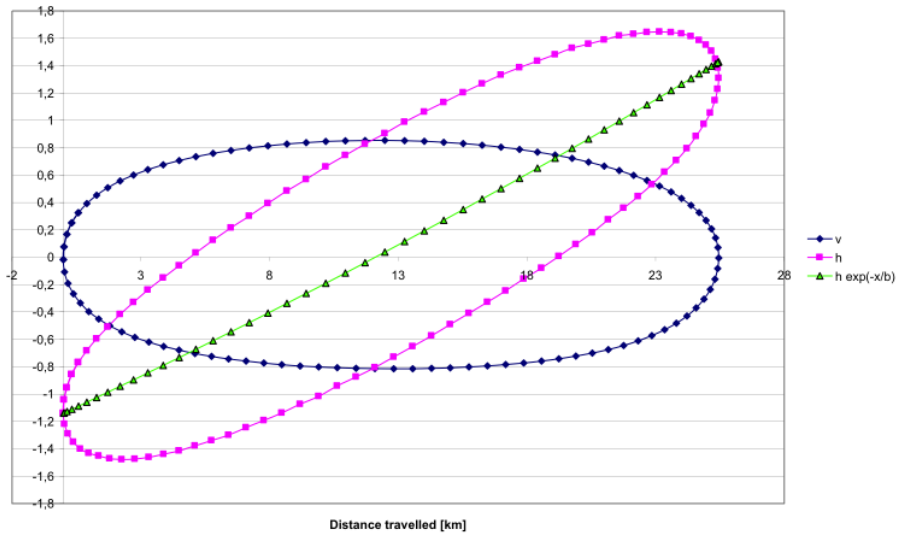

Figure 2.12: Velocity (m/s) and elevation (m) of a moving water particle as a function of the distance travelled (km).

2.3.4 Finding an expression for the phase lag

Equating the left hand side of (2.80) to zero and substitution of V from (2.70) and $\mathrm{d}V/\mathrm{d}t$ (from Intermezzo 2.3), allows the determination of the time at which high water (HW) and low water (LW) occur. Subsequent integration yields:

$$\omega t_{HW} = \pi - \arctan\left(\frac{\omega}{c}\frac{b}{(1-\delta_U b)}\right) \tag{2.83}$$

$$\omega t_{LW} = 2\pi - \arctan\left(\frac{\omega}{c}\frac{b}{(1-\delta_U b)}\right) \tag{2.84}$$

The phase lags for HW and LW are defined as: $\varepsilon_{HW} = \omega\,(T/2 - t_{HW})$ and $\varepsilon_{LW} = \omega\,(T - t_{LW})$. Assuming that the wave celerities for HW and LW are the same (which is acceptable as long as the tidal amplitude to depth ratio is small) the expression for the phase lag is:

$$\varepsilon = \arctan\left(\frac{\omega b}{c(1-\delta_U b)}\right) \tag{2.85}$$

The definition of the arc-tangent implies that $-\pi/2 < \varepsilon < \pi/2$. For damped or moderately amplified tidal waves the argument of the arc-tangent is positive (1-$\delta_U b \geq$0), therefore $0 \leq \varepsilon < \pi/2$.

Substitution of the times of occurrence of HW and LW in V (yielding V_{HW} and V_{LW}) and in S (yielding S_{HW} and S_{LW}) yields:

$$S_{HW} = \frac{v}{\omega}\,(1+\cos(\varepsilon)) = E\frac{1+\cos(\varepsilon)}{2} \tag{2.86}$$

$$S_{LW} = \frac{v}{\omega}\,(1-\cos(\varepsilon)) = E\frac{1-\cos(\varepsilon)}{2} \tag{2.87}$$

$$V_{HW} = v\sin(\varepsilon) \tag{2.88}$$

$$V_{LW} = -v\sin(\varepsilon) \tag{2.89}$$

2.3.5 The Geometry-Tide relation

We can integrate (2.81) to yield an analytical equation that links the estuary geometry to the tidal characteristics. For that purpose we integrate the equation between LWS and HWS:

$$\int_{LWS}^{HWS}\frac{\mathrm{d}h}{h} = \frac{1}{r_S c}\int_{LWS}^{HWS}\mathrm{d}V + \frac{(1-\delta_U b)}{r_S b}\int_{LWS}^{HWS}\mathrm{d}x \tag{2.90}$$

Starting at LWS at $x = 0$ this leads to:

$$\ln(h_{HWS}) - \ln(h_{LWS}) = \frac{1}{r_S c}\,(V_{HWS} - V_{LWS}) + \frac{(1-\delta_U b)}{r_S b}\,(E - 0) \tag{2.91}$$

and because the velocities at LWS and HWS are zero:

$$\frac{h_{HWS}}{h_{LWS}} = \frac{\bar{h} + H'/2}{\bar{h} - H'/2} = 1 + \frac{H'}{\bar{h} - H'/2} = \exp\left(\frac{(1-\delta_U b)}{r_S b}E\right) \tag{2.92}$$

We now develop the exponential function into a Taylor series, whereby $\exp(x) = 1+x+x^2/2+x^3/6...$ Comparing the Taylor series with (2.92) we can see that the argument of the exponential function is of the order $H'/\bar{h}$. We now define the dimensionless parameter $\zeta' = H'/\bar{h}$. We then obtain:

$$\frac{r_S H b\cos\varepsilon}{\bar{h}E\,(1-\delta_U b)} = (1-\zeta'/2) + \frac{1}{2}\,(1-\zeta'/2)\,\frac{1-\delta_U b}{r_S b}E + \frac{1}{6}\,(1-\zeta'/2)\left(\frac{1-\delta_U b}{r_S b}E\right)^2 + ...$$

If we substitute the argument of the exponential function by ζ', we obtain:

$$\frac{r_S H b\cos\varepsilon}{\bar{h}E\,(1-\delta_U b)} = 1 - \frac{1}{12}\zeta'^2 - \mathrm{O}\left(\frac{1}{24}\zeta'^3\right)$$

Hence for $0 < \zeta' < 1$, an accurate approximation of (2.91) is:

$$\frac{H}{E} = \frac{\eta\omega}{v} = \frac{\bar{h}}{r_S b}\frac{(1-\delta_U b)}{\cos(\varepsilon)} \tag{2.93}$$

which confirms that ζ' is indeed a correct approximation of the argument of the exponential function.

Equation (2.93) is essentially the same as (2.66), which we derived intuitively from the water balance equation. Now that the equation has been formally derived, it provides an accurate relation between H/E and h/b. This is the analytical relation we were looking for to relate the depth to the tidal excursion. We shall call it the "Geometry-Tide relation" since it presents a direct relation between the tidal scales H and E and the geometric scales h and b. It is important to realise that the ratio of the vertical to the horizontal tidal range (H/E) is directly proportional to the ratio of the vertical to the horizontal scales of the estuary shape (h/b). This is a very practical equation to derive an estimate of the estuary depth (notoriously difficult to observe) on the basis of observable tidal parameters (E, H, δ, ε) and the convergence length b.

An alternative derivation can be made on the basis of (2.27), which uses the cross-sectional area convergence length a and which is expressed in terms of the water elevation Z above the mean depth $\overline{h}$. Then the Lagrangean equation becomes:

$$r_S \frac{\mathrm{d}Z}{Z+\overline{h}} = \frac{(1-\delta_U a)}{a}\mathrm{d}x + \frac{1}{c}\mathrm{d}V \tag{2.94}$$

Subsequently, under the assumption that $Z << \overline{h}$ this leads to:

$$\frac{H}{E} = \frac{\eta\omega}{\upsilon} = \frac{\overline{h}}{r_S a}\frac{(1-\delta_U a)}{\cos(\varepsilon)} \tag{2.95}$$

Similarly we derive the expression for the phase lag:

$$\tan\varepsilon = \frac{\omega a}{c(1-\delta_U a)} \tag{2.96}$$

Although the assumption that $Z << \overline{h}$ seems more strict, these equations allow a bottom slope to be present in the estuary. In the following text, for reasons of convenience, we shall drop the over-bar and simply use h to describe the tidal average depth. If the tidal average depth is constant along the estuary we shall use h_0.

2.3.6 The Scaling equation

An interesting result is obtained if we combine (2.85) and (2.93):

$$\frac{\eta}{h} = \frac{1}{r_S}\frac{\upsilon}{c}\frac{1}{\sin(\varepsilon)} \approx \frac{\upsilon}{c}\frac{1}{\sin(\varepsilon)} \tag{2.97}$$

which is a direct relationship between the amplitude-to-depth ratio, the Froude number and the Wave-type number, N_E=sin(ε). This very useful equation provides a relationship between important hydraulic scales and is therefore named the "Scaling equation". This equation is also very useful to estimate the estuary depth on the basis of observable tidal parameters.

It is interesting to note that a simpler version of this equation is widely used in the literature, particularly in perturbation analysis (e.g. Jay, 1991; Friedrichs and Aubrey, 1994). In perturbation analysis it is customary to neglect sin(ε) in (2.97). This assumes ε=$\pi/2$, namely the case of a purely progressive wave. In perturbation analysis it is implicitly assumed that the wave behaves as a progressive wave, whereas we know that the tidal wave in an estuary is of mixed character (see Fig. 2.6). Because ε is small (typically in the order of 0.3), the error made by neglecting sin(ε) is substantial. In the author's experience the Froude number is always substantially smaller than the tidal amplitude to depth ratio. It is an illustration of how perturbation analysis can easily introduce unnecessary errors. While (2.97) is not more complicated, it is certainly more accurate than the equation used in perturbation analysis.

Friedrichs and Aubrey (1994) also present a version of (2.92) obtained from perturbation analysis, but in that equation, r_s, cos(ε) and (1-$\delta_U b$) are missing. Disregarding cos(ε) is the same as assuming that the tidal wave behaves like a standing wave. Because ε is small, the error may not seem so large, but combined with the neglect of damping and the effect of storage width, it can result in considerable deviation from the true value; a deviation which can be avoided by a more rigorous analytical derivation.

2.3.7 The damping assumption

The geometry-tide relation is also a very useful tool to analyse the relation between the damping of the tidal amplitude δ_η (which is the same as δ_H) and the damping of the tidal velocity amplitude δ_U. Under the condition that the tidal damping is either constant (exponential damping/amplification) or small ($|\delta_U b| << 1$), we can simply derive from Eq. (2.93):

$$\delta_H = \delta_U + \delta_h - \delta_{cos\varepsilon} = \delta_U + \delta_h + \tan\varepsilon \frac{\partial \varepsilon}{\partial x} = \delta_U + \Delta \tag{2.98}$$

where δ_h is relative depth gradient and Δ is the error made if we assume that $\delta_H \approx \delta_U$. On the basis of Eq. (2.40):

$$\delta_h = \frac{a-b}{ab} \tag{2.99}$$

In long estuaries, the depth gradient and phase lag gradient are generally small and $\delta_H \approx \delta_U$ applies. But in short estuaries, as we saw in section 1.2, there is generally a substantial depth gradient and the velocity amplitude reduces to zero near the estuary end, while the water level amplitude does not. Since in short estuaries the phase lag is very small ($\tan\varepsilon \approx 0$), for short estuaries $\delta_H \approx \delta_U + \delta_h$ applies.

However, in the more downstream part of coastal plain estuaries, both the depth and phase lag gradients are negligible and the tidal amplitude and tidal velocity amplitude are about equal. Hence:

$$\delta_H \approx \delta_U \tag{2.100}$$

This is a useful formula because in practice, δ_H is much easier to determine than δ_U.

2.4 Stokes' drift in alluvial estuaries

It is important to point out that Stokes' drift is not a physical phenomenon but an artefact of our mathematical definitions. The drift phenomenon was coined by George Stokes (1819-1903) (see for example, Longuet-Higgins (1969)). Formally, Stokes drift is defined as the difference between the average Lagrangean and the average Eulerian velocity. But in estuaries, Stokes drift is purely the result of observing the Eulerian velocity at a fixed point along the estuary axis. If there is a net zero transport of water through the estuary (Q_f=0), then in the Eulerian framework we observe an average upstream velocity equal to the Stokes drift velocity. Integrated over the tidal period, this is the Stokes drift. In a regular estuary with an average depth of about 10m, under a semi-diurnal tide with a tidal amplitude of 1 m/s, the Stokes drift amounts to about 2 km per tidal period. Not a negligible amount, only it is not real. It is a drift that results from the Eulerian perspective where we continuously observe a different particle that passes our point of observation. Heraclitus (quoted by Plato) said: "You can't step twice into the same river; for other waters are ever flowing on to you". Paraphrasing Heraclitus, we can say that: "Standing on the shoreline, you never observe the same water particle". However, if we observe the water particle in the Lagrangean way, then we see how the same water mass is continuously subject to the tidal forces of gravity and the friction exercised by the bottom shear. If the driving force is cyclic, as the tide is, then also the movement of the particle is cyclic; and if there is no river discharge, then the water balance requires that it returns to the same position. If there is an average downstream discharge, then this can be superimposed on the tidal movement and the water particle moves gradually downstream with the average velocity Q_f/A. Not so within the Eulerian framework. In the Eulerian framework, the water balance demands that the average tidal **discharge is zero** (or equal to the river discharge), but because the discharge is composed of two cyclic functions of velocity and water depth which are not in phase, the tidal average Eulerian **velocity is non-zero**. This is the Stokes drift phenomenon. A real 'Lagrangean' water particle does not experience a Stokes drift, but Eulerian particles do. There may be a Lagrangean drift due to wind, wave energy dissipation, or flow convergence, but at all times, the water balance requires that such a drift is compensated by a lateral or vertical return flow. In short, the Lagrangean tidal velocity is directly subject to conservation of mass; the Eulerian velocity only indirectly through the discharge.

We have seen before that the classical theory on tidal hydraulics has a preference for Eulerian theory. The literature is dominated by the assumption that the Eulerian velocity can be described by a standard harmonic function, and as a result, there is the suggestion that the Stokes drift is real. We saw in Figure 2.11 that the Lagrangean and Eulerian velocities are not the same. So if one of them is a pure sinus, then the other one is not. The Stokes drift velocity U_S is the difference between the Lagrangean velocity V and the Eulerian velocity U:

$$U_S = V - U \tag{2.101}$$

Hence in a Eulerian frame, U_S can be expressed as:

$$U_S = \int_0^t U(x,t)\mathrm{d}t \frac{\partial U(x,t)}{\partial x} \tag{2.102}$$

If we assume the Eulerian velocity U to be a pure harmonic, then it follows easily that:

$$\langle U_S \rangle = \frac{v^2}{2c} \tag{2.103}$$

But, as we saw from the numerical model simulation in Figure 2.11, the Eulerian velocity is not a pure harmonic. If we assume that the Lagrangean velocity is a pure harmonic, then the average Eulerian velocity is non-zero. In fact, we can see in Figure 2.11 that a pure sinus in the Lagrangean framework leads to a Eulerian velocity that has a residual velocity. The reverse is also true. If the Eulerian velocity has an average of zero, then the Lagrangean velocity should have a residual drift, equal to the Stokes drift. A simple thought experiment tells us which of the two is correct.

If we assume the Lagrangean velocity not to have a zero mean, then a water particle would gradually move upstream. What is true for one particle would apply to all particles, hence a non-zero mean Lagrangean velocity would lead to a residual upstream transport of matter. In a closed estuary with a constant or zero inflow from upstream, this is not possible. This is in contradiction with the water balance. Hence the Lagrangean velocity should have a zero mean or be equal to the fresh water discharge velocity.

In the Lagrangean framework, (2.102) modifies into (2.105) below. We do this by calculating U from V through a Taylor approximation, integrating backwards over S:

$$U = V + \frac{\partial U}{\partial x}(-S) + \frac{1}{2}\frac{\partial^2 U}{\partial x^2}(-S)^2 + ... \tag{2.104}$$

In a first order approximation it then follows that:

$$U_S = S\frac{\partial U}{\partial x} = \frac{v}{\omega}(1-\cos(\omega t))\left(-\frac{1}{c}\omega v \cos(\omega t) + \delta_U v \sin(\omega t)\right) \tag{2.105}$$

neglecting the damping for the time being, the time average residual velocity is:

$$\langle U_S \rangle = \frac{v^2}{cT}\int_0^T (1-\cos(\omega t))(-\cos(\omega t))\mathrm{d}t = \frac{v^2}{\omega cT}\int_0^{2\pi}\left(\cos^2(\omega t) - \cos(\omega t)\right)\mathrm{d}\omega t \tag{2.106}$$

The integral of the first term is π and of the second is zero, hence:

$$\langle U_S \rangle = \frac{v^2}{\omega cT}\pi = \frac{v^2}{2c} \tag{2.107}$$

This is the same result as in (2.103). The difference is that in classical literature it is assumed that the Lagrangean velocity equals this Stokes drift, whereas in alluvial estuaries it is the Eulerian average velocity that is equal and opposed to the Stokes drift. Hence:

$$\langle U \rangle = -\langle U_S \rangle = -\frac{v^2}{2c} \tag{2.108}$$

It follows from this equation that if the wave celerity goes to infinity (standing wave) that the Stokes drift is zero. This is because a standing wave is synchronous whereby (in an ideal estuary with zero damping) the longitudinal velocity gradient is zero.

Of course we have to take the damping/amplification into account, and also (e.g. according to Zimmerman, 1979) it is wise to consider the second order term in the implicit Taylor approximation of (2.104). The figures below illustrate the effect of damping/amplification on the Stokes drift, and also the importance of using the second order term for higher accuracy.

Figure 2.13 shows the Eulerian and Lagrangean velocities and displacements for the case where v=1.0 m/s, c=10 m/s, and T=44400 s. Figure 2.14 shows the Stokes residual velocity and Stokes drift varying over the tidal period. The second order term has only a slight influence but the effect of damping or amplification can be significant.

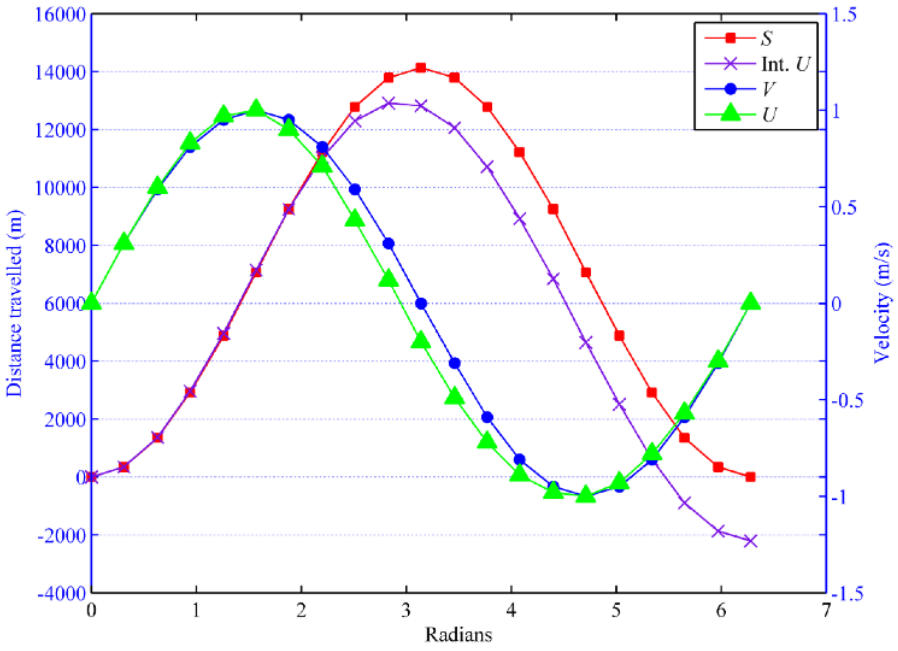

Figure 2.13: The Eulerian and Lagrangean velocities and displacements.

In conclusion, the Stokes drift is not a real phenomenon, as is often thought, but rather a mathematical artefact of the Eulerian reference frame. In open systems, however, there may be a throughflow. One can imagine this to happen in an estuary with two branches divided by an island. If the conditions for a residual flow (due to wind, gravitational effects, channel geometry, Coriolis effect, or wave energy dissipation) are better in one of the two channels, then there can be a residual upstream flow in that channel, which is compensated by a return flow in the other. But the drift that is caused by these pressures or shear stresses are Lagrangean drifts and not Stokes drifts. The forces act on the moving water particle that moves in response to the Newton's second law of motion. If there is a Lagrangean drift, then this may also manifest itself in a Eulerian drift - the Stokes drift is nothing more than the difference between the two. It is not a phenomenon in itself.

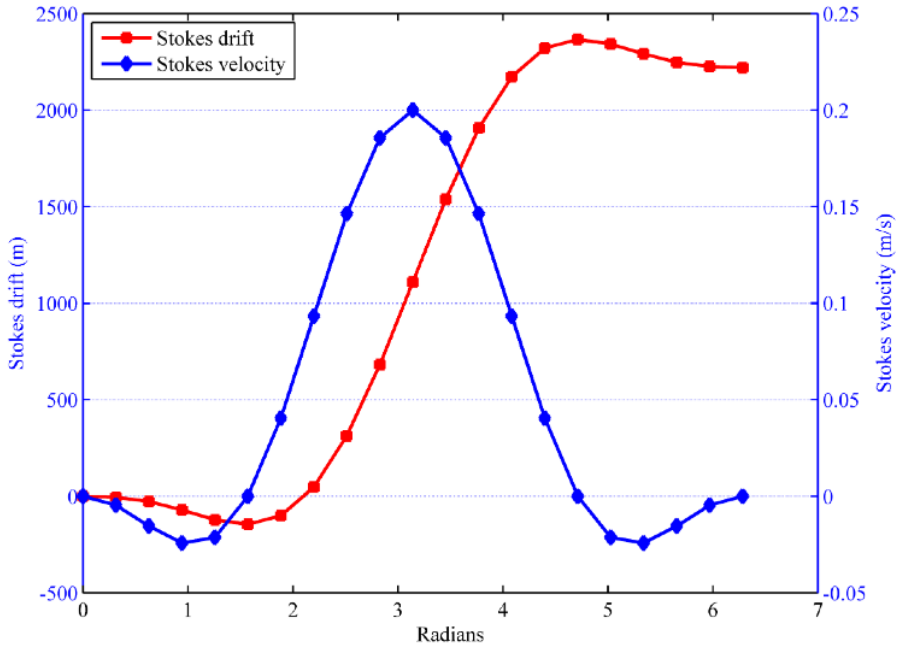

Figure 2.14: The Stokes residual velocity and Stokes drift varying over the tidal period.

2.5 The effect of river discharge on the Lagrangean water balance, the phase lag and the Geometry-Tide relation

The river discharge in the Lagrangean water balance

In the Lagrangean reference frame, the river discharge (pointing in downstream direction) comes in through the velocity with which the water moves:

$$V = v\sin(\omega t) - \frac{Q_f}{A} = v\sin(\omega t) - U_f = v\left(\sin(\omega t) - \varphi\right) \tag{2.109}$$

where $U_f = Q_f/A$ and we define $\varphi = U_f/v$ as the relative influence of the river discharge on the tidal flow. The Lagrangean derivative reads:

$$\frac{\mathrm{d}V}{\mathrm{d}t} = \omega v\cos(\omega t) - \frac{U_f}{a}V \tag{2.110}$$

As a result the distance travelled by the water particle is:

$$S = \frac{v}{\omega}\left(1 - \cos(\omega t)\right) - U_f t \tag{2.111}$$

In a Eulerian reference frame, the Eulerian velocity is:

$$U = v\sin(\xi) - U_f = v\left[\sin\left(\omega t - \frac{\omega}{c}\left(x - x_0 - S\right)\right) - \varphi\right] \tag{2.112}$$

Partial derivation of this equation results in the following expression:

$$\frac{\partial U}{\partial x} = \delta_U v\sin(\xi) + v\cos(\xi)\frac{\partial \xi}{\partial x} - \frac{U_f}{a} \tag{2.113}$$

where:

$$\frac{\partial \xi}{\partial x} = -\frac{\omega}{c}\left\{1 + \frac{U_f t}{a} - \delta_U S - \delta_U U_f t\right\} \tag{2.114}$$

In this derivative the last term is very small compared to the second since $\delta_U a \ll 1$, and also small compared to the other damping term if $U_f < v$. We can see in (2.114) that when φ approaches unity, the two damping terms more or less double the damping effect on $\partial\xi/\partial x$, because $S \approx Vt$. In the following we disregard the last term in $\partial\xi/\partial x$, assuming $\varphi < 1$, and explore what happens if it becomes more prominent. Combining (2.113) with the Lagrangean water balance where $x = S$ and $\xi = \omega t$ yields:

$$\frac{r_S}{hv}\frac{\mathrm{d}h}{\mathrm{d}t} = \frac{(1-\delta_U b)}{b}\sin(\omega t) - \frac{\partial \xi}{\partial x}\cos(\omega t) \tag{2.115}$$

Substitution of (2.109), (2.110) and (2.114) yields:

$$\frac{r_S}{h}\frac{\mathrm{d}h}{\mathrm{d}t} = \frac{(1-\delta_U b)}{b}(V+U_f) + \frac{1}{c}\left(\frac{\mathrm{d}V}{\mathrm{d}t}(1-\delta_U S) + U_f\frac{V}{a}(1-\delta_U S) + U_f\frac{t}{a}\frac{\mathrm{d}V}{\mathrm{d}t} + U_f\frac{t}{a}U_f\frac{V}{a}\right) \tag{2.116}$$

The last term is a factor $U_f t/a$ smaller than the other terms containing U_f, so it can be disregarded. Integration, from t_{LWS} until t, making use of the exponential shape of the cross-section yields:

$$r_S \ln\left(\frac{h}{h_{LWS}}\right) = \frac{(1-\delta_U b)}{b}S\left(1 + \frac{U_f t}{S}\right) + \frac{V}{c}\left(1 + \frac{U_f t}{a}\right) - \delta_U S\mathbf{F}\left(\frac{V}{v} + \frac{E}{S} - \varphi\frac{E}{2a}\right) \tag{2.117}$$

At t_{HWS}=$T/2$, this yields:

$$r_S \ln\left(\frac{h_{HWS}}{h_{LWS}}\right) = \frac{(1-\delta_U b)}{b}E\left(1 + \varphi\frac{\pi}{2}\right) - \delta_U E\mathbf{F}\left(1 - \varphi\frac{E}{2a}\right) \approx \frac{(1-\delta_U b)}{b}E\left(1 + \varphi\frac{\pi}{2}\right) \tag{2.118}$$

The last term is generally very small compared to the first, because $\mathbf{F}\delta_U b \ll 1$, and it is $\mathbf{F}$ times smaller than the damping in the first term. So the fresh water discharge impacts on the water level variation essentially through the impact is has on the distance travelled by the water particle $S(1 + U_f t/S)$. We can also see that the water depth at HWS is increased as a result of the river discharge if φ approaches unity.

If we would have made use of (2.27) instead of (2.26), then we could have replaced the width convergence length by the cross-sectional convergence length a.

The river discharge in the phase lag equation

The river discharge affects both the timing of HW and HWS, and similarly the timing of LW and LWS. We'll first look at the timing of HW and LW, and then at the timing of the slacks. The phase lag between HW and HWS will differ from the original phase lag that is unaffected by discharge. The original phase lag was defined as ε, while the new phase lags will be indicated by: $\varepsilon_{HW}(\varphi) = \omega(t_{HWS} - t_{HW})$ and $\varepsilon_{LW}(\varphi) = \omega(t_{LWS} - t_{LW})$ What we may expect is that, in line with Fig. 1.5, when $U_f \approx v (\varphi \approx 1)$ the HW phase lag reduces while the LW phase lag increases until the slacks coincide.

Influence of the river discharge on the timing of HW and LW

Considering the water balance of (2.114) at HW or LW, where dh=0, we find:

$$-(1-\delta_U b)\sin(\omega t) = b\left(\frac{\omega}{c} + \frac{\omega}{c}\frac{U_f}{a}t - \frac{1}{c}\delta_U v(1-\cos(\omega t))\right)\cos(\omega t) \tag{2.119}$$

and considering $a \approx b$ and $F = v/c$:

$$-(1-\delta_U b)\tan(\omega t) = \frac{\omega b}{c} + \mathbf{F}(\varphi\omega t - \delta_U b(1-\cos(\omega t))) \tag{2.120}$$

Let's first consider the situation of HW, where applies: $\omega t_{HW} = \pi - \varepsilon_{HW}$, $\cos(\omega t) = -1$. Assuming $\varepsilon_{HW} \ll \pi$ and subsequently $\cos(\varepsilon_{HW}) \approx 1$ and $t \approx T/2$, we find:

$$(1 - \delta_U b)\tan(\varepsilon_{HW}) = \frac{\omega b}{c} + \mathbf{F}(\varphi\pi - 2\delta_U b) \tag{2.121}$$

In order to study the relative importance of these terms we use the dimensionless numbers of Savenije et al. (2008), which will be further elaborated in the next chapter: $\gamma = c_0/(\omega b)$, $\lambda = c_0/c$, $\delta = \delta_U c_0/\omega$:

$$\left(1 - \frac{\delta}{\gamma}\right)\tan(\varepsilon_{HW}) = \frac{\lambda}{\gamma} + \mathbf{F}\left(\varphi\pi - 2\frac{\delta}{\gamma}\right) \tag{2.122}$$

A special case is the situation of the ideal estuary where there is no damping and the wave celerity is c_0 ($\delta = 0, \lambda = 1$). In that case:

$$\tan(\varepsilon_{HW,I}) = \frac{1}{\gamma} + \mathbf{F}\varphi\pi \tag{2.123}$$

Knowing that the order of magnitude of γ is 1, but the Froude number is in the order 0.1 or smaller, we can see that the impact of the river discharge is always small, unless γ is small, which is the case in prismatic channels.

The effect of the river discharge on the timing of HW is that it tends to delay the time of HW. The effect of damping is not clear. In the left hand member (the denominator) the damping reduces the delay, while in the second term it increases the delay.

Similarly for the timing of LW applies that $\omega t_{LW} = -\varepsilon_{LW}$ and $\cos(\omega t) = 1$. We again assume that $\varepsilon_{LW} \ll \pi$ and hence: $\cos(\varepsilon_{LW}) \approx 1$, $t \approx T$. It follows that:

$$(1 - \delta_U b)\tan(\varepsilon_{LW}) = \frac{\omega b}{c} + 2\mathbf{F}\varphi\pi \tag{2.124}$$

Using the dimensionless numbers we rewrite:

$$\left(1 - \frac{\delta}{\gamma}\right)\tan(\varepsilon_{LW}) = \frac{\lambda}{\gamma} + 2\mathbf{F}\varphi\pi \tag{2.125}$$

In the LW case there is no damping term in the right hand member, and the effect of the river discharge is doubled. Damping reduces the time of occurrence of LW through the denominator.

We can also consider the case of the ideal estuary where there is no damping ($\delta = 0, \lambda = 1$), hence:

$$\tan(\varepsilon_{LW,I}) = \frac{1}{\gamma} + 2\mathbf{F}\varphi\pi \tag{2.126}$$

So the river discharge delays the timing of both HW and LW, with LW delayed more. Damping reduces this delay. In strongly tapering funnel-shaped estuaries, this effect is minor, but in near prismatic estuaries the effect can be significant.

Influence of the river discharge on the timing of HWS and LWS

A much stronger effect on the phase lag between HW and HWS is provided by the shift in the occurrence of slack $\Delta\varepsilon$. Taking a fresh water discharge into account, the timing of the HWS and LWS is shifted:

$$\omega t_{HWS} = \pi + \Delta\varepsilon_{HWS} = \pi - \arcsin(\varphi) \tag{2.127}$$

$$\omega t_{LWS} = \Delta\varepsilon_{LWS} = \arcsin(\varphi) \tag{2.128}$$

Hence the phase lag between HWS and HW and between LWS and LW in the case of a fresh water discharge are:

$$\omega(t_{LWS} - t_{LW}) = \varepsilon_{LW}(\varphi) = \arcsin(\varphi) + \arctan\left(\frac{\lambda}{\gamma - \delta}\left(1 + 2\frac{\gamma}{\lambda}\mathbf{F}\varphi\pi\right)\right) \tag{2.129}$$

$$\omega(t_{HWS} - t_{HW}) = \varepsilon_{HW}(\varphi) = -\arcsin(\varphi) + \arctan\left(\frac{\lambda}{\gamma - \delta}\left(1 + \frac{\gamma}{\lambda}\mathbf{F}\varphi\pi - 2\frac{\delta}{\lambda}\right)\right) \tag{2.130}$$

Overall we see that the effect of the fresh water discharge on the occurrence of HW and LW is very minor (unless in prismatic estuaries), but that the effect of river discharge on the occurrence of HWS and LWS is direct through $\arcsin(\varphi)$, as depicted in Fig. 1.5.

The river discharge in the geometry-tide relation

Using the water balance of (2.122) and neglecting the terms with $\delta_U SF$, it follows:

$$r_S \ln\left(\frac{h}{h_{LWS}}\right) = \frac{(1-\delta_U b)}{b}\left(S + U_f t\right) + \frac{V}{c}\left(1 + \frac{U_f t}{a}\right) \tag{2.131}$$

We can substitute the conditions for HW and for LW in this equation, obtaining two equations, one for HW and one for LW. Subtraction of these equations yields:

$$r_S \ln\left(\frac{h_{HW}}{h_{LW}}\right) = \frac{(1-\delta_U b)}{b} E cos(\varepsilon) + 2\mathbf{F} sin(\varepsilon)\left(1 + \frac{U_f T}{2a}\right) \tag{2.132}$$

Assuming that $a \approx b$, and using the same operations as we used to derive (2.91), whereby we use the expression for $\tan(\varepsilon_{HW})$ above, it follows that the geometry tide relation is virtually unaffected by the fresh water discharge. The equation we obtain is the same as (2.91):

$$r_S \ln\left(\frac{h_{HW}}{h_{LW}}\right) \approx \frac{(1-\delta_U b)\, E}{b cos(\varepsilon)} \tag{2.133}$$

Influence of river discharge on the scaling equation

The average phase lag is not influenced by river discharge, since (2.128) and (2.130) are almost symmetrical. Hence the scaling equation is also almost unaffected by the fresh water discharge:

$$\frac{\eta}{h} \approx \frac{v}{c}\frac{1}{r_S \sin(\varepsilon)} \tag{2.134}$$

In summary, the influence of the river discharge on the Lagrangean water balance is minor. The only apparent effect is the shift in the occurrence of the slacks when the river discharge becomes prominent (φ approaching unity).

2.6 Concluding remarks

In this chapter we have derived three important analytical equations: the phase lag equation (2.85), the geometry-tide relation (2.93) and the scaling equation (2.97). In these equations the phase lag acts as a prominent variable. In alluvial estuaries it can vary over the full range between 0 and $\pi/2$, between a standing and a progressive wave, depending essentially on the degree of width convergence in the estuary. In classical analytical solutions people either assumed a standing or a progressive wave and, as a result, missed an essential characteristic of alluvial estuaries.

These three new equations, derived from the water balance equation, still contain four unknowns: the velocity amplitude, the water level amplitude, the wave celerity and the phase lag. Moreover, the last of these three equations contains no new information, being a combination of the previous two. So we have two equations with four unknowns. Although these are very useful equations to study the relationships between tidal flow parameters and estuary geometry, we still need two more analytical equations to solve the entire system. In the following chapter we shall do just that, and derive expressions for tidal damping (the derivative of the water level amplitude) and wave propagation (the wave celerity). We shall then have enough analytical equations to solve the St. Venant equations.

Chapter 3

TIDAL DYNAMICS

This chapter covers the remaining theory of tidal hydraulics, specifically dealing with equations that describe the effect of tidal damping and wave propagation.

In the previous chapter we derived relations between the hydraulic parameters of tidal flow and estuary geometry, essentially by analysing the conservation of mass equation in conjunction with the exponential shape of alluvial estuaries. In this chapter we shall derive analytical equations for tidal damping/amplification and for wave celerity by combining the conservation of mass and momentum equations. The damping equation is derived through the envelope method, while the celerity equation uses the methods of characteristics. We use analytical derivation and not scaling or perturbation analysis, as is often used. Scaling is useful for identifying the main mechanisms at play and for assessing orders of magnitude, but, as a tool for derivation, it does not always result in correct equations, as will be demonstrated. The analytical equations derived in this chapter are more general versions - or refinements - of well-known (classical) equations, such as Green's law and other rules of thumb derived by perturbation analysis. Most of these classical equations are only correct for frictionless channels or for channels with a constant topography, or for either progressive or standing waves. The general equations derived in this book apply to the full range of tidal waves (with a phase lag varying between 0 and $\pi/2$) and the natural topographies of alluvial estuaries. Moreover, we shall show that the set of equations can be reduced to 4 dimensionless relationships that can be solved explicitly.

3.1 Tidal movement and amplification

3.1.1 Why is the tidal wave amplified or damped?

We saw in the previous section that tidal amplification (or damping) has an effect on the water balance equation, and therefore on the ratio of E/H and (importantly) on the wave celerity. But what causes a tidal wave to be amplified or damped? Until now we have only analysed the mass balance equation, although the assumed Lagrangean velocity function is a solution of both St. Venant equations. To understand the reasons for tidal damping we have to look at the momentum balance equation.

Early authors like Langbein (1963) and Dyer (1973) suggested that tidal amplification is the result of the imbalance between topographic convergence and friction. If convergence is stronger than friction, the wave is amplified; if friction is stronger than convergence, the wave is damped; if they are equally strong, the tidal range is constant. This was indeed demonstrated by Jay (1991), who used perturbation theory, and by Savenije (1998) who combined the Lagrangean equations of the previous section with the momentum balance equation. In the following section we shall derive a relation for tidal amplification and damping.

3.1.2 Derivation of the tidal damping equation by the envelope method

We can rearrange (2.80) as follows:

$$\frac{\mathrm{d}V}{\mathrm{d}t} = r_S \frac{c}{h}\frac{\mathrm{d}h}{\mathrm{d}t} - \frac{cV}{b} + \frac{cV}{v}\frac{\mathrm{d}v}{\mathrm{d}x} \tag{3.1}$$

We shall now make use of (2.100), stating that the damping of the velocity amplitude is almost equal to the damping of the tidal range (including an error term Δ). This error term is zero when the phase lag ε and the damping/amplification are constant δ_u(implying exponential damping or no damping). This assumption is valid in long estuaries that gradually transform into a river. In short and closed estuaries this assumption may not be correct, but we'll see further on in Section 3.4 that in short estuaries we may use a simple linearised equation that performs well under those conditions. Making use of this assumption, (3.1) becomes:

$$\frac{\mathrm{d}V}{\mathrm{d}t} = r_S \frac{c}{h}\frac{\mathrm{d}h}{\mathrm{d}t} - \frac{cV}{b} + cV\left(\frac{1}{H}\frac{\mathrm{d}H}{\mathrm{d}x} - \Delta\right) \tag{3.2}$$

Next we combine (3.2) with the Lagrangean momentum balance equation (2.22). Written in a Lagrangean reference frame it reads:

$$\frac{\mathrm{d}V}{\mathrm{d}t} + g\frac{\partial h}{\partial x} + g\left(I_b - I_r\right) + g\frac{V|V|}{C^2 h} = 0 \tag{3.3}$$

Combination of (3.2) and (3.3), and making use of the Lagrangean relationship $V = \mathrm{d}v/\mathrm{d}t$, yields:

$$r_S \frac{cV}{gh}\frac{\mathrm{d}h}{\mathrm{d}x} - \frac{cV}{g}\left(\frac{1}{b} - \frac{1}{H}\frac{\mathrm{d}H}{\mathrm{d}x} + \Delta\right) + \frac{\partial h}{\partial x} + I_b - I_r + \frac{V|V|}{C^2 h} = 0 \tag{3.4}$$

To derive an explicit relation for the tidal damping, we shall condition this differential equation for the occurrence of HW and LW. We shall then obtain two differential equations describing the envelopes of the water levels at HW and LW. At HW and LW the special condition applies that $\partial h/\partial t = 0$, and hence:

$$\left.\frac{\mathrm{d}h}{\mathrm{d}x}\right|_{HW,LW} = \left.\frac{\partial h}{\partial x}\right|_{HW,LW} \tag{3.5}$$

Using this relation we can write (3.4) completely in Lagrangean derivatives for the conditions of HW and LW. Moreover, since the tidal range H is the difference between h_{HW} and h_{LW}, the Lagrangean gradient of the tidal range is defined by:

$$\frac{\mathrm{d}h_{HW}}{\mathrm{d}x} - \frac{\mathrm{d}h_{LW}}{dx} = \frac{\mathrm{d}H}{\mathrm{d}x} \tag{3.6}$$

And similarly because the sum of the two depth is twice the average depth (for a symmetrical wave), which we may assume to be correct if the tidal amplitude to depth ratio is small:

$$\frac{\mathrm{d}\,h_{HW}}{dx} + \frac{\mathrm{d}h_{LW}}{\mathrm{d}x} \approx 2\frac{\mathrm{d}\overline{h}}{\mathrm{d}x} \tag{3.7}$$

Finally the following conditions apply for HW and LW if the tidal amplitude to depth ratio is not too large:

$$h_{HW} \approx \overline{h} + \eta \tag{3.8}$$

$$h_{LW} \approx \overline{h} - \eta \tag{3.9}$$

where $\eta = H/2$. Moreover, if the velocity has a sinus shape:

$$V_{HW} = v\,\sin\varepsilon \tag{3.10}$$

$$V_{LW} = -v\,\sin\varepsilon \tag{3.11}$$

Combination of (3.4), (3.5), (3.8) and (3.10) yields for the condition of HW:

$$\frac{r_S c v \sin\varepsilon}{g(\overline{h}+\eta)}\frac{\mathrm{d}h_{HW}}{\mathrm{d}x} - \frac{cv\sin\varepsilon}{g}\left(\frac{1}{b} - \frac{1}{\eta}\frac{\mathrm{d}\eta}{\mathrm{d}x} + \Delta\right) + \frac{\mathrm{d}h_{HW}}{\mathrm{d}x} + \frac{(v\sin\varepsilon)^2}{C^2(\overline{h}+\eta)} = -I_b + I_r \tag{3.12}$$

This is the differential equation that describes the upper envelope of all water levels in the estuary, because no water level can rise above the point of HW. Similarly for the condition of LW we find the envelope for LW, which is the lower boundary of all the water levels in the estuary:

$$\frac{-r_S c v \sin\varepsilon}{g(\overline{h}-\eta)}\frac{\mathrm{d}h_{LW}}{\mathrm{d}x} + \frac{cv\sin\varepsilon}{g}\left(\frac{1}{b} - \frac{1}{\eta}\frac{\mathrm{d}\eta}{\mathrm{d}x} + \Delta\right) + \frac{\mathrm{d}h_{LW}}{\mathrm{d}x} - \frac{(v\sin\varepsilon)^2}{C^2(\overline{h}-\eta)} = -I_b + I_r \tag{3.13}$$

Subtraction of these two envelopes yields:

$$\frac{r_S c v \sin\varepsilon}{2\overline{h}}\left(\frac{\mathrm{d}h_{HW}}{\mathrm{d}x}\frac{\overline{h}}{(\overline{h}+\eta)} + \frac{\mathrm{d}h_{LW}}{\mathrm{d}x}\frac{\overline{h}}{(\overline{h}-\eta)}\right) - \frac{cv\sin\varepsilon}{\overline{h}}\left(\frac{\overline{h}}{b} - \frac{\overline{h}}{\eta}\frac{\mathrm{d}\eta}{\mathrm{d}x} + \overline{h}\Delta\right) + g\frac{\mathrm{d}\eta}{\mathrm{d}x} + f'\frac{(v\sin\varepsilon)^2}{\overline{h}} = 0 \tag{3.14}$$

with:

$$f' = \frac{g}{C^2}\left(1 - \left(\frac{\eta}{\overline{h}}\right)^2\right)^{-1} = f\left(1 - \left(\frac{\eta}{\overline{h}}\right)^2\right)^{-1} \tag{3.15}$$

where f' is the adjusted friction factor taking account of the friction being larger at LW than at HW. One could also determine this friction factor on the basis of Strickler's formula. It would then read:

$$f' = \frac{g}{K^2\overline{h}^{1/3}}\left(1 - \left(\frac{1.33\eta}{\overline{h}}\right)^2\right)^{-1} \tag{3.16}$$

The coefficient 1.33 in this equation follows from a Taylor series expansion of $(h+\eta)^{1.33} \approx h^{1.33}(1+1.33\eta/h)$, if $\eta < h$. Due to the factor 1.33, this equation only makes sense as long as $\eta/h < 0.7$ and may only be applied for smaller amplitude to depth ratios. We can see that if the tidal amplitude to depth ratio is small $f' \approx f = g/C^2$.

The part between brackets in the first term of (3.14) can be replaced by twice the residual water level slope $2I$, defined in (3.7), provided $\eta/h < 1$. Elaboration yields:

$$\frac{\overline{h}}{\eta}\frac{\mathrm{d}\eta}{\mathrm{d}x}\left(1 + \frac{g\eta}{cv\sin\varepsilon}\right) = \frac{\overline{h}}{b} - f'\frac{v\sin\varepsilon}{c} - r_S\frac{\mathrm{d}\overline{h}}{\mathrm{d}x} + \overline{h}\Delta \tag{3.17}$$

The width and the depth convergence in this equation can be combined into the cross-sectional convergence. For small values of r_S this leads to the simplified equation:

$$\frac{\overline{h}}{\eta}\frac{\mathrm{d}\eta}{\mathrm{d}x}\left(1 + \frac{g\eta}{cv\sin\varepsilon}\right) = \frac{\overline{h}}{a} - f'\frac{v\sin\varepsilon}{c} + \overline{h}\Delta \tag{3.18}$$

Regarding the term $\overline{h}\Delta$. It is zero in a near ideal estuary where: a) there is no bottom slope, b) the tide is modestly damped/amplified or δ_U is constant, and c) the phase lag is constant. In long coastal plain estuaries this is generally an acceptable assumption. If there is amplification or damping in a coastal plain estuary, then this is generally modest. In that case the term $\overline{h}\Delta$ is non-zero, but since the gradient of the tidal velocity amplitude is small compared to the convergence length ($\delta_u b < 0.1$), $\overline{h}\Delta$ is still much smaller than h/a. In short (amplified) estuaries, there may be a bottom gradient, a gradient in the phase lag (gradually moving towards a standing wave) and a gradient in the tidal velocity amplitude (gradually reducing to zero). So in short estuaries the $\overline{h}\Delta$ term may become prominent and may need to be accounted for. In coastal plain estuaries, however, particularly in the downstream part, this term may be disregarded.

Hence, the analytical solution of the St. Venant's equations yields:

$$\frac{1}{\eta}\frac{\mathrm{d}\eta}{\mathrm{d}x}\left(1 + \frac{g\eta}{cv\sin\varepsilon}\right) = \frac{1}{a} - f'\frac{v\sin\varepsilon}{\overline{h}c} \tag{3.19}$$

This is a differential equation describing the damping of the tidal amplitude as a function of the estuary shape, the friction and the residual slope. The subtraction of the two envelopes for HW and LW resulted in a differential equation that describes the tidal range. It will prove to be a very useful equation to elaborate further. In the following text, for convenience sake, we shall drop the over-bar for the average depth and h will stand for the tidal average depth.

It is interesting to check the origin of the terms in this equation. The first term on the right hand side obviously comes from the convergence term in the continuity equation. The second term stems from the friction term in the momentum balance equation. On the left hand side, it is less obvious. The 1 stems from the last term in (3.1) and is the term that determines the effect of tidal damping on the mass balance equation; the second term between brackets stems from the depth gradient in the momentum balance equation (clearly an important term). Scaling (see below) shows that this term is indeed larger than 1.

This equation is a general version of Green's law, a rule of thumb often quoted. Green (1837) assumed that the amount of energy in a progressive tidal wave ($E = 0.5\rho g\eta^2 BcT$) would remain constant under frictionless flow as it travels up a converging estuary. If we use the classical equation for wave propagation ($c^2 = gh$), this leads to the tidal range being inversely proportional to the square root of the width and the 0.25th power of the depth. In an ideal estuary with constant depth, it implies that $\delta_H = 1/(2b)$. We shall see further on in equation (3.64) that zero friction ($f' = 0$) indeed leads to Green's law. So Green's law is a special case of (3.19), and (3.19) is a general version of Green's law.

From (3.19), it can be seen that in an ideal estuary where there is no tidal damping or amplification:

$$\frac{1}{a} = f' \frac{v \sin\varepsilon}{\overline{h}c} = \frac{R'}{c} \tag{3.20}$$

This is a similar result as in (2.57), which was the condition for an ideal estuary to occur. The resistance term R'/c is also presented in Table 2.2. We can indeed verify the earlier remark that there is tidal amplification if $1/a > R'/c$ (see Figure 3.1). We can also verify that since a, f, h and v are constant along the estuary, the wave celerity and $\sin(\varepsilon)$ are proportional. Since $\sin(\varepsilon)$ indicates the type of tidal wave (it equals zero for a standing wave and 1 for a progressive wave) it is called the Wave-type number N_E (Savenije, 1998). In alluvial estuaries, where the tidal wave is of a mixed character, the Wave-type number is between 0 and 1. Since it has often been observed that the phase lag is constant along a near ideal estuary, the wave celerity also is, which can indeed be seen in alluvial estuaries, at least for considerable stretches where convergence and depth are constant.

Scaling the tidal damping equation

By scaling (3.19), we can study the behaviour of the damping equation. Therefore we introduce three parameters: the dimensionless tidal range y, the dimensionless velocity number μ, and the dimensionless wave celerity λ, which have been scaled using η_0 as the tidal amplitude at x=0, and c_0 as the classical wave celerity (see (3.27)):

$$y = \frac{\eta}{\eta_0} \tag{3.21}$$

$$\mu = \frac{v\overline{h}}{r_S c_0 \eta} \tag{3.22}$$

$$\lambda = \frac{c_0}{c} \tag{3.23}$$

It then follows from scaling (2.100) that:

$$\sin\varepsilon = \mu\lambda \tag{3.24}$$

And hence, the second term of the left hand part of (3.19) becomes:

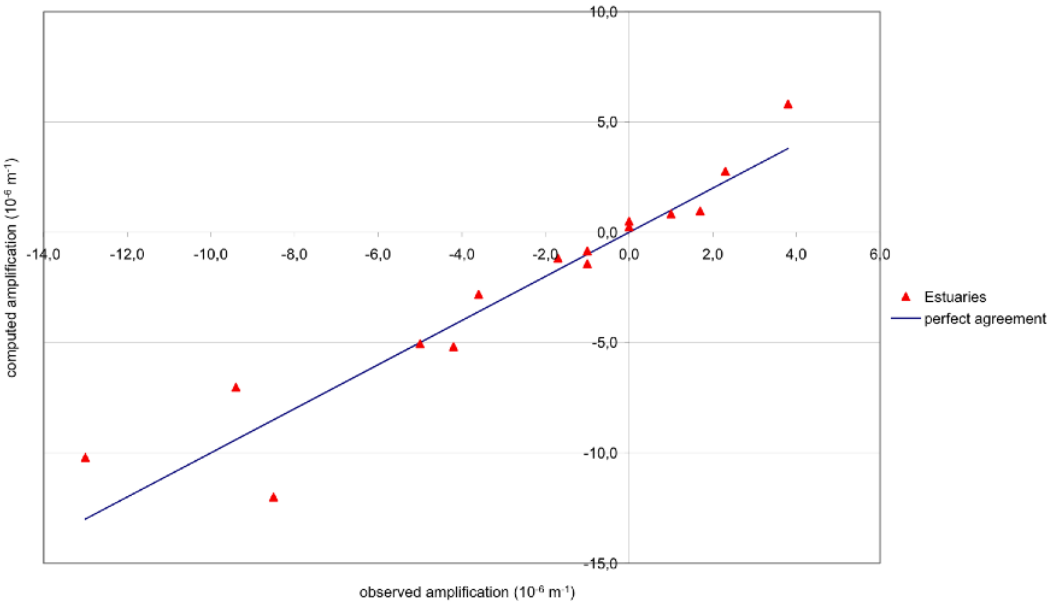

Figure 3.1: Computed and observed tidal damping and amplification (δ_H) in the estuaries of Table 2.2

$$\frac{g\eta}{cv\sin\varepsilon} = \frac{r_S {c_0}^2 \eta}{cv\bar{h}\sin\varepsilon} = \frac{1}{\mu^2} \tag{3.25}$$

Substitution of these dimensionless numbers in (3.19) leads to:

$$\frac{\mathrm{d}y}{\mathrm{d}x}\left(\frac{1+\mu^2}{\mu^2}\right) = \frac{y}{a} - f'\frac{\eta_0}{\bar{h}^2}y^2\sin^2\varepsilon \tag{3.26}$$

Since μ is O(1), we can see that the part between brackets is a number in the order of 2. Most studies in the literature assume that damping of a tidal wave is exponential (e.g., Jay, 1991; Friedrichs and Aubrey, 1994; Prandle, 2003; van Rijn, 2011). This would be the case if the second term on the right hand was linear in y and if all other factors were constant [1]. But, as we can see, the second term on the right hand side is quadratic in y. Moreover, μ and $\sin\varepsilon$ are not necessarily constant with x. As a result, it is not at all obvious that exponential damping or amplification may be assumed.

To study this relationship further, we first need to derive an analytical equation for the wave celerity (being part of $\sin\varepsilon$). We shall do this in the following section and then continue to look at the asymptotic behaviour of the damping equation.

3.2 Tidal wave propagation

Observations in estuaries indicate that an amplified tidal wave moves considerably faster than is indicated by the classical equation for wave propagation. Similarly, the celerity of propagation is lower if the tidal wave is damped. This phenomenon is clearly observed in the Schelde estuary

[1] Note that the quadratic of y and of $\sin\varepsilon$ stems from the quadratic velocity in the friction term. If the friction is linearized (e.g. by Lorentz's linearization), then the second part of (3.26) becomes linear in both y and $\sin\varepsilon$. Since this is how most of the classical literature linearizes the St. Venant equations, the classical literature uses exponential damping

(located in the Netherlands and Belgium) and in the Incomati estuary in Mozambique. In the Incomati, the tidal wave is damped throughout and the celerity of the wave is lower as expected. In the Schelde the tidal range increases from the estuary mouth as far as the city of Antwerp, after which it decreases until it reaches Gent. In harmony with the amplification and the damping the tidal wave moves faster than expected in the downstream reach and slower in the upstream reach. This section presents an analytical expression for the celerity of the tidal wave that takes into account the effect of tidal damping as an expansion of the classical equation for tidal wave propagation. The equation is successfully applied to observations in the Schelde and the Incomati. The equation, developed by Savenije and Veling (2005), is a fully analytical solution of the St. Venant equations and appears to perform better than methods developed by earlier authors.

3.2.1 The relation between tidal damping and wave celerity

The classical formula for wave propagation is widely used to describe the propagation of a tidal wave in estuaries. This equation has been derived for the propagation of a small amplitude gravity wave in a channel of constant cross-section with no friction or bottom slope (as in Section 2.2.2):

$$c_0^2 = \frac{1}{r_S} gh \tag{3.27}$$

where c_0 is the classical celerity of a progressive wave, and r_S is the storage width ratio defined earlier.

The fact that this equation is so widely used in estuaries is surprising since the conditions for its derivation (progressive wave with constant cross-section and no friction) do not apply in alluvial estuaries where the cross-section varies exponentially along the estuary axis and friction is clearly not negligible. It will be demonstrated that under special circumstances the classical wave equation also describes the propagation of a tidal wave in a converging channel, with a phase lag ε between high water (HW) and high water slack (HWS). This is the case when the wave does not gain or lose amplitude as it travels upstream and the energy per unit width that is present in the wave is constant. When the energy gain from convergence of the banks as the wave travels upstream is compensated by the energy lost by friction, we speak of an "ideal estuary" (Pillsbury, 1939). Ideal estuaries have constant depth, exponentially varying width, constant wave celerity and constant phase lag between water level and velocity (see Section 2.2.2). The exponential geometry being the natural shape of an estuary, it has been used widely to derive analytical equations for tidal wave propagation (see e.g., Hunt, 1964; Harleman, 1966; Jay, 1991; Savenije, 1992a; Friedrichs and Aubrey, 1994; Lanzoni and Seminara, 1998, 2002; Savenije and Veling, 2005). Although in an ideal estuary there is no tidal damping or amplification, in real estuaries there generally is, albeit modest. As a result, the length scale of tidal damping is generally large in relation to the length scale of bank convergence (see e.g., Friedrichs and Aubrey, 1994; Savenije, 1992a).

There appears to be a close relation between tidal damping (or amplification) and wave celerity. Tidal damping and tidal wave celerity both react to the imbalance between convergence and friction. In estuaries where tidal damping or amplification is apparent (e.g. the Thames, the Schelde or the Incomati), one can observe a prominent deviation from the classical wave celerity c_0. If the wave is amplified, such as in the lower parts of the Thames and the Schelde, then the wave moves considerably faster than the celerity computed by (3.27). When the wave is damped, as is the case in the Incomati and in the upper parts of the Thames and Schelde, then the wave travels considerably slower.

Observations of tidal wave celerity under tidal damping and amplification are presented in Figure 3.2 for the Schelde in The Netherlands and in Figure 3.8 for the Incomati in Mozambique. These observations are combined with a drawn line representing the classical equation for wave propagation of (3.27). Figure 3.7 shows observations at high water (HW) and low water (LW) in the Schelde and Figure 3.8 observations at high water slack (HWS) and low water slack (LWS) in the Incomati. It can be seen clearly that in an amplified estuary (the lower Schelde) the travel time of the wave is much shorter than the travel time computed by (3.27) (about half) and that the travel time is substantially larger in a damped estuary (the upper Schelde and the Incomati).

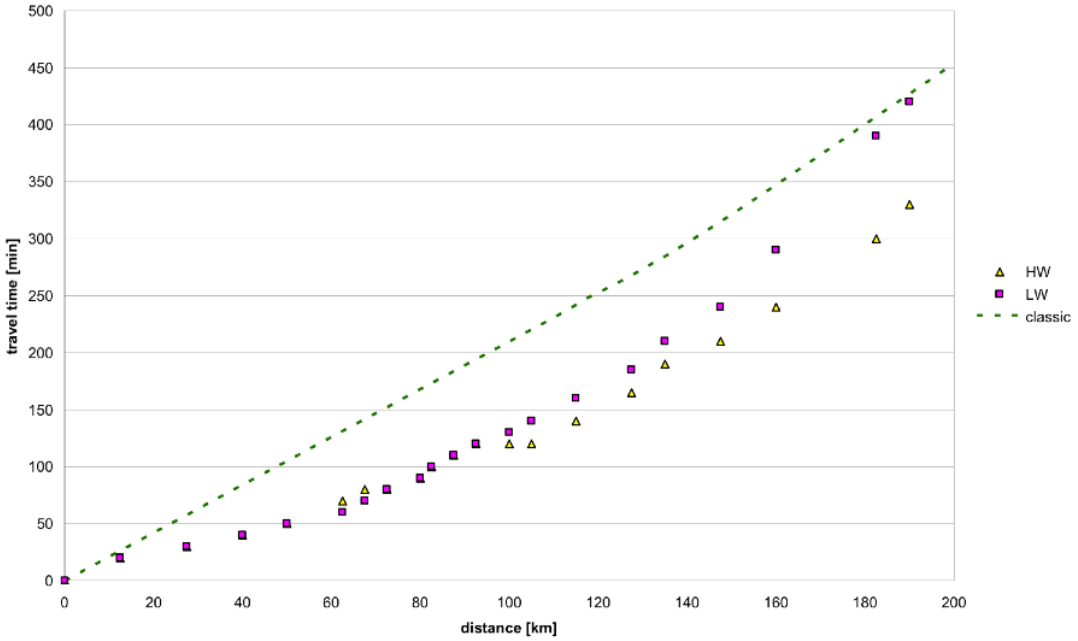

Figure 3.2: Observed propagation of the tidal wave at HW and LW on 21 June 1995 in the Schelde, compared to the propagation computed with the classical equation (Equation (3.27)).

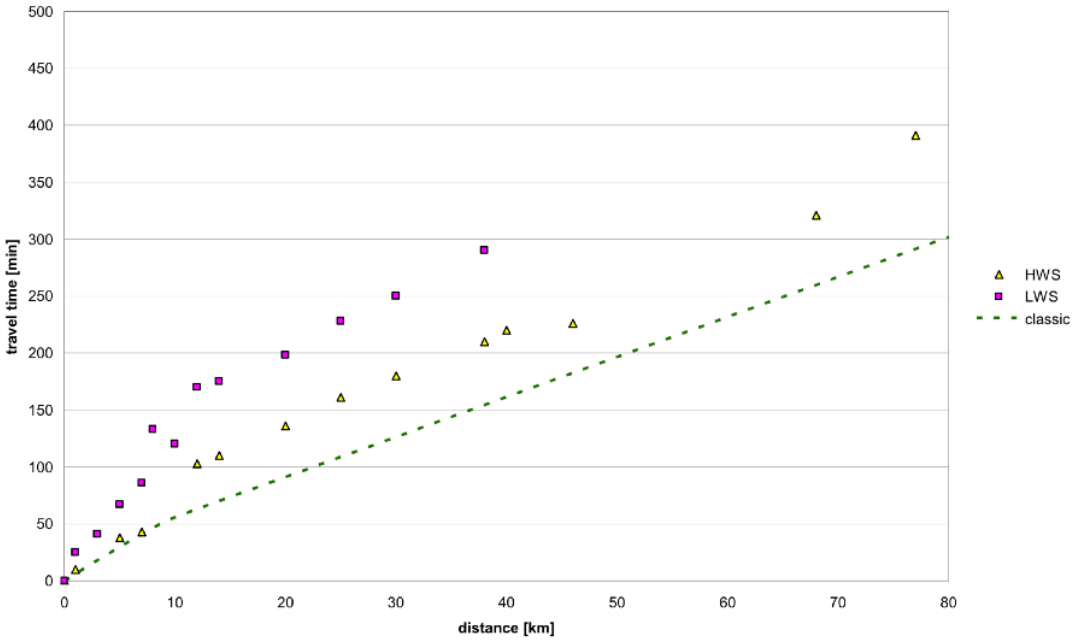

Figure 3.3: Observed propagation of the tidal wave at HWS and LWS on 23 June 1993 in the Incomati, compared to the propagation computed with the classical equation (Equation (3.27)).

To date not many efforts have been made to derive analytical equations for wave propagation in funnel shape estuaries under the influence of tidal damping or amplification. Ponce and Simons (1977) remarked that: "a coherent theory that accounts for celerity as well as attenuation characteristics has yet to be formulated". To date, the approach that made the most substantial contribution to solving this problem is the method of Friedrichs and Aubrey (1994), who addressed it by scaling the governing equations and subsequently solving the first and second order approximations analytically. This approach, called the perturbation approach, reduces the differential equation by neglecting higher order terms. In doing so, the effect of tidal damping generally disappears from the equation. Only in the second order solution of Friedrichs and Aubrey (1994) are the combined effects of tidal damping and wave propagation present. The equations obtained were fitted to observations in the Thames, Tamar and Delaware by calibration. Although the method was based on the linearised St. Venant equations, it was able to demonstrate a combined effect of damping/amplification and wave celerity by retaining an exponentially decaying or increasing tidal amplitude (although we know now that tidal damping or amplification is not exponential).

In this Section the method of characteristics (see e.g., Dronkers, 1964; Whitham, 1974) is used to derive an analytical equation for the combined effect of damping and wave celerity. This equation allows the computation of the celerity of propagation under damped or amplified conditions. The equation obtained is not very complicated and is an extension of the classical formula in which, besides the rate of amplification (or damping) the phase lag ε between high water and high water slack is essential. Conditions for these derivations are that the tidal amplitude to depth ratio and the Froude number are considerably smaller than unity and that the velocity of river discharge is small compared to the tidal velocity. In the lower part of alluvial estuaries this situation is the rule rather than the exception. Further down, in Section 3.5, we shall analyse the effect of river discharge on wave celerity.

3.2.2 Derivation of the celerity equation

Rewriting the St. Venant equations (2.22 and 2.27) and making use of the exponential convergence of the cross-section (Eq.2.38), gives us:

$$r_S \frac{\partial Z}{\partial t} + h\frac{\partial U}{\partial x} + U\frac{\partial Z}{\partial x} - \frac{Uh}{a} = 0 \tag{3.28}$$

$$\frac{\partial U}{\partial t} + U\frac{\partial U}{\partial x} + g\frac{\partial h}{\partial x} + gI_b - gI_r + f\frac{U\,|U|}{h} = 0 \tag{3.29}$$

where the parameters all have been defined earlier.

The main unknown parameters to be determined in the analysis, as functions of time and space, are the water depth h and the water velocity U. Both are considered periodic functions Φ and Ψ with a tidal period T and an angular velocity $\omega = 2\pi/T$.

Similar to the assumptions made on the character of the tidal wave in (2.48)-(2.50), the following periodic functions can be applied for velocity and depth in a Eulerian reference frame:

$$U = \upsilon(x)\Phi(\xi - \varepsilon) \approx -\upsilon(x)\sin(\xi - \varepsilon) \tag{3.30}$$

$$h = Z + \overline{h} = \eta(x)\Psi(\xi) + \overline{h} \approx \eta(x)\cos(\xi) + \overline{h} \tag{3.31}$$

$$\xi = \omega\left(t - \frac{x}{c}\right) + \xi_0 \tag{3.32}$$

The difference with (2.48)-(2.50) is that here we allow the velocity amplitude $\upsilon(x)$ and is the tidal amplitude $\eta(x)$ to vary as a function of x. Although defined earlier, here we recall that $\overline{h}$ is the tidal average depth, xi is the dimensionless argument of the periodic function, c is the celerity of the tidal wave, and ε is the phase lag between high water (HW) and high water slack (HWS), or between low water (LW) and low water slack (LWS). This phase lag may be assumed constant along the estuary axis if the tidal amplitude to depth ratio and φ are small. The functions Φ and Ψ are harmonics with unit amplitude, similar to sinusoids, but which do not have to be

sinusoids. In fact, they may contain higher order harmonics or be distorted. Note that in Section 2.4, when discussing Stokes' drift, we argued that the Eulerian harmonics are distorted while the Lagrangean harmonics are not. The approach followed here does not contradict this argument. The following derivation applies equally well to a distorted tidal wave. There are, however, a number of assumptions that have to be made. For the equations (3.30-3.32) to be correct, the following conditions should be met:

Assumptions made for the derivation:

1) The tidal velocity U in (3.30) should not be influenced by the river discharge Q_f. Hence,$v \gg Q_f/A$.
2) The amplitude of the tidal water level variation is smaller than the depth of flow. Hence, $\eta < h$.
3) The Froude number is small: $v \ll c$.
4) The phase lag ε is constant along the estuary.
5) 5) The wave celerity is constant along the estuary, or at least along a certain reach of the estuary, or $\partial c/\partial x = 0$.
6) 6) The scaled tidal wave (Ψ) does not significantly change shape as it travels upstream.

The first assumption is very common in tidal hydraulics and quite acceptable in the downstream part of alluvial estuaries. We shall evaluate the limits of this assumption in Section 3.5. The second is an important assumption made throughout this book. It is only valid in deep estuaries or estuaries with a very small amplitude. In a shallow estuary such as the Incomati this assumption is not valid near the estuary mouth, although it is further upstream. Assumption 3 is linked to the second assumption; we saw this in (2.97). The Froude number is always smaller than the amplitude to depth ratio by a factor $r_S \sin(\varepsilon)$. Assumption 4 corresponds to the theory of the ideal estuary, which in alluvial estuaries is a good approximation of reality. However, we know that if the tidal amplitude to depth ratio is large, or if the river discharge becomes dominant over the tidal flow, that this assumption is no longer valid. The fifth assumption is connected to the previous assumption. It is crucial for the derivations made. A constant wave celerity is in agreement with the theory of the ideal estuary, but in real estuaries, the celerity may show a trend. Often the solution is to consider different reaches where the celerity may be considered a constant. We shall check the validity of this assumption in Section 3.2.3 for the estuaries studied. Assumption 6, finally, is the methodological assumption. This assumption implies that higher order effects are negligible, but it is less restrictive than the assumption made for the derivation of the classical equation. Assumption 6 is acceptable as long as assumptions 1-3 are valid, and therefore it is not really an additional assumption.

If we look at Figure 3.4, we see the different stages of the tidal wave as it travels up the Schelde estuary. We see that the wave is first amplified and subsequently damped. We also see that it is gradually deformed by over-tides and secondary effects, particularly by the fact that friction is higher during LW and less during HW. Overall, however, the scaled wave, divided by its tidal range, retains its shape represented by the periodic function Ψ. When applying the analytical theory that assumes the wave celerity to be constant, the practical solution is to sub-divide the estuary in reaches of limited length where a constant celerity may be assumed (see Toffolon and Savenije, 2011).

The following partial derivatives can be derived for the argument of the harmonic functions:

$$\frac{\partial \xi}{\partial t} = \omega \tag{3.33}$$

$$\frac{\partial \xi}{\partial x} = -\frac{\omega}{c} \tag{3.34}$$

The average water depth gradient can be found by averaging (3.29) over time. It leads to a residual depth gradient I_R consisting of three terms, the density gradient, the bottom slope and

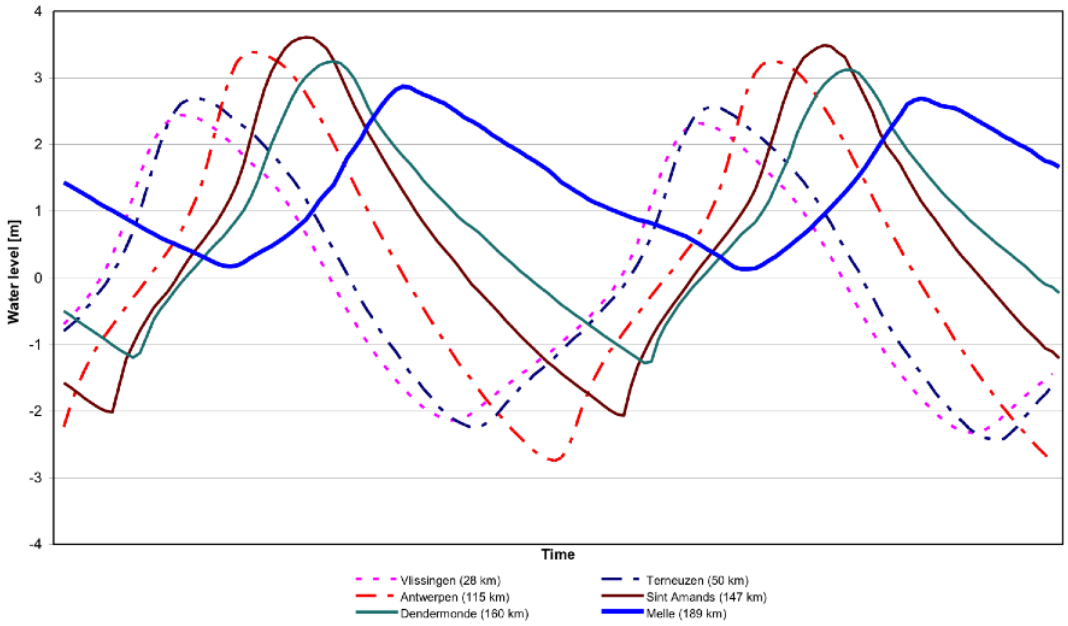

Figure 3.4: Observed tidal waves at different points along the Schelde estuary on 23 June 2001.

the residual friction slope I_f. The latter is also affected by river discharge, as we shall see in Section 3.5. Hence:

$$\frac{\partial \overline{h}}{\partial x} = I_R = I_r - I_b + I_f \tag{3.35}$$

Subsequently, the following partial derivatives of velocity and depth can be written:

$$\frac{\partial U}{\partial t} = \upsilon \Phi' \frac{\partial \xi}{\partial t} = \upsilon \omega \Phi' \tag{3.36}$$

$$\frac{\partial U}{\partial x} = \upsilon \Phi' \frac{\partial \xi}{\partial x} + \Phi \frac{\partial \upsilon}{\partial x} = -\frac{\upsilon}{c} \omega \Phi' + \upsilon \delta_u \Phi \tag{3.37}$$

$$\frac{\partial Z}{\partial t} = \eta \Psi' \frac{\partial \xi}{\partial t} = \eta \omega \Psi' \tag{3.38}$$

$$\frac{\partial h}{\partial x} = \frac{\partial Z}{\partial x} + \frac{\partial \overline{h}}{\partial x} = \eta \Psi' \frac{\partial \xi}{\partial x} + \Psi \frac{\partial \eta}{\partial x} + I_R = -\eta \frac{\omega}{c} \Psi' + \eta \delta_H \Psi + I_R \tag{3.39}$$

where δ_U and δ_H are the tidal damping rate for the tidal velocity amplitude and the tidal range, which were defined earlier in (2.58) and (2.72), respectively. Note that for these derivatives it is not necessary to assume that the periodic functions are simple harmonics.

Essential for further derivation is the assumption that the wave may be amplified or damped, but that the scaled tidal wave (Ψ) is not deformed, as long as the observer travels along a characteristic at the wave celerity (Ψ is constant with time if ξ is constant with time, implying that $\mathrm{d}x/\mathrm{d}t = c$). As we can see from Figure 3.4, showing the propagation of tidal waves in the Schelde estuary, the tide has a higher order M_4 component resulting from the non-linear resistance term. The shape of the scaled tidal wave, however, remains similar as the wave travels upstream.

Hence, for an observer travelling at the celerity of the tidal wave:

$$\frac{\mathrm{d}\Psi(x,t)}{\mathrm{d}t} = \frac{\partial \Psi}{\partial t} + c\frac{\partial \Psi}{\partial x} = \frac{\partial \Psi}{\partial \xi}\frac{\partial \xi}{\partial t} + c\frac{\partial \Psi}{\partial \xi}\frac{\partial \xi}{\partial x} = \Psi'\left(\frac{\partial \xi}{\partial t} + c\frac{\partial \xi}{\partial x}\right) = 0 \tag{3.40}$$

The crux of the method is that application of (3.40) to the combined Saint Venant equations implies that the sum of all terms containing Ψ' should be zero. These terms should be found in a linear combination of the two equations. Thus, the equation of continuity (3.28) is multiplied by a constant factor m and added to the equation of motion (3.29), after which the sum of all terms containing Ψ' are equated to zero. Such a method is more often used to determine the celerity of propagation, for example by Sobey (2001), who applied it to a channel of constant cross-section and disregarded the effect of tidal damping. Our approach generates more terms.

To enhance insight into the terms, the St. Venant equations are represented in Table 3.1 in a format where each column lists the coefficients of the equations belonging to the variables Ψ', Φ', Ψ and Φ for each term of the equations. In this Table there are a number of cells that contain non-linear terms. These terms could also have been placed in another column. The reason why certain columns are chosen is to provide a logical overview. The position of these terms is not affecting the further analysis. What is essential for the following analysis is to see which terms belong to Ψ'.

Table 3.1: Representation of the terms of the St. Venant equations as functions of Ψ', Φ', Ψ and Φ.

term	Ψ'	Φ'	Ψ	Φ	**constant**
$r_s\frac{\partial Z}{\partial t}$	$r_s\eta\omega$				
$-\frac{Uh}{a}$				$-\frac{\upsilon h}{a}$	
$h\frac{\partial U}{\partial x}$		$-h\frac{\upsilon\omega}{c}$		$+h\upsilon\delta_U$	
$U\frac{\partial Z}{\partial x}$	$-U\frac{\omega}{c}\eta$		$U\eta\delta_H$		
$\frac{\partial U}{\partial t}$		$\upsilon\omega$			
$U\frac{\partial U}{\partial x}$		$-U\frac{\upsilon\omega}{c}$		$+U\upsilon\delta_U$	
$g\frac{\partial h}{\partial x}$	$-g\frac{\omega}{c}\eta$		$g\eta\delta_H$		gI_R
$-gI_R$					$-gI_R$
$\frac{fU\lvert U\rvert}{h}$				$\frac{f\upsilon\lvert U\rvert}{h}$	

The combined equation can be split into two parts: the equation where the sum of the coefficients of the terms containing Ψ' is zero (corresponding to (3.40)), and the equation where the sum of the remaining terms is zero. The first equation yields:

$$m = \frac{g}{(cr_S - U)} \tag{3.41}$$

where m is the multiplication factor for the equation of continuity.

The second equation reads:

$$m\left\{-h\frac{\upsilon\omega}{c}\Phi' - \upsilon h\left(\frac{1}{b} - \delta_u\right)\Phi + \upsilon\Phi\left(\eta\delta_H\Psi + I_R\right)\right\} + \upsilon\omega\left(1 - \frac{U}{c}\right)\Phi' + g\eta\delta_H\Psi + \left(\frac{f\upsilon\,|U|}{h} + U\upsilon\delta_u\right)\Phi = 0 \tag{3.42}$$

Substitution of m and rearrangement yields:

$$(cr_S - U)(c - U) = gh\frac{1 + C_c + D_2 + D_3}{1 - (R_c + D_1 + D_4)(c/(c-U))} = ghF_c(\Phi, \Psi) \tag{3.43}$$

with $F_c(\Phi, \Psi)$ being the damping/amplification function of the celerity, consisting of the following terms:

$$C_c = \frac{\Phi c}{\Phi' \omega}\frac{1}{a}$$

$$R_c = -\frac{\Phi}{\Phi' \omega}\frac{f|U|}{h}$$

$$D_1 = -\frac{g}{\Phi' \upsilon \omega}\eta \Psi \delta_H$$

$$D_2 = -\frac{\Phi c}{\Phi' \omega}\delta_u$$

$$D_3 = -\frac{\Phi c}{\Phi' h \omega}\eta \Psi \delta_H$$

$$D_4 = -\frac{\Phi}{\Phi' \omega}\upsilon \Phi \delta_u$$

These terms are all functions of U and h, and hence of time and space. Here C_c is the term that determines the acceleration of the wave due to the convergence of the banks. S_c determines the influence of the residual slope. R_c determines the deceleration due to friction and the D_i terms ($i = 1, ..., 4$) contain the effect of tidal amplification or damping. The terms are defined in such a way that if they are positive, they cause the wave to move faster. If they are negative they slow down the propagation of the wave. Because in alluvial estuaries the Froude number ($F = U/c$) is much smaller than unity: $|D_4| \ll |D_2|$ and $|D_3 \ll |D_1|$. As a result, D_4 and D_3 can generally be disregarded, but we retain them here.

Airy's Equation

Besides that $F_c(\Phi, \Psi)$ is a function of $U$and h, equation (3.43) contains the flow velocity and the depth explicitly. This dependency on U and h can be simplified using an adjusted Airy equation. Airy (1845), quoted by (Lamb, 1932, art.175), presented the following equation for a frictionless undamped progressive wave ($\sin\varepsilon = \pi/2$) in a prismatic channel with no bottom slope:

$$c = \overline{c_0}\left(1 + \frac{3\eta}{2\overline{h}}\right) \tag{3.44}$$

where $\overline{c_0}$ is the classical celerity of the tidal wave at mean depth. In our case, where there is friction, tidal damping and a strong topography, this equation is different. For a small Froude number, (3.43) can be modified as:

$$(c - v)^2 = \overline{c_0}^2\left(1 + \frac{h - \overline{h}}{\overline{h}}\right)F_c(\Phi, \Psi) \tag{3.45}$$

Let us consider the situation at HW. At HW: $h - \overline{h} = \eta$ and $U = v\sin\varepsilon$. Making use of the Scaling Equation, (2.97), this leads to:

$$c_{HW} = \overline{c_0}\left(1 + \frac{\eta}{\overline{h}}\right)^{0.5} F_{cHW}^{0.5} + \overline{c_0} r_S \frac{\eta}{\overline{h}}\sin^2\varepsilon \tag{3.46}$$

The root in the first term can be replaced by the first terms of a Taylor series expansion, if $\eta/h < 1$. Hence:

$$c_{HW} = \overline{c_0}\left(1 + \frac{\eta}{2\overline{h}}\right)F_{cHW}^{0.5} + \overline{c_0} r_S \frac{\eta}{\overline{h}}\sin^2\varepsilon = \overline{c_0}\left(1 + \frac{\eta}{\overline{h}}\left(\frac{1}{2} + r_S\frac{\sin^2\varepsilon}{F_{cHW}^{0.5}}\right)\right)F_{cHW}^{0.5} \tag{3.47}$$

Now it can be seen that for $r_S = 1$, $F_c(\Psi, \Phi) = 1$ and $\varepsilon = \pi/2$ (the case of an undamped progressive wave in a prismatic channel) this is the same as Airy's equation. In alluvial estuaries, however, the value of $\sin^2 \varepsilon$ is O(0.1). With $F_c(\Psi, \Phi)$ and r_S being close to unity, this implies that in alluvial estuaries the effect of the wave amplitude on the wave celerity is less strong than Airy's equation suggests. The general equation for the effect of depth and velocity variation on wave propagation can be derived similarly as:

$$c = \overline{c_0}\left(1 - \frac{\eta}{2\overline{h}}\Psi\right)F_c^{0.5} - \overline{c_0} r_S \frac{\eta}{\overline{h}}\Phi\sin\varepsilon = \overline{c_0}\left(1 - \frac{\eta}{\overline{h}}\left(\frac{\Psi}{2} + r_S\frac{\Phi\sin\varepsilon}{F_c^{0.5}}\right)\right)F_c^{0.5} \tag{3.48}$$

This modified Airy equation, or (3.45), is useful to calculate the celerity at different moments within the tidal wave, such as HW, LW, HWS, LWS or TA. For a small amplitude-to-depth ratio, the direct effect of the water level fluctuation on the wave celerity will be small, but for large amplitude waves, the wave celerity between HW and LW can differ substantially. In extreme cases, the HW following LW can catch up with the previous LW, resulting in a tidal bore.

But in case of a damped or amplified wave, the effect of the function $F_c(\Psi, \Phi)$ can be much stronger. So let us first explore the behaviour of this function.

A solution for HWS and LWS

The values of C_c, S_c, R_c, and D_i vary during the tidal cycle. In Table 3.2 the values of these terms are presented for special moments during the tidal cycle: HW, LW, HWS, LWS, the tidal average situation (TA) and at maximum flow (MAX) during ebb and flood respectively. In this Table, it is assumed that the functions Φ and Ψ behave like sinusoids.

Table 3.2: Values of terms determining tidal propagation for HW, HWS, LW, LWS, TA and MAX flow situations.

	HW	**LW**	**HWS**	**LWS**	**TA ebb**	**TA flood**	**MAX ebb**	**MAX flood**
ζ	0	π	ε	$\pi+\varepsilon$	$\pi/2$	$3\pi/2$	$\pi/2+\varepsilon$	$3\pi/2+\varepsilon$
Φ	$\sin\varepsilon$	$-\sin\varepsilon$	0	0	$-\cos\varepsilon$	$\cos\varepsilon$	-1	+1
Φ'	$\cos\varepsilon$	-1	1	$-\sin\varepsilon$	$\sin\varepsilon$	0	0	
Ψ	1	-1	$\cos\varepsilon$	$-\cos\varepsilon$	0	0	$-\sin\varepsilon$	$\sin\varepsilon$
C_c	$-\frac{c\tan\varepsilon}{\omega}\frac{1}{a}$	$-\frac{c\tan\varepsilon}{\omega}\frac{1}{a}$	0	0	$\frac{c}{\omega a\tan\varepsilon}$	$\frac{c}{\omega a\tan\varepsilon}$	$-\frac{c}{\omega a}$	$\frac{c}{\omega a}$
R_c	$\frac{fv(\sin\varepsilon)^2}{h_{HW}\omega\cos\varepsilon}$	$\frac{fv(\sin\varepsilon)^2}{h_{LW}\omega\cos\varepsilon}$	0	0	$\frac{-fv\cos\varepsilon}{\overline{h}\omega}$	$\frac{-fv\cos\varepsilon}{\overline{h}\omega}$	$\frac{fv}{\overline{h}\omega}$	$-\frac{fv}{\overline{h}\omega}$
D_1	$\frac{g\eta\delta_H}{v\omega}\frac{1}{\cos\varepsilon}$	$\frac{g\eta\delta_H}{v\omega}\frac{1}{\cos\varepsilon}$	$\frac{g\eta\delta_H}{v\omega}\cos\varepsilon$	$\frac{g\eta\delta_H}{v\omega}\cos\varepsilon$	0	0	$\frac{g\eta\delta_H}{v\omega}\sin\varepsilon$	$-\frac{g\eta\delta_H}{v\omega}\sin\varepsilon$
D_2	$\frac{c\tan\varepsilon}{\omega}\delta_U$	$\frac{c\tan\varepsilon}{\omega}\delta_U$	0	0	$\frac{-c}{\omega\tan\varepsilon}\delta_U$	$\frac{-c}{\omega\tan\varepsilon}\delta_U$	$\frac{c}{\omega}\delta_U$	$-\frac{c}{\omega}\delta_U$
D_3	$\frac{c\tan\varepsilon}{h_{HW}\omega}\eta\delta_H$	$-\frac{c\tan\varepsilon}{h_{LW}\omega}\eta\delta_H$	0	0	0	0	$-\frac{c\sin\varepsilon}{\overline{h}\omega}\eta\delta_H$	$-\frac{c\sin\varepsilon}{\overline{h}\omega}\eta\delta_H$
D_4	$\frac{v\sin\varepsilon\tan\varepsilon}{\omega}\delta_U$	$-\frac{v\sin\varepsilon\tan\varepsilon}{\omega}\delta_U$	0	0	$\frac{v\cos\varepsilon}{\omega\tan\varepsilon}\delta_U$	$-\frac{v\cos\varepsilon}{\omega\tan\varepsilon}\delta_U$	$-\frac{v}{\omega}\delta_U$	$-\frac{v}{\omega}\delta_U$

If the tidal wave progresses as a non-deformed wave, any convenient moment during the tidal cycle can be selected to determine the wave celerity. It can be seen from Table 3.2 that it is very attractive to solve the equation for the moments of HWS and LWS where: $U = 0$, $C_c = 0$, $R_c = 0$, $D_2 = 0$, $D_3 = 0$, and $D_4 = 0$. Hence, the expression for the function $F_{cHWS,LWS}$ reads:

$$F_c\left(0, \cos\varepsilon\right) = \frac{1}{1 - D_c} = 1/\left(1 - \frac{g\eta\delta_H}{v\omega}\cos\varepsilon\right) \tag{3.49}$$

and the equation for the celerity of the wave (at slack time) reads:

$$c^2 = \frac{1}{r_S} g h F_{cHWS,LWS} = \frac{c_0^2}{\left(1 - \frac{g}{\upsilon\omega}\frac{\mathrm{d}\eta}{\mathrm{d}x}\cos\varepsilon\right)} \tag{3.50}$$

where $D_c = D_1$ and h is the water depth at slack time. Since the water depth at HWS is larger than at LWS, the celerity of the wave is higher at HWS than at LWS. Hence, the assumption that the wave is non-deformed is only valid if the depth at HWS is not much different from the depth at LWS, or if $\eta\cos\varepsilon \ll h$. In that case the average depth may be used.

Equation (3.50) is an expansion of the classical equation for wave propagation by a simple damping factor $F = 1/(1-D)$. The expression for D can be made even simpler if we make use of subsequently eqs. (2.97) and (2.96):

$$D = \frac{g}{\upsilon\omega}\frac{\mathrm{d}\eta}{\mathrm{d}x}\cos\varepsilon = \frac{g\eta}{\upsilon\omega}\delta_H\cos\varepsilon = \frac{gh}{r_S\omega c}\delta_H\frac{1}{\tan\varepsilon} = \left(\frac{c_0}{\omega}\right)^2\delta_H\frac{(1-\delta_H a)}{a} \tag{3.51}$$

The equation thus obtained is surprisingly simple and provides clear insight into the factors that influence tidal propagation. It can be seen directly that: the classical equation is obtained if convergence balances friction and there is no tidal damping or amplification (if $\delta_H = 0$). The wave is slowed down under tidal damping ($\mathrm{d}\eta/\mathrm{d}x < 0$) and accelerated under tidal amplification ($\mathrm{d}\eta/\mathrm{d}x > 0$). If we analyse the origin of the terms in the denominator, we see that the 1 represents the acceleration term in the momentum balance equation, while the second term represents the damping component of the depth gradient in the momentum balance equation.

What can we say of the wave celerity at TA? At TA the depth is the same for the flood and ebb tide. The asymmetry between TA-flood and TA-ebb is in the D4-term and in the left hand member of (3.43) where the velocity has a different sign. Both cases of asymmetry are negligible if the Froude number is small. Disregarding the D_4-term one can demonstrate that the celerity at TA and HWS/LWS is the same, making use of the damping equation. Hence we can use equation (3.45) with $F_c = 1/(1-D_c)$, using the expression for D derived for HWS/LWS also for HW, LW and TA, provided we take account of the correct water depth and velocity at these moments in time.

Rearrangement of (3.19) yields the expression for tidal damping or amplification:

$$\frac{\mathrm{d}\eta}{\mathrm{d}x} = \eta\frac{\left(\frac{1}{a} - f'\frac{\upsilon\sin\varepsilon}{\bar{h}c}\right)}{\left(1 + \frac{g\eta}{c\upsilon\sin\varepsilon}\right)} = \eta\alpha\frac{\left(\frac{1}{a} - f'\frac{\upsilon\sin\varepsilon}{\bar{h}c}\right)}{(1+\alpha)} \tag{3.52}$$

which we can use to substitute into (3.50), so as to obtain an implicit relation for the wave celerity with:

$$1 - \left(\frac{c_0}{c}\right)^2 = D_c = \frac{\sin\varepsilon\cos\varepsilon}{(1+\alpha)}\left(\frac{c}{\omega a} - f'\frac{\upsilon\sin\varepsilon}{\omega\bar{h}}\right) = \frac{\sin 2\varepsilon}{2\,(1+\alpha)}\left(\frac{c}{\omega a} - \frac{R'}{\omega}\right) \tag{3.53}$$

In (3.53) both the nominator and denominator of D_c have been multiplied by α. As a result, the denominator $(1+\alpha)$ has a value close to unity. In the right hand side of (3.53) the friction term of Jay (1991) is used, with $R' = f'\upsilon\sin\varepsilon/h$. It can be seen clearly that $c = c_0$ when the convergence and the friction terms are equal.

It is interesting to look at what would happen if D_c equals unity. Since the 1 in the denominator corresponds with the acceleration term, it implies that critical convergence occurs when convergence and acceleration cancel out. This was termed critical convergence by Jay (1991). In Section 3.3 we shall see that the situation of critical convergence is the transition to a standing wave, where the wave celerity becomes infinite and the estuary synchronous (HW and LW occurring everywhere at the same time).

Simplifying the damping equation

Now that we have an expression for the wave celerity, we can simplify the damping equation as expressed by Eq. (3.19). In Intermezzo 3.1 the details of this algebraic manipulation are

presented, resulting in a much simpler damping equation:

$$\delta_H = \frac{1}{2a} - f' \frac{v^2}{2\eta g \bar{h}} \tag{3.54}$$

Intermezzo 3.1: Simplification of Eq. (3.19)
We make use of the goniometric equality:

$$(\cos\varepsilon)^{-2} = 1 + (\tan\varepsilon)^2$$

and substitution of the Eq's for the tangent of ε (2.96) and the cosine of ε (2.95), this becomes:

$$\left(\frac{\eta\omega}{v}\frac{r_S a}{h\,(1-\delta_H a)}\right)^2 = 1 + \left(\frac{\omega a}{c\,(1-\delta_H a)}\right)^2$$

or:

$$\left(\frac{\eta\omega r_S}{vh}\right)^2 - \left(\frac{\omega}{c}\right)^2 = \left(\frac{1-\delta_H a}{a}\right)^2$$

Reworking the damping equation (3.19), making use of (2.97):

$$\left(\frac{1-\delta_H a}{a}\right) = f'\frac{v^2}{c^2}\frac{1}{\eta r_S} + \delta_H\left(\frac{c_0\eta r_S}{vh}\right)^2$$

and reworking the celerity equation (3.50) using the expression for $\cos\varepsilon$ en c_0:

$$\left(\frac{c_0}{c}\right)^2 = 1 - \delta_H\left(\frac{c_0}{\omega}\right)^2\left(\frac{1-\delta_H a}{a}\right)$$

or:

$$\left(\frac{1-\delta_H a}{a}\right) = \left(\frac{\omega}{c_0}\right)^2\frac{1-(c_0/c)^2}{\delta_H}$$

Substitution of the left hand members of the reworked (3.19) and (3.50) in the goniometric equation:

$$\left(\frac{\eta\omega r_S}{vh}\right)^2 - \left(\frac{\omega}{c}\right)^2 = \left\{f'\frac{v^2}{c^2}\frac{1}{\eta r_S} + \delta_H\left(\frac{c_0\eta r_S}{vh}\right)^2\right\}\left(\frac{\omega}{c_0}\right)^2\frac{1-(c_0/c)^2}{\delta_H}$$

or:

$$\delta_H\left\{\left(\frac{c_0\eta r_S}{vh}\right)^2 - \left(\frac{c_0}{c}\right)^2\right\} = \left\{f'\frac{v^2}{c^2}\frac{1}{\eta r_S} + \delta_H\left(\frac{c_0\eta r_S}{vh}\right)^2\right\}\left(1-\left(\frac{c_0}{c}\right)^2\right)$$

$$\delta_H\left\{\left(\frac{c_0}{c}\right)^2\right\} = \left\{f'\frac{v^2}{c^2}\frac{1}{\eta r_S} + \delta_H\left(\frac{c_0\eta r_S}{vh}\right)^2\right\}\left(\left(\frac{c_0}{c}\right)^2\right) - f'\frac{v^2}{c^2}\frac{1}{\eta r_S}$$

Division by $(c_0/c)^2 \neq 0$:

$$\delta_H = \left\{f'\frac{v^2}{c^2}\frac{1}{\eta r_S} + \delta_H\left(\frac{c_0\eta r_S}{vh}\right)^2\right\} - f'\frac{v^2}{{c_0}^2}\frac{1}{\eta r_S}$$

Re-substitution of the reworked damping equation:

$$\delta_H = \left(\frac{1-\delta_H a}{a}\right) - f'\frac{v^2}{{c_0}^2}\frac{1}{\eta r_S}$$

or:

$$2\delta_H = \frac{1}{a} - f'\frac{v^2}{{c_0}^2}\frac{1}{\eta r_S} = \frac{1}{a} - f'\frac{v^2}{\eta g\bar{h}}$$

We can now use the simplified damping equation to, in turn, simplify the celerity equation, which then reduces to:

$$1 - \left(\frac{c_0}{c}\right)^2 = \frac{g\eta\cos\varepsilon}{2v\omega}\left(\frac{1}{a} - f'\frac{v^2}{\eta g\bar{h}}\right) = \left(\frac{c_0}{\omega}\right)^2\frac{(1-\delta_H a)}{2a}\left(\frac{1}{a} - f'\frac{v^2}{\eta g\bar{h}}\right) = \left(\frac{c_0}{\omega}\right)^2\left(\frac{1-\delta_H a}{a}\right)\delta_H \tag{3.55}$$

3.2.3 Empirical verification in the Schelde and Incomati estuaries

The theory described in the previous section has been confronted with observations made in the Schelde and Incomati estuaries. Figures 3.5 and 3.6 show the application of the theory to wave celerity in the two estuaries. The equation performs considerably better than the classical equation. In the Incomati the correspondence is very good, with the exception of the part nearest the mouth. In the Schelde the line for HW is very good, but the line for LW shows a deviation upstream from the point located 150 km from the mouth. The reasons for these deviations should be sought in the relatively high ratio of tidal amplitude to depth and the effect of river discharge, of which the details are given by Savenije and Veling (2005). For the sake of comparison, Figure 3.5 also shows the relation derived by Friedrichs and Aubrey (1994) for the tidal average situation.

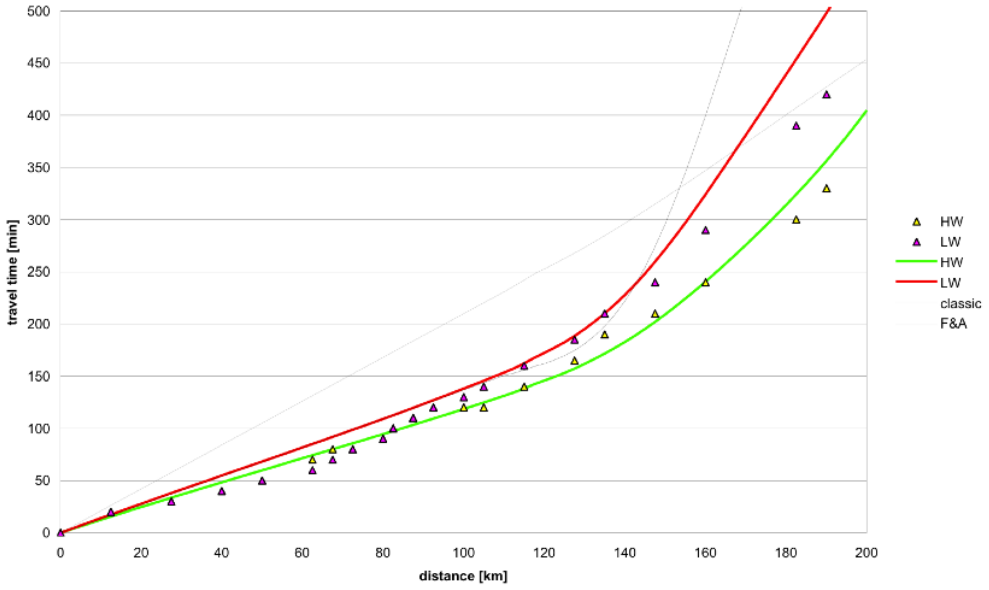

Figure 3.5: Propagation of the tidal wave in the Schelde estuary observed at high water (HW) and low water (LW) 21 June 1995 (indicated by triangles). The thick drawn lines represent the computed wave propagation. The thin drawn line represents the wave propagation according to the method of Friedrichs and Aubrey (1994).

Figure 3.7, shows the variation of the damping term D_c as a function of x in the Schelde estuary. The thick line is the value obtained by (3.50) using observed values of $\mathrm{d}\eta/\mathrm{d}x$. The line indicated by D'' is obtained with (3.53). The reason why this line deviates from the previous line upstream from 140 km is because it does not take into account the effect of river discharge on tidal damping. This can be seen if we consider the thin line (indicated by D'), which was obtained by using a slightly more sophisticated formula than (3.52), developed by Horrevoets et al. (2004) taking into account the effect of river discharge. The theory on the effect of river discharge on tidal damping is presented in Section 3.5. The line that takes river discharge into account fits the observed data very well.

3.2.4 Overview of the set of equations

With the derivations made in this and the previous chapter, we have formulated a set of analytical equations with which the St Venant equations can be solved analytically. These equations are new in that they are based on a consistent set of assumptions and that they have general applicability, whether the wave is progressive, standing or of mixed character. The equations are

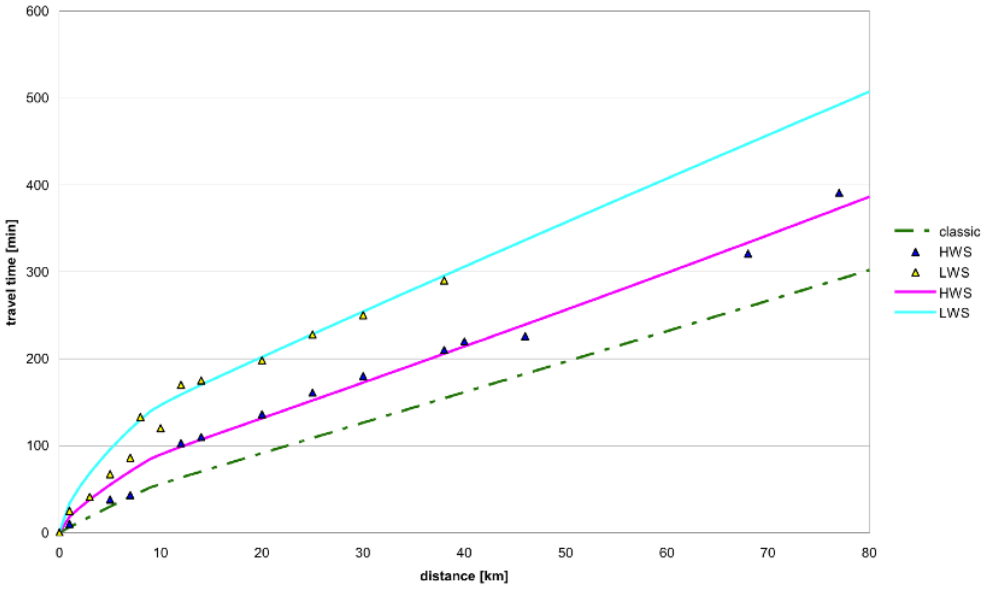

Figure 3.6: Propagation of the tidal wave in the Incomati estuary observed at high water (HW) and low water (LW) 23 June 1993 (indicated by triangles). The thick drawn lines represent the computed wave propagation. The thin drawn line represents the classical wave propagation.

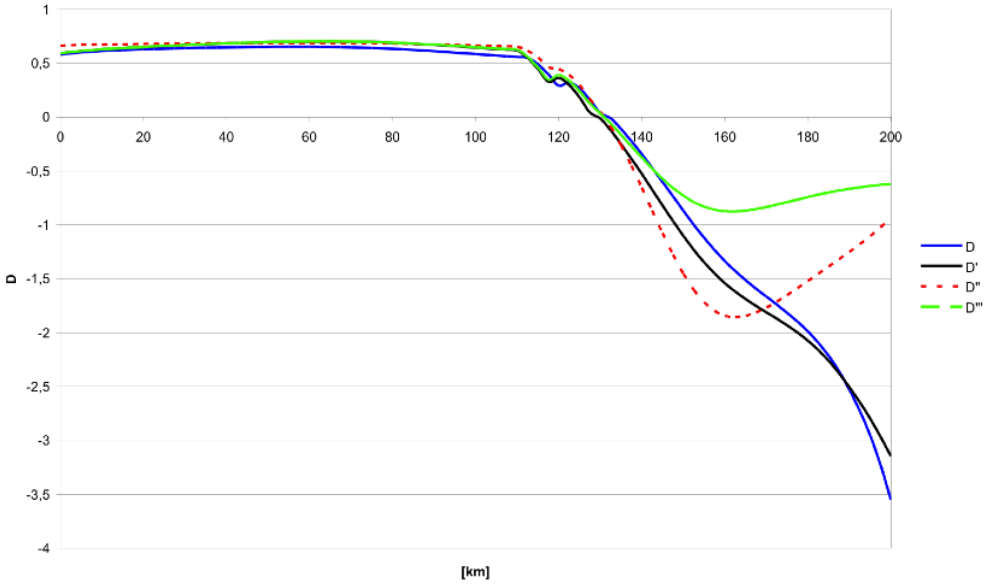

Figure 3.7: The variation of the damping term along the axis of the Schelde estuary. D indicates the damping term obtained by Equation (3.50), using observed values of $\mathrm{d}\eta/\mathrm{d}x$. D'' was obtained with Equation (3.53), D''' by substituting (2.93) in (3.50), and D' by using the equation of Horrevoets et al. (2004) that accounts for the effect of river discharge on tidal damping.

summarised in Table 3.3. They constitute: the "Phase Lag equation" (Eq. 2.85), the "Geometry-Tide relation" (Eq. 2.93), the "Scaling equation" (Eq.2.97), the "Damping equation" (Eq.3.19) and the "Celerity equation" (Eq.3.53). These equations are also compared to their "classical" counterparts, which have been used widely in the past. The basic requirement for these equations to apply is that the geometry should be exponential and that the estuary should be 'long'. But even for short estuaries the equations can be used if we relax the assumption that the damping of the tidal amplitude and the tidal velocity are equal.

Table 3.3: Overview of the set of analytical equations

Name	Equation number	Newly derived equation	"Classical" equation
Phase Lag equation	(2.96)	$\tan\varepsilon = \frac{\omega a}{c(1-\delta_U a)}$	
Geometry-Tide relation	(2.95)	$\frac{H}{E} = \frac{\eta\omega}{\upsilon} = \frac{\overline{h}}{r_s a}\frac{(1-\delta_U a)}{\cos(\varepsilon)}$	$\frac{\eta\omega}{\upsilon} = \frac{\overline{h}}{r_s a}$
Scaling equation	(2.97)	$r_s\frac{\eta}{h} = \frac{\upsilon}{c}\frac{1}{\sin(\varepsilon)}$	$r_s\frac{\eta}{h} = \frac{\upsilon}{c}$
Damping equation	(3.54)	$\frac{1}{\eta}\frac{\mathrm{d}\eta}{\mathrm{dx}} = \delta_H = \frac{1}{2}\left(\frac{1}{a} - f'\frac{\upsilon^2}{\eta g\overline{h}}\right)$	$\frac{1}{\eta}\frac{\mathrm{d}\eta}{\mathrm{dx}} = \frac{1}{2b}$
Celerity equation	(3.55)	$c^2 = c_0^2/\left[1 - \frac{c_0^2}{\omega^2}\frac{(1-\delta_H a)}{a}\delta_H\right]$	$c^2 = c_0^2 = \frac{1}{r_s}g\overline{h}$

The main innovation of these equations compared to their classical counterparts is: 1) the prominent presence of the phase lag ε, 2) the role attributed to tidal damping, and 3) the balance between convergence and friction. These three effects are often disregarded in classical analysis or treated in conflicting ways. In analysing the effect of these factors, it is interesting to look at when an equation collapses into its classical counterpart. The Geometry-Tide relation equals the classical equation when damping is zero and $\varepsilon = 0$ (a standing wave). The scaling equation, however, is the same as the classical counterpart when $\varepsilon = \pi/2$ (a progressive wave). Obviously if one uses these two classical equations jointly in a certain situation there is a serious lack of compatibility.

The classical counterpart of the Damping equation is "Green's law" derived from the conservation of energy equation for a frictionless tidal wave. Jay (1991) demonstrated its limitations, but it is interesting to see the similarity with the more general equation derived here. Green's law coincides with the damping equation for zero friction ($f' = 0$). In fact, Green's law is a special case of the Damping equation.

The celerity equation equals its classical counterpart if friction and convergence are balanced so that damping is zero (the condition for the ideal estuary). Moreover, we see that the celerity equation collapses into the classical equation when $\cos\varepsilon = 0$, which is the case of a progressive wave.

Where the classical equations are contradictory in their assumptions (some assume a standing wave, some a progressive wave; some assume friction or convergence, while others don't) the equations in Table 3.3 are consistent and compatible. They are general versions of their "classical" counterparts, with the most important difference being the account they take of the phase lag between HW and HWS. This makes the Estuary-Type Number ($N_E = \sin\varepsilon$) a key parameter in tidal hydraulics. One can conclude that the analytical equations, while remaining simple, are a substantial improvement over the classical equations and that they provide new insight into the propagation of tidal waves under damped or amplified conditions. They are the result of an integrated theory for wave celerity and wave attenuation in which the phase lag between high water and high water slack plays a key role; the phase lag being a fundamental characteristic of an alluvial estuary, which is generally disregarded in perturbation analysis.

3.3 Explicit solution of the set of equations

The beauty of the set of equations is not only that they form a consistent set of analytical solutions of the St Venant equations, but also that they can be solved explicitly. Until here we have presented them as implicit equations, meaning that each equation contains parameters of the other, whereby it is not simple to express one of the variables explicitly as a function of known input parameters. In this section, based on Toffolon et al. (2006) and Savenije et al. (2008), we show that by scaling and subsequent mathematical manipulation this is indeed possible, and thereafter we shall explore the asymptotic behaviour of these equations.

3.3.1 Scaling the equations

We shall introduce a number of dimensionless parameters, some of which have been used before, but for completeness we shall here present the full set:

$$\zeta = \eta/\bar{h} \tag{3.56}$$

$$\lambda = c_0/c \tag{3.57}$$

where ζ is the dimensionless tidal amplitude and λ is the celerity number indicating the ratio of the classical wave celerity to the actual wave celerity. We then introduce the dimensionless friction parameter χ, the dimensionless estuary shape number γ, and the velocity number μ:

$$\gamma = \frac{c_0}{\omega a} \tag{3.58}$$

$$\chi = r_S f \frac{c_0}{\omega \bar{h}} \zeta = \chi_0 \zeta \tag{3.59}$$

$$\mu = \frac{1}{r_S} \frac{v}{\zeta c_0} = \frac{1}{r_S} \frac{v\bar{h}}{\eta c_0} \tag{3.60}$$

The estuary shape number γ depends on the ratio of the square root of the depth to the convergence length and on the storage width ratio. It is the main indicator for estuary shape. In γ we use the cross-sectional convergence length instead of the width convergence length. This means that we base the derivations on (2.27) instead of (2.26). Note that the independent variables are generally γ and χ_0, which depend on the estuary shape and friction; ζ, λ and μ are dependent variables. Since μ represents the proportion of the Froude number to the tidal amplitude to depth ratio, it is the key variable in the scaling equation. Finally, we need a dimensionless damping/amplification number:

$$\delta = \frac{1}{\eta} \frac{\mathrm{d}\eta}{\mathrm{d}x} \frac{c_0}{\omega} \tag{3.61}$$

With these parameters we shall scale the "phase lag equation" based on (2.85), the "scaling equation" based on (2.97), the "damping equation" based on (3.19), and the "celerity equation" based on (3.53). We then obtain the following scaled and far more simple equations:

The phase lag equation

$$\tan\varepsilon = \frac{\lambda}{\gamma - \delta} \tag{3.62}$$

The scaling equation

$$\mu = \frac{\sin\varepsilon}{\lambda} = \frac{\cos\varepsilon}{\gamma - \delta} \tag{3.63}$$

The damping/amplification equation

$$\delta = \frac{\mu^2}{\mu^2 + 1}\left(\gamma - \chi\mu^2\lambda^2\right) \tag{3.64}$$

The celerity equation

$$\lambda^2 = 1 - D = 1 - \delta\frac{\cos\varepsilon}{\mu} = 1 - \delta\left(\gamma - \delta\right) \tag{3.65}$$

The second form of the scaling equation corresponds with the "geometry-tide" relation, which in fact is a combination of the scaling equation and the phase lag equation. All these are relatively simple algebraic expressions, which is surprising, knowing how complex the set of partial differential equations is. Of the 4 equations the damping equation is the most complex one, but we shall see in the following that this equation can be simplified even further.

3.3.2 Solving the equations explicitly

This set of equations can in principle be solved iteratively, but it is also amenable to an analytical solution, as was shown by Toffolon et al. (2006) and Savenije et al. (2008). Given the non-linear character of the system, two families of solutions appear to exist: the standing wave solution and the mixed wave solution, separated by the point of critical convergence.

Making use of the trigonometric equation $\cos^{-2}\varepsilon = 1 + \tan^2\varepsilon$, (3.62) and (3.63) can be combined to eliminate the phase lag, giving:

$$\left(\gamma - \delta\right)^2 = \frac{1}{\mu^2} - \lambda^2 \tag{3.66}$$

Equations (3.64) and (3.65) can be rewritten as:

$$\gamma - \delta = \chi\mu^2\lambda^2 + \frac{\delta}{\mu^2} \tag{3.67}$$

$$\gamma - \delta = \frac{1 - \lambda^2}{\delta} \tag{3.68}$$

Isolating λ^2 from (3.68) and substituting into (3.66) and (3.67), we can write two equations in the unknowns δ and μ. After some algebra, it is possible to obtain a single tenth order equation for μ:

$$\frac{\left(\chi^2\mu^6 + \gamma\chi\mu^4 + 2\mu^2 - 2\right)\left(\mu^2 - \gamma\mu + 1\right)\left(\mu^2 + \gamma\mu + 1\right)}{\mu^2\left(\gamma\chi\mu^4 + 2\mu^2 + 2\right)} = 0 \tag{3.69}$$

The denominator of (3.69) is always strictly positive in physically meaningful cases. Concerning the numerator, the relationships delimited by the first and second parentheses give rise to two different families of solutions (the first family representing the mixed tidal wave and the second family the standing wave), which will be considered separately below. The equation delimited by the third parenthesis gives no positive roots for μ.

Solution for the mixed wave (the first family of solutions)

We can now derive simpler relationships considering only a single family of solutions. Introducing (3.67) and (3.68) into (3.66), we end up with

$$\lambda^2\left[\delta\left(1 - \frac{1}{\mu^2}\right) + \chi\mu^2\left(1 - \lambda^2\right)\right] = 0 \tag{3.70}$$

which can be simplified for $\lambda^2 \neq 0$, neglecting the second family of solution. In this case, (3.70) along with (3.67) gives a simple expression for the damping/amplification equation, relating δ to μ:

$$\delta_m = \frac{1}{2}\left(\gamma - \chi\mu_m^2\right) \tag{3.71}$$

where the subscript m denotes the mixed tidal wave. In dimensional form, this is the same equation as the Damping equation (3.54).

Where (3.64) is a general version of the damping equation (including the occurrence of a standing wave), (3.71) is a much simpler equation, which is similar to damping equations derived by others, as we shall see in Section 3.4. In (3.71) we still see the balance between friction and convergence, where the condition for an ideal estuary is that $\gamma = \chi\mu_m^2$.

Substituting (3.71) into (3.68) it is also possible to find

$$\lambda_m^2 = \frac{\chi^2\mu_m^4 - \gamma^2}{4} + 1 \tag{3.72}$$

These two equations for δ_m and λ_m can be used to eliminate δ and λ from (3.66). This leads to a single equation for μ_m:

$$\chi^2\mu_m^6 + \gamma\chi\mu_m^4 + 2\mu_m^2 - 2 = 0 \tag{3.73}$$

which corresponds to the first family of solution of (3.69) and represents the propagation of a mixed wave with $0 < \varepsilon < \pi/2$. It can be solved as a third-order equation in μ^2. The real solution is:

$$\mu_m = \sqrt{\frac{1}{3\chi}\left(m - \gamma + \frac{\gamma^2 - 6}{m}\right)} \tag{3.74}$$

with:

$$m = \left[27\chi + \left(9 - \gamma^2\right)\gamma + 3\sqrt{3}\sqrt{27\chi^2 + 2\left(9 - \gamma^2\right)\gamma\chi + 8 - \gamma^2}\right]^{1/3}, \tag{3.75}$$

With this solution for μ_m, explicit solutions can be obtained for λ_m, δ_m, and ε_m, by substitution in (3.72), (3.71) and (3.62), respectively.

Critical convergence

Equations analogous to (3.73) can be written also for the other unknowns. For instance, the equation for λ reads

$$16\lambda_m^6 + 8\left(\gamma^2 - 4\right)\lambda_m^4 + \left[\left(\gamma^2 - 4\right)^2 + 4\left(\gamma\chi + 1\right)\right]\lambda_m^2 - \left[\chi^2 - \left(\gamma^2 - 4\right)\left(\gamma\chi + 1\right)\right] = 0, \tag{3.76}$$

which can be seen as a third-order equation in λ_m^2. The solution is physical only if real roots exist, i.e. if $\lambda^2 \geq 0$. If $\lambda^2 = 0$ the threshold condition, according to (3.76), reads

$$\chi^2 - \left(\gamma_c^2 - 4\right)\left(\gamma_c\chi + 1\right) = 0, \tag{3.77}$$

where γ_c is the limit for critical convergence, defined as the threshold condition for the transition from the mixed tidal wave (first family of solutions) to the standing wave (second family). Below we show that the second family of solution is completely determined by the convergence alone. Hence, critical convergence can also be defined as the limit for which the solution is influenced by friction. For weak friction, this boundary for critical convergence is similar to the one defined by Jay [1991] as the convergence rate at which convergence and acceleration effects are equal and opposed. For a frictionless tidal wave $\gamma_c = 2$, which is the same value as obtained by Jay (1991). At this point the phase lag approaches zero, which is similar to the impedance phase ϕ of 90°, obtained by Jay (1991). On the other hand, when friction becomes important, the two definitions of critical convergence lead to different results.

The relationship (3.77) defines the region of existence of critical convergence in the $\chi - \gamma$ plane and can be solved for one of the two parameters as a function of the other one. The expression for χ where $\gamma = \gamma_c$ reads:

$$\chi(\gamma_c) = \frac{1}{2}\gamma_c\left(\gamma_c^2 - 4\right) + \frac{1}{2}\left(\gamma_c^2 - 2\right)\sqrt{\gamma_c^2 - 4} \tag{3.78}$$

where the condition $\gamma_c \geq \sqrt{2}$ (which is always satisfied, because $\gamma_c \geq 2$) has been used to simplify the solution. The inverse solution for γ is a more complex expression:

$$\gamma_c = \frac{1}{3\chi}\left[\frac{m_1}{2} - 1 + 2\frac{\left(12\chi^2 + 1\right)}{m_1}\right] \tag{3.79}$$

with

$$m_1 = \left[36\chi^2\left(3\chi^2 + 8\right) - 8 + 12\chi\sqrt{3}\sqrt{\left(\chi^2 - 2\right)^2\left(27\chi^2 - 4\right)}\right]^{1/3} \tag{3.80}$$

The threshold condition is shown in Figure 3.8: the solution for the mixed wave exists for $\gamma < \gamma_c(\chi)$, where γ_c is the threshold for critical convergence, which increases with starting from $\gamma_c = 2$ for the frictionless case.

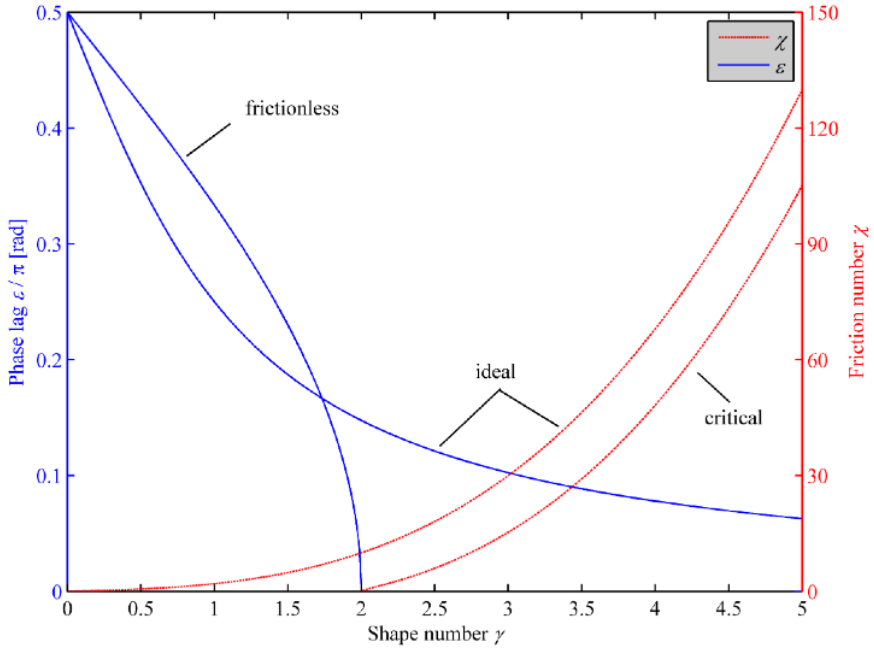

Figure 3.8: Phase lag ε and friction parameter χ as a function of convergence parameter γ under special conditions:.

Solution for the standing wave (the second family of solutions)

Beyond critical convergence, the tidal wave behaves as a synchronous standing wave, where HW and LW are reached simultaneously along the estuary. This is the second family of solutions. For a standing wave $\lambda = 0$ applies, which is the solution we have excluded in the simplification of equation (3.70) used to derive the first case. Imposing $\lambda = 0$ in the set of equations, we find that (3.66) is redundant since it is exactly the product of (3.67) and (3.68). Then, equating the latter two equations, one easily obtains:

$$\mu_s^2 - \gamma\mu_s + 1 = 0 \tag{3.81}$$

$$\mu_s = \delta_s \tag{3.82}$$

$$\varepsilon_s = 0 \tag{3.83}$$

where the subscript s stands for the standing wave solution, which pertains to the case where $\gamma > \gamma_c(\chi)$. Equation (3.83) follows directly from (3.62).

These equations corresponds to the second family of solutions of equation (3.69). Equation (3.81) gives real solutions only if $\gamma \geq 2$, which means beyond critical convergence; the physical solution hence reads:

$$\mu_s = \frac{1}{2}\left(\gamma - \sqrt{\gamma^2 - 4}\right) \tag{3.84}$$

If γ goes to infinity, this equation will approach $\mu_s = 1/\gamma$. Similarly we can derive the damping equation for a standing wave:

$$\delta_s = \frac{1}{2}\left(\gamma - \sqrt{\gamma^2 - 4}\right) \tag{3.85}$$

which again gives the limit $\delta_s = 1/\gamma$ when γ goes to infinity.

The threshold condition (3.77) ensures that the transition between the two families of solution is smooth from the mixed tidal wave, given by (3.76), to the apparent standing wave where $\lambda = 0$. It is possible to demonstrate that also the transition between the solutions (3.74) and (3.84) is continuous.

We now have explicit solutions for the variables mu, lambda, delta and epsilon for both the standing and the mixed wave. In the following we shall consider a number of special solutions and we shall explore the asymptotic behaviour of the equations.

3.3.3 Specific solutions and asymptotic behaviour of the equations

In the following we analyse particular (asymptotic) solutions of the mixed wave that correspond with the situation 1) a constant cross-section, or 2) the ideal estuary, or 3) the frictionless estuary. Finally we shall analyse the asymptotic behaviour of the damping equation as x goes to infinity.

Solution for an estuary with constant cross-section

A special case of the mixed wave solution is the situation where there is no convergence, i.e. when $\gamma = 0$. In that case equations (3.71), (3.63) and (3.65) yield:

$$\delta_0 = -\mu_0^2 \frac{\chi}{2} \tag{3.86}$$

$$\cos\varepsilon_0 = -\mu_0\delta_0 = \frac{\chi}{2}\mu_0^3 \tag{3.87}$$

$$\tan\varepsilon_0 = -\frac{\lambda_0}{\delta_0} = -\frac{\sqrt{1+\delta_0^2}}{\delta_0} \tag{3.88}$$

$$\lambda_0^2 = 1 + \left(\frac{\chi\mu_0^2}{2}\right)^2 \tag{3.89}$$

where the subscript 0 denotes the zero convergence situation. Using (3.74), and the condition that $\gamma = 0$, we can derive explicit expressions for μ_0, δ_0, ε_0 and λ_0:

$$\mu_0 = \sqrt{\frac{m_0^2 - 6}{3m_0\chi}} \tag{3.90}$$

with:

$$m_0 = 3\left(\chi + \sqrt{\chi^2 + \frac{8}{27}}\right)^{1/3} \tag{3.91}$$

$$\delta_0 = -\frac{m_0^2 - 6}{6m_0} \tag{3.92}$$

$$\cos\varepsilon_0 = \frac{1}{2\sqrt{\chi}}\left(\frac{m_0^2 - 6}{3m_0}\right)^{3/2} \tag{3.93}$$

$$\tan\varepsilon_0 = \sqrt{1 + \left(\frac{6m_0}{m_0^2 - 6}\right)^2} \tag{3.94}$$

$$\lambda_0^2 = 1 + \left(\frac{m_0^2 - 6}{6m_0}\right)^2 \tag{3.95}$$

With these equations the damping and phase lag of a wave in an estuary with a constant cross-section can be computed. We see that the damping, wave propagation and phase lag purely depend on the friction ratio, which is in agreement with the literature (e.g., Lorentz, 1926; Lamb, 1932; Dronkers, 1964; Ippen, 1966a; Van Rijn, 1990). In these solutions the tidal amplitude is damped exponentially and the tidal wave celerity is reduced accordingly. All these authors used linearized St Venant equations and a constant damping number (exponential damping). As a result, their equations for the tidal wave propagation in a channel of constant cross-section under the influence of friction are less accurate and less general than the solution presented here.

In the special case of no friction we obtain $m_0 = \sqrt{6}$ and hence, as expected, that $\lambda_0 = 1$ (the classical wave celerity) and $\delta_0 = 0$ (no damping). One can also demonstrate that as χ approaches zero, μ_0 approaches unity and ε_0 approaches $\pi/2$: the case of the undamped progressive wave.

Solution for an ideal estuary

An interesting special case of the first family of solutions (the mixed tidal wave) is that of the ideal estuary (subscript I), where there is neither tidal damping nor amplification. Hence, where:

$$\delta_I = 0 \tag{3.96}$$

In this case, the system (3.66)-(3.68) yields:

$$\lambda_I^2 = 1 \tag{3.97}$$

$$\mu_I^2 = \frac{1}{\gamma^2 + 1} = \frac{\gamma}{\chi_I} \tag{3.98}$$

which is the condition of solubility (representing the relationship between friction and convergence parameters necessary to obtain a balance between damping and amplification of the wave amplitude). This yields:

$$\chi_I = \gamma\left(\gamma^2 + 1\right) \tag{3.99}$$

which has been tested against numerical results in Toffolon et al. (2006). The phase lag can be estimated from equation (3.62):

$$\tan\varepsilon_I = \frac{1}{\gamma} \tag{3.100}$$

In addition, it follows from substitution of these values in (3.63) that:

$$sin\varepsilon_I = \mu_I = \sqrt{\frac{\gamma}{\chi_I}} = \sqrt{\frac{1}{\gamma^2 + 1}} \tag{3.101}$$

$$cos\varepsilon_I = \gamma\mu_I = \sqrt{\frac{\gamma^3}{\chi_I}} = \sqrt{\frac{\gamma^2}{\gamma^2 + 1}} \tag{3.102}$$

These relations for χ_I and ε_I are also presented in Figure 3.8.

Solution for a frictionless estuary

Finally, a special case of the first family of solutions is the frictionless estuary. The second family of solutions, already is independent of friction. This is because in the damping equation (3.19) the friction is neutralised if $\varepsilon = 0$. In fact, an apparent standing wave has zero velocity at HW and LW and, as a result, the friction term falls out of the equation in the derivation of (3.19) (Savenije, 2001b). If a mixed wave has an infinitely small tidal amplitude, or if the estuary is frictionless, we also obtain $\chi = 0$. Under that condition, the expression for the velocity number (3.73) simplifies substantially, leading to:

$$\mu_f = 1 \tag{3.103}$$

where the subscript f denotes the frictionless situation. In addition we find:

$$\delta_f = \gamma/2 \tag{3.104}$$

$$\lambda_f^2 = 1 - (\gamma/2)^2 \tag{3.105}$$

and

$$\cos\varepsilon_f = \gamma/2 \tag{3.106}$$

$$sin\varepsilon_f = \lambda_f \tag{3.107}$$

The special case of a frictionless estuary with constant cross-section ($\gamma = 0$) results in a purely progressive wave, with $\varepsilon = \pi/2$, $\delta = 0$ and $\lambda = 1$.

In Figures 3.13 3.16 we present diagrams of the solution of the mixed and standing wave, indicated by the red lines. The curves representing the frictionless situation are clearly visible as thick lines in the graphical representations. The mixed wave equations for δ_f and $\cos(\varepsilon_f)$ are simply straight lines; the equation for λ_f^2 is a parabola. Surprisingly, the equations describing $\cos(\varepsilon)$ and δ appear to behave as near-straight lines for the cases with friction as well.

Table 3.4 present a summary of the 5 equations in the mixed wave, the standing wave, and for constant cross-section.

Table 3.4: Dimensionless equations for tidal wave propagation in alluvial estuaries.

Name	**Mixed wave**	**Standing wave**	**Constant Cross-section**
Phase Lag equation	$\tan\varepsilon = \frac{\lambda}{\gamma-\delta}$	$\varepsilon = 0$	$\tan\varepsilon = -\frac{\lambda}{\delta}$
Geometry-Tide relation	$\mu = \frac{\cos(\varepsilon)}{\gamma-\delta}$	$\mu = \frac{1}{2}\left(\gamma - \sqrt{\gamma^2-4}\right)$	$\mu = -\frac{\cos(\varepsilon)}{\delta}$
Scaling equation	$\mu = \frac{\sin(\varepsilon)}{\lambda}$		$\mu = \frac{\sin(\varepsilon)}{\lambda}$
Damping equation	$\delta = \frac{1}{2}\left(\gamma - \chi\mu^2\right)$	$\delta = \frac{1}{2}\left(\gamma - \sqrt{\gamma^2-4}\right)$	$\delta = -\frac{1}{2}\chi\mu^2$
Celerity equation	$\lambda^2 = 1 - \delta\left(\gamma - \delta\right)$	$\lambda = 0$	$\lambda^2 = 1 + \delta^2$

Asymptotic behaviour of the damping equation

We start from the damping equation of the mixed wave. If we introduce the dimensionless tidal amplitude $y = \eta/\eta_0$, then the damping equation can be written as:

$$\frac{\mathrm{d}y}{\mathrm{d}x} = \frac{y}{2a}\left(1 - \frac{y}{\beta}\right) \tag{3.108}$$

where β is the ideal dimensionless amplitude defined as:

$$\beta = \frac{\gamma}{\chi_0 \mu^2} \frac{h}{\eta_0} \tag{3.109}$$

Because (3.108) applies to the mixed wave alone, it is a simpler equation than the general dimensionless equation of (3.26). Analogous to that equation we see that convergence and friction are in balance if $y = \beta$, so that there is no tidal damping or amplification. In fact there are two situations where there is no damping. The first one is the trivial situation where $y = 0$, and the other is where $y = \beta$.

We can integrate this equation if we assume that β is constant with x, which is correct if μ is constant along the estuary axis. From the definition of μ, this is the case when there is no bottom slope, the storage ratio is constant, and the ratio of the velocity amplitude and the tidal amplitude is fixed ($\delta_u = \delta_H$). For a general performance analysis this is a reasonable assumption. Further down we shall check specifically if this is a correct assumption for the asymptotic solution.

Upstream asymptotic behaviour

For constant β we can integrate x as a function of y, resulting in:

$$\int \frac{\mathrm{d}x}{2a} = \int \frac{\mathrm{d}y}{y\,(1 - y/\beta_c)} \tag{3.110}$$

where β_c is the constant β-value. Using the boundary condition that $y = 1$ at $x = 0$ yields:

$$\frac{x}{2a} = ln\left(\frac{1 - \beta_c}{1 - \beta_c / y}\right) \tag{3.111}$$

or:

$$y = \frac{\beta_c}{1 - (1 - \beta_c)\, exp\,(-x/(2a))} \tag{3.112}$$

In the asymptotic situation where x goes to infinity, this implies that:

$$y_{inf} = \beta_c = \frac{\gamma}{\chi_0 \mu^2} \frac{h}{\eta_0} = \frac{\chi_I \mu_I^2}{\chi \mu^2} \frac{\eta_{inf}}{\eta_0} \tag{3.113}$$

where the second step in (3.113) follows from using expression (3.98) for μ. This implies that in the upstream asymptotic situation the amplitude tends to an ideal estuary with constant amplitude. If $y_{inf} > 1$, then the estuary is amplified; if $y_{inf} < 1$, then it is damped; and if $y_{inf} = 1$, the estuary is ideal.

Using (3.98) for μ of an ideal estuary, the amplitude then becomes:

$$\eta_{inf} = \beta \eta_0 = \frac{\gamma\left(\gamma^2 + 1\right)}{\chi_0} \frac{h}{\eta_0} = \frac{\omega}{c_0} \gamma\left(\gamma^2 + 1\right) \frac{h^2}{r_S f} \tag{3.114}$$

or:

$$\zeta_{inf} = \frac{h}{a} \frac{\left(\gamma^2 + 1\right)}{r_S f} \tag{3.115}$$

which are expressions that only depend on the geometry and the friction, and are independent on the boundary conditions. The caveat is that the equation applies to long estuaries where we may assume that $\delta_u \approx \delta_H$. We can see that in deep convergent estuaries (with large γ), this can lead to a large equilibrium amplitude. Using the scaling equation to elaborate this equation together with (3.97) and (3.101) implies that:

$$\frac{v_{inf}}{c_0} = \frac{h}{a} \frac{\sqrt{\gamma^2 + 1}}{f} \tag{3.116}$$

It is interesting to note that if an estuary is long enough, the system will readjust until the conditions of the ideal estuary are achieved. This is an indication that the ideal estuary is the energetically stable state of an estuary to which the forces of nature converge. Also note that the variables in these equations are all independent variables related to the geometry and the friction, and hence that the asymptotic state is independent of the tidal forcing.

Downstream asymptotic behaviour

Near the estuary mouth, we can also look at the asymptotic behaviour. To what extent is the damping exponential? We can approach the longitudinal damping or amplification of the tidal amplitude by a Taylor series:

$$y \approx y_0 + y_0' x + y_0'' \frac{x^2}{2} + ... \tag{3.117}$$

On the basis of (3.108) we can determine the second derivative, but in this case we cannot assume β to be constant:

$$y'' = \frac{\mathrm{d}^2 y}{\mathrm{d}x^2} = \frac{1}{(2a)^2}\left(y - (3 - 2\delta_\beta a)\frac{y^2}{\beta} + 2\frac{y^3}{\beta^2}\right) \tag{3.118}$$

Substitution of $y_0 = 1$ yields:

$$y \approx 1 + \frac{x}{2a}\left(1 - \frac{1}{\beta}\right) + \frac{1}{2}\left(\frac{x}{2a}\right)^2\left(1 - \frac{3 - 2\delta_\beta a}{\beta} + \frac{2}{\beta^2}\right) + ... \tag{3.119}$$

In a region close enough to the mouth where $x < 2a$, we can see that, if β is constant, the damping or amplification behaves as a linear function. If β is very large, then the slope is $1/(2a)$. For small values of β the gradient becomes negative and the steeper it gets, the less linear the behaviour. A large value of β occurs in deep and strongly converging estuaries, which are generally amplified. Hence we see that amplification is often linear, as is the case in the Schelde. The region where amplification is linear may extend over quite some distance into the estuary. The non-linear (exponential) effect only becomes apparent when we move further upstream. In contrast we see that the process of damping is never linear but closer to an exponential function.

To see if the above Taylor series is similar to a Taylor series of exponential damping with $y = \exp(\delta_H x)$, we can develop the exponential equation in a Taylor series (making use of (3.108) to determine δ_H). We can then see that the first two terms are only the same as in (3.119) if $y = 1$, but that the third term has a different structure. So the exponential approximation is not correct in general, but not too bad in near ideal estuaries where y is close to unity.

3.4 Other formulations for the friction term

The most difficult nut to crack in solving the St. Venant equations analytically is how to deal with the non-linear friction term. The classical way is to use Lorentz' linearization, that dissipates the same amount of energy as the non-linear friction term. Dronkers (1964) did the same, but considered an over-tide and by doing so catered for the major part of the non-linearity inherent in the friction term. Our approach presented in section 3.2 does also retain the nonlinearity inherent in the friction term, by considering the envelopes at HW and LW and assuming that the tidal velocities at these point in time can be adequately described by $v \sin\varepsilon$ and $-v \sin\varepsilon$ respectively, which is another way of solving the non-linearity problem. Because it still uses the sine function to describe the velocity at HW and LW it is called a quasi-nonlinear method.

In this section we shall compare different formulations of the friction term and see how they compare to observations. It is largely based on the work of Cai et al. (2012b). We'll see that a combination of the linear and quasi-nonlinear approach performs remarkably well, while still allowing simple analytical solution.

3.4.1 Different formulations of the damping equation

The linearised friction term

Lorentz's linearization (Lorentz, 1926) of the friction term R reads:

$$R_L = \frac{8}{3\pi}\frac{v}{K^2 \overline{h}^{4/3}}U \tag{3.120}$$

which is a slightly different formulation as in (2.47).

Following the procedure proposed by Savenije (2005) and considering the linearized friction term (3.120), instead of the quasi-nonlinear friction term (2.5), in the momentum equation, it is possible to obtain the linear damping equation Toffolon and Savenije (2011):

$$\delta = \frac{\gamma}{2} - \frac{4}{3\pi}\frac{\chi\mu}{\lambda} \tag{3.121}$$

Dronkers' friction term

Dronkers (1964, p. 302) suggested an interesting higher order formulation for the friction term (see also Cartwright (1968)), leading to results that are comparable to those obtained using the fully nonlinear formulation for the friction term. Dronkers (1964) took account of overtide generation by including a third order term (cubic velocity) in the friction term, while also assuming that U is a periodic function with zero mean:

$$R_D = \frac{16}{15\pi}\frac{v^2}{K^2\overline{h}^{4/3}}\left[\frac{U}{v} + 2\left(\frac{U}{v}\right)^3\right] \tag{3.122}$$

Note that this equation does not account for the time variable depth in the friction term. In our symbols the expression for the tidal damping using Dronkers' friction term would read:

$$\delta = \frac{\gamma}{2} - \frac{8}{15\pi}\frac{\chi\mu}{\lambda} - \frac{16}{15\pi}\chi\mu^3\lambda \tag{3.123}$$

3.4.2 Performance of the different friction formulations

In order to investigate the performance of the analytical solutions, they have been compared with a fully nonlinear numerical solution of the governing equations (2.1) and (2.2). The numerical model (Toffolon et al., 2006) is based on the explicit MacCormack method, which is second order accurate both in space and in time. A total variation diminishing (TVD) filter is applied to avoid spurious oscillations, especially when the wave steepens because of frictional or geometrical effects.

Since we focus on the tidal damping in this study, in this section we present a comparison between the values of the dimensionless damping number δ estimated using analytical methods against the fully nonlinear numerical results. We consider a wide range of parameters (with $1 \le \gamma \le 3$, $0.1 \le \zeta \le 0.3$, $10\ \mathrm{m^{1/3}s^{-1}} \le K \le 50\ \mathrm{m^{1/3}s^{-1}}$ and $\overline{h}$=10 m) covering a wide spectrum of tidal channels. In order to present dimensionless results, distance x is scaled by the frictionless wavelength in prismatic channels:

$$x^* = \frac{\omega}{c_0}x \tag{3.124}$$

Figure 3.9 shows the performance of the different analytical models at a single position $x^* = 0.426$ (corresponding to 30 km for a 10 m deep estuary). Both the linear (Toffolon and Savenije, 2011) and the quasi-nonlinear (Savenije et al., 2008) solution behave reasonably well, but none of them is fully correct for a finite amplitude wave. It appears that Dronkers' approach lies closest to the numerical solution, and that Savenije et al. (2008) and Toffolon and Savenije (2011) have a consistent bias from the numerical solution. The former method underestimates the tidal damping, while the latter overestimates it.

The reason for this behavior lies in the different simplifications used in the friction term F. Toffolon and Savenije (2011) used Lorentz's linearization (3.120), which is based on the equal energy dissipated by linear and quadratic friction during a tidal cycle (assuming a sinusoidal tide). On the other hand, working within an original Lagrangean-based approach, Savenije et al. (2008) obtained the effective friction $\widehat{F}_S$ acting over a tidal cycle by subtracting the high water (HW) and low water (LW) envelopes, leading to:

$$\widehat{F}_S = \frac{1}{2}\left[\frac{U_{HW}^2}{K^2\left(\overline{h}+\eta_{HW}\right)^{4/3}} + \frac{U_{LW}^2}{K^2\left(\overline{h}-\eta_{LW}\right)^{4/3}}\right] \tag{3.125}$$

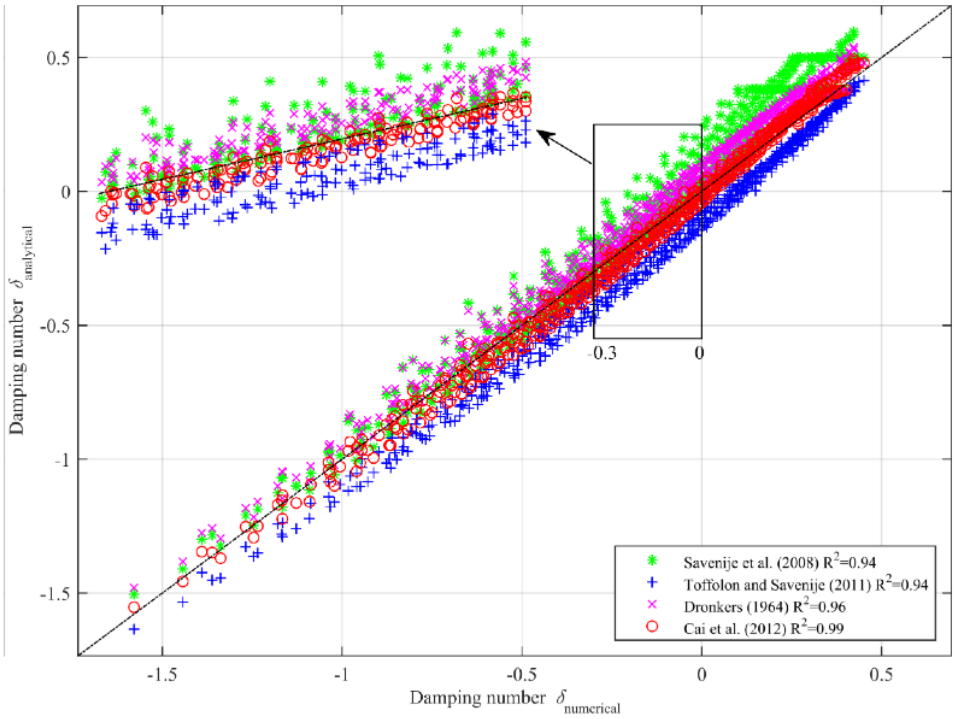

Figure 3.9: Tidal damping δ at $x^* = 0.426$ obtained with four different analytical models, compared to numerical results: The weighted equation by Cai et al. (2012b), i.e. Eq. (3.127); Dronkers (1964), i.e. Eq. (3.123); Savenije et al. (2008), i.e. Eq. (3.64); and Toffolon and Savenije (2011)), i.e. Eq. (3.121). R^2 is the coefficient of determination, which provides an estimate of the average deviation of the estimates of the different analytical models from the assumed correct value (numerical model): the closer R^2 is to unit, the better is the model.

where the two velocities at HW and LW follow from equations (3.10) and (3.11).

These approaches (linearized and quasi-nonlinear), which are correct for the strictly linear case where the tidal wave is a simple harmonic, yield opposite biases in the damping equation for finite-amplitude waves.

This behavior can be clearly seen from Figure 3.10, which compares the friction effectively acting during a tidal cycle considering the different options. The damping in the three standard Eulerian approaches (see also Vignoli et al., 2003)) is based on the definition of a tidally average friction term $\langle |F| \rangle = T^{-1} \int_T |F| \, \mathrm{d}\, t$, where F is estimated as follows: the fully nonlinear definition from (2.5) (blue line), Lorentz's linearization F_L from (3.120) (red dashed line), and Dronkers' relationship F_D from (3.122) (black dash-dot line). On the contrary, Savenije's Lagrangean approach (3.125) directly provides the effective friction $\widehat{F}_S$ (green dashed line), which can be consistently compared with the previous ones. All quantities used in Figure 3.10 are obtained by the numerical model, so the only difference is the approximation used for the friction term. The comparison suggests that the tidally averaged friction term obtained with Lorentz's linearization overestimates the friction along the estuary, while Savenije et al. (2008) model tends to underestimate it. In the middle, the third-order approximation by Dronkers (1964) is very close to the complete nonlinear friction.

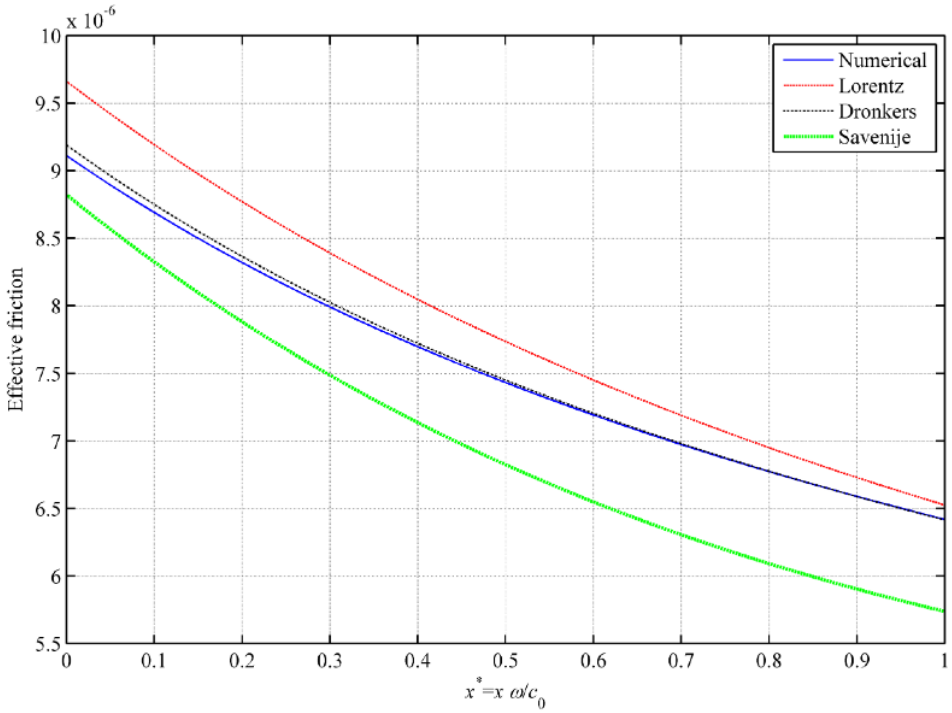

Figure 3.10: Comparison of the tidally averaged friction term $\langle |F| \rangle$ computed with different formulations of the friction term: fully nonlinear (2.5) (blue line), Lorentz's linearization (3.120) (red dashed line), Dronkers' expansion (3.122) (black dash-dot line); and for Savenije's effective friction $\widehat{F}_S$ (3.125) (green dashed line). All estimates are based on variables obtained from numerical results (γ=1, ζ=0.1, K=30 $\mathrm{m}^{1/3}s^{-1}$ and $\overline{h}$=10 m).

3.4.3 A combination of the linear and quasi-non-linear equation

Cai et al. (2012b) demonstrated that, as a whole, the two approaches to calculate the frictional dissipation (i.e., using the linearized friction term or the envelopes of HW and LW) consistently have an opposite bias. Because of this, Cai et al. (2012b) explored if the 'true' damping could be obtained by taking the weighted average of equations (3.121) and (3.71):

$$\delta = \frac{\gamma}{2} - \alpha\frac{4}{3\pi}\frac{\chi\mu}{\lambda} - (1-\alpha)\frac{1}{2}\chi\mu^2 \tag{3.126}$$

For different weights of the linearized friction term α (from 0 to 1), it is possible to compare the values of δ obtained by equation (3.126) with the damping observed in the numerical results for the same wide range of parameters as for Figure 3.9. Figure 3.11 presents the optimum weight α with its standard error at different locations along the estuary and the corresponding coefficient of determination R^2. We can see that the optimum weight α becomes stable from $x^* \simeq 0.35$ onward and that the equilibrium weight for α is about 1/3. The fact that the weight is approximately 1 near the estuary mouth is the result of the imposed harmonic boundary condition without overtides, which is consistent with the linear assumption. The stable values of α that develop in the landward direction indicates that the wave adjusts its shape toward an equilibrium shape.

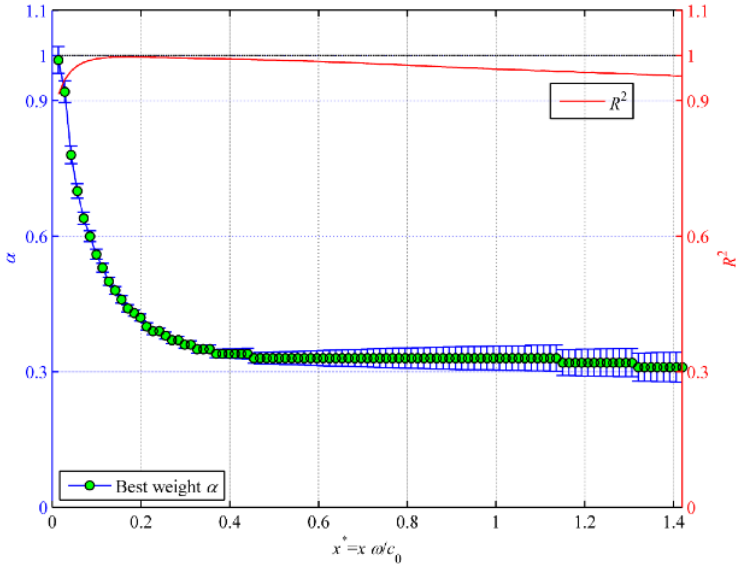

Figure 3.11: Optimum weight of the linearized friction term α with its standard error along the estuary axis and the corresponding coefficient of determination R^2.

Assuming $\alpha = 1/3$, Cai et al. (2012b) obtained a weighted damping equation, which reads:

$$\delta = \frac{\gamma}{2} - \frac{4}{9\pi}\frac{\chi\mu}{\lambda} - \frac{\chi\mu^2}{3} \tag{3.127}$$

This equation is very similar to Dronkers' equation (3.123), which can be rearranged using (3.63) in the following form:

$$\delta = \frac{\gamma}{2} - \frac{2}{5}\frac{4}{3\pi}\frac{\chi\mu}{\lambda} - \frac{32}{15\pi}\sin(\varepsilon)\frac{1}{2}\chi\mu^2 \tag{3.128}$$

Similarly to (3.126), the last two terms of equation (3.128) can be seen as a combination of (3.121) and (3.71), whereby the weights of the linearized and nonlinear models would be $\alpha = 0.4$ and $1-\alpha = 0.68\sin(\varepsilon)$, respectively, which is satisfied if $\varepsilon \simeq \pi/3$, a reasonable value for modestly convergent estuaries.

By iteratively solving the set of four analytical equations (3.62), (3.63), (3.65) and (3.127), we obtain a new analytical solution for the dimensionless parameters μ, δ, λ, and ε. The damping number δ has been compared with the other solutions in Figure 3.9, and we can see that the agreement of equations (3.123) and (3.127) with the numerical model is very good, but the

latter obtains the best result with the highest coefficient of determination $R^2 = 0.99$. Moreover, as we can see from Figure 3.12, where different versions of analytical solutions are compared with numerical results, the weighted damping equation obtains the best result with the highest coefficient of determination R^2 along the estuary axis, except near the mouth of the estuary where the modified linear model (Toffolon and Savenije, 2011) achieves the best result due to the purely harmonic wave imposed at the seaward boundary.

Apparently, by combining the two approaches of Toffolon and Savenije (2011) and Savenije et al. (2008), we have obtained a more accurate analytical model, which is closer to the fully nonlinear numerical solution.

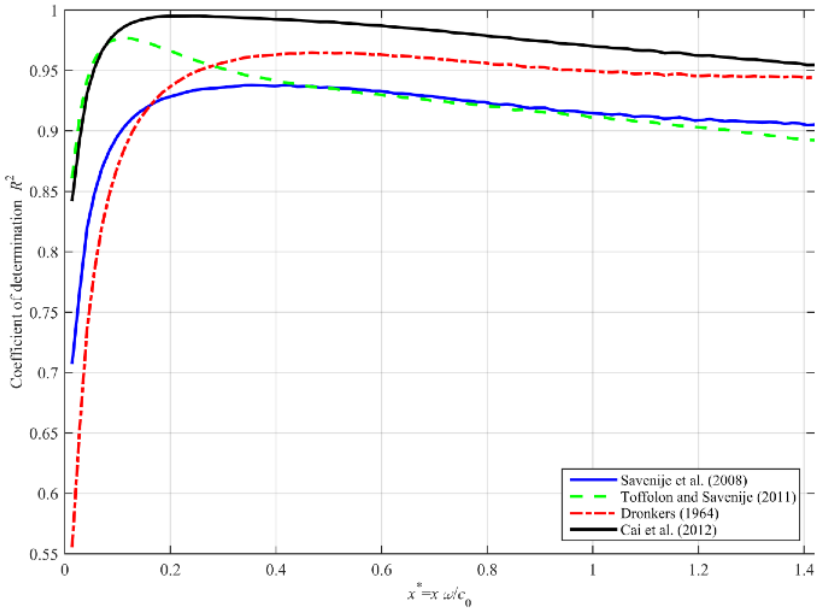

Figure 3.12: Longitudinal variation of the coefficient of determination R^2 between numerical model and different analytical models for a wide range of parameters with $1 \leq \gamma \leq 3$, $0.1 \leq \zeta \leq 0.3$, 10 $\mathrm{m}^{1/3}\mathrm{s}^{-1} \leq K \leq 50$ $\mathrm{m}^{1/3}\mathrm{s}^{-1}$ and $\overline{h}$=10 m.

3.4.4 Performance of the weighted damping equation

Figures 3.13–3.16 present the solution of the velocity number, the damping number, the celerity number, and the phase lag obtained with the different analytical models as a function of γ and χ. In these graphs, the blue symbols represent the weighted method by Cai et al. (2012b) using equation (3.127), whereas the dashed red lines represent the solution of Savenije et al. (2008), the drawn black lines the solution of Toffolon and Savenije (2011), and the dashed-dotted green lines the solution with Dronkers (1964)' friction term. Unlike the equation of Savenije et al. (2008), which had two families of solutions for mixed and standing waves, both the weighted solution and the solutions of Toffolon and Savenije (2011) and Dronkers' approach provide continuous solutions in the transition zone of critical convergence (Jay, 1991) where γ is close to 2. In the weighted method, a clear separation between the subcritical and the supercritical cases exists only for vanishing friction ($\chi = 0$).

Comparing the weighted model with the other three models, we can see in Figures 3.13 3.16 that three zones can be distinguished. For small values of γ (weakly convergent estuaries), the main dimensionless parameters (μ, δ, λ and ε) obtained with the weighted model are closer to the linear solution of Toffolon and Savenije (2011). In the transition zone where critical convergence occurs in the model of Savenije et al. (2008), the result is about the average of Savenije et al. (2008) and Toffolon and Savenije (2011). For larger values of γ (the strongly

convergent estuaries), we can see that the weighted solution is closer to the frictionless case. Moreover, it appears that Dronkers' solution is very close to the weighted solution for an amplified wave with bigger γ, while it is similar to Savenije et al. (2008) for waves with $\gamma < 2$. For an ideal estuary (where friction balances convergence), the four methods are identical.

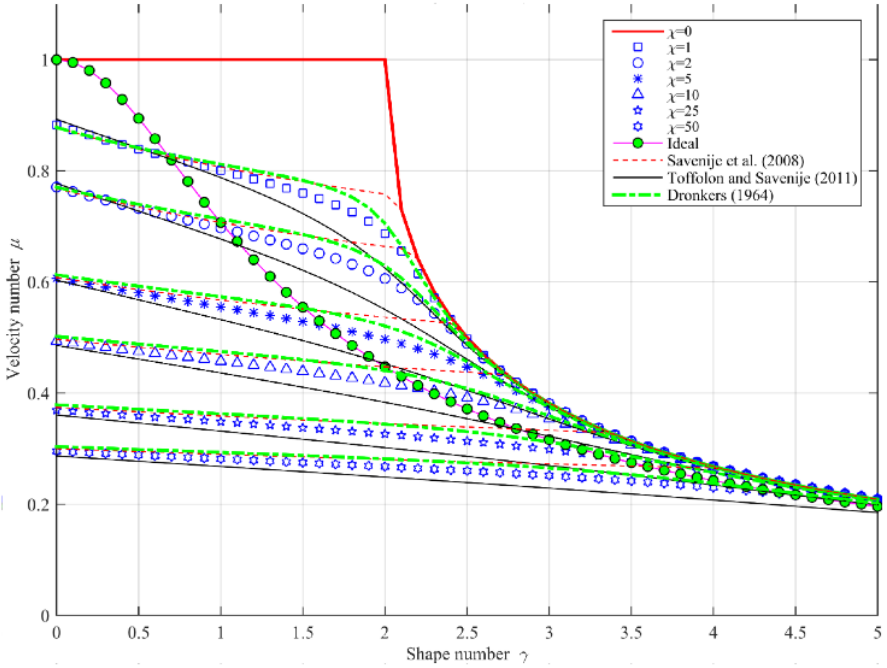

Figure 3.13: Relationship between the velocity number μ (3.60) and the estuary shape number γ (3.58) for different values of the friction number χ (3.59). The blue symbols indicate the weighted model exploiting equation (3.127). The red drawn line represents the frictionless estuary (χ=0). The dashed red lines, drawn black lines, and dashed-dotted green lines represent the solutions obtained by Savenije et al. (2008), Toffolon and Savenije (2011), and Dronkers' approach, respectively. The green round symbols indicate the ideal estuary ($\mu = \sqrt{\frac{1}{1+\gamma^2}}$).

3.4.5 Application to the Schelde estuary

For given geometry, friction, and tidal amplitude at the downstream boundary, the dimensional values of the tidal amplitude η, the velocity amplitude v, the wave celerity c, and the phase lag ε can be computed by using the analytical model presented in section 3.4.4. We have applied the weighted equation to the geometry of the Scheldt estuary, assuming a convergence length for the cross-sectional area a=27 km (see also Horrevoets et al. (2004)). Until 110 km from the mouth of the estuary the flow depth is approximately constant ($\bar{h}$=11 m), while more landward the depth reduces gradually to 2.6 m (assumed estuary length L=200 km). At the estuary mouth (x=0 m), we assume a harmonic tide characterized by a tidal amplitude η_0=2.3 m (spring tide) and a tidal period T=44400 s.

The four analytical models have been compared with observations made in the Scheldt estuary during spring tide on 14-15 June 1995. All models can potentially be made to fit the observations if a suitable friction coefficient is used. However, this calibration provides significantly different values of the Manning-Strickler coefficient: K=32 $\mathrm{m^{1/3}s^{-1}}$ for Savenije et al. (2008)'s model, K=33 $\mathrm{m^{1/3}s^{-1}}$ for Dronkers' approach, K=39 $\mathrm{m^{1/3}s^{-1}}$ for the present model, and K=46 $\mathrm{m^{1/3}s^{-1}}$ for Toffolon and Savenije (2011)'s model. Apparently the differences introduced by using different friction formulations can be compensated by decreasing or increasing the friction coefficient. Therefore, the different analytical models have also been compared with a 1D numerical model in

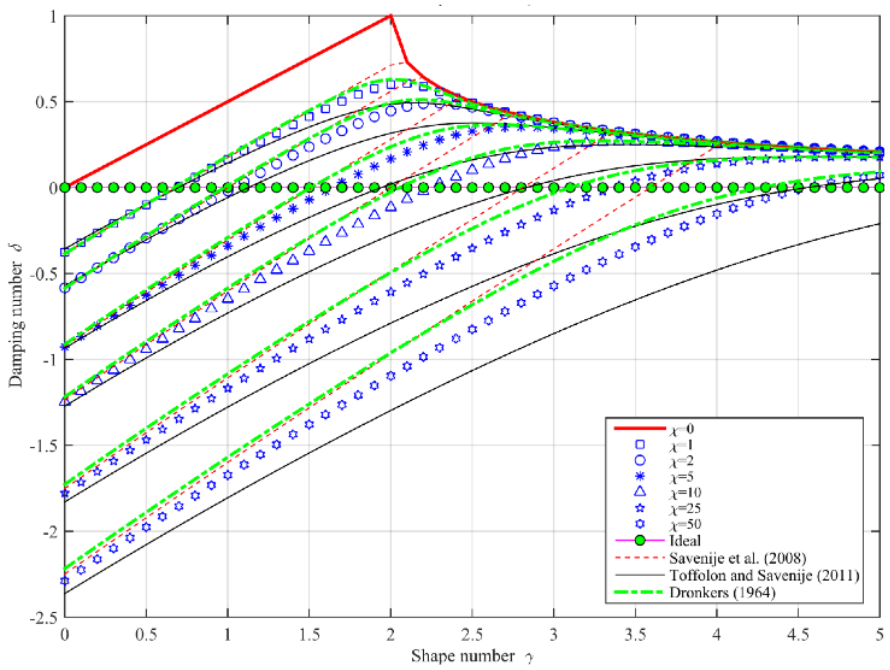

Figure 3.14: Relationship between the damping number δ (3.61) and the estuary shape number γ (3.58) for different values of the friction number χ (3.59). The symbols are as in Figure 3.13. The ideal estuary is defined by δ=0.

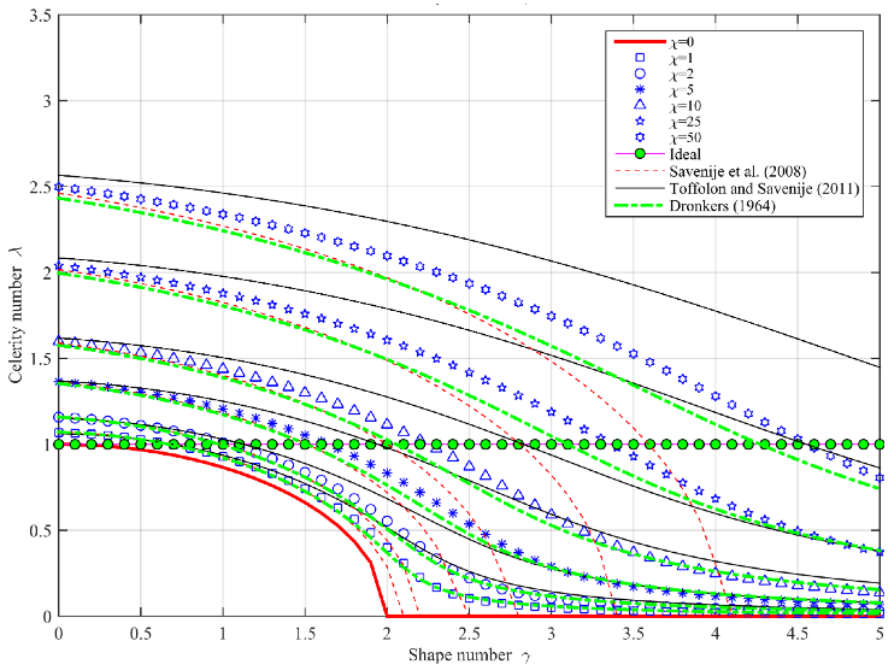

Figure 3.15: Relationship between the celerity number λ (3.57) and the estuary shape number γ (3.58) for different values of the friction number χ (3.59). The symbols are as in Figure 3.13. The ideal estuary is defined by λ=1.

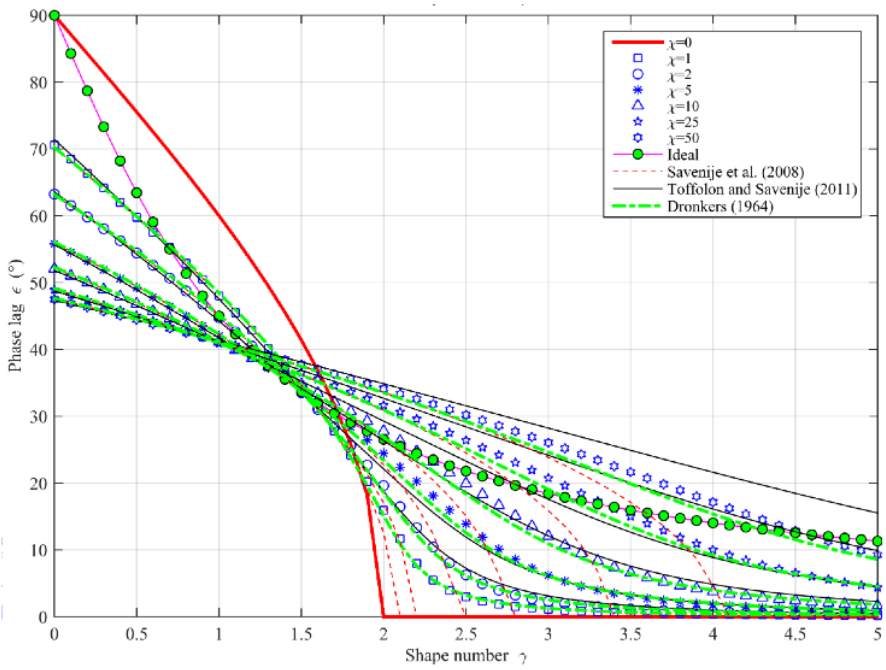

Figure 3.16: Relationship between the phase lag ε and the estuary shape number γ (3.58) for different values of the friction number χ (3.59). The symbols are as in Figure 3.13. The ideal estuary is defined by $\varepsilon = \arctan(1/\gamma)$.

the Scheldt estuary. The calibrated Manning-Strickler friction coefficient K used in the numerical model (38 $m^{1/3}s^{-1}$) appears to be almost the same as the friction coefficient of the weighted model (39 $m^{1/3}s^{-1}$), which is to be expected since the weighted damping equation (3.127) was obtained by calibration of K against numerical solutions. In Figure 3.17, all models use the same friction coefficient K=38 $m^{1/3}s^{-1}$. It can be clearly seen that the quasi-nonlinear model (Savenije et al., 2008) and Dronkers' method underestimate the tidal damping while the linear model (Toffolon and Savenije, 2011) overestimates it. The reason for the overestimation of the travel time at LW in the landward part in both the analytical and numerical models is due to the neglect of river discharge and the high tidal amplitude to depth ratio.

Finally, the tidal characteristics of the Scheldt estuary, as computed with the weighted model, are presented in diagrams for the velocity number, damping number, celerity number and phase lag. In Figure 3.18, the Scheldt estuary is represented by red line segments. Next to the segments, the distance from the estuary mouth in kilometers is written, indicating the length over which a segment is representative. We can see that in the Scheldt the seaward part (0-110 km) has a vertical line segment with a constant estuary shape number (this is due to the constant convergence length and depth assumed over that reach). At the inflection point, at 110 km, the tidal wave approaches a standing wave, although a pure standing wave cannot occur in the weighted method. Further upstream the pattern becomes irregular due to shallowing.

3.4.6 Final words on the friction term

We have seen that the set of analytical equations presented in Section 3.3 is a proper analytical framework to test different friction formulations. Because the celerity equation is in principle independent on wave shape, the dominant term to account for the non-linearity in the equations is the friction term in the damping equation. We have seen that it is relatively simple to adjust this term so as to better account for over-tides or other non-linear effects. The combined linear and quasi-nonlinear method appears to work remarkably well.

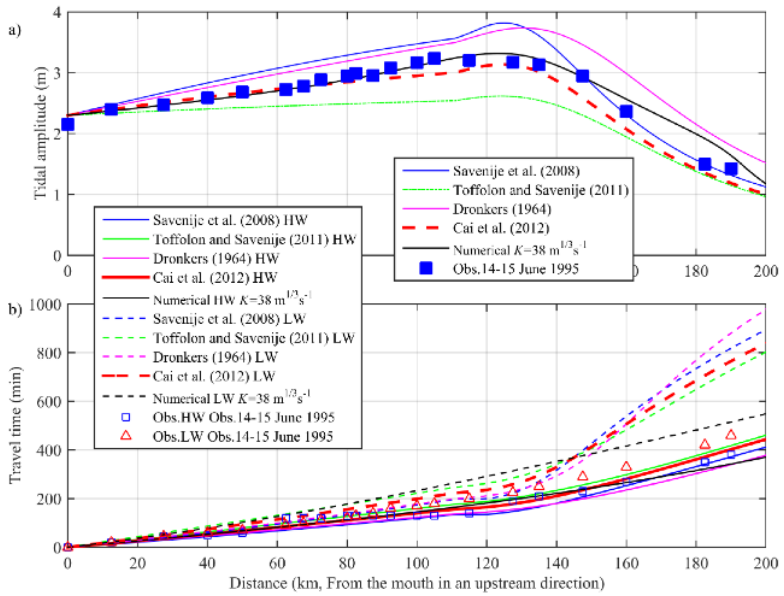

Figure 3.17: Comparison between different analytical models, numerical solution and field data: (a) tidal amplitude, and (b) travel time at HW and LW in the Scheldt estuary observed on 14-15 June 1995.

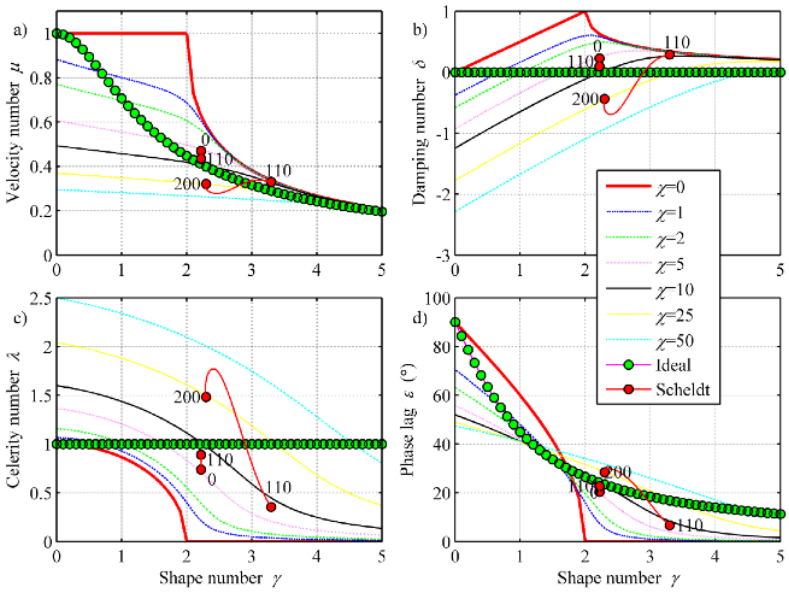

Figure 3.18: Positioning of the Scheldt estuary (red circles) in: (a) velocity number diagram, (b) damping number diagram, (c) celerity number, and (d) phase lag diagram. The numbers at the inflection points indicate the distance from the estuary mouth (in kilometers). The background shows the lines of the weighted model with different values of the friction number χ (3.59). The drawn line with dots represents the ideal estuary.

3.5 Effect of river discharge and other higher order effects on tidal damping

3.5.1 Which higher order effects are important

In the previous sections a number of assumptions have been made regarding estuary hydraulics and shape. The most important were that:

1 . The topography is that of an ideal estuary, with an exponentially varying width and no (or very modest) bottom slope;

2 . The Froude number is small;

3 . The tidal amplitude-to-depth ratio is small;

4 . The river discharge is small compared to the tidal discharge;

5 . The phase lag is near constant with x;

6 . The celerity is near constant with x.

It appears that in the upstream part of the estuary the third and fourth assumptions become restrictive, particularly where it concerns the derivation of the Damping equation (as we saw in Figure 3.5). The effect of river discharge is not always negligible and the tidal amplitude to depth ratio is not always very small. In shallow estuaries, or in estuaries that experience tidal amplification the tidal amplitude to depth ratio can approach unity. Both have a noticeable effect on the friction term: the discharge because the velocity during ebb is stronger than during flood and the depth because Chézy's roughness coefficient is depth-dependent and hence friction is stronger during ebb than during flood.

In the following, the effect of river discharge and a large amplitude-to-depth ratio on the derivation of the tidal damping equation is explored. Subsequently a more accurate version is derived for a situation where river discharge can no longer be neglected. It will be shown that taking account of these effects primarily lead to a revised expression for the friction term.

In the derivation of the equation for wave celerity, similar assumptions have been made. We shall see that river discharge does not influence the derivation of the celerity equation itself. If however we use the revised expression for the friction term, then we can significantly improve the prediction of the wave celerity in the upstream part of an amplified estuary such as the Schelde where the river discharge is not small compared to the tidal flow. The derivations presented in this Section are based on the work of Horrevoets et al. (2004).

3.5.2 Incorporating river discharge into the derivation of the Celerity equation

In section 2.5 we analysed the effect of river discharge on the water balance equation. We shall now further build on these findings to assess the effect on the damping and celerity equation. The river discharge affects the celerity equation through U as in (3.129) and (3.130):

$$U = v\sin(\xi) - \phi \tag{3.129}$$

$$\frac{\partial U}{\partial x} \approx v\left(\delta_u \sin(\xi) - \frac{\omega}{c}\cos(\xi) - \frac{\phi}{a}\right) \tag{3.130}$$

where $\phi = U_f/v$.

Subsequently, the effect of the river discharge on the velocity gradient can be accounted for in the damping term D_4:

$$D_4 = -\frac{\Phi}{\Phi'\omega} v\Phi\left(\delta_u + \frac{\phi}{a}\right) \tag{3.131}$$

Although D_4 is normally an order of magnitude smaller than D_2 because it is scaled by the Froude number, it may no longer be negligible if the river discharge is large compared to the tidal flow. However, at HWS and LWS (even with a significant upstream discharge) $D_4 \approx 0$ since$\Phi \approx 0$ and hence there is no effect of the river discharge on this damping term.

The other possible effect of river discharge on wave propagation is through the friction term. The friction term of (3.43) then needs to be adjusted as follows:

$$R_c = -\frac{\upsilon}{\Phi'\omega}\frac{f}{h}\left(\sin\xi - \phi\right)\left|\sin\xi - \phi\right| \tag{3.132}$$

Slack is defined as the situation where the flow velocity is zero, which is the case when $\sin\zeta = \phi$ and $R_c = 0$. So there is no effect of river discharge on the friction term, but there is an influence through the phase lag. The river discharge causes a shift in the occurrence of slack with HWS occurring earlier and LWS occurring later (as we saw in section 2.5). Hence, these terms of the celerity equation remain largely unaffected by river discharge. The largest effect is through the damping equation, which is reflected in the terms D_1 and D_3, of which, as we saw, $D_1 = D_c$ is the most important term. So the approach is to first adjust the damping equation for river discharge and then to use this adjusted damping equation to account for the effect of river discharge on the celerity equation. In addition (3.45) can be used to take account of the direct discharge effect on the flow velocity.

In the following section we shall analyse the effect of the river discharge on the damping term.

3.5.3 Incorporating river discharge into the derivation of the damping equation through the envelope method

In the following we shall use the Manning-Strickler equation (3.16) instead of the Chézy equation (3.15) since the Chézy roughness coefficient C is depth-dependent, whereas Manning's K is not. Hence (3.4) is modified into:

$$r_S\frac{cV}{gh}\frac{\mathrm{d}h}{\mathrm{d}x} - \frac{cV}{g}\left(\frac{1}{b} - \frac{1}{H}\frac{\mathrm{d}H}{\mathrm{d}x}\right) + \frac{\partial h}{\partial x} + I_b - I_r + \frac{V\left|V\right|}{K^2h^{1.33}} = 0 \tag{3.133}$$

where $K(=1/n)$ is Manning's coefficient and V is the velocity of a water particle in a Lagrangean reference frame that moves with the water.

The same equations are used as in Section 3.1.2 for the depth and the depth gradients at HW and LW (3.5)-(3.9). However we modify the velocity to account for river discharge:

$$V_{HW} = \upsilon\left(\sin(\varepsilon) - \phi\right) \tag{3.134}$$

and similarly for LW:

$$V_{LW} = -\upsilon\left(\sin(\varepsilon) + \phi\right) \tag{3.135}$$

Here the assumption is made that the cross-sectional area of the stream at HW and LW is not much different. This simplification is acceptable as long as the tidal amplitude is small compared to the depth of flow. Combination of these equations leads to the following expression for HW:

$$r_S\frac{c_{HW}\upsilon(\sin(\varepsilon)-\phi)}{gh_{HW}}\frac{\mathrm{d}h_{HW}}{\mathrm{d}x} - \frac{c_{HW}\upsilon(\sin(\varepsilon)-\phi)}{g}\left(\frac{1}{b} - \frac{1}{H}\frac{\mathrm{d}H}{\mathrm{d}x}\right) + \frac{\mathrm{d}h_{HW}}{\mathrm{d}x} \pm \frac{(\upsilon(sin(\varepsilon)-\phi))^2}{K^2h_{HW}^{1.33}} = -I_b + I_r \tag{3.136}$$

The last term is the friction term and has a positive value if $\sin\varepsilon > \phi$ and a negative value if $\sin\varepsilon < \phi$.

Similarly for LW it follows that:

$$-r_S\frac{c_{LW}\upsilon(\sin(\varepsilon)+\phi)}{gh_{LW}}\frac{\mathrm{d}h_{LW}}{\mathrm{d}x} + \frac{c_{LW}\upsilon(\sin(\varepsilon)+\phi)}{g}\left(\frac{1}{b} - \frac{1}{H}\frac{\mathrm{d}H}{\mathrm{d}x}\right) + \frac{\mathrm{d}h_{LW}}{\mathrm{d}x} - \frac{(\upsilon(sin(\varepsilon)+\phi))^2}{K^2h_{LW}^{1.33}} = -I_b + I_r \tag{3.137}$$

To arrive at an expression for the tidal range H, these equations should be subtracted, leading to terms containing $\mathrm{d}H/\mathrm{d}x$ or I. This is straightforward if the coefficients of the terms are the same, otherwise it leads to correction factors.

Interestingly, the ratio of c/h in the first term is similar for HW and LW since both the celerity and the depth are higher than average at HW and lower than average at LW. We shall therefore assume that these two coefficients are similar, so that the terms can be subtracted. As was observed in Section 3.1.2, the coefficients of the first term of (3.136) and (3.137) are scaled a Froude number smaller than that of the third term, while the sum of dh/dx for HW and LW is equal to the residual slope I, which is small compared to $\mathrm{d}H/\mathrm{d}x$. Hence, the first terms in (3.136) and (3.137) are small compared to the other terms.

In the second term of (3.136) and (3.137), the celerity is different at HW and LW. As a result a correction factor appears in the subsequent subtraction of these terms. In the last term (the resistance term), the water depth is different at HW and at LW. This also leads to a correction factor (f'').

Subsequently, (3.136) and (3.137) are subtracted and combined with (3.4) and (3.7). Details on the subtraction of individual terms are presented in Horrevoets et al. (2004). Subtraction yields the following expressions:

for **zone I**, where $\sin\varepsilon > \phi$:

$$\frac{1}{\eta}\frac{\mathrm{d}\eta}{\mathrm{d}x}\left(\frac{1}{\alpha} - r_S\frac{\phi\zeta}{\sin(\varepsilon)} + \vartheta\right) = \frac{\vartheta}{b} - \frac{f'v\sin(\varepsilon)}{\overline{h}c}\left[1 + \frac{8}{3}\zeta\frac{\phi}{\sin(\varepsilon)} + \frac{\phi^2}{\sin^2(\varepsilon)}\right] - \frac{r_S I}{\overline{h}} \tag{3.138}$$

for **zone II**, where $\sin\varepsilon < \phi$:

$$\frac{1}{\eta}\frac{\mathrm{d}\eta}{\mathrm{d}x}\left(\frac{1}{\alpha} - r_S\frac{\phi\zeta}{\sin(\varepsilon)} + \vartheta\right) = \frac{\vartheta}{b} - \frac{f'v\sin(\varepsilon)}{\overline{h}c}\left[\frac{4}{3}\zeta + \frac{2\phi}{\sin(\varepsilon)} + \frac{4}{3}\zeta\frac{\phi^2}{\sin^2(\varepsilon)}\right] - \frac{r_S I}{\overline{h}} \tag{3.139}$$

where α is the tidal Froude number defined by (3.25) and equals μ^2, $\zeta = \eta/\overline{h}$ is the tidal amplitude to depth ratio, I is the residual slope of the average water level, f' is the adjusted friction factor of (3.16), and ϑ is a correction factor for wave celerity defined as:

$$\vartheta = 1 - \frac{(c_{HW} - c)}{c}\frac{\phi}{\sin(\varepsilon)} \approx 1 - \left(\sqrt{1+\zeta} - 1\right)\frac{\phi}{\sin(\varepsilon)} \tag{3.140}$$

The friction factor f' compensates for the fact that friction is larger at LW than at HW and is always larger than unity. It enhances the effect of friction. If $\zeta \ll 1$, $f' \approx f$. In the upper reaches of an amplified estuary however, the friction factor can become very important as ζ approaches unity (e.g. if $\zeta = 0.5$, $f' = 1.8f$). The coefficient 4/3 in these equations follows from a Taylor series expansion of $(h+\eta)^{1.33} \approx h^{1.33}(1 + 1.33\zeta)$, if $\zeta < h$. Due to the factor 4/3, (3.16) only makes sense as long as $\zeta < 0.7$.

The correction factor ϑ compensates for the difference in wave celerity at HW and LW in the second term of (3.136) and (3.137). It has a value smaller than unity, but is close to unity as long as $\zeta \ll 1$ and $\phi/\sin\varepsilon$ is in the order of magnitude of 1 or less. In practice, $\vartheta \approx 1$.

Just like we saw in Section 3.1.2, the term $r_S I/h$ (the I-term) in (3.138) and (3.139) is generally small compared to the convergence term ϑ/b. The average water level slope can be scaled at less than h/L, with L being the length of the tidal influence (the length of the estuary). Hence the ratio of the I-term to the convergence term is less than b/L. In estuaries with a strong topography where $b \ll L$, the I-term can be disregarded, as for example in the Schelde, an estuary with a strong topography (b=28 km and L=200 km), b/L=28/200=0.28. The Incomati in Mozambique is an example of an estuary with a strong topography in the lower segment but with moderately converging banks upstream, where the ratio in the lower segment is b/L=6/100=0.06, whereas in the upper segment it is b/L=42/100=0.42, thereby implying that the I-term may become important in that part. Since the residual slope I is determined by the bottom slope, the effect of the I-term may become important in the upstream part of an estuary. It implies that when the bottom slope becomes important near the upstream end of the estuary, the I-term gains prominence, the tidal amplitude is damped stronger and the tide dies out.

The main difference between (3.138) and the earlier derived (3.17) is the introduction of $\phi/\sin\varepsilon$ both in the friction term and in the denominator (which is the part between brackets in the left hand member).

It can be seen from (3.138) that, since in alluvial estuaries $\zeta < 1$, the impact of the river discharge on the denominator is small, as long as ϕ is in the order of magnitude of 1 or less. If $Q_f = 0$ then (3.138) is the same equation as (3.17).

We can also write these equations in the dimensionless variables we introduced in section 3.3. The equations then read:

for **zone I**, where $\sin\varepsilon > \phi$:

$$\delta = \frac{\mu^2}{\mu^2\left(\vartheta - r_S\frac{\phi}{\mu\lambda}\zeta\right)+1}\left[\vartheta\gamma - \chi\left(\phi^2 + \frac{8}{3}\mu\lambda\phi\zeta + \mu^2\lambda^2\right) - \frac{r_S c_0}{\omega h}I\right] \tag{3.141}$$

for **zone II**, where $\sin\varepsilon < \phi$:

$$\delta = \frac{\mu^2}{\mu^2\left(\vartheta - r_S\frac{\phi}{\mu\lambda}\zeta\right)+1}\left[\vartheta\gamma - \chi\left(\frac{4}{3}\phi^2\zeta + 2\mu\lambda\phi + \frac{4}{3}\mu^2\lambda^2\zeta\right) - \frac{r_S c_0}{\omega h}I\right] \tag{3.142}$$

Equation (3.141) is the same as (3.64) when $\phi = 0$.

Cai et al. (2012b) applied these equations in the Modaomen estuary of the Pearl river in China. In the upstream part of the estuary the influence of the river discharge is strong. They used (3.141) to analyse the effect of upstream water diversions and dredging on the tidal damping and wave propagation. Over time there appeared to be a significant trend as a result of these human interferences and an increased risk for the propagation of storm surges.

3.5.4 Application to the Schelde estuary

With (3.138) and (3.139) an analytical model can be made that can be compared to observations made in the Schelde on 14-15 June 1995. The characteristics of the model are based on the Schelde geometry. The length of the estuary $L = 200$ km. The width at the estuary mouth $B_0 = 26$ km. The convergence length $b = 28$ km. Up to 110 km from the mouth the depth of flow $h = 10.5$ m. There is no bottom slope before 110 km from the mouth, after which the depth reduces gradually to 2.6 m. The estuary is subject to a harmonic tide at the mouth of the estuary ($x = 0$) with a tidal range of $H_0 = 4.4$ m (corresponding with spring tide), a tidal velocity amplitude of v= 1.2 m/s and a tidal period of $T = 44400$ s. The tidal velocity is amplified and damped in agreement with the damping and amplification of the tidal range, as observed by Graas (2001).

At the upstream end of the model ($x = 200$ km) there is a weir barrage where a river discharge of 38 m^3/s passed downstream on 14-15 June 1995. This weir corresponds to the weir in Gent. The total river discharge amounted to 112 m^3/s since there was an additional 74 m^3/s coming from the Rupel tributary at x=128 km.

A phase lag of 40 min has been used throughout the estuary in accordance with observations made by Graas (2001). For the celerity of propagation the average between HW and LW has been taken, corresponding with the mean tidal situation.

Since it is not possible to solve the differential (3.84) and (3.85) analytically, a numerical equation has been used: $y_{n+1} = y_n + \mathrm{d}y/\mathrm{d}x^*\Delta x$, with a length step $x = 2.5$ km. The equation can be solved simply in a spreadsheet.

In Figure 3.5, the results of the spreadsheet model are compared to the observed water levels in the Schelde during dead tide on 21 June 1995 (Q_f=41 m^3/s). The model fits the observations using a constant Manning coefficient K=38 $m^{0.33}/s$ (n=0.026) along the estuary axis. This implies that in the lower part of the estuary a Chézy roughness of 57 $m^{0.5}/s$ applies. One may conclude that by the introduction of the river discharge in Savenije (2001b) model an almost perfect fit with observations has been obtained. In Figure 3.5, the weighted model is compared to the original model (Q_f=0) and to a situation of high river discharge (Q_f=100 m^3/s). The effect of the river discharge on the tidal damping is considerable in the upstream part. It appears that the tidal range close to Gent is substantially reduced by the river discharge. This is primarily due to the LW levels being higher. The HW levels are less affected by the river discharge.

It can be concluded that β is strongly affected by river discharge if Q_f/A approaches $v \sin \varepsilon$. This also may have a significant impact on the damping term D in the Celerity equation (Eq.3.58), which is directly proportional to $1/\beta$. The influence of river discharge on wave celerity is therefore primarily felt through the effect of river discharge on tidal damping. Finally, the deviation seen in Figure 3.10 between the observed and computed wave celerity for HW and LW in the upper reach of the estuary may have three causes:

1 . The tidal amplitude to depth ratio at LW approaches unity in the area near the 150 km mark; however, the ratio of the tidal amplitude to the average depth remains below 0.5;

2 . The ratio of river discharge to tidal flow approaches unity near the 180 km mark;

3 . The shift in ε causes the celerity near HW to be close to c_0 and the celerity near LW to be slower.

It is not completely clear which of these effects is most important. It is a fact however, that the analytical solutions become less applicable as we move further upstream and the estuary gradually gains a riverine character.

3.5.5 Conclusion

In the upper reach of the Schelde estuary, there appears to be an important influence of the river discharge on the tidal range. The river discharge is largely responsible for the considerable tidal damping that occurs upstream. The effect of the river discharge on tidal damping is primarily through the friction term. An important point along the estuary is the point where the two moments of slack occur at the same time, upstream of which the tidal flow no longer changes direction and where the river discharge becomes dominant over the tidal flows. At this point, which varies with river discharge, the friction term is dominated by the river discharge. The reduction of the tidal range is primarily caused by higher water levels at LW, as a consequence of the river discharge forcing itself through a narrow cross-section.

In this Section an equation has been presented that accounts for the effect of the river discharge on tidal damping and tidal wave propagation. By the introduction of the river discharge into the derivations, a considerable improvement of the existing analytical equation for tidal damping could be obtained. The comparison of the equation with observations is quite good. The equation is not complicated and can be easily applied e.g. in a spreadsheet. Although the equation enhances our insight into the effect of river discharge on tidal damping and propagation, we can't use the equation far beyond the point where the river discharge and the tidal flow are of equal magnitude.

3.6 The influence of climate change and human interference on estuaries

The equations presented in the previous sections provide us with a very useful tool to assess the possible impacts of human interference in the estuarine system as well as the effects of climatic change. Man and climate can impact on the estuary through a number of ways:

- Dredging and deepening of access and shipping channels
- Bank stabilisation, canalisation and constrictions
- Closure of tidal branches and inlets
- Construction of harbours
- Sea level rise
- Changed rainfall and evaporation patterns
- Modified river discharge regime

Dredging can have a large impact on tidal hydraulics, particularly if it leads to general deepening. If dredging is done in a way that the spill is dumped elsewhere in the cross-section, then dredging does not lead to an increase of the cross-sectional average depth. If the spill is moved out of the estuary, however, the average depth increases, which has various implications. There is a difference in the short-term and the long-term reaction. The long-term reaction is a morphological reaction which may change the shape of the estuary and particularly the convergence length. Such a morphological reaction is slow and would most probably be counteracted by engineering works of bank stabilisation, the estuary being a focus of engineering attention already. The short-term reaction can be seen from both the Scaling equation (Eq.2.92), the Damping equation and the Celerity equation (Eq.3.58). As the depth increases, the scaling equation suggests that the tidal velocity would decrease and the celerity increase. The tidal range is fixed by the downstream boundary, but could increase if a shallow sill near the estuary mouth is removed. These changes all point towards decreasing friction in the Damping equation, leading to either reduced tidal damping or increased tidal amplification. As a result, the wave celerity increases. What happens to the Wave-type Number ($\sin\varepsilon$) is not so clear. We can see form the Phase lag equation (Eq. 2.88) that the increase in both c and δ counteract each other, leading to a minor change in ε, if at all. We also see in the Geometry-tide relation that the deepening and the reduced damping (or increased amplification) counteract each other, which leads to a more or less unchanged tidal range to tidal excursion ratio, suggesting that the tidal velocity amplitude remains more or less the same. Both the tidal range and the tidal excursions, however, will amplify in upstream direction.

Bank stabilisation affects the storage width ratio. Fixed banks and closure of tidal creeks and inlets, often in combination with dredging, leads to less storage on banks on tidal flats and in creeks resulting in a value of rS close to unity. The celerity equation shows that a reduced value of r_S directly leads to a higher velocity of propagation, being inversely proportional to the root of r_S. As a second order effect, the celerity increases even further because the convergence term in (3.58) increases compared to the friction term. A higher wave celerity in the Damping equation leads to less damping and more amplification. The Phase Lag equation again provides negative feedback. An increased wave celerity and increased tidal damping counteract each other in the Phase Lag equation, yielding a more or less constant phase lag. In the Scaling equation the celerity increases with the root of r_S, so the tidal velocity amplitude (and hence the tidal excursion) is expected to increase at a similar rate. So in conclusion, bank stabilisation leads to higher tidal velocity, higher wave celerity and a longer tidal excursion.

Constrictions primarily have local influence. A constriction imposed by bank stabilisation, as is the case for instance in the Schelde near the city of Vlissingen (Flushing), leads to channel deepening, while maintaining the cross-sectional area. This is mainly a local effect that does not have a noticeable impact on the overall hydraulic behaviour. Canalisation has a larger impact. Besides affecting the storage width ratio, it may also change the convergence, as happened with the Rotterdam waterway. In canals with a long convergence length, the Wave-type number will approach unity (progressive wave), leading to tidal damping and a strong tidal velocity gradient. Construction of harbours on tidal channels will lead to more storage, reduced wave propagation and more tidal damping. In principle, the loss of storage width caused by dredging and vertical walls can be compensated by the gain in storage through harbour construction.

The possible impact of sea level rise is a topical issue. Over the coming century the rate of sea level rise could be in the order of 0.5 m, but it could also be more. Let us assume that sea level rise will be accompanied by the raising of estuary banks, and hence loss of storage width. This implies that sea level rise will be much the same as a combination of deepening and storage width reduction. On top of that, sea level rise may increase the tidal range at the downstream boundary, particularly in estuaries that have a shallow sill near the mouth (such as the Incomati). The combination of these effects, which strengthen each other, leads to a higher wave celerity, more tidal amplification, and a larger tidal excursion. So on top of the sea level rise, people living along an estuary will have to reckon with a larger tidal range (so higher HW) and a shorter travel time of the tidal wave. How much this effect will be depends strongly on the characteristics of the estuary. Because of the non-linearity of the Damping equation, the reaction of the estuary system very much depends on the values of the hydraulic parameters. With a simple spreadsheet model however, the combination of the equations presented in Table

3.3 can provide good indications of what should be expected if certain changes are made to the geometry and the hydrological boundary conditions of an estuary.

Finally, there is the effect of hydrology and climate. We have seen that the river discharge affects the hydraulics of the estuary, particularly the tidal damping and the wave celerity in the riverine part of the estuary. These effects are not as dramatic as the ones discussed above. However, the impact of climate and hydrology on salinity, water quality and ecosystem behaviour can be substantial, possibly leading to drastic changes in overall system behaviour. These effects will be discussed further on in Chapter 4.

Chapter 4

MIXING IN ALLUVIAL ESTUARIES

This chapter deals with how salt and fresh water mix and how we can describe this process with analytical equations.

In well-mixed estuaries salinity penetrates through the process of mixing while the river discharge flushes the salinity back towards the sea. This struggle for dominance can have two winners: the mixing, and in that case we observe an increasing salinity over time; or the flushing by the river flow, and in that case we see the estuary water become fresher. When the two mechanisms tie, we have a steady state situation where the salinity remains constant over time. What remains is a longitudinal gradient of the salinity, gradually diminishing in upstream direction from sea salinity at the mouth to fresh water at the toe of the salt intrusion curve.

There are several mixing mechanisms that vary in importance depending on: the shape of the estuary, the location, the level of stratification, the density, and the strength of the tide. One can distinguish different types of mixing, such as: mixing by turbulence, mixing by tidal shear, mixing by residual currents, mixing by trapping and density driven mixing. These mechanisms will be described in the following sections. All these mixing mechanisms together drive longitudinal dispersion of salinity, which can be decomposed into many smaller constituting fluxes. There are different methods for flux decomposition, but we shall see that this approach does not really lead to practical results. In order to obtain a predictive model, we require a predictive equation for what is called the effective longitudinal dispersion. This one-dimensional predictive equation will be derived and illustrated by empirical data. A general equation that integrates all mixing processes will be presented. But first let's be clear about the terminology: what is dispersion, what is effective longitudinal dispersion and how does it relate to mixing?

4.1 What is dispersion and how does it relate to mixing?

Dispersion is a mathematical artefact. Dispersion follows from averaging over time when we follow a water particle. If we follow a water particle over - let's say - a day, then we can see the distance that the particle travelled between the beginning and the end of the day (the distance covered). This is the average distance travelled by the water particle. If the movement is described by a sine function and we average over the tidal period, then average - the distance travelled - is zero. But we can also look at all the places the where the particle has been. The water particle may well have diverted from the direct trajectory linking the start and finish position. During this trajectory if has been in contact with other particles and it may have exchanged diluted substances. If the water is of homogeneous density (or salt concentration) then the water does not change its properties during its diversions, but if the water had a variable density, then the diversion would have allowed the water to mix with other particles, which would have changed its density or salt concentration. In the latter case the density is different from what it would have been if the particle had travelled in a straight line connecting start and finish. The difference between the straight line (which we call advection) and the actual detour we call the dispersion of water particles. It may be clear that if we integrate the water movement over a very short time step, say a few seconds, that the dispersion is very small: over a very small distance, there is no diversion. But if we integrate over a longer period, say a day

or a week, then the straight line connecting start to finish is probably a bad indicator of the trajectory that the water particle actually covered. So dispersion is completely scale dependent and, in fact, an artefact of our averaging.

The question remains: Is dispersion a real physical mechanism, or is it just a mathematical invention? Of course, dispersion is real. And if there is a density (or concentration) gradient, dispersion leads to mixing. But how can we make a mathematical artefact into something physical? The answer to this question is the correct scale over which we average. If we select the physically relevant temporal or spatial scale, then the dispersion becomes a physical process connected to that scale. In tidal mixing, the proper temporal scale is the tidal period T. In a 1-dimensional situation with no river discharge, the water particle starts its travel at LWS moving upstream over a tidal excursion E. At HWS it starts to flow back ending up in the starting position after one tidal cycle. If there is a river discharge, then the average distance the water particle travelled during the tidal period is $Q_f T/A$, which is the advective transport, but it covered quite some more ground. It travelled over a distance E up and down the estuary, and probably also moved laterally and vertically through the cross-section. In the process it had the opportunity to mix with particles of different density and as a result, the density of the water would have changed as a result of the circulations. This is what we call the dispersive transport. Under the influence of a density gradient, exchange of water particles (mixing) leads to a transport of dissolved substances in the direction of the gradient (moving from high concentration to low concentration).

So the proper temporal and spatial scales of tidal mixing in alluvial estuaries are the tidal period T and the tidal excursion E. The tidal excursion is the mixing length of the longitudinal mixing process. The width - or half the width as some say - is the spatial scale of the lateral mixing, and the depth is the scale of the vertical mixing. If we consider dispersion at these temporal and spatial scales, then the dispersion has physical meaning and we may be able to develop a predictive equation that connects this dispersion to physically meaningful parameters.

Finally, there is the term diffusion. Mathematically diffusion and dispersion are the same thing, but physically they are not. The term diffusion is used for molecular processes (Brownian motion) we also find in stagnant water. Transport by diffusion is orders of magnitude smaller than the process of dispersion that we see in moving water under tidal influence. On top of this, tidal dispersion is much larger than dispersion in unidirectional flow, partly because the water moves up and down with the tide, which stirs the water in a physical sense, but also because of the strong density gradients that are present in tidal waters. As a result, the combination of different mixing mechanisms in estuaries is more complex than in rivers or canals and we can identify different types of mixing. In the next section we shall elaborate on these different mechanisms.

4.2 Types of mixing, their relative importance and interaction

Mixing is the mechanism through which salt travels upstream. Every tidal cycle, on the flood tide, an amount of salt water enters the estuary, but if that amount of water would not mix, then the same water would again leave the estuary on the ebb tide without any salinity penetrating the estuary. We shall see that if we want to analyse mixing in detail by looking at all the different mixing mechanisms at their particular spatial and temporal scales, the picture becomes very fuzzy. Several authors have tried to split up the mixing process into smaller components resulting from spatial and temporal averaging, but without enhancing the insight into how mixing works. Jay et al. (1997) conclude that the track record of determining these fluxes is discouraging, among others because of the low accuracy that can be reached in subtracting fluxes. Others have looked at the driving mechanisms of mixing and what this teaches us about the main hydraulic parameters that influence mixing. Although this approach may enhance our insight, to date, it has failed to come up with a predictive method to forecast the effective dispersion. The most important reason being that we do not know how these individual mechanisms interact and how they provide feedback on each other.

In analogy with Sivapalan et al. (2003), we may call this approach, where we try to build-

up the dispersion from analysing the detailed mixing processes, a reductionist or "upward" approach. Like in hydrology, this reductionist approach, although physically appealing, does not generate workable models that predict system behaviour. The reasons lie partly in a phenomenon called 'equifinality' and partly in the fact that these individual components do not function independently but interact according to certain laws of "self-organisation". In tidal dispersion similar processes are at work. Therefore it is worthwhile to look at the concept of equifinality and self-organisation in somewhat more detail.

The concept of equifinality is notorious in hydrology. It was introduced by Beven (1993) to describe the fact that distributed rainfall-runoff models may perform well, but often for the wrong reasons. Distributed physically based rainfall-runoff models use large sets of spatially distributed parameters. It appears that the same hydrological behaviour can be simulated adequately by a sheer infinite combination of parameters, which often are not even close to their expected value. As a result, these complex hydrological models cannot do much more than mimic hydrological behaviour, but their predictive value, to forecast what would happen if we changed something in the land-use of the catchment, is low. At first sight this is a disappointing result. It implies that a purely physically based approach of looking at sub-processes at detailed scale, and subsequently scaling these up to the larger scale, does not yield satisfactory results. On the other hand, equifinality is an indication of the existence of a physical law that apparently translates a plethora of detailed processes (in a strongly heterogeneous environment) into consistent system functioning. As a result, Savenije (2001a) called "equifinality, a blessing in disguise". Equifinality is the reason why relatively simple hydrological laws exist, which are able to describe hydrological processes under highly variable conditions, in different physical environments and in far from homogeneous situations. Coming to grips with the underlying physical law that govern equifinality is one of the biggest challenges in hydrology. And the same may be true for mixing in estuaries.

The main question is: what causes equifinality? One important cause is that hydrology is a complex system of interacting processes that provide feedback on each other while attenuating extremes. The physical process underlying this is entropy. To say it popularly, entropy does not like extremes. The Second Law of thermodynamics implies that average behaviour becomes overwhelmingly likely in a very large system, implying that exceptions will no longer be observable in the output signal of large systems. In the end all energy is transferred into heat. Within a large system, this energy is dissipated as gradually as possible.

A watershed is a large complex system, and so is an alluvial estuary. Just like an alluvial estuary, a watershed shapes the medium through which the water flows. Erosion, deposition and biological activity are the main shaping forces, but the underlying physical law is the maximisation of entropy driving self-organisation in a way that energy is dissipated as homogeneously as possible. Friction is the most important force that translates energy into heat. Different processes interact to spread the energy smoothly over the water trajectory. If one process is over-loaded it triggers another. The feedback between these processes results in an overall system performance obeying a physical law at a higher level of aggregation, and there are many ways that this behaviour can be reached.

Mixing works the same way. Mixing is spreading of energy. If one mixing mechanisms is under-performing, another takes over; not because they communicate, but because the physical processes that shape the geometry, and that drive the mixing processes, are connected by the second law of thermodynamics. Hence there are feedback mechanisms that lead to efficient and gradual dissipation of mixing energy. The law to describe this overall mixing behaviour still has to be derived, but in this chapter a formula will be presented (Van der Burgh's equation) that comes very close to it, judging from its excellent performance and closeness to the theoretical knowledge available to date.

Following the analogy of Sivapalan, Van der Burgh's method is a "downward" approach, which is mainly empirical and based on what the data "tell us". We observe certain system behaviour, we derive an equation that describes it and we relate the key parameters of the equation to the physical parameters that we know are the main drivers of the process. This is the way that many physical laws have been discovered: the Gas law, Darcy's law, Manning's law, Newton's law of gravity, etc. There is nothing wrong with it. The only problem is that we feel uncomfortable if we cannot make the connection between what we observe at a small scale

and what we observe at the aggregated system-scale. We feel dissatisfied, as with the magician who just fooled us into believing that the girl has been cut into two and we have no clue how the trick works. At the same time it triggers our curiosity. Many physical scientists are still trying to work out how gravity works. Yet nobody contests Newton's law describing it.

It is clear that for an empirically derived physical law to be credible, it has to be 1) based on solid empirical evidence in a wide range of situations, 2) consistent with other certified physical laws, 3) based on the dominant physical drivers that we know, and 4) connected to the physical processes we observe at smaller scales. The last condition implies that we bring the "downward" and "upward" approach together, similarly to what is advocated by Sivapalan. So let us look at the mixing mechanisms and at what drives them. Although detailed study of the mixing processes may not be the right way to understand system performance, we have to understand them to find the middle ground between the downward and the upward approach.

There is virtually no limit to the number of mixing processes that can be identified. Fischer et al. (1979) separated the small-scale turbulent diffusion (periodicity less than a few minutes) from the larger scale advective processes, although the separation between the two is arbitrary. Turbulence essentially is the mechanism that transfers the friction from the estuary/river bottom into the body of the flowing water. Gravity works on all water particles, but the friction only along the interface between land and water. The sheer stress exercised on the interface is transferred into the fluid by viscous interaction and turbulent eddies that dissipate energy within the fluid. This causes mixing by turbulent eddies at spatial scales of a few meters and time scales of less than a few minutes, but also interactions at larger scales. The flow can be considered to exist of different streamlines that flow in different directions and at different velocities. There is a shear stress exercised between these streamlines, which we call tidal shear. Where streamlines interact, cross-over, or meet to exchange fluid, we talk of advective dispersion. An essential difference between a river and an estuary is that in an estuary the magnitude, the direction and even the existence of these streamlines is continuously changing over time and space, as a result of tidal forcing. The direction of the flow lines in an estuary is seldom parallel to the estuary axis, but is shearing between flood and ebb channels. This makes the mixing highly dynamic.

Besides tidal-forced mixing there is also mixing by wind and by the river. Hence, we can distinguish three main driving forces for mixing:

- The wind that drives both vertical and horizontal circulation. The vertical circulation is driven by wind shear inducing a surface current of relatively fresh water and a water level slope in the direction of the wind, while the surface slope triggers a relatively saline return flow close to the bottom (see Fig. 4.1). Mixing occurs along the interface between these two currents and through upwelling of relatively saline water from the bottom. The wind also can cause horizontal circulation depending on the shape of the estuary. Particularly irregular estuaries, such as Rias, can experience net circulation over shallow bays due to wind (see Fischer et al., 1979). Although in lakes and coastal lagoons wind-driven mixing can be dominant, in alluvial estuaries this mixing mechanism is considered less important than the following two.

- The river provides potential energy with buoyant fresh water driving vertical gravitational circulation. Gravitational circulation is an important mechanism in the part of the estuary where the longitudinal salinity gradient is largest. In estuaries with a strong funnel shape (and hence a dome-shaped salt intrusion curve) this region is located in the central part of the salt intrusion length. In the downstream part of these estuaries, where the salinity gradient is small, tide-driven mixing is dominant. In narrow estuaries, with a recession-shaped salt intrusion curve and a rather constant salinity gradient, gravitational circulation is the main mixing mechanism throughout.

- The tide provides kinetic energy to the estuary that drive the mixing of saline and fresh water. The tide rocks the estuary water back and forth and dissipates tidal energy through mixing. The tide generates different types of mixing: 1) turbulent mixing at small spatial and temporal scales, 2) tidal shear between streamlines with different velocities; 3) spring-neap interaction; 4) trapping of water on tidal flats and in dead ends; 5) residual currents in the cross-section; 6) residual currents over tidal flats and shallows; 7) exchange between

ebb and flood channels that meet and mix at cross-over points. The latter mechanism is dominant in the downstream part of estuaries with a dome-shaped salt intrusion curve.

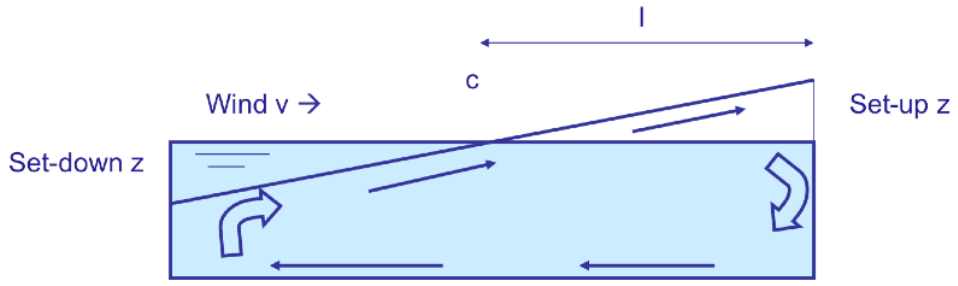

Figure 4.1: Wind-driven vertical circulation.

We saw earlier, in Chapter 1, that the balance between the potential energy difference and the tidal kinetic energy is reflected in the Estuarine Richardson number N_R (introduced by Fischer, 1972), which is represented here:

$$N_R = \frac{\Delta\rho}{\rho}\frac{gh}{v^2}\frac{Q_f T}{P_t} \tag{4.1}$$

Hence the Estuarine Richardson number is a measure for the relative importance of gravitational circulation compared to tidal mixing. The ultimate form of gravitational circulation is the saline wedge, which corresponds with a high Estuarine Richardson number.

In the following sections we shall discuss the mixing by the tide and by the density difference in more detail. We shall pay no further attention to wind-driven mixing and concentrate on the main mechanisms. Gravitational circulation and mixing by tidal shear have been well documented in the literature. These mechanisms will be briefly summarised. Still poorly known are the mixing mechanisms by tidal pumping and residual circulation. Here we shall try to explore new terrain.

4.3 Gravitational circulation

Hansen and Rattray (1965) started a discussion on which of the two mechanisms (density driven or tide driven) is dominant in a certain estuary. Their classification method makes use of the parameter v reflecting the relative importance of tide driven dispersion versus the total dispersion. Several researchers spent time on investigating which of the two is the dominant mechanism in certain estuaries. Smith (1980), who called density driven dispersion buoyancy driven dispersion, stated that in wide estuaries buoyancy effects are dominant. West and Broyd (1981) confirmed this and concluded that transverse oscillatory (i.e. tide driven) shear mechanisms dominated for narrow, shallow estuaries; whereas transverse gravitational (i.e. density driven) shear mechanisms dominated in wide estuaries.

Here we come to a different conclusion. Gravitational circulation is dependent on the longitudinal salinity gradient and is driven by the moment M per unit of volume that results from the two opposed hydrostatic forces (of the fresher upstream section and the more saline downstream section) that are equal in magnitude but do not work along the same line of action (see Fig. 2.2). (2.32) that describes the moment exercised on the fluid is represented here:

$$M = \frac{1}{12}\frac{\partial\rho}{\partial x}gh^2 \tag{4.2}$$

We see that the longitudinal salinity gradient is modest in wide estuaries because wide estuaries (with a short convergence length) have a dome-shaped intrusion curve, which has a very small salinity gradient in the wider part of the estuary. Only as the estuary narrows does the salinity gradient become stronger. The observations by earlier researchers are often biased by two shortcomings. The first is that much work has been done on the basis of laboratory flumes or

mathematical models that assume constant width (e.g. Hansen and Rattray, 1965). These results are of limited use in real estuaries with converging banks. The second is that if observations were made in real estuaries, they were merely done in selected cross-sections of the estuary (often only one), which may not be representative at all for the overall longitudinal dispersion

Instead we see that gravitational circulation is dominant in near prismatic estuaries (with a long convergence length), such as the Limpopo, the Chao Phya or the Rotterdam Waterway, experiencing a steep salinity gradient, but which are generally narrow compared to estuaries with a short convergence length.

The apparent paradox between what e.g. Smith (1980) observed (that gravitational circulation is larger in wide estuaries) and what is stated here can be explained if we distinguish between width and convergence. An estuary with a short convergence length is wide at the mouth. If we look at the estuary from the upstream end, then the width increases gradually from the river width to the sea. The shorter the convergence length, the wider the estuary becomes. Because the tidal influence in alluvial estuaries always exceeds a quarter of the tidal wave length, which is in the order of 100 km or more, estuaries with a short convergence length are always wide. Similarly estuaries with a long convergence length are generally narrow, having a width not much larger than the river width. We saw that estuaries with a short convergence length (i.e. wide estuaries) are dominated by tidal mixing, and estuaries with a long convergence length (i.e. narrow estuaries) by gravitational circulation. In the wider part of the estuary the salinity gradient is small and hence the gravitational circulation is small. But if there is a salinity gradient then we can indeed conclude that the wider an estuary is, the more powerful the gravitational circulation.

Fischer et al. (1979) observed that the density gradient drives lateral mixing rather than vertical mixing, as a result of the varying depth over the cross-section. Because estuaries are much wider than deep, lateral gravitational circulation is much more important than vertical circulation. Overall effective longitudinal dispersion by gravitation circulation D_g, according to Fischer, is proportional to the width squared and the depth to the sixth power:

$$D_g \propto \left(\frac{g}{\rho}\frac{\partial \rho}{\partial x}\right)^2 h^6 B^2 \tag{4.3}$$

Hence we see that this gravitational dispersion is both a function of the width and the salinity gradient. Both should be significant for this type of dispersion to be dominant. An estuary that is wide, but has no salinity gradient will not experience much gravitational circulation.

Fischer concludes by saying that although we have started to understand the mechanisms at work in tidal and gravitational mixing, we must be very cautious to apply formulas that have been derived under laboratory conditions or on the basis of spot observations in real estuaries. *"We have given several formulas for estimating the value of the longitudinal dispersion coefficient, but each one has been based on an analysis of one mechanism at the neglect of others"*. It is especially interesting to find out how these mechanisms interact. One of the few papers that deal with the combined effect of gravitational circulation and tidal dynamics is by Mccarthy (1993), which will be briefly presented in the next section where we discuss residual circulation.

4.4 Mixing by the tide

We saw that the tide generates different types of mixing which we shall describe in somewhat more detail below.

Turbulent mixing is the weakest of the mechanisms occurring at small spatial (a few meters) and temporal scales (a few minutes). Fischer et al. (1979) consider it inferior to the other tide driven mechanisms that can be classified as **advective mixing**. The latter results from water flowing in streamlines that move at different velocities, in different directions and that vary over time. These streamlines interact and exchange fluid. A practical distinction between turbulent and advective mixing is that a three-dimensional hydraulic model is able to model the salt fluxes resulting from advective dispersion by the combination of the velocity field with the salinity field. The turbulent dispersion is imposed through the eddy diffusivity of turbulent flow that these models use. Hence a good 3-dimensional hydraulic model should in principle be able to simulate

tidal mixing adequately. But because of schematisations implicit in most 3-D models, this is unfortunately not yet the case.

Uncles and Stephens (1996) emphasised the importance of **spring-neap interaction** (Uncles and Stephens, 1996). During neap tide, estuaries tend to be more stratified, as the Estuarine Richardson number is larger. The strength of tidally driven mixing may vary significantly between spring and neap tides (Jay and Smith, 1990b). The transition from neap to spring tide can generate significant mixing.

Schijf and Schönfeld (1953) introduced the concept of **tidal trapping**. Tidal trapping results from the phase difference between the main estuary branch and a dead-end tidal branch, bay or tidal flat. In a dead-end branch slack occurs at HW, whereas the water in the estuary is still flowing upstream at HW. Between HW and HWS the water level drops and the dead-end branch already starts emptying while the estuary still flows upstream with relatively saline water. Hence a tidal flat discharges relatively fresh water into the flood flow. In estuaries with an irregular topography trapping can be an important mechanism. Because trapping occurs only along the sides of the estuary, its relative importance is less in very wide estuaries. The typical length scale of tidal trapping is the tidal excursion E.

A phenomenon receiving more attention in recent years is **residual circulation** in the cross-section. Unfortunately, also here, most of the research has been done on estuaries with constant cross-section and 2-D vertical mathematical models (e.g. Li and O'Donnell (1997)), or on observations in a single cross-section (e.g Turrell et al., 1996; Jay and Smith, 1990a,b; Stacey et al., 2001). Mccarthy (1993) is an exception. He presented one of the very few papers on residual circulation generated by the combined effect of tide and gravitational circulation in an estuary with exponentially varying width. He used a 2-D vertical model and perturbation analysis to identify the mixing mechanisms that combine into longitudinal dispersion. In the estuary with exponentially varying width, McCarthy indeed obtained a dome-shaped intrusion curve and hence a very slight density gradient near the mouth. He concluded that density driven mixing is weak at the estuary mouth and tidal induced landward buoyancy transport is dominant. Further inland, the density driven mixing takes over to counteract the seaward Lagrangean advection of salt. The density driven mixing is a function of the salinity gradient, whereas the tide driven mixing is rather a function of the salinity and the width.

Finally there is the type of residual circulation not considered by (Mccarthy, 1993), which Fischer et al. (1979) call **tidal pumping**. It is partly the result of an irregular topography (as is prominent in Rias but not in alluvial estuaries) and partly of the existence of separate ebb and flood channels that have cross-over points. The latter is a dominant mechanism in the wider part of funnel-shaped estuaries and is discussed in the next section.

4.5 Residual circulation through flood and ebb channels

Strongly funnel shaped estuaries develop separate flood and ebb channels. The Schelde presented in Fig. 4.2 is a good example, but similar patterns can be observed in other funnel-shaped estuaries such as the Pungue, the Columbia and the Thames. In the flood channel the amplitude of the landward tidal velocity is about 20% larger than in the ebb channel. Also the flood channel is about 20% shorter than the ebb channel. As a result, on the incoming tide, the relatively saline water flowing through the flood channel arrives earlier at the cross-over point than the relatively fresh water in the ebb channel. On the ebb tide, the amplitude of the tidal velocity in the ebb channel is substantially higher than in the flood channel, about 40%. Although the ebb channel is 20% longer than the flood channel, the relatively fresh water flowing through the ebb channel reaches the cross-over point earlier than the relatively saline water ebbing through the flood channel.

In the following a relation is derived for the salt dispersion by this type of residual circulation based on a box model, see Fig. 4.3. The box model represents one ebb-flood channel loop of length L_{ef}. We assume that in the flood channel the transfer of salt is Lagrangean with little mixing (since at the mouth the longitudinal salinity gradient is small and there is no significant connection between the ebb and flood channel). Through the flood channel, over a tidal cycle, a

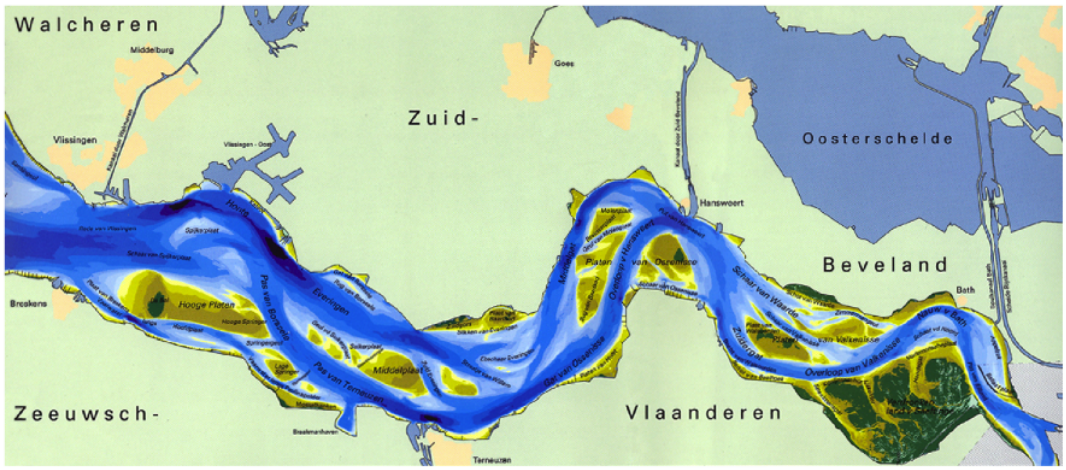

Figure 4.2: Flood and ebb channels in the Schelde.

salt flux F_f is conveyed to the next cell equal to:

$$F_f = S_0 A_f \frac{E}{T} \frac{\Delta v}{v} \tag{4.4}$$

where S_0 is the salinity at the estuary mouth, A_f is the cross-sectional area of the flood channel, E is the tidal excursion, T is the tidal period, and $e_p = \Delta v / v$ is the relative difference of the tidal velocity amplitude between the flood and ebb currents in the flood channel, which is the **tidal pumping efficiency**. In order to close the salt balance, assuming a steady state situation, this flux should be counteracted by the salt flux F_e in downstream direction through the ebb channel:

$$F_e = -S_1 \left(A_f \frac{E}{T} \frac{\Delta v}{v} - Q_f \right) \tag{4.5}$$

where Q_f is the fresh water discharge, which is a scalar with a positive value. The sum of these fluxes should be zero, yielding:

$$(S_1 - S_0) A_f \frac{E}{T} \frac{\Delta v}{v} = -Q_f S_1 \tag{4.6}$$

or:

$$\frac{\partial S}{\partial x} L_{ef} A_f \frac{E}{T} \frac{\Delta v}{v} = -Q_f S \tag{4.7}$$

Because the positive x-axis points upstream, the salinity gradient is negative.

We can compare (4.7) to the general steady state salt dispersion equation:

$$DA \frac{\partial S}{\partial x} = -Q_f S \tag{4.8}$$

where D is the longitudinal effective tidal average dispersion coefficient. The derivation of this equation is presented in detail in the next chapter (equation (5.16)), but is merely represented here. If we compare (4.7) and (4.8) we immediately see the expression for D_{ef}, the effective tidal average dispersion coefficient resulting from residual circulation in the ebb-flood channel system:

$$D_{ef} = \frac{A_f}{A} \frac{\Delta v}{v} \frac{E}{T} L_{ef} = 0.5 e_p \frac{E}{T} L_{ef} \tag{4.9}$$

This is a very straightforward and simple result. It implies that salt intrusion due to residual circulation between ebb and flood channels is proportional to: 1) the length of ebb-flood interaction loop, 2) the tidal excursion, and 3) a tidal pumping efficiency $\Delta v / v$. The ratio of A_f / A

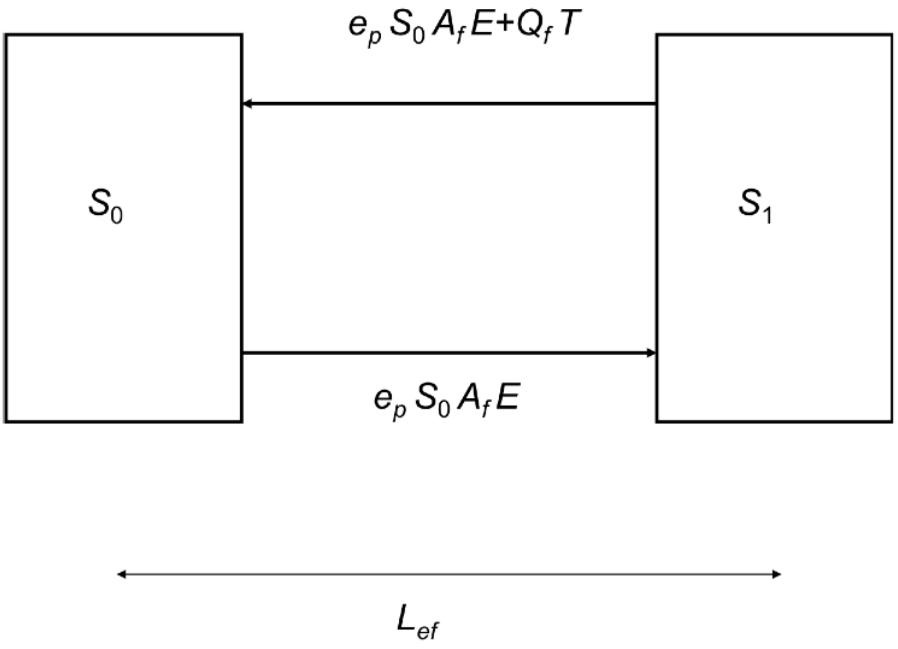

Figure 4.3: Box model for ebb-flood channel dispersion.

may be assumed to be close to 0.5. A possible deviation from 0.5 can be included in the pumping efficiency e_p.

Relation (4.9) was tested by Nguyen et al. (2008b) using a simple Lagrangean model where mixing only takes place at the cross-over points. The model shows that in the most downstream loop pure seawater fills the flood channel, while mixed, somewhat fresher, water flows down the ebb channel. In the second loop the same happens, resulting in a decreasing salinity following a 'stair-case' pattern (see Figure 4.4). The intrusion follows a dome-shape. We also see that the longer the loop length, the stronger the dome-shape is. If the loop length and the tidal pumping efficiency is increased the longitudinal dispersion increases proportionally, in agreement with (4.9). Subsequently, we studied the relation between the loop length and the estuary geometry, the loop length being a crucial parameter that appears to become smaller as the estuary becomes narrower. Figure 4.2 presents an illustration of the flood-ebb channel pattern in the Schelde estuary. The following approach was followed. Since the loop length scales at the width convergence b, the dimensionless ratio of L_{ef} to b was analysed. It appears that there is a certain width at which separate ebb and flood channels no longer develop. This width B_L depends on the width to depth ratio of a stable channel, so it is logical to assume that there is a fixed ratio of B_L/h that forms the threshold for separate ebb and flood channels to develop. In the Schelde and the Columbia this ratio lies at about 100. The values of B_L in the Schelde and Columbia are both about 1000 m, the average depth in both estuaries being about 10 m. Now the geometric relation sought should be a relation between the loop length and the width at the cross-over point between two loops. One can see the analogy with a standing wave of which the nodes are located at the constriction point where the ebb and flood currents cross-over. The width of the constrictions and the angle of the banks determine the space within which the sinus wave can develop. Fig. 4.5 shows a relation between L_{ef}/b and B/B_L for the Schelde and the Columbia. The points of both estuaries fit the same pattern. The equation describing this relation is based on the equation derived for the effective longitudinal dispersion presented in Section 4.8.

Because near the mouth of a funnel shaped estuary the salinity gradient is very small, the dominant mechanism near the mouth is the residual circulation by ebb-flood channel interaction.

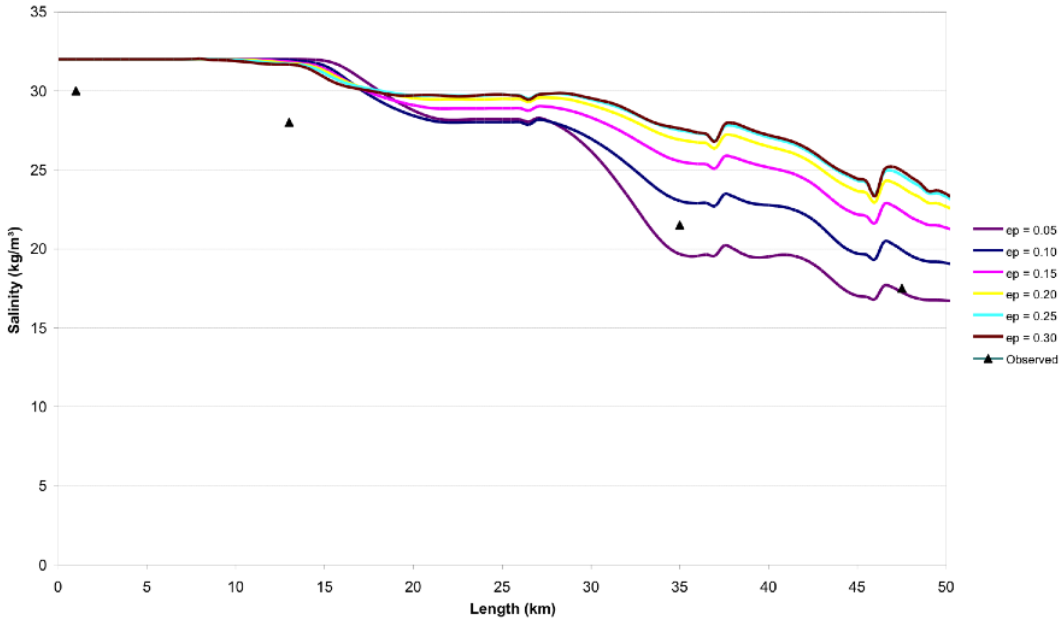

Figure 4.4: Lagrangean model for ebb-flood channel interaction considering different pumping efficiencies (e_p).

So near the mouth of funnel-shaped estuaries the dispersion by the ebb-flood channel interaction may be assumed to be equal to the effective longitudinal dispersion. We saw that the dispersion generated by this mechanism is proportional to the length of the ebb-flood channel loop. As a result, the loop length L_{ef} should obey a similar equation as the effective longitudinal dispersion presented in (4.36). The equation, hence has to be of the following type:

$$\frac{L_{ef}}{b} = \alpha_L \left(1 - \beta_L \left(\frac{B_0}{B} - 1\right)\right) \tag{4.10}$$

The condition that $L_{ef} = 0$ at $B = B_L$ yields an expression for β_L, resulting into:

$$\frac{L_{ef}}{b} = \alpha_L \left(1 - \left(\frac{B_L}{B_0 - B_L}\frac{B_0 - B}{B}\right)\right) = \alpha_L \left(\frac{1 - B_L/B}{1 - B_L/B_0}\right) \tag{4.11}$$

This equation indeed fits the data points very well, as we can see in Figure 4.5. It yields a value for α_L of 0.5. In view of the straightforward analysis made the result looks surprisingly accurate. The good fit is a confirmation of the adequacy of the box model and the assumption that ebb-flood channel interaction is the main mechanism in the lower part of funnel-shaped estuaries and it supports the validity of the equation for the effective longitudinal dispersion equation. However, certainly for the time being, we should consider (4.11) as a result obtained by curve fitting rather than as a physical law.

The resulting equation for the dispersion generated by the residual circulation in ebb and flood channels then reads:

$$D_{ef} = \frac{e_p}{4}\frac{Eb}{T}\left(\frac{1 - B_L/B_0\ \exp(x/b)}{1 - B_L/B_0}\right) \tag{4.12}$$

This equation is only valid if $B > B_L$. If $B \leq B_L$ then $D_{ef} = 0$. If $B > B_L$ we see from (4.12) that at $x = 0$ the dispersion due to residual circulation equals $e_p Eb/(4T)$. This is a surprisingly simple result.

In summary, we have seen that in funnel-shaped estuaries ebb and flood channels occur if the estuary is wide enough for these channels to develop. In the Schelde and Columbia this happens downstream from the point where the width to depth ratio is about 100. Downstream from this point, the residual circulation between ebb and flood channels becomes a dominant mechanism (if the salinity gradient is small). The mixing by this mechanism strongly depends on the estuary width, which forces the loop length. The effective longitudinal dispersion generated by the flood-ebb channel interaction is directly proportional to: the loop length, the tidal excursion and the efficiency of the tidal pumping.

Being such a dominant mechanism, it is surprising that so little research has been done on this type of circulation. There may be a number of reasons for this apparent lack of knowledge:

1. To study this mechanism in the field implies a major operation. A survey would involve a dense network of monitoring points and have to stretch over a considerable period of time to monitor the spring-neap interaction.

2. Three-dimensional hydraulic models can reproduce the mixing by flood and ebb-channel interaction. There does not appear to be a need for understanding how the mechanism works, if our models can mimic it.

3. The theoretical research on mixing is still too much focussed on 2-D mathematical modelling and analysis in a single cross-section. Or as Jay et al. (1997) put it: *"estuarine circulation theory has focused on two-dimensional analyses that treat either vertical or lateral variations but not both."*

4.6 The decomposition method and why it is not very useful

Another way of differentiating between mechanisms is by decomposing the longitudinal salt flux through a cross-section into different components. Following the maximum generality scaling approach, Smith (1980) arrived at four dominant mechanisms for well-mixed estuaries: the oscillatory vertical shear (earlier described by Bowden, 1967, 1981), the oscillatory transverse shear (earlier described by Okubo, 1967); the interaction between tidal and buoyancy effects; and the buoyancy driven steady horizontal circulation. Another approach, originally considered by Hansen (1965), was followed by many researchers who arrived at a considerable number of decomposed mixing mechanisms such as: vertical and transverse shear dispersion (West and Mangat, 1986); transverse net circulation (tide driven, density driven and boundary-induced, analyzed by Fischer, 1972); vertical net circulation (earlier analyzed by Hansen, 1965); transverse (and vertical) oscillatory shear (analyzed by Holley et al., 1970); and transverse (and vertical) gravitational net circulation (West and Broyd, 1981). In Hansen's approach, the salinity, the velocity and cross-sectional area are considered to be the sum of a tidal mean value (subscript 0), a tidally varying (subscript 1) and a turbulent value (subscript 2):

$$s(x,y,z,t) = s_0(x) + s_1(x,t) + s_2(x,y,z,t) \tag{4.13}$$

$$U(x,y,z,t) = U_0(x) + U_1(x,t) + U_2(x,y,z,t) \tag{4.14}$$

$$A(x,y,z,t) = A_0(x) + A_1(x,t) \tag{4.15}$$

The salt flux F can be defined as:

$$F = \int U s \mathrm{d}A \tag{4.16}$$

The tidal average salt flux can then be decomposed in six terms (Fischer, 1972):

$$\langle F \rangle = A_0 U_0 s_0 + \langle A_1 U_1 \rangle s_0 + A_0 \langle U_1 s_1 \rangle + U_0 \langle A_1 s_1 \rangle + \langle A_1 (U_1 s_1)' \rangle + \langle A U_2 s_2 \rangle \tag{4.17}$$

in which $(U_1 s_1)'$ is the deviation of $U_1 s_1$ from its tidal mean and where the angle brackets denote a tidal average value.

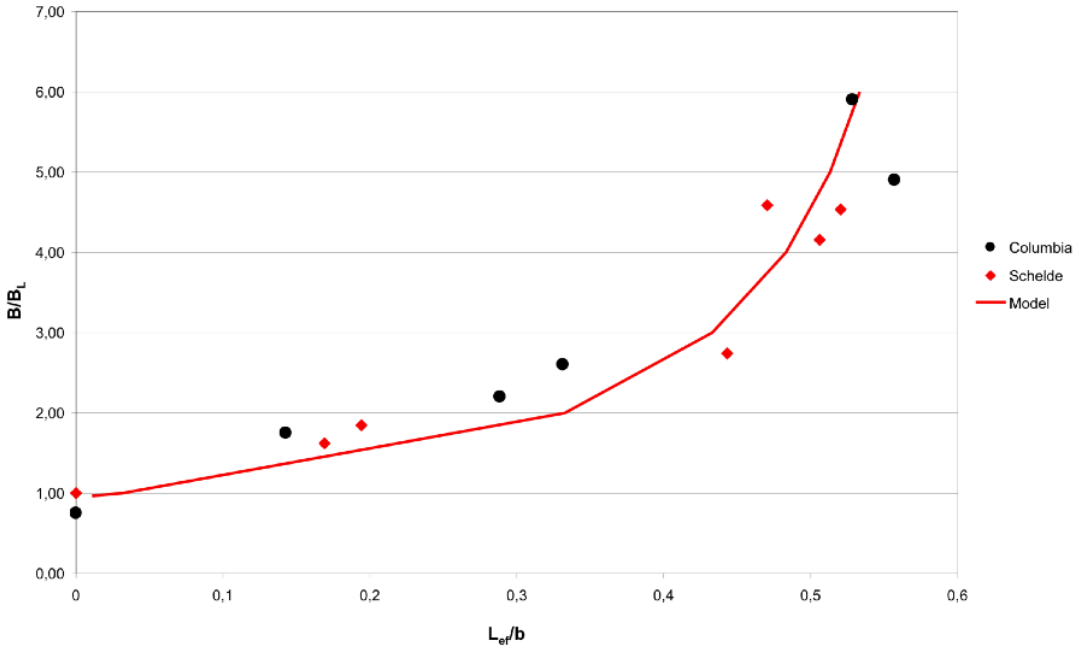

Figure 4.5: Relationship between the loop length to convergence length ratio L_{ef}/b and the dimensionless width B/B_L.

Lagrange versus Euler and the importance of Stokes' drift in the decomposition

The first two terms on the right hand member constitute the advective salt flux caused by the fresh water discharge Q_f. The advective Lagrangean salt transport resulting of the river discharge $A_0 U_f s_0$ is not equal to the first term only, which is the Eulerian average salt transport, directed downstream. Dyer (1973) indicated that the second term, the salt transport by Stokes' drift, is part of the Lagrangean transport and follows from the river discharge not being equal to the Eulerian integral, as the cross-sectional area varies over time. We saw in Section 2.4 that Stokes' drift is a mathematical artefact of the Eulerian reference frame and not a real mechanism. We can see how in the decomposition method this may cause problems. We can analyse the importance of these terms as follows:

$$-Q_f = \frac{1}{T}\int AU\mathrm{d}t = \overline{AU} - \frac{1}{2\pi}\int \hat{A}v\sin(\omega t - \varepsilon)\cos(\omega t)\mathrm{d}t \tag{4.18}$$

where Q_f has received a negative sign because it is directed downstream and $\hat{A}$ is the amplitude of the tidal cross-sectional area variation. The harmonics are chosen in correspondence with the definition for h and U in Chapter 3: (3.30)-(3.32). The first term on the right hand side is the Eulerian mean discharge which is directed downstream, whereas the second term represents the Stokes drift, which is directed upstream (the mean Eulerian velocity is negative, pointing downstream, as we can also see in Figure 2.11). It implies that in absolute terms the Eulerian discharge should be larger than the Stokes drift by an amount equal to Q_f. We can see that the Stokes drift is zero for a standing wave (ε=0); since the integral of $\sin(2\alpha)$ over 2π is zero. In that case the Eulerian discharge equals Q_f. For a progressive wave, however, with $\varepsilon = \pi/2$, the harmonics are exactly in phase. The argument of the integral then is -$\cos^2\alpha$, of which the integral is -π. Hence for a progressive wave, the Stokes drift is at its maximum equaling $\hat{A}u = B\eta v$ (in upstream direction). If we scale the salt transport by this Stokes drift against the Lagrangean salt transport, then the proportion is $\eta v/hU_f$ (with U_f as the velocity of the fresh water discharge), which is equal to ξ/φ. φ is unity at the point where there is only one moment of slack (point P

in Fig. 1.6 where $U_f = v$). Near the mouth of a funnel shaped estuary φ becomes very small, smaller than ξ, and the relative contribution of the Stokes drift to the salt transport becomes larger, in absolute terms larger than the Lagrangean salt flux. Because the Lagrangean salt flux remains the same, the Eulerian (downstream) salt transport should increase at the same rate (their sum being equal to the Lagrangean salt flux). So in an alluvial (positive) estuary, where $\varepsilon > 0$, the Stokes drift salt transport is not negligible compared to the Lagrangean salt flux, the balance between them being the tidal average Eulerian discharge. The worrying thing is that the Stokes drift salt transport is not a real transport (as we saw in section 2.4), but a mathematical artefact, which makes this decomposition method tricky.

The usefulness of decomposition

Van de Kreeke and Zimmerman (1990), following the suggestion of Fischer (1972), split-up s_2 and U_2 even further into vertical and transverse components, but neglected tidal variations in A, leading to 6 components containing: advection, geometry induced dispersion, residual lateral circulation, vertical density circulation, lateral oscillatory shear and vertical shear. Park and James (1990), who (after Dyer, 1974) in addition considered the tidal variation, decomposed the salt flux into 66 components, grouped into an equation of 11 terms. These components had to be grouped to be able to attribute some physical meaning to them. Jay et al. (1997) observed: *"Little attempt has been made to connect estuarine circulation to the salt fluxes that must maintain it. The result has been a welter of confusing transport expansions filled with terms of uncertain meaning".*

Hence, the approach followed in this study is quite different from the decomposition method. We start with the observed salt fluxes and derive the dispersion from the observed salinity distribution. This is a 'downward' approach as discussed in section 4.2. In contrast, the decomposition method is a reductionist 'upward' approach that does not yield directly applicable practical equations, but which in combination with the 'downward' approach can yield insight into the mechanisms at work. Subsequently we may be able to attribute physical meaning to the relationships found by 'downward' analysis. However, there are a number of problems with the decomposition method:

1. It is done in cross-sections, whereas mixing is a 3-dimensional process that acts mainly in the longitudinal direction. For observations in a cross-section to have significance, a large number of cross-sections need to be monitored. Moreover the dominant mixing mechanism changes from cross-section to cross-section. In one section (for instance in an ebb-channel) gravitational circulation may be dominant, but in another (for instance in a cross-over point of a flood and ebb channel) it may be shear by cross-over currents and residual circulation. So an observation in one cross-section does not tell us much.

2. The relative error that we make if we subtract fluxes can be very large, particularly if the residual fluxes are small compared to the momentary fluxes. In tidal hydraulics the momentary fluxes are several orders of magnitude larger than the residual fluxes and hence the errors in the residual fluxes are often larger than the residual fluxes themselves.

3. It is highly data-intensive. To determine a residual flux in a cross-section one has to continue monitoring in the cross-section during several tidal periods (also to account for spring-neap interaction) and sample the entire cross-section at many points over the width and depth. This is both data-intensive and labour-intensive, and hence expensive.

To investigate which of the many components is the dominant mechanism in a particular estuary under given hydrological conditions is, at the least, time consuming. Moreover, several scientists question the usefulness of decomposition and the correctness of linear superposition of mixing mechanisms. Important mixing processes such as the alternation between different degrees of stratification or the breaking of internal waves cannot be adequately described by the decomposition method. Rattray and Dworski (1980) state that the different components are closely interrelated, and that conclusions to be derived from this method of analysis (such as the relative importance of vertical and transverse variations to the total flux) depend on the details of the decomposition, details which are chosen by the analyst. Chatwin and Allen (1985) remark that

in view of this dependency, the question of whether the transverse or the vertical dispersion is the most important salt intrusion mechanism may be less fundamental than was once believed, in that the issue is to some extent prejudged by the method of decomposition chosen.

Jay et al. (1997) observed that much research on the decomposition was done in cross-sections without consideration for the larger scale salt fluxes that should support the individual mechanisms. Moreover, they observed that *"the importance of the lateral terms emphasizes the three-dimensionality of estuarine transport and clearly demonstrate that two-dimensional theory cannot totally explain transport, even in narrow channelized estuaries"* (where the effect of temporal width variation due to the tide is small). Hence the three-dimensional character of mixing is crucial.

One wonders why researchers have lingered so long on two-dimensional analyses. There are probably two reasons. One is that much of the research to date started with laboratory flume analysis and once you are on that track, it may be difficult to explore another. The second reason may be that most of the hydraulic engineers who ventured into mixing theory started from the analysis of stratified systems, which were originally studied in 2-D.

The most advanced decomposition method used is by Mccarthy (1993), who integrated the 2-D hydraulic and salt balance equations in an estuary with an exponential shape and found the resulting fluxes by perturbation analysis. He distinguished five components (with his terminology between quotes): 1) the landward tide-driven transport ("tidal buoyancy transport"), 2) the seaward Eulerian (non-tidal) discharge ("Eulerian buoyancy transport"), 3) the landward Stokes drift ("Stokes buoyancy transport"), 4) the landward "diffusive buoyancy transport", and 5) the seaward "variable breadth diffusive transport". The second and third components (as we have seen) are opposed and their sum equals the Lagrangean seaward salt flux. The fourth and fifth components constitute the transport driven by the salinity gradient, representing the process driven by the gravitational circulation, both vertically and laterally, but mostly laterally since the width is so much larger than the depth. Although his study did not consider the important transport mechanism by ebb-flood channel interaction, it clearly illustrated that tide-driven transport is dominant in the downstream part of estuaries, while density-driven transport is dominant at the upstream part of the salt intrusion curve. In doing so, he also emphasized the importance of the width variation and the interconnectedness of lateral, vertical and longitudinal mixing processes. Had he included the ebb-flood channel interaction, then this would have yielded a different combination of mixing mechanisms, but still the same amount of net seaward and net landward fluxes. Hence the inclusion of a new mechanism affects the magnitude of the others. This is also what happens in the real world. The mixing mechanisms provide feedback on each other. As a result, for the study of effective longitudinal salt intrusion it is more important to look at the mixing process as a whole than to look at each of the individual mixing mechanism.

Hence in this book it is not the objective to further study the array of separate processes involved in dispersion. If dispersion is symbolized by an instrument, then the approach followed here is to study what the instrument does and what outer effect it has on the salt balance rather than coming to grips with all the intricacies of its inner functioning. In short, the study focuses on the apparent functioning of dispersion: how dispersion counteracts the advective downstream salt transport, as a function of geometry, hydrodynamics and density differences. Dronkers and Van Os (1981) supported this approach by stating that for most practical purposes, for example to determine the total salt intrusion length, it is sufficient to know the overall effect of the mixing processes rather than to understand the individual mechanisms. The analysis of the individual mixing mechanisms will help our physical understanding of how mixing works, but the addition of individual mechanisms will not yield a workable equation with which the salt intrusion can be computed and predicted in a real-life situation.

In the following, therefore, we shall focus on the effective, also called apparent, tidal average and cross-sectional average longitudinal x-dependent dispersion and how it contributes to salt intrusion. In the derivation we shall incorporate the insight gained from analysing the decomposition methods.

4.7 Longitudinal effective dispersion

The effective dispersion incorporates all the dispersion mechanisms that counteract the advective salt transport. In a positive estuary where the salinity decreases in upstream direction, these dispersion mechanisms result in a landward transport of salt. If the dispersive salt transport is stronger than the advective salt transport then the salinity at a certain location increases with time; if it is weaker, then the salinity decreases with time. If the dispersive and advective transports are equally strong, then a tidal-average state of equilibrium occurs.

In the case of equilibrium, with the salinity distribution known, the apparent tidal average dispersion coefficient D can be computed from (4.8). This approach of determining the effective horizontal dispersion coefficient on the basis of the steady state conservation of mass equation was first suggested by Stommel (1953) and later recommended by Bowden (1967). Before using this method, however, one has to check if a state of (tidal average) equilibrium indeed occurs.

Chatwin and Allen (1985) derived the following conditions under which the use of one-dimensional mixing models is justified:

1) the estuary should be long compared to the cross-sectional dimensions and the tidal excursion;

2) changes of geometry in the x-direction must be gradual.

Surely in the estuaries under study here, these conditions do not put any serious constraint on the applicability of one-dimensional mixing models. Dronkers (1982) gave an additional condition for applying 1-D mixing models, the most important of which is that:

3) the time of averaging (e.g. one tidal period) should be larger than "the time scale of cross-sectional mixing" which is defined as the average time required for turbulent mixing in the cross-section.

In very wide estuaries this third condition may require longer averaging times (e.g. several tidal periods), but in the Schelde, an estuary more than 10 km wide, the condition was amply met, according to Dronkers (1982). Again this condition does not pose a strict limitation on the applicability of 1-D mixing models. It may be concluded that if the salt intrusion in an estuary can be adequately described by a one-dimensional tidal averaged model, then its use is apparently justified. This is in agreement with the observation by Fischer et al. (1979) that it is better to consider the one-dimensional tidal average dispersion model as an empirical model, which should be verified in practise. Fortunately, practice has shown that the domain of applicability of the 1-D model in estuaries is large.

If we follow this approach then the application of the one-dimensional dispersion model depends on finding a suitable relation for D. Of the different types of relations tried in the literature, Prandle (1981) gave a good overview. He suggested the following types of relations:

$$D = D_0 \tag{4.19}$$

$$D \propto \frac{\partial S}{\partial x} \tag{4.20}$$

$$D \propto \left(\frac{\partial S}{\partial x}\right)^2 \tag{4.21}$$

which can be summarized as:

$$D \propto \left(\frac{\partial S}{\partial x}\right)^k \tag{4.22}$$

with k=0, 1, 2, respectively.

As far as theoretical backing is concerned, the first relation (k=0) occurs when the amount of energy available for mixing is uniformly distributed over the estuary. Such a situation occurs where the mixing is fully tide driven and where both the tidal range and the tidal excursion are constant along the estuary (i.e. in an ideal estuary). The second relation (k=1) corresponds with the case where the mixing is fully density driven and where the dispersion is proportional to

the moment M, see (4.2), exerted by the two hydrostatic forces shown in Figure 2.3. Hence, the density driven dispersion is proportional to the salinity gradient. If the density driven dispersion has a strong lateral component, then Fischer et al. (1979) suggested to use (4.3). This is an equation type with k=2.

With regard to estuary shape, Prandle (1981) obtained some unexpected results. He showed that in flumes and in estuaries with almost constant cross-section (Rotterdam Waterway) (4.20) and (4.21) performed best, but that in estuaries with a pronounced funnel shape, such as the Thames, the St. Lawrence, the Delaware and the Bristol Channel, very good results were obtained with the simple (4.19).

What is surprising is that some researchers suggested the opposite. Several (among others West and Broyd, 1981) mentioned that density driven dispersion (k=1) prevails in deep and wide estuaries and tide driven dispersion (k=0) in narrow and shallow estuaries. This appears in contradiction with what we found earlier that estuaries with a pronounced funnel shape have dome-shaped salt intrusion curves, whereas estuaries with almost a constant cross-section have recession type intrusion curves. Near the mouth of an estuary with a dome type intrusion curve (being an estuary with a pronounced funnel shape where the mixing process is claimed to be density driven) hardly any density gradient occurs, and hence hardly any density driven mixing can occur. One reason for this paradox is that the researchers who studied deep and wide estuaries with dome shaped intrusion curves and who concluded that the mixing was primarily density driven, carried out their investigations somewhere in the middle reach of the salt intrusion curve. So, although they were correct in identifying density driven mixing as the dominant mechanism in the middle reach of wide estuaries, hardly any density driven mixing occurred in the wider part, near the mouth, of these estuaries.

So it is more correct to draw another conclusion. A narrow and prismatic estuary like the Rotterdam Waterway has a high level of stratification and a rather steep (recession-type) salt intrusion curve. The dominant mixing mechanism is gravitational circulation, which is best described by (4.20) or (4.21). A wide funnel shaped estuary, such as the Thames, the Delaware or the Schelde, has a dome-shaped intrusion curve and a small density gradient near the mouth. In the downstream part of such an estuary the dominant mechanism is tide-driven mixing in the form of ebb and flood channel interaction (as long as the estuary is wide enough for separate ebb and flood channels to develop: B/h >100). In the reach where the dome shaped intrusion curves bends down, and hence the salinity gradient is strong, gravitational circulation becomes dominant with a strong lateral component.

As a result, the dispersion is highest near the estuary mouth, decreasing in upstream direction. Because the gravitational circulation is proportional to the density gradient, the gravitational dispersion reduces with the salinity gradient until it becomes very small near the toe of the intrusion curve. Beyond the toe of the intrusion curve the dispersion is dominated by turbulent diffusion, which is small compared to the other mechanisms.

Many researchers, such as Preddy (1954), Kent (1958), Ippen and Harleman (1961), and Stigter and Siemons (1967), recognised that the effective dispersion is highest near the estuary mouth and that it decreases upstream to become zero, or virtually zero, near the toe of the salt intrusion curve. The challenge now is to find a relation that applies well in all estuaries, whether funnel shaped or of almost uniform cross-section, which is easy to incorporate in a predictive model and which is physically appealing. More specifically:

a) The relation should be dimensionally sound, with dimensionless coefficients,

b) The dispersion should decrease in upstream direction,

c) The dispersion should be large near the mouth of funnel shaped estuaries,

d) The relation should be continuous and easy to apply.

The following relation suggested by Savenije (1986, 1989, 1993a,b) performs well against these criteria:

$$\frac{D}{D_0} = \left(\frac{S}{S_0}\right)^K \tag{4.23}$$

where K is the dimensionless Van der Burgh's coefficient (Van der Burgh, 1972) which lies between zero and unity. This relation has been widely tested and successfully applied in about 20 estuaries world-wide. It is interesting to see that in contrast to Prandle's relations, summarized by (4.22), in this equation the salinity is used instead of the salinity gradient.

If we use this simple relation, then a dome shaped intrusion curve (which occurs in wide and deep estuaries) results in a high value of the dispersion coefficient near the mouth, decreasing slowly in upstream direction to become zero at the toe of the intrusion curve. In a narrow estuary, where the salinity decreases steeply, the salinity curve has an exponential decline (recession shape). In an exponential function, the function value is directly proportional to its gradient. So $\mathrm{d}S/\mathrm{d}x$ is proportional to S, and the dispersion is still proportional to the salinity gradient to the power K. This is in agreement with the theory. So (4.23) both applies to tidal driven dispersion (particularly ebb-flood channel exchange) and to gravitational circulation. This equation describes the mixing process well: near the mouth, in the middle and near the toe, and both in funnel shaped estuaries and in estuaries with a long convergence length. The coefficient K is obtained through calibration.

Fig. 4.6 illustrates how (4.23) performs in relation to an observed salt intrusion curve in the Pungue estuary with a dome-shaped intrusion curve. The thick line is a dimensionless salt intrusion curve S/S_0 that fits the observations made on 3 October 1993. The observations at HWS have been translated half a tidal excursion to the left and the observations at LWS half a tidal excursion to the right. The dimensionless dispersion curve has been computed with the steady state salt balance equation (Eq. 4.8), but it also completely corresponds with (4.23). For the case where K=1, the curves of D/D_0 and S/S_0 coincide. So the line indicated by D/D_0 is the line that fits the observed effective 1-D tidal average dispersion.

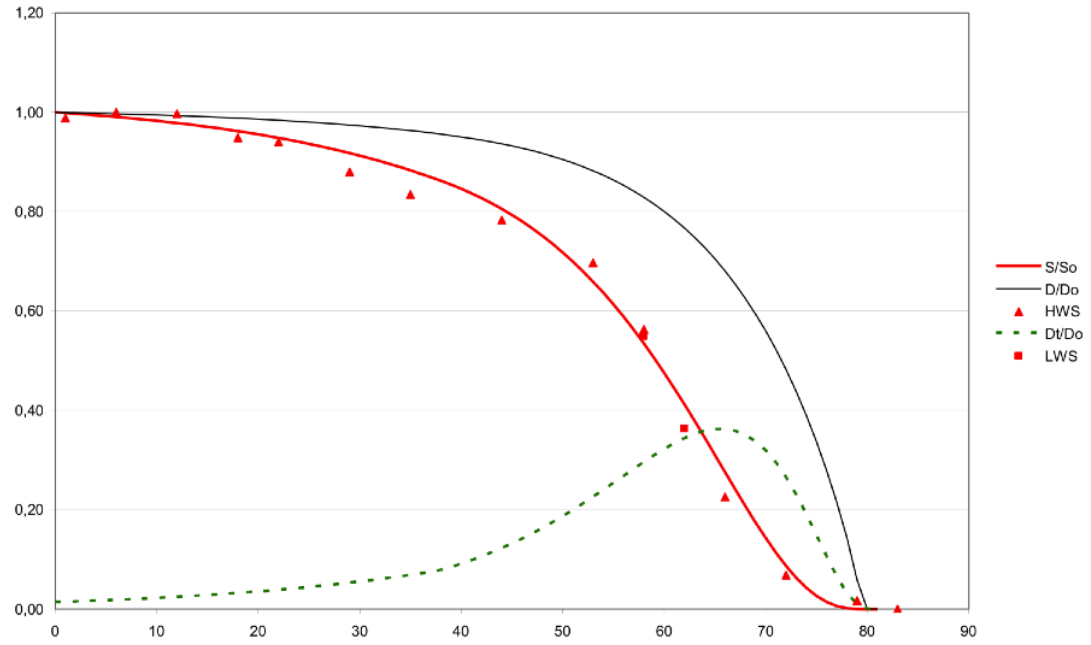

Figure 4.6: Dispersion equation derived from the salt intrusion curve measured in the Pungué estuary on 3/10/1993.

Finally, the dashed line corresponds with (4.20), and reflects the density driven dispersion. It is not possible to scale the density driven mixing exactly; the position of the curve is merely indicative. If we assume that the total dispersion is the sum of the tide driven dispersion and the density driven dispersion, then the difference between these two curves equals the tide driven dispersion. It can be seen in Fig. 4.6 that the tide driven dispersion near the mouth is very

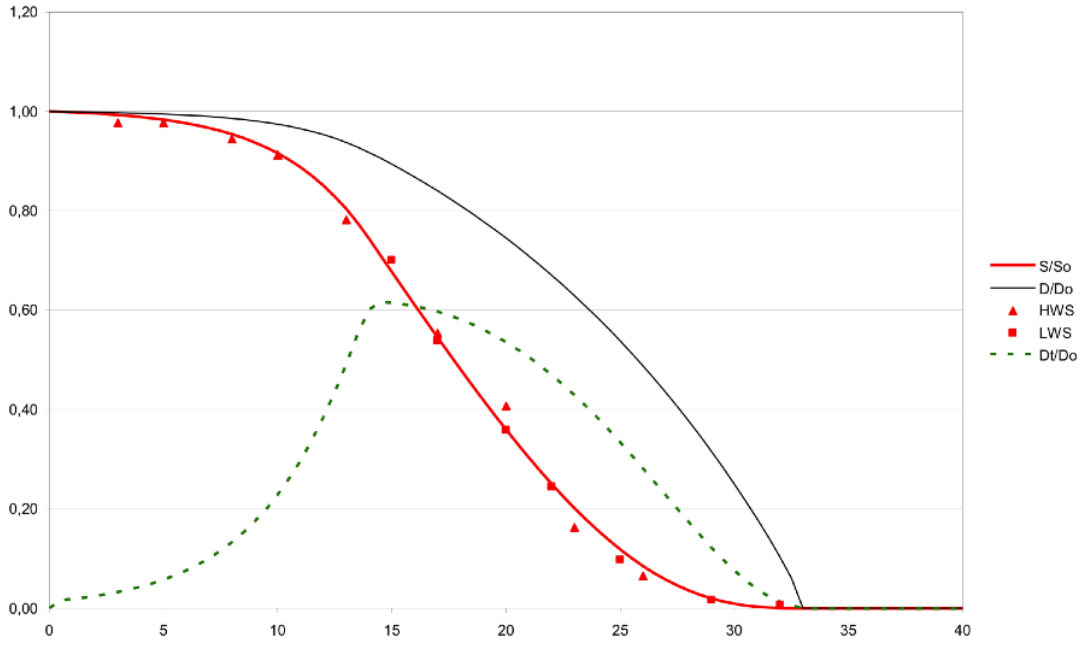

Figure 4.7: Dispersion equation derived from the salt intrusion curve measured in the Maputo estuary on 29/5/1984.

large due to ebb-flood channel interaction and reduces as the estuary becomes narrower. After the point where the salinity gradient is at its steepest the density driven mixing becomes more important. The value of K obtained in this estuary is 0.3, suggesting that tide-driven mixing is more important than density driven mixing.

Fig. 4.7 shows a similar graph for the Maputo estuary with a bell-shaped intrusion curve. It is based on observations made on 29 May 1984. Here we also see that tide-driven mixing is dominant in the wider part of the estuary, but less so as in the strongly funnel-shaped Pungue estuary. Upstream from the point where the salinity gradient has its maximum, the density driven mixing is dominant. The Maputo has a trumpet shape with a short convergence length near the mouth (of 3.5 km) and a longer convergence length upstream (16 km). The inflection point of the density driven mixing lies exactly at the point where the change of the convergence length takes place: the upper reach having a more prismatic character and the lower reach a pronounced funnel shape. The value of K in this estuary is also 0.3, with tide-driven mixing being more important than density driven mixing.

Fig. 4.8, finally, presents an estuary with a near prismatic channel: The Limpopo, with a convergence length of 130 km in the upstream reach (and 50 km in the downstream reach). As a result the intrusion curve has a recession shape, which is an indication of gravitational circulation being the dominant mechanism. We see that this is indeed the case. Consequently we expect a higher value of K which is indeed the case K being equal to 0.5.

We see that (4.23) can describe the longitudinal salinity distribution very well in different types of estuaries. (4.23) has a much wider range of applicability than either one of (4.19)-(4.22). It can be used to describe tide-driven mixing as well as gravitational mixing and it is a relatively simple and dimensionally correct formula. In the following we look further into the physical meaning of (4.23).

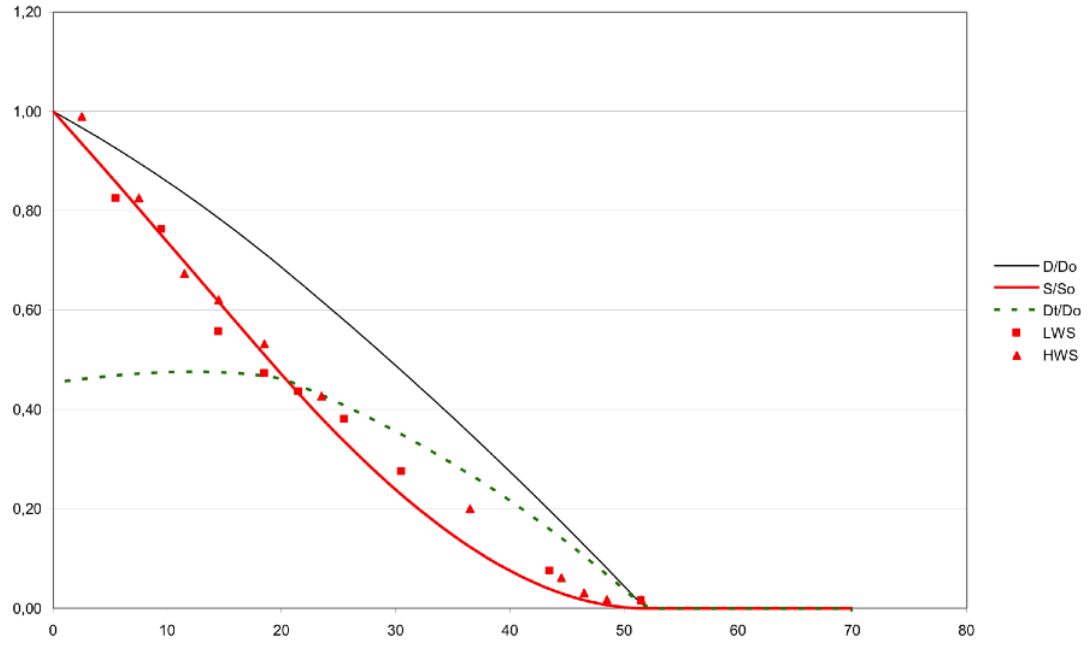

Figure 4.8: Dispersion equation derived from the salt intrusion curve measured in the Limpopo estuary on 24/7/1994.

4.8 Van der Burgh's equation

Van der Burgh (1972) developed a purely empirical method on the basis of the effective tidal average dispersion under equilibrium conditions. He made use of a considerable number of salinity measurements carried out in the Rotterdam Waterway (excavated in 1868) over a period of 80 years (1892-1971), the first of which were published in a handwritten document by Canter Cremers (1905). In addition he used salt measurements carried out in a number of tidal inlets of the Dutch delta system, including the Schelde. He based his analysis on the steady state salt balance equation (4.8), and assumed that the HWS and LWS salinities could be obtained through longitudinal translation over half the tidal excursion, which indeed is correct.

Van der Burgh analysed the salt distributions surveyed in the Rotterdam Waterway over the period 1905-1971. This is a period over which the channel was deepened several times, so the data set covers various depths. He observed that the effective dispersion obtained from (4.8) consistently decreased in upstream direction. Plotting the longitudinal variation of the effective dispersion against the velocity of the fresh water discharge (see Fig. 5.2), he found a direct proportionality:

$$\frac{\partial D}{\partial x} = -K\frac{Q_f}{A} = -KU_f \tag{4.24}$$

where K is Van der Burgh's dimensionless coefficient. Here Q_f and U_f are positive scalars, so the minus sign stems from the fact that the dispersion decreases in upstream direction. This relation, known as Van der Burgh's equation, can be shown to be the same as (4.23). Differentiation of (4.23) with respect to x yields:

$$\frac{\partial D}{\partial x} = -K\frac{D_0}{S}\left(\frac{S}{S_0}\right)^K\frac{\partial S}{\partial x} = -K\frac{D}{S}\frac{\partial S}{\partial x} \tag{4.25}$$

It can be directly seen that combination of this equation with the steady state salt balance equation, (4.8), yields (4.24). This relation is known as Van der Burgh's equation.

A major difficulty Van der Burgh had in determining the effective dispersion was that the exact amount of fresh water discharge in the estuary was not always well known. Although a good estimate was available of the Rhine discharge on entering The Netherlands (at Lobith), the division of the water over the many branches was difficult to determine at that time. In addition, the time required for the salinity distribution in the estuary to adjust to the flow recorded at Lobith was not known. Van der Burgh used the results of an electro-analogous model of the Rhine delta to obtain the fresh flows in the estuary. However, the inaccuracy in the methodology was probably still great, which makes it the more surprising that he came up with this important relationship.

Van der Burgh named his approach the "advective method". His method has the advantage that, for its derivation, it does not require a constant cross-section. Moreover, the relation between $\partial D/\partial x$ and U_f is dimensionally sound.

4.8.1 The physical meaning of Van der Burgh's K

It can be shown mathematically that Van der Burgh's coefficient is a sort of "shape factor" influencing the shape of the salt intrusion curve. Kranenburg, in a personal communication, indicated this to the author for a channel of constant cross-section. The application of this approach to a channel with an exponentially varying cross-section is explored in the following.

Differentiation of (4.8) with respect to x yields:

$$Q_f S' = DA'S + D'AS' + DAS'' \tag{4.26}$$

where a single accent indicates the first partial derivative and a double accent the second partial derivative with respect to x.

Since $A'/A = -1/a$ and $D = -(U_f S/S')$, (4.26) can be elaborated into:

$$D' = -U_f - \frac{DA'}{A} - \frac{DS''}{S'} = -U_f \left(1 + \frac{S}{aS'} - \frac{SS''}{(S')^2}\right) \tag{4.27}$$

Substitution of Van der Burgh's equation yields:

$$K = 1 + \frac{S}{aS'} - \frac{SS''}{(S')^2} \tag{4.28}$$

The influence of K and a on the shape of the salt intrusion curves can be made clear by scaling. We scale S by the sea salinity to obtain the dimensionless salinity:

$$\varsigma(\xi) = \frac{S}{S_0} \tag{4.29}$$

where ξ=x/L. Elaboration of (4.28) then leads to:

$$\frac{\varsigma\varsigma''}{(\varsigma')^2} = (1-K) + \frac{\varsigma}{\varsigma'}\frac{L}{a} \tag{4.30}$$

where ς' is the first derivative of ς with respect to ξ, and ς" is the second derivative. The left hand member is the shape-function which is influenced by two terms on the right hand side. It can be easily seen that the shape function is positive if the curvature ς" is positive (because $\varsigma/\varsigma'^2 \geq 0$ for all ξ on [0,1]).

In the integration of the steady state salt balance equation the boundary condition used is that ς'=0 where ς=0, at the upstream end of the intrusion curve. Since, in a positive estuary, the gradient of the salinity is negative for all ς on [0,1], ς' can only become zero at the toe of the intrusion curve if somewhere within this interval the curvature ς", and hence the shape function, becomes positive. Because the second term of the right hand side of (4.30) is always negative in a positive estuary (since $\varsigma' < 0$), the curvature can only become positive in the interval [0,1] if the first term on the right hand side is positive; this is the case when $K < 1$. Hence there is an upper limit to the value of K. Since the lower boundary of K is zero, it follows that $0 < K < 1$.

Dome shaped (type 3) intrusion curves have a negative curvature ($\varsigma" < 0$), at least in the downstream part of the estuary, and recession shaped (type 1) intrusion curves have a positive curvature ($\varsigma" > 0$). The bell shaped (type 2) intrusion curve is a mixture of these two: dome shaped near the mouth of the estuary and recession shaped at the toe of the intrusion curve. Hence the left hand side of (4.30) is negative in type 3 estuaries, and positive in type 1 estuaries. Therefore, dome shaped intrusion curves occur when the term containing K is small with respect to the absolute value of the term containing L/a (meaning a large value of K and a large value of L/a) and recession shaped intrusion curves in the opposite case (K is small and L/a is small). This is interesting since it implies that K and L/a are shape factors influencing the shape of the salt intrusion curves.

4.8.2 Correspondence with other methods

Van der Burgh's method has similarities with a number of methods developed by other authors. Preddy (1954), Kent (1958), Ippen and Harleman (1961), and Stigter and Siemons (1967) already recognised that the effective dispersion decreased in upstream direction. Mccarthy (1993) clearly demonstrated how the dispersion decreases in upstream direction, to become zero near the toe of the salt intrusion curve.

The theory demonstrating the largest similarity with Van der Burgh's method is that of Hansen (1965). They limited their theory to the central zone of a narrow estuary of constant cross-section. In addition, they assumed that the salinity in the central zone would decrease linearly (no curvature: $S"=0$) in upstream direction. Both are very strong limitations which Van der Burgh's method does not have. On the basis of these strong assumptions, they arrived at three so-called similarity conditions for the two-dimensional vertical description of velocity and salinity, being: that the vertical turbulent viscosity and dispersion were constant along the estuary and that the horizontal tide driven dispersion D_t was defined by:

$$\frac{\partial D_t}{\partial x} = -\frac{Q_f}{A} = -U_f \tag{4.31}$$

which is indeed what we would obtained from (4.27) by substitution of a$\rightarrow \infty$ (constant cross-section) and $S"=0$ (no curvature).

Moreover, they defined the parameter υ by: the fraction of the salt advected seaward with the river discharge ($\upsilon U_f S$) that is balanced by the upstream salt flux associated with tidal dispersion ($D_t \partial S/\partial x$) only. Consequently, by using the steady state conservation of mass equation for salt it can be seen that, υ equals the ratio of the tide driven dispersion D_t to the effective (=total) dispersion D:

$$\nu = \frac{D_t}{D} \tag{4.32}$$

Fischer et al. (1979) gave a wider definition of ν as the fraction of the total landward transport of salinity caused by all dispersion mechanisms other than the density driven circulation, meaning that D_t incorporates all dispersion mechanisms other than density driven dispersion. If $\nu = 0$ then the dispersion is fully density driven; if $\nu = 1$, the dispersion is driven by other mechanisms. Thus combination of (4.31) and (4.32) leads to:

$$\frac{\partial D}{\partial x} = -\frac{1}{\nu}\frac{Q_f}{A} \tag{4.33}$$

which is identical to Van der Burgh's equation for $K=1/\nu$. Apparently, in an estuary with constant cross-section and with a salinity distribution without curvature, Van der Burgh's $K=1/\nu$. In Hansen & Rattray's definition, Van der Burgh's coefficient is the proportion of total effective dispersion to the tide driven dispersion. If $K=1$, the dispersion is fully tide driven. If $K > 1$ the influence of density driven dispersion becomes more pronounced. This is in conflict with the limits to K earlier found, but one should realize that Hansen & Rattray's relation was derived under strongly limiting assumptions such as a constant cross-sectional area and $S"=0$. In an exponentially shaped estuary or in an estuary with a non-linear salinity distribution, Hansen & Rattray's result would have been different, and K would not necessarily have to be larger than unity.

Shaha and Cho (2011) looked at the variability of both K and ν along the axis of the Sumjin River Estuary. They found indeed that K was inversely proportional to ν and that ν decreased from almost unity near the mouth to zero near the toe of the intrusion curve, indicating the transition from tide driven to salinity driven mixing. By differentiation of (4.32) and combination with (4.33) and the Van der Burgh equation, they showed that:

$$K = \frac{1}{\nu}\left(1 - \frac{DA}{Q_f}\frac{\partial \nu}{\partial x}\right) = \frac{1}{\nu}\left(1 + \left(\frac{\partial \nu}{\partial x}\right) / \left(\frac{1}{S}\frac{\partial S}{\partial x}\right)\right) \tag{4.34}$$

Clearly this is based on the assumption that (4.33) is correct, which is doubtful in an exponential estuary. Application of (4.33) in exponential estuaries led to values of K larger than unity, which is not possible, as we saw. Therefore, Shaha and Cho (2011) modified (4.34) to account for an exponential shape, resulting in:

$$K = \frac{1}{\exp(\nu)}\left(1 - \frac{DA}{Q_f}\frac{\partial \nu}{\partial x}\right) = \frac{1}{\exp(\nu)}\left(1 + \left(\frac{\partial \nu}{\partial x}\right) / \left(\frac{1}{S}\frac{\partial S}{\partial x}\right)\right) \tag{4.35}$$

which led to realistic values of K in the Sumjin River estuary (see Figure 3 in Shaha and Cho (2011)). In a positive estuary both the gradient of S and ν are negative. The salinity reduces in upstream direction and the mixing becomes more gravitationally driven as we move upstream. The two reduce more or less in parallel. Of course, as a result of the definitions of K and ν, both are limited within the interval [0,1]. The exponential function of ν prevents K to become too large when ν approaches zero. We have to realise, though that (4.34) is based on the assumption of (4.33), and that (4.35) implicitly uses a modification of this assumption. Whether this is correct needs still to be seen.

For the moment we have to assume that K can be used as a constant value in the range of the estuary where K matters, which is near the toe of the salt intrusion.

4.9 General equation for longitudinal dispersion

Integration of Van der Burgh's equation assuming K to be constant and taking into account the exponential variation of the cross-sectional area yields the following equation:

$$\frac{D}{D_0} = 1 - \beta\left(\exp\left(\frac{x}{a}\right) - 1\right) \tag{4.36}$$

where:

$$\beta = \frac{KaQ_f}{D_0 A_0} \tag{4.37}$$

where D_0 is the dispersion and the estuary mouth, A_0 is the cross-sectional area at the estuary mouth, a is the convergence length and Q_f is the fresh water discharge. This is a simple equation relating the longitudinal effective dispersion to the longitudinal ordinate, the estuary geometry and the river discharge. We can see that estuary shape is prominently present through both a and A_0. For the equation to become predictive, an expression for D_0 and K needs to be found. This is done in the following chapter.

We have seen that Van der Burgh's equation is a very attractive equation to use for describing the longitudinal variation of the dispersion in alluvial estuaries. We have also seen from, amongst others, the work of Shaha and Cho, that it is probably not correct to assume K to be constant with x. The reason why a constant K works well in practice is because the impact of K on the salinity is very small in the wider part of the estuary and only becomes prominent near the toe of the salt intrusion. So the K value used is generally the K value that belongs to the tail of the salt intrusion curve. In the next chapter we shall discuss the limits of the Van der Burgh equation further in the light of recent developments.

Chapter 5

SALT INTRUSION IN ALLUVIAL ESTUARIES

This chapter presents an analytical method to calculate the salinity distribution in alluvial estuaries, applicable to a wide range of estuaries under different tidal and hydrologic conditions. The method is predictive in the sense that we can determine the salinity distribution on the basis of the geometry and the tidal and hydrologic boundary conditions.

There are different types of salt intrusion, depending on topography, hydrology and tide. These estuaries range from estuaries with a very strong exponential shape to estuaries with almost a prismatic shape, and from estuaries that experience strong tidal drivers to estuaries that are riverine in character. In this chapter we classify them on the basis of their salt intrusion curve, which appears to be strongly linked to the geometry.

The salt intrusion in alluvial estuaries is generally of the well mixed or partially mixed type, particularly in the period when it matters: the dry season. This chapter shows that salt intrusion can be adequately described by the one-dimensional dispersion equation. When this equation is combined with equations describing topography and dispersion it yields a predictive equation that can be used for both unsteady and steady state. This equation applies to the tidal average situation, but also to high water slack and low water slack. The influence of rainfall and evaporation on salt intrusion can also be taken into account, which sometimes is crucial to understand the salinity distribution. Under extreme circumstances hypersalinity can occur, which is illustrated with case material.

5.1 Types of salt intrusion and shapes of salt intrusion curves

In an estuary of the well mixed type the variation of the salinity along the longitudinal axis of the estuary is gradual. This implies that if a continuous survey is done along an estuary, e.g. by a moving boat or by simultaneous observations along the estuary, a smooth curve can be fitted through the observed cross-sectional averaged salinities. The shape of the curve, however, can differ widely depending on the situation at hand.

A number of designations will be used to characterize salt intrusion curves of a particular shape. It is a classification to help identify certain types of salt intrusion, which, as will be shown further on, have certain relations to both the geometric shape of an estuary and the hydrology. The following types are distinguished (see Fig. 5.1):

- type 1, recession shape
- type 2, bell shape
- type 3, dome shape
- type 4, humpback shape

Type 1 is an intrusion curve with a logarithmic convex shape; the salinity gradient at the estuary mouth is steep. Examples of this type are (see Table 2.2): the Chao Phya in Thailand

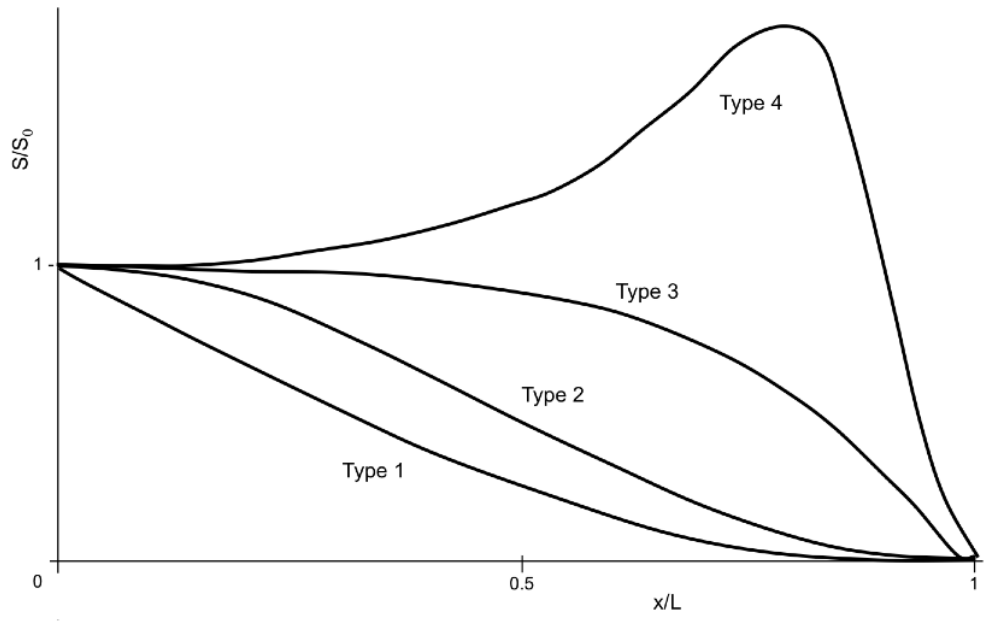

Figure 5.1: Four types of salt intrusion curves.

and the Limpopo in Mozambique, which are close to prismatic, straight and narrow estuaries (a large value of b). Type 3 shows completely the opposite: it has a concave shape and the salinity gradient at the mouth is small. Examples of this type are: the Delaware in the USA, the Thames in the UK and the Schelde in the Netherlands. These are all wide channels with a pronounced funnel shape (a small value of b). Type 2 is not a transition from type 1 to 3, it is rather a mixture of the two. It starts concave, but within 50% of the salt intrusion length, it changes into a convex shape. Examples are the Maputo in Mozambique and the Mae Klong in Thailand. These estuaries have an inflection point in their width function. They are close to prismatic upstream (a large value of b), but strongly funnel-shaped near the mouth (a small value of b).

Apparently, these three types of intrusion curves are very much linked to the geometry of the estuary. All estuaries studied appear to belong to a certain type of curve shape irrespective of the hydrological conditions (within the hydrological limits between which well mixed salt intrusion occurs): the intrusion may increase or decrease, the shape type remains unchanged.

The fourth type is an exception in this respect. A humpback shape is entirely the result of a rainfall deficit or an evaporation excess. Evaporation can change a bell shaped intrusion into a dome shaped intrusion and eventually into a hypersaline intrusion. Generally, in well mixed estuaries, the salinity reduces in upstream direction. Such an estuary is a normal or "positive" estuary (see Section 1.2). In a positive estuary, the sum of the fresh water inflow and the direct rainfall on the estuary surface exceeds the evaporation (Dyer, 1973). In some arid parts of the world, however, so-called hypersaline or "negative" estuaries occur where evaporation exceeds the sum of rainfall and runoff. In a hypersaline estuary the salinity increases in upstream direction until it reaches a maximum after which it decreases depending on the amount of fresh water inflow. The maximum salinity to be reached is saturation level (363 kg/m^3 at 20^{o}C). Such hypersaline estuaries occur for example in the Sahel: the Saloum and the Casamance (Pagés and Citeau, 1990), and in some tropical North Australian estuaries (Wolanski, 1986). Although in all estuaries there is, in principle, an influence of direct rainfall and evaporation on the salinity of the estuary water, this effect is not important in most of the estuaries. In Sections 5.3 and 5.7 more attention is paid to this phenomenon.

This classification of salt intrusion curves is a purely descriptive one. In the following sections the salt intrusion will be analyzed in an analytical way making use of the equations of conservation

of mass for water and salt.

5.2 Salt balance equation

In analogy with the 1-D mass balance equation for water, the mass balance equation for dissolved salt states that the sum of the change in salt load over time and the change of the salt fluxes over the distance should be zero or, in case of a source of salt, should be equal to the source. Hence the cross-sectional averaged salt balance equation reads:

$$r_S \frac{\partial As}{\partial t} + \frac{\partial F}{\partial x} = 0 \tag{5.1}$$

where:

— r_S is the storage width ratio defined earlier in Chapter 2
— F=$F(x,t)$ is the mass flux of salt in kg/s averaged over the cross-sectional area A
— s=$s(x,t)$ is the salinity in kg/m^3

In contrast to the water balance of (2.2), the salt balance equation does not have a source term. In (5.1) the source term can be disregarded, unless salt is picked up from the bottom or from marginal salt flats. Salt deposition by rainfall is marginal and evaporation does not carry any salt either, so for all practical purposes in alluvial estuaries the source term may be disregarded.

Subsequently, the mass flux is defined as:

$$F = \int\int U s \mathrm{d}z \mathrm{d}y \tag{5.2}$$

where U=$U(x,y,z,t)$ and s=$s(x,y,z,t)$ are the water velocity and salt concentration at a certain point (y,z) in the cross-section. Equation (5.1) can be elaborated by making use of (2.2), the continuity equation of water, eliminating the temporal variation of the cross-sectional area:

$$r_S A \frac{\partial s}{\partial t} - s\frac{\partial Q}{\partial x} + \frac{\partial F}{\partial x} = -sR_S \tag{5.3}$$

where Q is the discharge. We see that through the water balance the source term enters into the equation.

The mass flux F is generally decomposed into an advective and a dispersive term:

$$F = Qs - AD\frac{\partial s}{\partial x} \tag{5.4}$$

where D=$D(x,t)$ is the longitudinal dispersion coefficient in m^2/s. Differentiation of (5.4) leads to:

$$\frac{\partial F}{\partial x} = Q\frac{\partial s}{\partial x} + s\frac{\partial Q}{\partial x} - \frac{\partial}{\partial x}\left(AD\frac{\partial s}{\partial x}\right) \tag{5.5}$$

where D=$D(x,t)$ is the longitudinal dispersion coefficient in m^2/s. Differentiation of (5.4) leads to:

$$r_S A \frac{\partial s}{\partial t} + Q\frac{\partial s}{\partial x} - \frac{\partial}{\partial x}\left(AD\frac{\partial s}{\partial x}\right) = -sR_S \tag{5.6}$$

where we note that the second term of (5.3) was cancelled out by the second term of (5.5).

In the literature, the storage width ratio in (5.6) is often disregarded. This is not correct, but in steady state models the effect of the storage width is obviously not present. In dynamic models where it is disregarded, it can be compensated in the first term by increasing the value of A_0 (assuming a larger cross-sectional area at the mouth), but obviously, that would require an adjustment of the dispersion as well to correct the error thus introduced in the third term.

Equation (5.6) is the unsteady state one-dimensional salt balance equation. Separation of the discharge Q into a tidal component and a fresh water component yields:

$$r_S A\frac{\partial s}{\partial t} + (Q_t - Q_f)\frac{\partial s}{\partial x} - \frac{\partial}{\partial x}\left(AD\frac{\partial s}{\partial x}\right) = -sR_S \tag{5.7}$$

where Q_t=$Q_t(x,t)$ is the tidal discharge, which has a time-average value of zero, and Q_f=$Q_f(t)$ is the fresh water discharge of the river(s) entering the estuary, which is a scalar with a positive value. The time scale of the temporal variation of the two discharges is different. The tidal discharge variation has a time scale of hours, whereas the fresh water discharge variation has a time scale of days to months. In the remainder of this section, the source term (which stems from the water balance equation, not from the salt balance equation) will be neglected. However, in Section 5.3, the effect of rainfall and evaporation on this term will be dealt with in detail.

Situation at High Water Slack and Low Water Slack

A special case of (5.7) occurs at high water slack (HWS), when the direction of flow changes from upstream into downstream. At HWS - by definition - the tidal discharge Q_t is zero. In case of a mixed-type wave (see Section 2.2) the time at which HWS occurs - some time after reaching high water (HW) - propagates upstream with the celerity of the wave. The moment of HWS occurs later as the tidal wave moves further upstream. Hence at each point along the estuary HWS occurs at a different time.

Similar to the discharge, the rate of change of the salinity $\partial s/\partial t$ can also be decomposed into a tidal component - with a periodicity equal to the tidal period - and a long-term component. Since in a situation where the fresh water discharge is constant, the maximum salinity is reached when Q_t is zero at HWS, it is reasonable to assume that even when Q_f varies over time the tidal component of $\partial s/\partial t$ is zero at HWS. Hence (5.7) can be modified for HWS into:

$$r_S A\frac{\partial s_{HWS}}{\partial t} - Q_f\frac{\partial s_{HWS}}{\partial x} - \frac{\partial}{\partial x}\left(A_{HWS}D_{HWS}\frac{\partial s_{HWS}}{\partial x}\right) = 0 \tag{5.8}$$

where $\partial s_{HWS}/\partial t$ is the long term variation of the salinity at HWS. If the long-term variation is negligible (Q_f is constant), a situation of equilibrium occurs in which there is a balance between the second and the third terms. In that case, (5.8) can be integrated with respect to x. The uppercase S=$S(x)$ is used to indicate the steady state salinity. Since the fresh water discharge Q_f may be considered invariant with x, integration under the boundary condition that S=S_f (the fresh water salinity) and $\partial S/\partial x = 0$ when $x \to \infty$, yields:

$$Q_f\,(S_{HWS} - S_f) + A_{HWS}D_{HWS}\frac{\partial S_{HWS}}{\partial x} = 0 \tag{5.9}$$

An analogous derivation can be made for low water slack (LWS):

$$Q_f\,(S_{LWS} - S_f) + A_{LWS}D_{LWS}\frac{\partial S_{LWS}}{\partial x} = 0 \tag{5.10}$$

The subscript LWS refers to the situation at LWS. The curves described by (5.9) and (5.10) represent the two sets of points in the S-x plane that occur at HWS and LWS respectively. Since HWS and LWS represent the upper and lower extremes of the salt intrusion, they form two envelope curves between which the salinity varies (see Fig. 5.2). Instantaneous salt intrusion curves fall within the two envelopes.

Mean tidal situation

Another special case is the tidal average situation, which follows from averaging over a tidal cycle under the following first order approximations:

$$\frac{1}{T}\int_0^T A\frac{\partial s}{\partial t}\mathrm{d}t \approx A_{TA}\frac{\partial s_{TA}}{\partial t} \tag{5.11}$$

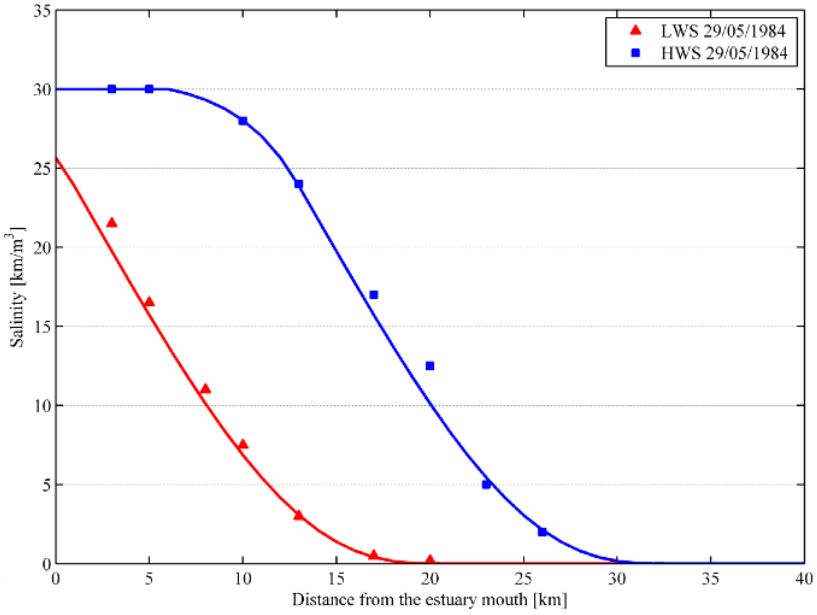

Figure 5.2: Envelope curves of salinity intrusion at High Water Slack (HWS) and Low Water Slack (LWS). The example is taken from the Maputo estuary. The observations made on 29/5/1984 are indicated by symbols, the envelope curves by drawn lines.

$$\frac{1}{T}\int_0^T Q_t \frac{\partial s}{\partial x} \mathrm{d}t \approx 0 \tag{5.12}$$

$$\frac{1}{T}\int_0^T Q_f \frac{\partial s}{\partial x} \mathrm{d}t \approx Q_f \frac{\partial s_{TA}}{\partial x} \tag{5.13}$$

$$\frac{1}{T}\int_0^T \frac{\partial}{\partial x}\left(AD\frac{\partial s}{\partial x}\right) \mathrm{d}t \approx \frac{\partial}{\partial x}\left(A_{TA}D_{TA}\frac{\partial s_{TA}}{\partial x}\right) \tag{5.14}$$

where the subscript TA refers to the tidal average (TA) situation, and D_{TA} is the tidal and cross-sectional average, x-dependent, dispersion. In particular the latter three assumptions are inaccurate near the toe of the salt intrusion curve, where $\partial s/\partial x$ may vary strongly with time. This led Fischer et al. (1979, p.270) to remark that efforts made to derive a time-averaged dispersion equation starting from (5.7) have not been wholly satisfactory because of the assumptions required. Making use of the above assumptions (5.7) can be modified into:

$$r_S A_{TA}\frac{\partial s_{TA}}{\partial t} - Q_f \frac{\partial s_{TA}}{\partial x} - \frac{\partial}{\partial x}\left(A_{TA}D_{TA}\frac{\partial s_{TA}}{\partial x}\right) = 0 \tag{5.15}$$

Fischer et al. (1979) remark that in view of the weakness of the assumptions, it is better to consider (5.15) as an empirical model that should be verified in practice. However, the fact that (5.15) has been used successfully in many mathematical models appears to be sufficient reason to adopt this model as sufficiently adequate.

In support of this, O'Kane (1980) demonstrated that (5.15) follows from (5.7) in an oscillating framework, where the observer maintains a constant volume of water between himself and the head of the estuary. The only assumption required in his derivation is that the dispersion is devoid of harmonics. In fact, in a one-dimensional model, O'Kane's framework is Lagrangean as long as the amount of fresh water inflow is negligible compared to the tidal volume. In well-mixed

estuaries this is an acceptable assumption. O'Kane's equation can be applied equally well to the tidal average situation, or to slack; the difference between HWS, LWS or TA being merely a longitudinal translation (see Fig. 5.2. In all three cases, the rate of change $\partial s/\partial t$ reflects the long-term variation of the salinity. In this respect, the dispersion D_{TA} should be considered as an "effective" tidal average dispersion, since it is a bulk parameter that expresses the result of all mixing processes that occur within a tidal cycle.

Although (5.15) may be considered correct, in this book, we shall not focus on the TA situation. In our approach the HWS and the LWS situations are considered more relevant, providing the extremes between which salt intrusion is bound. Particularly the HWS situation is important since it determines the maximum salt intrusion that during a given day occurs. For design purposes, this is the critical situation.

In the special case where equilibrium occurs between the advective and dispersive terms: $\partial s_{TA}/\partial t = 0$ and steady state occurs. In that case (5.15) can be integrated with respect to x to yield:

$$Q_f\,(S_{TA} - S_f) + A_{TA} D_{TA} \frac{\partial S_{TA}}{\partial x} = 0 \tag{5.16}$$

where S_{TA} represents the mean tidal steady-state salinity. The boundary condition used is that $S_{TA} = S_f$ and $\partial S_{TA}/\partial x = 0$ when $x \to \infty$. The river water salinity S_f is generally small as compared to the salinity in the estuary ($S_{TA} \gg S_f$) and is often disregarded.

In contrast to what some researchers (Ippen, 1966a; Hansen, 1965) did, it is not at all necessary to assume that A_{TA} and D_{TA} be constant with x. Hence, both A_{TA} and D_{TA} are still functions of x. In the following we will give a solution of these steady state equations for a cross-section and dispersion that vary with x.

Similarity between HWS, LWS and TA situation

There is a large similarity between (5.9), (5.10) and (5.16). All three equations, in the particular situation for which they apply (HWS, LWS or TA) are of the form:

$$S_i - S_f = c_i \frac{\partial S_i}{\partial x} \tag{5.17}$$

where i=1,2,3 indicates the three different states: HWS, LWS and TA, and where c_i is an x-dependent coefficient equal to the ratio between the dispersion coefficient and the fresh water velocity, which is different for each state. Hence, the difference between the three equations lies in c_i and in the different downstream boundary conditions belonging to each state. It will be shown in Section 5.5 that, as a result of the expression used for c_i, the three curves have identical shapes but different positions along the x-axis.

5.3 Influence of rainfall and evaporation

The direct rainfall on an estuary and the evaporation from an estuary are described mathematically by the parameter P_n, representing net rainfall in m/s (the balance of rainfall and evaporation). If P_n is negative, then evaporation predominates.

The continuity equation for water, (2.2) changes if rainfall is added to the water balance:

$$r_S \frac{\partial A}{\partial t} = -\frac{\partial Q}{\partial x} + r_S B P_n \tag{5.18}$$

where B is the estuary width and r_S accounts for the fact that the rainfall acts over the entire width, including the storage width. Combination of (5.18) with (5.1) and comparison with (5.3) yields an expression for the source term, as an effect of rainfall or evaporation:

$$r_S A \frac{\partial s}{\partial t} - s\frac{\partial Q}{\partial x} + \frac{\partial F}{\partial x} = -r_S s B P_n \tag{5.19}$$

The source term has a negative sign. It is negative if rainfall is added to the system, leading to a dilution of saline water, and positive in case of evaporation, leading to a higher concentration of salt.

To simulate the effect of rainfall and evaporation, use is made of the mean tidal salt balance equation, (5.15), to which the source term is added:

$$r_S A\frac{\partial s}{\partial t} - Q_f\frac{\partial s}{\partial x} - \frac{\partial}{\partial x}\left(AD\frac{\partial s}{\partial x}\right) = -r_S s B P_n \tag{5.20}$$

Rainfall and evaporation affect the salt balance in two ways. One is through the source term, the other is through the fresh discharge Q_f.

Integration of (5.18) with respect to x for the mean tidal situation where $Q{=}{-}Q_f$ and under the assumption that the long term variation in the cross-sectional area $\partial A/\partial t$ is negligible, leads to:

$$\int_x^\infty \mathrm{d}Q_f = -\int_x^\infty r_S B P_n \mathrm{d}x \tag{5.21}$$

The integration is done to infinity, signifying the length over which the tidal influence is felt, which is a length several times larger than the width convergence length b. There, the fresh water discharge equals the river discharge Q_r which is supposed to be measured outside the tidal influence. Elaboration of (5.21) yields:

$$Q_f(x) = Q_r + r_S B P_n b \tag{5.22}$$

Meaning that if r is positive, $Q_f(x)$ reduces in upstream direction and increases towards the mouth of the estuary. If P_n is negative, then there is a point where Q_f becomes zero, after which it becomes negative, attracting water from the sea.

The salt balance equation hence modifies into:

$$r_S A\frac{\partial s}{\partial t} - (Q_r + r_S B P_n b)\frac{\partial s}{\partial x} - \frac{\partial}{\partial x}\left(AD\frac{\partial s}{\partial x}\right) = -r_S B P_n s \tag{5.23}$$

Depending on the relative size of each term in (5.23), the effect of rainfall and evaporation is important or small. The relative size of each term depends on both hydrological and geometrical parameters, which can vary strongly from estuary to estuary. In most estuaries, however, the importance is small, which is one of the reasons that not much attention is given to this issue in the literature. Savenije (1988) showed that evaporation is important to describe the salinity distribution in the Gambia. Savenije and Pagés (1992) showed that this was also the case for the estuaries north and south of the Gambia: the Saloum and the Casamance, leading to hypersaline conditions.

Scaling of the salt balance equation

To analyse the relative size of the terms in (5.23) the terms of the equation are scaled. Elaboration yields:

$$r_S A\frac{\partial s}{\partial t} - (Q_r + r_S B P_n b)\frac{\partial s}{\partial x} - \frac{\partial A}{\partial x}D\frac{\partial s}{\partial x} - \frac{\partial D}{\partial x}A\frac{\partial s}{\partial x} - AD\frac{\partial^2 s}{\partial x^2} = -r_S B P_n s \tag{5.24}$$

Using the exponentially varying cross-sectional area of (2.38), (5.24) can be further elaborated:

$$r_S\frac{\partial s}{\partial t} - \frac{Q_r}{A}\frac{\partial s}{\partial x} - r_S\frac{P_n b}{\bar{h}}\frac{\partial s}{\partial x} + \frac{D}{a}\frac{\partial s}{\partial x} - \frac{\partial D}{\partial x}\frac{\partial s}{\partial x} - D\frac{\partial^2 s}{\partial x^2} + r_S\frac{P_n}{\bar{h}}s = 0 \tag{5.25}$$

This is a linear differential equation of s with x-dependent coefficients. The relative importance of the terms in (5.25), and in particular the rainfall (and evaporation) terms, is analysed through scaling of the terms. The parameters are transformed into non-dimensional parameters in a way that the non-dimensional salinity and its derivatives are of the order unity, and that hence the

coefficients determine the relative importance of the terms. The following transformations are made:

$$t' = t/T$$
$$x' = x/L$$
$$s' = s/S_0$$
$$Q' = Q_r/Q_0$$
$$P_n' = P_n/P_0$$
$$D' = D/D_0$$

where Q_0 is the dry season fresh water discharge, P_0 is the net rainfall rate during the dry season (negative in case of net evaporation) and L is the tidal average salt intrusion length that corresponds to Q_0. With these transformations (5.25) can be scaled:

$$\frac{\partial s'}{\partial t'} + N_1 {P_n}' s' + \left(-N_2 {P_n}' - N_3 Q' + N_4 D'\right) \frac{\partial s'}{\partial x'} - N_5 \left(\frac{\partial D'}{\partial x'} \frac{\partial s'}{\partial x'} + D' \frac{\partial^2 s'}{\partial {x'}^2} \right) = 0 \qquad (5.26)$$

where the following non-dimensional coefficients determine the relative importance of the terms with respect to the rate of change of the salinity, $\partial s'/\partial t'$.

$$N_1 = P_0 T/h$$
$$N_2 = P_0 T b/(hL)$$
$$N_3 = Q_0 T/(r_S A_0 L \exp(-x'L/a))$$
$$N_4 = D_0 T/(r_S a L)$$
$$N_5 = D_0 T/r_S L^2$$

where N_1 and N_2 weigh the impact of the net rainfall P_n on the rate of change of the salinity, N_1 through dilution and N_2 through advection; N_3 weighs the impact of the river discharge on the rate of change of the salinity; and N_4 and N_5 weigh the importance of the dispersion at the downstream boundary to the rate of change of the salinity. In Table 5.1 the values of the coefficients are presented for the estuaries studied.

In evaluating the importance of the terms of (5.26), the following should be taken into account. Firstly, although s' varies between 0 and 1, this is not the case for its derivatives. Secondly, the coefficient N_3 depends on x', and, hence, is not a constant. The choice was made to incorporate the factor exp(-$x'L/a$) in N_3 (instead of leaving it in the equation) to make the variables independent of the estuary under consideration, and to let the estuary-dependent coefficients determine the relative importance of the terms.

Consequently, a certain value of x' should be selected to allow comparison between estuaries. At the downstream boundary, where $x' = 0$, the salinity is determined by the ocean salinity, and evaporation has no effect. At the upstream boundary, where $x' = 1$, the salinity equals the fresh water salinity and the effect of evaporation is negligible. The part of the estuary where evaporation has the largest effect is in the central part of the salinity zone, where $x' = 0.5$, $D' \approx 0.5$, $s' \approx 0.5$, $\partial D'/\partial x' \approx -1$ and $\partial s'/\partial x' \approx -1$. Hence $x' = 0.5$ has been selected for the comparison.

To evaluate the importance of rainfall and evaporation in relation to other terms, the non-dimensional coefficients are grouped (see Table 5.2). In combining coefficients, it is assumed that $D' \approx$0.5, $s' \approx$0.5, $\partial D'/\partial x' \approx$-1 and $\partial s'/\partial x' =$-1, and that the magnitude of $D'\partial^2 s'/\partial {x'}^2$ is small as compared to the others. These assumptions are not exact since the values depend on the type of the salt intrusion curve: in case of a dome shaped intrusion curve, $s' > 0.5$, $\partial s'/\partial x' >$1, and $\partial^2 s'/\partial {x'}^2 < 0$; in case of a recession shaped intrusion curve $s' < 0.5$, $\partial s'/\partial x' < -1$, and $\partial^2 s'/\partial {x'}^2 > 0$. They are, however, sufficiently accurate to evaluate the relative importance of the terms in orders of magnitude. This results in three coefficients: one coefficient N_P, which weighs the overall importance of rainfall:

$$N_P = N_1/2 + N_2$$

another coefficient which weighs the importance of fresh water inflow:

$$N_Q = N_3$$

and a third coefficient which weighs the overall impact of the dispersion:

$$N_D = 0.5N_4 + N_5$$

In Table 5.2 these coefficients are presented, as well as the ratios of N_P to N_Q and N_D respectively. It can be concluded from Table 5.2 that: 1) the effect of evaporation is important in the Gambia, 2) there is some influence during minimum flow in the Incomati, and 3) the influence is not significant in the other estuaries studied.

Table 5.1: Non-dimensional coefficients determining the relative importance of terms to salt intrusion.

Estuaries	h (m)	a (km)	b (km)	A'_0 (m^2)	L (km)	Q_0 (m^3/s)	P_0T (mm)	D_0 (m^2/s)	N_1 (10^{-3})	N_2 (10^{-3})	N_3 (10^{-3})	N_4 (10^{-3})	N_5 (10^{-3})
Mae Klong	5.2	102	155	1400	26	30	-1.9	190	-0.37	-2.18	41.6	3.18	12.48
Solo	9.2	226	226	2070	35	10	-1.9	238	-0.21	-1.33	6.6	1.34	8.63
Lalang	10.6	217	96	2550	65	50	-2.0	892	-0.19	-0.28	15.6	2.81	9.37
Limpopo	7	100	50	1340	60	5	-2.0	145	-0.29	-0.24	3.7	1.07	1.79
Tha Chin	5.3	87	87	1380	70	10	-1.9	273	-0.36	-0.45	6.9	1.99	2.47
Chao Phya	7.2	109	109	4300	50	30	-1.9	332	-0.26	-0.58	7.8	2.70	5.90
Incomati	2.9	42	42	1750	50	1	-1.8	9	-0.62	-0.52	0.9	0.19	0.16
Pungue	3.5	21	21	28000	70	20	-2.4	138	-0.69	-0.21	2.4	5.17	1.25
Maputo	3.6	16	16	6460	40	10	-1.8	105	-0.50	-0.20	6.0	7.28	2.91
Thames	7.1	23	23	58500	90	20	-1.0	77	-0.14	-0.04	1.2	1.65	0.42
Corantijn	6.5	64	64	34600	50	500	-2.0	230	-0.31	-0.39	19.0	3.19	5.08
Sinnamary	3.8	39	39	1210	16	100	-2.4	560	-0.63	-1.54	281.6	39.85	97.13
Gambia	8.7	121	121	27200	300	2	-2.4	200	-0.28	-0.11	0.04	0.24	0.10
Schelde	10.5	28	28	150000	110	90	-1.0	264	-0.10	-0.02	1.7	3.81	0.97
Delaware	6.6	41	41	255000	140	300	-1.0	312	-0.15	-0.04	2.1	2.41	0.71

Table 5.2: Non-dimensional coefficients indicating the relative importance of rainfall and evaporation in relation to discharge and dispersion.

Estuaries	N_P (10^{-3})	N_Q (10^{-3})	N_D (10^{-3})	N_P/N_Q	N_P/N_D
Mae Klong	-2.4	41.6	15.1	-0.1	-0.2
Solo	-1.4	6.6	9.3	-0.2	-0.2
Lalang	-0.4	15.6	10.8	-0.0	-0.0
Limpopo	-0.4	3.7	2.3	-0.1	-0.2
Tha Chin	-0.6	6.9	3.5	-0.1	-0.2
Chao Phya	-0.7	7.8	7.2	-0.1	-0.1
Incomati	-0.8	0.9	0.3	-0.9	-3.3
Pungue	-0.5	2.4	3.3	-0.2	-0.2
Maputo	-0.5	6.0	6.6	-0.1	-0.1
Thames	-0.1	1.2	1.2	-0.1	-0.1
Corantijn	-0.5	19.0	5.7	-0.0	-0.1
Sinnamary	-1.9	281.6	117.0	-0.0	-0.0
Gambia	-0.2	0.0	0.2	-6.6	-1.1
Schelde	-0.1	1.7	2.9	-0.0	-0.0
Delaware	-0.1	2.1	1.9	-0.1	-0.1

5.4 Time scales and conditions for steady state

The assumption made in (5.16) to arrive at the steady state equation for conservation of mass, requires that in the estuary an equilibrium condition is reached between, on the one hand, advective salt transport through the downstream flushing of salt by the fresh water discharge, and, on the other hand, the full range of mixing processes induced by the tidal movement and the gravitational circulation. The time required for an equilibrium to occur depends on 1) the rate at which the boundary conditions vary, in particular the rate of change of the fresh water discharge, and 2) the time required for the estuary system to adjust itself to a new situation. During the dry season, when the problem of salt intrusion is most acute, the variation of the fresh water discharge is generally slow. The question is: does the system react at the same pace as the boundary conditions, or does it need more time? In the latter case, the system lags behind steady state.

The estuary system reacts quite differently to an increase and to a decrease in the fresh water discharge. Generally the estuary reacts relatively quickly to an increase of the discharge. The new volume added at the upstream end of the estuary propagates as a mass wave through the system. However, the reaction to a decrease in the fresh water discharge is slow, since the process of salinization, gradually replacing the fresh water by saline water through mixing, takes time. In this respect, Van Dam and Schönfeld (1967) remark about the Schelde and Eems estuaries in The Netherlands that "the characteristic time for reaching a new equilibrium, for example from a wet period to a dry period, is in the order of one year for the Schelde, so that a final state is usually never reached". Although for the Schelde this observation will prove to be somewhat exaggerated, in the Gambia, the process of adjustment to a reduction of the fresh water discharge is so slow that the salt intrusion always lags far behind steady state. This phenomenon is important. In the Gambia, it is due to the slowness of the mixing process that so much fresh water remains available in the upper part of the estuary, during the dry season. If equilibrium were reached, the salt intrusion would go much further upstream.

It is important to investigate in a given estuary how quickly the system adjusts to a new situation. If the time required for the system to reach equilibrium is too long in relation to the variation of the boundary conditions, then a steady state model may not be used.

System response time scale

Kranenburg (1986) developed a time scale for system response to a variation in discharge, which is based on the comparison of a steady state model with an unsteady state model. If the salinity difference per unit of time between subsequent steady states at a certain point along the estuary axis (as a result of a change in fresh water discharge) is defined as $\partial S_{TA}/\partial t$ then a steady state is not reached as long as the mean tidal salinity adjustment rate $\partial sTA/\partial t$ is smaller, in absolute terms, than $\partial S_{TA}/\partial t$, for an infinitely small time step Δt. Hence a condition for steady state is that:

$$\left|\frac{\partial s_{TA}}{\partial t}\right| \geq \lim_{\Delta t \to 0} \left|\frac{\Delta S_{TA}}{\Delta t}\right| \tag{5.27}$$

However, when the unsteady salinity variation is larger than the variation between subsequent steady states, the unrealistic situation occurs where the system reacts stronger than the forces driving the system. Hence, for the state of equilibrium to be reached it is sufficient to assume that the unsteady state salinity variation should be approximately equal to the variation between steady states:

$$\frac{\partial s_{TA}}{\partial t} \approx \lim_{\Delta t \to 0} \frac{\Delta S_{TA}}{\Delta t} \tag{5.28}$$

In the following elaboration of (5.28), for reasons of simplicity, the subscript TA for the tidal average situation in S, s, A and D is removed. Combination with (5.15) yields:

$$\frac{\partial}{\partial x}\left(Q_f s + AD\frac{\partial s}{\partial x}\right) \approx A \lim_{\Delta t \to 0} \frac{\Delta S}{\Delta t} \tag{5.29}$$

In fact, the integral of (5.29) with respect to x represents the balance between, on the one hand, the salt flux, see (5.4), which the system can produce, and on the other hand, the amount of salt per unit of time required to follow up subsequent steady states.

Since the time dependency of the steady state salinity S is merely through Q'_f:

$$\lim_{\Delta t \to 0} \frac{\Delta S}{\Delta t} = \frac{\partial S}{\partial Q_f} \frac{\mathrm{d}Q_f}{\mathrm{d}t} \tag{5.30}$$

The most interesting case for the rapid assessment technique is the situation of extreme salt intrusion during the dry season, when the discharge is gradually diminishing. During the dry season the depletion of the fresh discharge is exponential, following the normal recession curve used in hydrology:

$$\frac{\mathrm{d}Q_f}{\mathrm{d}t} = -\frac{Q_f}{T_Q} \tag{5.31}$$

where T_Q is the time scale of the discharge reduction (which corresponds to the residence time of the renewable groundwater in the river basin).

Integration of (5.29) with respect to x, under the boundary condition that $s = 0$ at $x = L$, and combination with Eqs. (5.30), (5.31) and (5.16), disregarding S_f, yields:

$$(S - s) + \frac{A}{Q_f}\left(D_{SS}\frac{\partial S}{\partial x} - D\frac{\partial s}{\partial x}\right) \approx \frac{1}{T_Q}\int_x^L A\frac{\partial S}{\partial Q_f}\mathrm{d}x \tag{5.32}$$

where D_{SS} refers to the steady-state dispersion of (5.16) and D to the unsteady-state dispersion. Depending on the theory used, the tidal average dispersion coefficient D is a function of x, Q_f, $\partial s/\partial x$, s or any combination of them. If the dispersion coefficient was only a function of x and Q_f, then D would be equal to D_{SS}. If, however, the dispersion coefficient is assumed to depend on s or $\partial s/\partial x$, as is the case in several theories, then they can be different, although percentage-wise they can't differ much. However, since also the salinity gradients between steady state and unsteady state are different, the dispersion terms are different, and don't annihilate.

Kranenburg solves this problem in the following way. He observes that $(s - S) = 0$ both at $x = 0$ and at $x = L$, and that somewhere in the middle of the estuary a point should lie where $(s - S)$ reaches a maximum value, and where, hence, $\partial s/\partial x = \partial S/\partial x$. With $D \approx D_{SS}$, this implies that there is a point $x = X$ where the steady state and unsteady state dispersion terms of (5.23) annihilate each other whether or not D depends on $\partial S/\partial x$. Hence:

$$(S - s)|_X \approx \frac{1}{T_Q}\int_X^L A\frac{\partial S}{\partial Q_f}\mathrm{d}x \tag{5.33}$$

Subsequently, the time scale for system response can be defined as:

$$T_K = \frac{1}{S(X)}\int_X^L A\frac{\partial S}{\partial Q_f}\mathrm{d}x \tag{5.34}$$

Combination with (5.33) yields:

$$T_K \approx T_Q\left(\frac{(S - s)}{S}\right)_X \tag{5.35}$$

Assuming that the maximum difference between steady and unsteady state salinity lies at about half the salt intrusion length (X=$L/2$). This implies that to reach a state of 90% equilibrium at $x = L/2$, $(S - s)/S$=10%, and T_K should not be more than $0.1T_Q$. To reach a further state of equilibrium T_K should be less.

A more simple approach to determine the system response time is on the basis of the time required for the system to adjust itself to a new steady state S. The time scale is defined as:

$$\frac{\partial s}{\partial t} = \frac{S - s}{T_S} \tag{5.36}$$

In analogy with the operations carried out to obtain T_K, (5.36) is modified into:

$$Q_f(S-s) + A\left(D_{SS}\frac{\partial S}{\partial x} - D\frac{\partial s}{\partial x}\right) \approx \frac{1}{T_S}\int_x^L A(S-s)\mathrm{d}x \tag{5.37}$$

If Kranenburg's assumption is applied that at $x = X$: $D\partial s/\partial x = D_{SS}\partial S/\partial x$, then (5.37) yields:

$$Q_f T_S(S-s) \approx \int_X^L A(S-s)\mathrm{d}x \tag{5.38}$$

Because the spatial distribution of s is not known, it is assumed that in reaching the new steady state, the difference in salinity $(S-s)$ is a proportion of S. For the reach between X and L, this seems a reasonable assumption:

$$T_S \approx \frac{1}{Q_f S(X)}\int_X^L AS\mathrm{d}x \tag{5.39}$$

This is the time required for the fresh water discharge, with a salinity $S(X)$, to replace the salt accumulated upstream of X. For a steady state to occur, this time scale should not be larger than the time scale of the discharge reduction.

Particle travel time

A good time scale to compare T_S or T_K with is the average time T_f required for a fresh water particle to travel over the salt intrusion length:

$$T_f = \int_0^L \frac{A}{Q_f}\mathrm{d}x \tag{5.40}$$

One could call this the flushing time scale, since it equals the time required to flush the estuary with fresh water. In an exponentially shaped channel with a convergence length a, (5.40) yields:

$$T_f = \frac{A_0 a}{Q_f}\left(1 - \exp\left(-\frac{L}{a}\right)\right) \tag{5.41}$$

If the exponential function describing the cross-sectional area consists of two branches (as we saw in Chapter 2 sometimes happens), the upstream branch is considered most important since for the determination of T_S integration is done between X and L, and consequently in (5.41) the convergence length of the upstream branch is used and a value A_0' instead of A_0 which is obtained by extrapolation of the upstream branch to the estuary mouth. This value has been used for the computation of T_f in Table 5.6.

The ratio of T_S to T_f is an interesting parameter for further study, since it no longer depends on the fresh water discharge Q_f, and hence only includes geometric variables of the estuary under study.

Given a mathematical model for the steady state salinity distribution, (5.39) can be solved, and the system time scale T_S determined. This is done in Section 5.6, after we have obtained an expression for the salt intrusion length L.

5.5 Predictive model for steady state

5.5.1 Expressions for HWS, LWS and TA

Steady state salt intrusion models can be divided into three types, depending on their derivation: low water slack (LWS) models, e.g. Ippen and Harleman (1961); tidal average (TA) models, e.g. Van der Burgh (1972); and high water slack (HWS) models, e.g. Savenije (1989). A LWS

model is calibrated on measurements carried out at LWS, and a HWS model with measurements carried out at HWS. For the calibration of a TA model, the average salinity has to be derived from measurements carried out during a full tidal cycle at several points along the estuary axis, which, if done well, is very elaborate and time consuming.

Although HWS models are not commonly used, they are the most practical models because the best moment to carry out a salt intrusion measurement is at HWS; this is for the following reasons:

1. The moment that HWS occurs is easily determined. The observer measures the salinity, when the in-going current slacks. Although the same advantage applies to LWS, the accessibility at LWS is generally poor. The estuary is shallow and sometimes it is very difficult to reach the waterside. Inaccessible mud flats often separate the river from the banks.

2. If the salinity at the downstream boundary is not known, it can easiest be estimated at HWS. At HWS, the salinity at the estuary mouth is generally equal or almost equal to the sea salinity, which is not, or not much, affected by the fresh water discharge from the estuary.

3. At HWS the salt intrusion is at its maximum. Generally, it is the maximum intrusion that is of interest to planners.

4. A single observer in a small outboard driven boat can travel with the tidal wave and measure the entire salt intrusion curve at HWS. If the intrusion length is not too long, he may even return to the estuary mouth and repeat the measurement for LWS.

As it seems logical to assume that the TA salt intrusion is directly related to the fresh water discharge, many predictive models are of the TA type. These models, however, do not provide information on the maximum and minimum salinity reached at a certain location as a function of the tide. This is especially important, when during part of the day, the water is fresh, while during another part of the day the water is brackish. In this Section, it will be shown that the model used in the rapid assessment technique can be calibrated on HWS - which has all the advantages mentioned above -, can be used to compute the situation at LWS and TA, and that the calibration parameters obtained can be well related to hydrological, hydraulic and geometrical parameters.

Section 5.2 it has been shown that the same type of (5.17) can be used to describe the three situations of HWS, LWS and TA. Because in a steady state situation the $\partial S/\partial t = 0$, and hence $\partial S/\partial x = \mathrm{d}S/\mathrm{d}x$, no partial derivatives are used in the subsequent derivations in this Section. (5.17) can be combined with Van der Burgh's equation, described in Chapter 4, and the geometric assumptions, described in Chapter 2, to yield HWS, LWS and TA analytical equations that are mathematically related. In the following paragraphs relations are derived between the salinity distributions at HWS, LWS and TA. These relations allow the determination of the dispersion at LWS and TA, and the corresponding salinity distributions on the basis of the calibrated dispersion at HWS.

To this end, in agreement with (5.9), (5.10) and (5.16), (5.17) is expanded to read:

$$S_i - S_f = -\frac{A}{Q_f} D_i \frac{\mathrm{d}S_i}{\mathrm{d}x} \tag{5.42}$$

where A is the tidal average cross-sectional area, D_i=$D_i(x)$ is the dispersion coefficient at HWS, LWS and TA respectively. It should be noted that the values of Q_f and A are assumed to be the same for HWS, LWS, and TA. The error made by using the same value for A is compensated by D_i, which then also incorporates the effect of a smaller cross-sectional area at LWS and a larger cross-sectional area at HWS. In this way all the differences between HWS, LWS and TA are incorporated in one variable D_i.

In Chapter 3 the Van der Burgh equation has been presented. Van der Burgh assumed that his relation, which was derived for the TA situation, could be used for LWS and HWS as well: he assumed that the salt intrusion curve obtained for the TA situation could be shifted upstream over half the tidal excursion to obtain the HWS situation, and downstream over half the tidal

excursion to obtain the LWS situation. This is in agreement with what was observed by O'Kane (1980) in his oscillating framework approach (see Section 5.2) and by Park and James (1990) who stated that the instantaneous - not tidal average - salt flux F was found to arise predominantly from the product of the tidal average salinity S and the tidal velocity U. This means that the tidal average salinity variation represented by the terms in (5.15) is small as compared to the instantaneous advection $UA\partial S/\partial x$. Hence, over one tidal cycle, a short time compared to the time required to adjust the terms in (5.15), it is justified to assume average mixing conditions corresponding to the TA situation.

Hence Van der Burgh's expression is used for HWS, LWS and TA:

$$\frac{\mathrm{d}D_i}{dx} = -K\frac{Q_f}{A} \tag{5.43}$$

Combination of (5.42) with (5.43) yields:

$$\frac{\mathrm{d}S}{S-S_f} = \frac{1}{K}\frac{\mathrm{d}D}{D} \tag{5.44}$$

where the subscript i has been disregarded for the sake of simplicity, but it is understood that (5.44) can be applied to the HWS, LWS and TA situation. Integration results in:

$$\frac{S-S_f}{S_0-S_f} = \left(\frac{D}{D_0}\right)^{\frac{1}{K}} \tag{5.45}$$

where S_0 and D_0 are boundary conditions at $x = 0$ for the HWS, TA or LWS condition. In addition, integration of (5.43) in combination with an exponentially varying cross-section yields:

$$\frac{D}{D_0} = 1 - \beta\left(\exp\left(\frac{x}{a}\right) - 1\right) \tag{5.46}$$

where:

$$\beta = \frac{KaQ_f}{D_0A_0} \tag{5.47}$$

where β is the dispersion reduction rate, which is always positive, determining the longitudinal variation of D. From (5.45) it can be seen that $S = S_f$ when $D = 0$. Since $S = S_f$ at $x = L$, the intrusion length, (5.46) can be elaborated to yield an expression for the intrusion length:

$$L = a\ln\left(\frac{1}{\beta} + 1\right) \tag{5.48}$$

Since β is positive, the argument of the natural logarithm is always larger than unity.

Application of (5.45) and (5.46) to the HWS situation, disregarding S_f for reasons of convenience, yields:

$$\frac{S^{HWS}}{S_0^{HWS}} = \left(\frac{D^{HWS}}{D_0^{HWS}}\right)^{\frac{1}{K}} \tag{5.49}$$

$$\frac{D^{HWS}}{D_0^{HWS}} = 1 - \frac{KaQ_f}{D_0^{HWS}A_0}\left(\exp\left(\frac{x}{a}\right) - 1\right) \tag{5.50}$$

Since the tidal excursion may be assumed to be independent of x, the envelope lines of the salinity at HWS and LWS should have the same shape. The line at TA is obtained through a horizontal translation over a distance equal to half the tidal excursion. Hence:

$$S_0^{TA} = S^{HWS}(x = E/2) \tag{5.51}$$

$$S^{TA}(x = E/2) = S^{HWS}(x = E) \tag{5.52}$$

Application of the combined (5.9) and (5.10) at $x = E/2$ and $x = E$, division of the results, some elaboration and substitution of (5.51) and (5.52) yields:

$$\frac{S^{HWS}(x=E)}{S^{HWS}(x=E/2)} = \frac{S^{TA}(x=E/2)}{S_0^{TA}} = \left(1 - \frac{KaQ_f}{A_0D^{HWS}(x=E/2)}\frac{\exp\left(\frac{E}{2a}\right)-1}{\exp\left(-\frac{E}{2a}\right)}\right)^{\frac{1}{K}} \tag{5.53}$$

If one uses (5.45) and (5.46) for TA, and substitutes $x = E/2$, then comparison of the result with (5.53) learns that:

$$D_0^{TA} = \left\{ \frac{D^{HWS}}{{D_0}^{HWS}} = 1 - \frac{KaQ_f}{D_0^{HWS} A_0} \left(\exp\left(\frac{E}{2a}\right) - 1 \right) \right\} \exp\left(-\frac{E}{2a}\right) \tag{5.54}$$

Similarly for LWS, one obtains:

$$S_0^{LWS} = S^{HWS}(x = E) \tag{5.55}$$

$$D_0^{LWS} = \left\{ \frac{D^{HWS}}{{D_0}^{HWS}} = 1 - \frac{KaQ_f}{D_0^{HWS} A_0} \left(\exp\left(\frac{E}{a}\right) - 1 \right) \right\} \exp\left(-\frac{E}{a}\right) \tag{5.56}$$

Estuaries with a complex geometry

In some estuaries the geometry cannot be described by a single exponential function. Several estuaries require two branches to describe the longitudinal variation of A, see for instance the Incomati estuary of Fig. 2.9. In fact there are many estuaries like that. In Table 5.3 there are: the Limpopo, the Tha Chin, the Incomati, the Pungue, the Maputo, the Corantijn, and the Sinnamary. In fact most of the estuaries have two branches, often accounting for a trumpet shape near the estuary mouth. In those estuaries the above equations can be solved stepwise. The geometry is given by:

$$A = A_0 exp\left(-\frac{x}{a_1}\right), \text{ if } 0 < x < x_1 \tag{5.57}$$

$$A = A_1 exp\left(-\frac{x - x_1}{a_2}\right), \text{ if } x > x_1 \tag{5.58}$$

where x_1 is the inflection point, $A_1 = A(x_1)$, a_1 is the convergence length of the downstream branch, and a_2 of the upstream branch. In general, the downstream convergence length is shorter than the upstream one, resulting in the said trumpet shape.

The (5.45) and (5.46) can be applied normally for the downstream part, using a_1 for a. Subsequently, a value for the dispersion at the inflection point D_1 needs to be determined, as well as the salinity at the inflection point: S_1. This is done by substitution of x_1 for x in (5.45)-(5.47), using a_1 for a. Subsequently, (5.45) and (5.46) can be used for the upstream end, taking D_1 and S_1 as the downstream boundary conditions. The intrusion length can be computed as follows:

$$L^{HWS} = x_1 + a_2 \ln\left(\frac{1}{\beta_1} + 1\right) \tag{5.59}$$

where β_1 is defined by:

$$\beta_1 = \frac{Ka_2Q_f}{D_1 A_1} \tag{5.60}$$

using the value of D_1 determined at the inflection point.

After calibration of the model on HWS observations, the values of S_0^{HWS} and D_0^{HWS} are known. Consequently, the salinities and dispersion coefficients at any point along the estuary for HWS can be calculated with Eqs. (5.49) and (5.50).

By substitution of these HWS values into equations (5.51), (5.54), (5.55) and (5.56), the TA salinities and the LWS salinities can be computed using (5.45) and (5.46) for TA and LWS, respectively.

In the above equations there remain two unknown model parameters: K and D_0^{HWS}. In addition, there is another variable that is often unknown: the fresh river discharge Q_f, which in an estuary is one of the most difficult parameters to determine. Fortunately, in the above equations, Q_f always occurs in the same term as the dispersion coefficient, which permits them to be combined into only one variable, the mixing coefficient $\alpha(m^{-1})$:

$$\alpha = \frac{D}{Q_f} \tag{5.61}$$

The value of α at the estuary mouth, α_0, is a model parameter that can be obtained through calibration. The two remaining calibration parameters function differently: K is a value that is fixed for a certain estuary, whereas α_0 varies over time, responding to the tidal range and the river discharge. They affect the equations differently and can be easily found by fitting the model to observations.

To be able to determine the fresh water discharge from α_0, an additional relation is needed between α_0 and Q_f. This relation, which is required to make the model predictive, is established in the next section.

Some applications as illustration

The steady state model has been applied in numerous estuaries for a wide range of river flows and tidal ranges. The data of these measurements are summarised in Table 5.3 In Fig. 5.2 already the example of the Maputo estuary in Mozambique was presented. Here some more illustrations are given of the steady state model applied to three other Mozambican estuaries: the Pungué (Fig. 5.3), the Incomati (Fig. 5.4) and the Limpopo (Fig. 5.5). These measurements were conducted by different persons: the ones in the 1980s by the author, the ones in the 1990s by H.A. Zanting and the ones in 2002 by S. Graas.

It can be seen that the model performs very well, although the estuaries are very different in character. The Pungué has a "dome-shaped" intrusion curve, the Limpopo has a "recession-shaped" intrusion curve, and the Incomati and the Maputo have a "bell-shaped" intrusion curve. The toes of the curves are also different. The toe of the Incomati is very flat, corresponding with a very small value of K (K=0.15), whereas the limpopo and The Pungué have a steeper toe (K=0.5 and 0.3 respectively).

When calibrating the model to measurements, one tries different values of K and α_0. Because these two parameters affect the fit in different ways, it is generally possible to find a satisfactory combination of K and α_0. One should realise that, K should be independent of the river discharge and the tide, whereas α_0 should vary with river discharge and tide. So if observations during different flow regimes are collected, then different values of α_0 should be obtained using the same value of K. This can also be seen in Table 5.3.

In general it is important that sufficient measurements along the estuary axis are taken, because individual measurements can have considerable errors due to: timing errors, variation of salinity over the cross-section, and local mixing effects (trapping etc.). The best way to derive a longitudinal distribution is to travel by boat during HWS and LWS. But this may require a very fast boat in some estuaries, since the tidal wave can travel fast (see Section 3.2).

Empirical relations for the predictive model

To turn the steady state model into a predictive model, (semi-) empirical relations are required that relate the two calibration parameters K and α_0 to hydrodynamic and geometrical bulk parameters. These bulk parameters are dimensionless numbers composed of geometrical (a, b, A_0, B_0, h_0), hydrological (Q_f) and hydraulic (H, E, C, v) parameters that influence the process of mixing and advection. In the past, several researchers searched for significant bulk parameters to be used for predicting model parameters from directly measurable physical quantities. In the following, a short review is given of empirical work by Rigter (1973), Fischer (1974), Van der Burgh (1972) and Van Os and Abraham (1990). With the exception of Van der Burgh, all these investigators based their analysis on laboratory tests and prototype measurements in estuaries with constant cross-section.

Classical approaches

Combination of (5.47) and (5.48) yields an explicit analytical relation between the salt intrusion length L and the effective dispersion at the estuary mouth D_0, or, for that matter, between L and α_0 if (5.61) is used. Prominent in this equation is the presence of the convergence length and the logarithmic function; both stemming from the exponential shape of alluvial estuaries. Classical literature on the intrusion length, however, is almost entirely based on prismatic channels. This may be difficult to understand in hindsight, since natural, alluvial, estuaries are never prismatic,

Table 5.3: Measured salinity distributions and calibrated values of K and α_0 for different estauries.

Estuary	date	T (s)	H_0 (m)	E_0 (km)	Q_f (m^3/s)	S_0 (kg/m^3)	f	K	a_1 (km)	x_1 (km)	a_2 (km)	A_0 (10^3 m^2)	h (m)	N	F_2	F_d	a (km)	α_0 (m^{-1})	α_0' (m^{-1})	D_0 (m^2/s)	D_0' (m^2/s)
Mae Klong	20/01/77	86400	2	11	120	28	0.028	0.3			102	1.4	5.20	0.673	0.003	0.157		7.2	5.4	864	647
	08/03/77	44400	1.5	10	60	30	0.028	0.3			102	1.4	5.20	0.190	0.010	0.458		6.2	5.4	372	324
	09/04/77	44400	2	14	36	29	0.028	0.3			102	1.4	5.20	0.082	0.019	0.929		9.0	8.1	324	292
Solo	26/07/88	86400	0.8	9	50	35	0.023	0.6			226	2.07	9.20	0.232	0.001	0.047		9.2	7.4	460	369
	08/09/88	86400	0.4	5	7	35	0.023	0.6			226	2.07	9.20	0.058	0.000	0.015		12.5	15.7	88	103
Lalang	20/10/89	86400	2.6	27	120	25	0.023	0.7			217	2.55	10.60	0.151	0.009	0.519		9.0	8.1	1080	970
Limpopo	04/04/80	44400	1.1	7	150	30	0.026	0.5	50.4	20	130	1.71	7.00	0.557	0.004	0.166	58	9.0	7.7	1350	1158
	31/12/82	44400	1.1	8	2	35	0.026	0.5	50.4	20	130	1.71	7.00	0.006	0.005	0.186	105	38.0	42.3	76	85
	22/04/83	44400	0.5	4	1	33	0.026	0.5	50.4	20	130	1.71	7.00	0.006	0.001	0.049	108	45.0	40.2	45	40
	24/07/94	44400	0.9	6.8	5	35	0.026	0.5	50.4	20	130	1.71	7.00	0.019	0.003	0.135	101	25.0	25.7	125	128
	10/08/94	44400	1.0	7.1	3	35	0.026	0.5	50.4	20	130	1.71	7.00	0.011	0.004	0.147	103	29.0	33.1	87	99
Tha Chin	16/04/81	86400	1.6	12	55	26	0.039	0.4	22	22	87	3	5.30	0.132	0.004	0.197	55	15.5	10.4	853	572
	27/02/86	44400	2.6	20	40	31	0.039	0.4	22	22	87	3	5.30	0.030	0.039	1.739	54	15.0	12.7	600	507
	01/03/86	86400	1.8	14	40	34	0.039	0.4	22	22	87	3	5.30	0.082	0.005	0.205	61	16.5	13.7	660	550
	13/08/87	44400	2	15	39	27	0.039	0.4	22	22	87	3	5.30	0.038	0.022	1.123	51	12.0	10.9	468	424
Chao Phya	05/06/62	86400	2.2	22	63	29	0.031	0.8			109	5.3	7.20	0.058	0.009	0.437		11.4	9.3	718	587
	17/03/80	86400	1.5	18	43	32	0.031	0.8			109	5.3	7.20	0.048	0.006	0.265		15.2	10.7	654	461
	28/03/80	86400	1.7	20	31	34	0.031	0.8			109	5.3	7.20	0.031	0.007	0.308		17.7	13.7	549	425
	29/01/83	86400	2.4	26	90	33	0.031	0.8			109	5.3	7.20	0.070	0.013	0.537		12.0	9.0	1080	813
	23/02/83	86400	1.6	19	100	28	0.031	0.8			109	5.3	7.20	0.106	0.007	0.338		9.4	6.7	940	675
	16/01/87	86400	2.5	15	180	20	0.031	0.8			109	5.3	7.20	0.241	0.004	0.295		5.4	3.8	972	680
Incomati	30/07/80	44400	1.4	7	3	32	0.022	0.2	7.5	14	42	8.1	2.90	0.002	0.009	0.377	33	9.5	11.2	29	34
	05/09/82	44400	1.4	7	2	35	0.022	0.2	7.5	14	42	8.1	2.90	0.002	0.009	0.344	35	16.0	13.5	32	27
	10/02/83	44400	1.2	8	1	35	0.022	0.2	7.5	14	42	8.1	2.90	0.001	0.011	0.450	37	30.0	19.5	30	19
	23/06/93	44400	1.4	8	4	35	0.022	0.2	7.5	14	42	8.1	2.90	0.003	0.011	0.450	32	10.0	11.0	40	44
	07/07/93	44400	2.6	9	4	35	0.022	0.2	7.5	14	42	8.1	2.90	0.002	0.014	0.569	32	9.4	11.7	38	47
Pungue	26/09/80	44400	6.3	20	22	34	0.031	0.3	21	38	12	26.4	3.50	0.002	0.058	2.397	16	19.0	10.8	308	238
	26/05/82	44400	5	10	50	32	0.031	0.3	21	38	12	26.4	3.50	0.008	0.015	0.637	18	5.2	5.5	210	225
	06/08/82	44400	5.2	14	36	34	0.031	0.3	21	38	12	26.4	3.50	0.004	0.029	1.175	17	5.3	6.6	191	237
	22/09/82	44400	5.2	14	26	35	0.031	0.3	21	38	12	26.4	3.50	0.003	0.029	1.141	17	8.0	8.1	208	212
	29/10/82	44400	6	16	60	34	0.031	0.3	21	38	12	26.4	3.50	0.006	0.037	1.534	17	5.0	5.4	300	326
	03/10/93	44400	5.3	15	10	35	0.031	0.3	21	38	12	26.4	3.50	0.001	0.033	1.310	16	28.0	15.0	280	140
	12/10/93	44400	3.8	15	10	35.5	0.031	0.3	21	38	12	26.4	3.50	0.001	0.033	1.292	17	15.0	13.5	150	135
	16/10/93	44400	6.4	16	10	35.5	0.031	0.3	21	38	12	26.4	3.50	0.001	0.037	1.469	16	26.0	15.0	260	150
	31/01/02	44400	6.2	20	262	28	0.031	0.3	21	38	12	26.4	3.50	0.022	0.058	2.911	19	1.9	2.4	498	622
	27/02/02	44400	6.1	20	200	29	0.031	0.3	21	38	12	26.4	3.50	0.017	0.058	2.811	19	2.3	2.8	460	562
	01/03/02	44400	6.7	24	150	28	0.031	0.3	21	38	12	26.4	3.50	0.011	0.084	5.192	18	2.8	3.7	420	549
Maputo	28/04/82	44400	2.8	13	25	35	0.022	0.4	4	8	16	40	3.60	0.002	0.024	0.957	13	5.5	8.8	113	221
	15/07/82	44400	1.5	6	8	35	0.022	0.4	4	8	16	40	3.60	0.001	0.005	0.204	14	7.2	10.0	58	80
	06/04/82	44400	2.9	10	180	35	0.022	0.4	4	8	16	40	3.60	0.020	0.014	0.566	12	3.0	3.0	540	547
	19/04/82	44400	3.3	12	120	35	0.022	0.4	4	8	16	40	3.60	0.011	0.020	0.815	12	3.6	5.0	432	478
	02/05/84	44400	3.4	13	70	28	0.022	0.4	4	8	16	40	3.60	0.006	0.024	1.196	13	3.9	5.8	273	337
	17/05/84	44400	3.3	14	50	31	0.022	0.4	4	8	16	40	3.60	0.004	0.028	1.253	13	5.0	6.2	200	311
	29/05/84	44400	2.8	12	40	30	0.022	0.4	4	8	16	40	3.60	0.004	0.020	0.951	13	5.8	6.1	192	245
	02/08/84	44400	2.8	11	49	31	0.022	0.4	4	8	16	40	3.60	0.005	0.017	0.773	13	3.9	5.6	191	273
Thames	07/04/49	44400	5.3	14	40	33	0.026	0.2			23	58.5	7.10	0.002	0.014	0.597		6.3	9.0	252	359
Corantijn	02/07/65	44400	2	11	1995	35	0.026	0.2	19	18	64	69	6.50	0.117	0.009	0.379	48	0.4	0.5	798	898
	16/08/65	44400	2.2	12	680	35	0.026	0.2	19	18	64	69	6.50	0.036	0.011	0.451	53	0.8	0.7	544	498
	08/12/78	44400	1.8	10	115	20	0.026	0.2	19	18	64	69	6.50	0.007	0.008	0.549	54	1.0	1.2	115	137
	14/12/78	44400	2.3	12	130	19	0.026	0.2	19	18	64	69	6.50	0.007	0.011	0.832	55	1.2	1.2	156	153
	20/12/78	44400	1.6	9	220	18	0.026	0.2	19	18	64	69	6.50	0.016	0.006	0.494	55	1.1	0.8	242	169
Sinnamary	12/11/93	44400	2.6	10	148	26.5	0.031	0.5	2.64	3	39	3.5	3.80	0.188	0.013	0.708	28	3.4	5.6	503	685
	27/04/94	44400	2.9	12	108	22.8	0.031	0.5	2.64	3	39	3.5	3.80	0.114	0.019	1.185	28	5.5	5.5	486	595
	02/11/94	44400	2.7	11	106	29.1	0.031	0.5	2.64	3	39	3.5	3.80	0.122	0.016	0.780	32	6.5	5.2	689	556
	03/11/94	44400	2.9	12	106	26.4	0.031	0.5	2.64	3	39	3.5	3.80	0.112	0.019	1.024	31	5.5	5.3	583	566
Delaware	23/08/32	44400	1.7	8	120	32	0.026	0.2			41	255	6.60	0.003	0.005	0.216		1.2	0.9	144	111
	04/10/32	44400	1.7	8	72	32	0.026	0.2			41	255	6.60	0.002	0.005	0.216		1.7	1.2	122	86

but it is not so strange if we consider the reasons behind it. Pioneers in the development of formulas to predict the intrusion length were the U.S. Army Corps of Engineers, and the Dutch Ministry of Public Works, both of which were involved in the design of shipping access channels, waterways and harbours, particularly in the Mississippi delta and the Rotterdam Waterway. These channels, which were often man-made and artificially kept at depth, had a prismatic, or near prismatic form. An important research question was what would happen to the salt intrusion if these channels were deepened. As a result intensive laboratory experiments were done at Waterways Experimental Station (WES) in Vicksburg, Mississippi and at Delft Hydraulics in The Netherlands, all in flumes with a constant cross-section.

Since the early research on salt intrusion started in prismatic channels, this sort of set the scene for further research, also the analytical research which did not have the drawback of having to construct complicated flumes with a varying cross-section. Apparently, it is difficult to change course once you are on a certain track. We shall see further on, however, that the formulas derived for prismatic channels perform very poorly in natural channels. But let's first see how the equations derived above perform under prismatic conditions

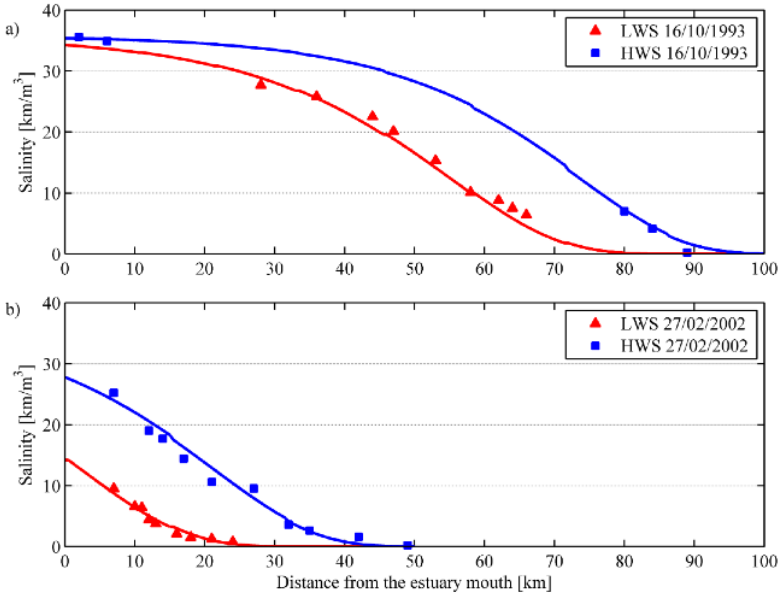

Figure 5.3: Measured and computed salt intrusion curves in the Pungué estuary: a) on 16/10/1993, b) on 27/2/2002. The draw lines are computed, the symbols indicate the measurements.

Prismatic channels

In an estuary with constant cross-section, D decreases linearly in upstream direction ($D = D_0 - KU_f x$), which follows directly from integration of Eq. (5.43) with $A = A_0$. Substitution into (5.45) and considering that $S = S_f$ for $x = L$ yields the following expression:

$$L = \frac{D_0 A_0}{K Q_f} \tag{5.62}$$

If this equation is combined with an empirical relation for the intrusion length L, then an empirical relation is obtained for D_0 or α_0.

Rigter (1973), on the basis of flume data of the Waterways Experiment Station (WES), arrived at the following empirical relation:

$$L^{LWS} = 1.5\pi \frac{h_0}{f_D}(F_d^{-1}N^{-1} - 1.7) \approx 4.7 \frac{h_0}{f_D} F_d^{-1} N^{-1} \tag{5.63}$$

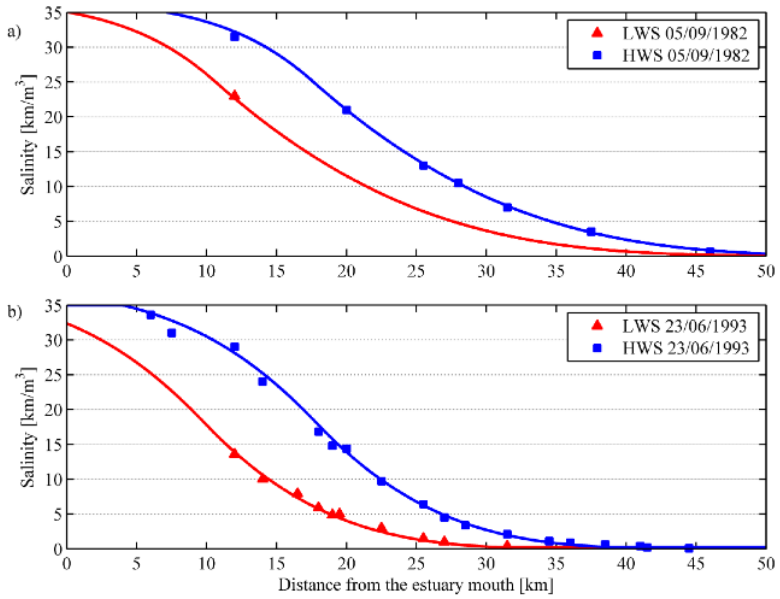

Figure 5.4: Measured and computed salt intrusion curves in the Incomati estuary: a) on 05/09/1982, b) on 23/06/1993. The draw lines are computed, the symbols indicate the measurements.

where h_0 is the tidal average depth at the estuary mouth, f_D is the Darcy-Weisbach friction factor ($f_D = 8g/C^2$), N is Canter Cremers' estuary number defined in Section 2.1 as the ratio of the fresh water entering the estuary during a tidal cycle ($Q_f T$) to the flood volume of salt water entering the estuary over a tidal cycle, P_t:

$$N = \frac{Q_f T}{P_t} = \frac{U_0 T}{E} = \pi \frac{U_0}{\upsilon_0} \tag{5.64}$$

where $U_0 = U_f(0) = Q_f/A_0$ and υ_0 is the tidal velocity amplitude at the estuary mouth. In (5.64), use has been made of (2.65) and (2.74). Finally, the densimetric Froude number F_d is defined as:

$$F_d = \frac{\rho \upsilon_0^2}{\Delta\rho g h_0} = \frac{\rho}{\Delta\rho} F^2 \tag{5.65}$$

where F is the Froude number ($F = \upsilon/\sqrt{gh}$). It is observed that, since in alluvial estuaries both N and F_d are much smaller than unity, the number 1.7 in (5.63) can be disregarded, and that Rigter's intrusion length is inversely proportional to N and F_d.

Fischer (1974), in a discussion of Rigter's results, and using the same data, derived the following formula:

$$L^{LWS} = 17.7 \frac{h_0}{f_D^{0.625}} F_d^{-0.75} N^{-0.25} \tag{5.66}$$

Van der Burgh (1972) made use of limited field observations in real estuaries: the Rotterdam Waterway, the Schelde, the Haringvliet (a tidal branch of the Rhine-Meuse delta) and the Eems. He reached at a quite similar relation as the earlier researchers. He found that the mean tidal dispersion at the mouth obeyed the following relation:

$$D_0^{TA} = 26(Ng)^{0.5} h_0^{1.5} \tag{5.67}$$

In combination with Eqs. (5.62), (5.64)and (5.65) this yields for prismatic channels:

$$L^{TA} = \frac{26 h_0}{K} \frac{\sqrt{g h_0}}{\upsilon_0} \frac{\upsilon_0}{U_0}^{0.5} N = 26\pi \frac{h_0}{K} F^{-1} N^{-0.5} \tag{5.68}$$

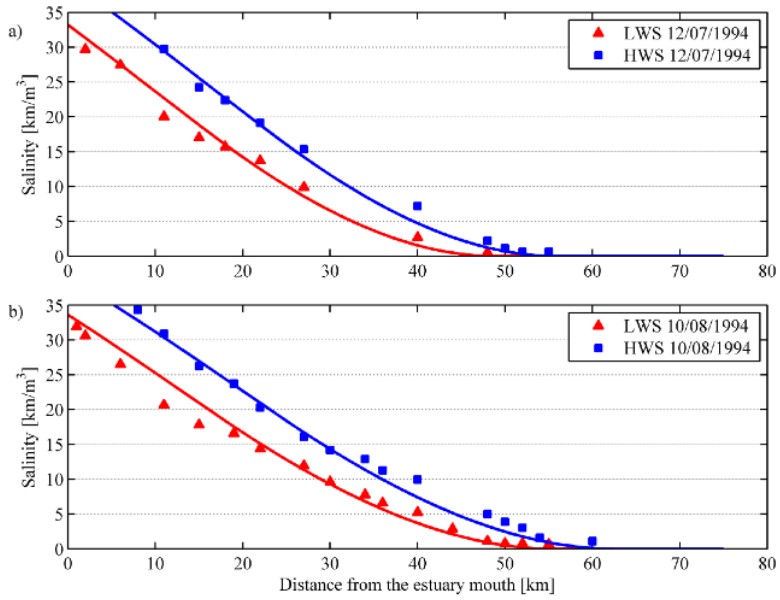

Figure 5.5: Measured and computed salt intrusion curves in the Limpopo estuary: a) on 24/07/1994, b) on 10/08/1994. The draw lines are computed, the symbols indicate the measurements.

It is clear that, although Van der Burgh used F^2 instead of F_d, there is similarity between the methods presented; most importantly, they are all linear in h_0. Since the relative density difference $\Delta\rho$ over the intrusion length of a well mixed estuary does not significantly vary from estuary to estuary - sea salinity being virtually the same everywhere ($\Delta\rho$=25kg/m^3) -, and the same applies to the roughness, which has been said to be low and not much different in the various estuaries, the major difference between the methods lies in the exponents used for the two bulk parameters: the Froude number F and Canter Cremers' number N. This was also observed Van Os and Abraham (1990) who developed a formula similar to Rigter's for use at Delft Hydraulics:

$$L^{LWS} = 4.4 \frac{h_0}{f_D} {F_d}^{-1} N^{-1} \tag{5.69}$$

About the exponents in (5.69), it can be observed that the exponent of N is negative since the salt intrusion length reduces if Q_f increases. Similarly, the intrusion length decreases with an increase in the tidal velocity (F_d^{-1} decreases with the second power of v_0 and N^{-1} increases linearly with v_0), which is understandable since the salt intrusion length at LWS is short if E is large.

Expression for the dispersion at the mouth and the salt intrusion length

Based on a large number of observations in real estuaries, a predictive expression for α_0^{HWS}, and hence for the dispersion D_0^{HWS} can be obtained. The observations made over the years in 13 estuaries, worldwide, are summarised in Table 5.3.

As the earlier researchers did, a relation has been sought with non-dimensional parameters affecting dispersion such as: the Canter Cremers number N, the densimetric Froude number F_d, and the Estuarine Richardson number $N_R = N/F_d$, defined earlier in (2.36). The dispersion coefficient is made dimensionless dividing it by the tidal excursion and the tidal velocity amplitude. This is the correct scaling, because the tidal excursion is the mixing length of the longitudinal dispersion process and the velocity amplitude is the scale for the velocity of the shear and subsequent mixing. As a result, the following empirical relation was obtained by Savenije

(1993c):

$$\frac{D_0^{HWS}}{v_0 E_0} = 1400 \frac{h_0}{a} N_R^{0.5} \tag{5.70}$$

Apparently, the HWS dispersion coefficient at the mouth D_0^{HWS} varies with the root of the Estuarine Richardson number. Another prominent dimensionless ratio is h/a, which accounts for the estuary geometry, which classical approaches neglect. It is interesting to note that the left hand member is the inverse of a Péclet number, being the ratio of the advection to the dispersion of a transport process. If the Péclet number is large (or when (5.70) is small) then advection dominates over dispersion.

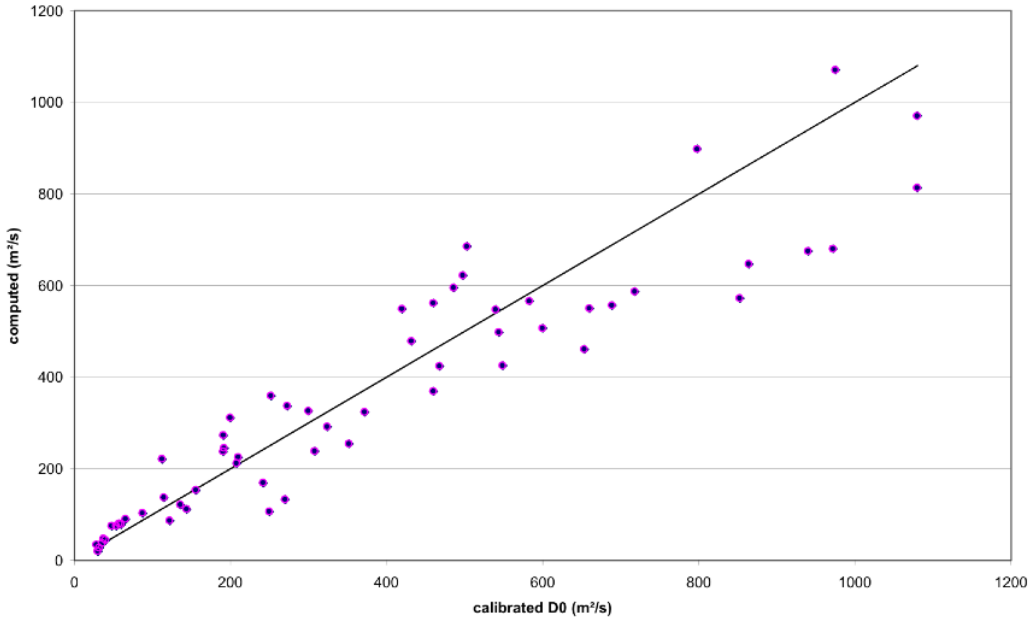

Figure 5.6: Empirical relation between values of D_0 at HWS computed with Equation 5.70 and values obtained from calibration.

In (5.70) a weighed value of a has been taken for those estuaries that demonstrate two branches in the function describing the longitudinal variation of the cross-sectional area. An average value of a is taken, weighed between a1 and a2 over the intrusion length. For these estuaries the weighed value is shown in Table 5.3. It can be seen that the longer the salt intrusion length is, the closer a is to a_2.

A plot of (5.70) against observations is presented in Fig. 5.6. We can see that this very simple equation agrees surprisingly well with the observations, particularly taking into account the inaccuracies present in both the geometry and the hydrology. Fig. 5.3 is a linear plot (not logarithmic, which tends to reduce the scatter). The middle drawn line is the line of perfect agreement, and it can be seen that line fits the data points for a wide range of values. The R_2 correlation coefficient equals 0.88, with a standard error of 106 m^2/s, which is 30% of the average value of the observations. Due to the large uncertainty in the determination of the fresh water discharge, a large scatter in the data points is unavoidable. A relative error of 30% in the determination of D_0 could result form an error of 60% in Q_f. In estuaries, an error of 60% in determining the freshet may very well occur, particularly during low flow. Hence the relation obtained is quite satisfactory. The only way to improve the reliability of (5.70) is by increasing the number of data points still further.

Van der Burgh's coefficient

It appears not so easy to find an adequate predictive equation for Van der Burgh's coefficient. Since Van den Burg's K is not depending on time-dependent factors, but is a characteristic value for a certain estuary, it would be logical to look for a relation between K and dimensionless numbers defining the general state of the estuary, such as the geometry, tidal characteristics (e.g. tidal damping) and channel roughness.

The following ratios have been correlated with K:

1. E/H, as a key tidal parameter that is related to the geometry through the Geometry-Tide relation of (2.92);
2. E/C^2, as a channel roughness indicator, which still has a time dimension, but since this time dimension is governed by the tidal period inclusion is not significant;
3. $(1-\delta_b)$, accounting for tidal amplification or damping;
4. b/a, accounting for bottom slope, if present;
5. E_a/A_0', as a ratio of tidal excursion to convergence for the second branch (if applicable);
6. H/h, as a key relation between tide and estuary shape.

Where A_0' is the cross-sectional area at $x=0$ which is obtained by extending the second branch of the exponential function of the cross-sectional area to $x=0$. In single branch estuaries this value is, of course, equal to A_0.

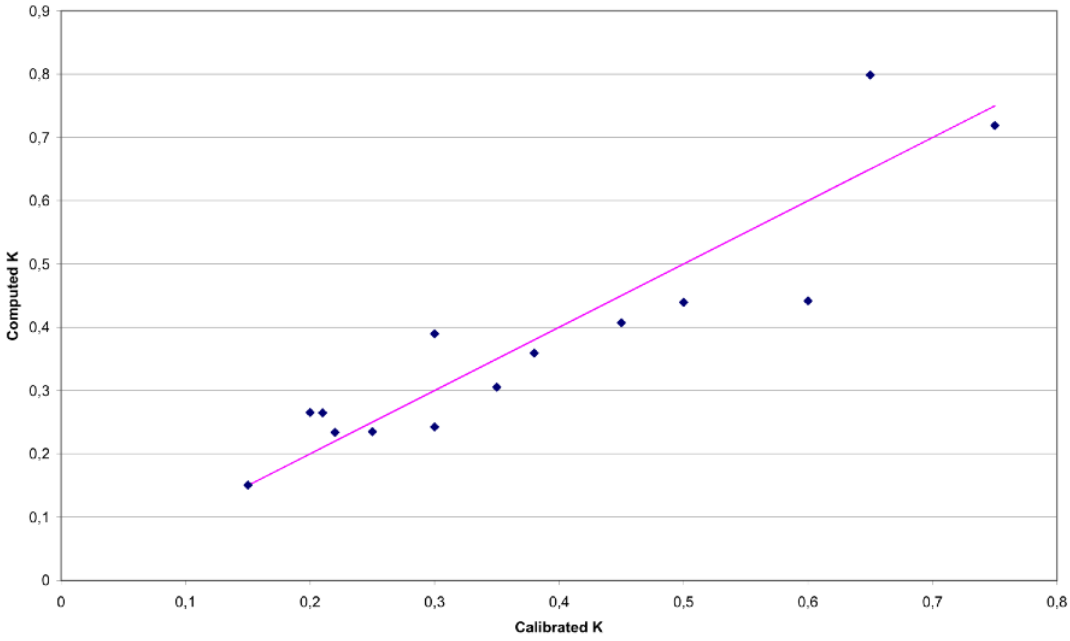

Figure 5.7: Van den Burgh's K computed by Equation 5.71 versus the values obtained from calibration.

The data for the regression analysis are presented in Table 5.4. The following relation has been obtained with a correlation coefficient R^2=0.93, which is reasonable but not always accurate. Surprisingly, the tidal range to depth ratio did not have a significant contribution in the multiple regression. This is correct because all the other parameters of the Geometry-Tide equation are already present in the regression analysis. We also see that tidal damping has a very strong

impact on the value of K. Strongly damped estuaries with a high friction apparently have a small value of K. We can understand this if we consider that a high damping and roughness implies that a high amount of tidal energy is converted into mixing, which results into a relatively high importance of tidal mixing and relatively low importance of gravitational mixing.

Fig. 5.7 presents the relation between calibrated values obtained in the various estuaries and the computed values with the following equation:

$$K = 0.3 * 10^{-3} \left(\frac{E}{H}\right)^{0.65} \left(\frac{E}{C^2}\right)^{0.39} (1 - \delta b)^{-2.0} \left(\frac{b}{a}\right)^{0.58} \left(\frac{Ea}{A'_0}\right)^{0.14} \tag{5.71}$$

We should keep in mind that the value of K should always be between zero and unity. The equation does not provide for that. We can see that K is particularly sensitive to tidal damping, channel roughness, and the tidal excursion. This equation should be used with caution. Its predictive value is weak. It should be used as a first estimate of K. Subsequently, a moving boat survey on a HWS or LWS situation will provide a more reliable value for K.

Table 5.4: Parameters used for the equation to predict Van der Burgh's coefficient.

Estuary	K	T (s)	H_0 (m)	E_0 (km)	f	C^2 (m/s^2)	a (km)	b (km)	A'_0 (10^3 m^2)	h (m)	δ_H (10^{-6}m^{-1})
Mae Klong	0.3	44400	2	14	0.028	2809	102	155	1.4	5.20	-5.20
Lalang	0.65	86400	3	31	0.023	3481	217	96	2.55	10.60	-1.00
Limpopo	0.5	44400	1.1	8	0.026	3025	130	50	1.34	7.00	1.70
Tha Chin	0.35	86400	2	15	0.039	2025	87	87	1.38	5.30	-9.40
Chao Phya	0.75	86400	2.4	26	0.031	2500	109	109	5.3	7.20	-3.60
Incomati	0.15	44400	1.4	7	0.022	3600	42	42	1.75	2.90	-13.0
Pungue	0.3	44400	6.3	20	0.031	2500	21	21	26.4	3.50	-8.50
Maputo	0.38	44400	2.8	13	0.022	3600	16	16	6.46	3.60	1.00
Thames	0.2	44400	5.3	14	0.026	3025	23	23	58.5	7.10	2.30
Corantijn	0.21	44400	2	11	0.026	3025	64	48	35.6	6.50	-1.70
Sinnamary	0.45	44400	2.6	10	0.031	2500	39	39	1.21	3.80	-1.00
Gambia	0.6	44400	1.2	10	0.031	2500	121	121	27.2	8.7	-1.00
Delaware	0.22	44400	1.7	8	0.026	3025	41	42	255	6.60	1.70
Schelde	0.25	44400	4	12	0.026	3025	28	28	150	10.50	3.80

5.5.2 The predictive model compared to other methods

Combination of the empirical (5.70) with (5.47) and (5.48) yields:

$$L^{HWS} = a \ln \left(1400 \frac{h_0 E_0 v_0}{K a^2 U_0} N_R^{0.5} + 1\right) \tag{5.72}$$

Since on the interval $x(0,1)$: $\ln(x+1) \approx x$, as a first order approximation, (5.72) can be simplified to facilitate comparison with the results of earlier researchers:

$$L^{HWS} \approx 1400 \frac{h_0 E_0 v_0}{K a U_0} N_R^{0.5} \tag{5.73}$$

But this is seldom the case: only in prismatic channels. However, the earlier researchers based their theory on estuaries with constant cross-section, or estuaries where $a \to \infty$. Hence (5.73) may be compared with the work of these researchers. Elaboration yields:

$$L^{HWS} \approx 1400 \pi \frac{h_0 E_0}{K a} F_d^{-0.5} N^{-0.5} \tag{5.74}$$

The correspondence with the relations obtained by Rigter (1973), Fischer (1974) and Van Os and Abraham (1990) presented in (5.63), (5.66) and (5.69) is high, but it is highest with Van der Burgh's relation, (5.68). The difference with Van der Burgh's, besides the logarithmic function of (5.72), lies in the use of E/a. The tidal excursion is a very important longitudinal mixing length

scale, and the convergence length a accounts for the lateral mixing through residual ebb and flood currents. If the estuary has a more pronounced funnel shape (a is small), this results in a large salt intrusion. Apparently the salt intrusion through lateral mixing is easier in a funnel shaped estuary than in a prismatic estuary. This corresponds with what one would think intuitively. Hence the new formula takes better account of the topography, through the logarithmic function, and of the main mixing processes: N_R for gravitational circulation; E for longitudinal circulation through trapping; and a for lateral circulation between ebb and flood channels.

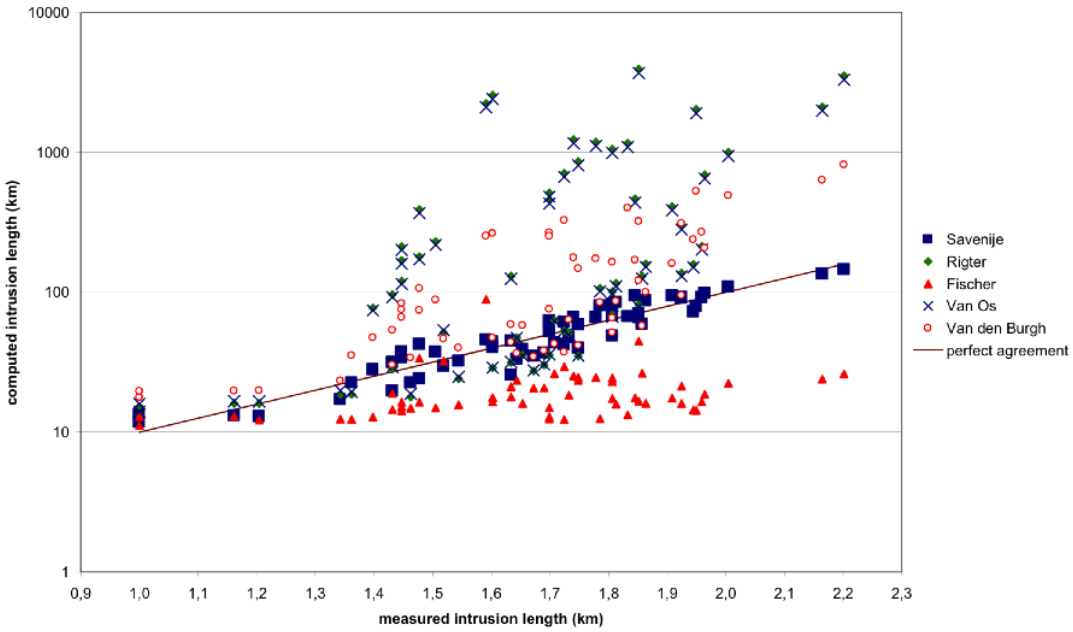

Figure 5.8: Comparison of various predictive models for the salt intrusion length at HWS.

In Fig. 5.8 the different predictive formulas for the salt intrusion length at HWS are compared for the estuaries studied. The data are presented in Table 5.5. It can be clearly seen that the new method predicts the salt intrusion length quite adequately, and much better than other methods.

Conclusion

The set of estuaries studied covers a wide range of dispersion coefficients as can be seen from Fig. 5.6. The relation obtained is quite acceptable and is a considerable improvement over classical methods. The application of the steady state model in 15 estuaries with quite different tidal and geometrical characteristics has proven successful. The empirical relations for α and K turn the technique into a predictive method which can be used as a management tool to evaluate the effect of changes in the hydrology or the geometry of the estuary involved.

5.6 Unsteady state model

5.6.1 System response time

In Section 5.4 expressions have been derived for the system response time as a function of the steady state salinity distribution $S(x)$. The first expression (T_K) is based on equating the unsteady salinity variation to the variation of the salinity between subsequent steady states as a result of fresh water flow depletion, which yielded (5.34). In this case, the system is assumed to

Table 5.5: Measured and predicted salt intrusion length in different estuaries

Estuary	date	H_0 (m)	E_0 (km)	Q_f (m^3/s)	f	A_0 (10^3 m^2)	h (m)	N	F_2	F_d	L_{HWS} (km)	Savenije (km)	Rigter (km)	Fischer (km)	V.Os (km)	Burgh (km)
Mae Klong	20/01/77	2.0	11	120	0.028	1.4	5.2	0.67	0.00	0.16	29	22	18	15	19	34
	08/03/77	1.5	10	60	0.028	1.4	5.2	0.19	0.01	0.46	23	22	19	12	19	35
	09/04/77	2.0	14	36	0.028	1.4	5.2	0.08	0.02	0.93	35	32	24	16	25	40
Solo	26/07/88	0.8	9	50	0.023	2.07	9.2	0.23	0.00	0.05	30	24	180	34	172	74
	08/09/88	0.4	5	7	0.023	2.07	9.2	0.06	0.00	0.01	39	46	2242	89	2102	252
Lalang	20/10/89	2.6	27	120	0.023	2.55	10.6	0.15	0.01	0.52	33	30	52	32	53	46
Limpopo	04/04/80	1.1	7	150	0.026	1.71	7	0.56	0.00	0.17	22	21	19	12	20	27
	31/12/82	1.1	8	2	0.026	1.71	7	0.01	0.00	0.19	64	83	1054	23	989	196
	22/04/83	0.5	4	1	0.026	1.71	7	0.01	0.00	0.05	71	80	3953	45	3703	386
	24/07/94	0.9	6.8	2	0.026	1.71	7	0.02	0.00	0.14	55	57	498	21	468	135
	10/08/94	1.0	7.1	2	0.026	1.71	7	0.01	0.00	0.15	60	69	792	23	744	170
Tha Chin	16/04/81	1.6	12	55	0.039	3	5.3	0.13	0.00	0.20	45	39	36	16	35	58
	27/02/86	2.6	20	40	0.039	3	5.3	0.03	0.04	1.74	43	45	31	21	32	44
	01/03/86	1.8	14	40	0.039	3	5.3	0.08	0.00	0.21	54	47	51	18	50	63
	13/08/87	2.0	15	39	0.039	3	5.3	0.04	0.02	1.12	40	40	29	16	29	47
Chao Phya	05/06/62	2.2	22	63	0.031	5.3	7.2	0.06	0.01	0.44	51	43	63	26	62	43
	17/03/80	1.5	18	43	0.031	5.3	7.2	0.05	0.01	0.27	64	49	101	24	97	51
	28/03/80	1.7	20	31	0.031	5.3	7.2	0.03	0.01	0.31	72	59	130	26	125	57
	29/01/83	2.4	26	90	0.031	5.3	7.2	0.07	0.01	0.54	53	42	53	29	53	37
	23/02/83	1.6	19	100	0.031	5.3	7.2	0.11	0.01	0.34	44	33	47	23	47	37
	16/01/87	2.5	15	180	0.031	5.3	7.2	0.24	0.00	0.29	27	20	28	19	29	30
Incomati	30/07/80	1.4	7	3	0.022	8.1	2.9	0.00	0.01	0.38	53	61	712	12	668	327
	05/09/82	1.4	7	2	0.022	8.1	2.9	0.00	0.01	0.34	68	67	1164	13	1092	400
	10/02/83	1.2	8	1	0.022	8.1	2.9	0.00	0.01	0.45	89	79	2034	14	1906	529
	23/06/93	1.4	8	4	0.022	8.1	2.9	0.00	0.01	0.45	50	61	514	12	482	266
	07/07/93	2.6	9	4	0.022	8.1	2.9	0.00	0.01	0.57	50	63	458	13	431	252
Pungue	26/09/80	6.3	20	22	0.031	26.4	3.5	0.00	0.06	2.40	84	91	137	21	131	95
	26/05/82	5.0	10	50	0.031	26.4	3.5	0.01	0.01	0.64	61	80	107	12	102	84
	06/08/82	5.2	14	36	0.031	26.4	3.5	0.00	0.03	1.17	65	85	116	16	110	86
	22/09/82	5.2	14	26	0.031	26.4	3.5	0.00	0.03	1.14	73	87	160	16	152	100
	29/10/82	6.0	16	60	0.031	26.4	3.5	0.01	0.04	1.53	64	83	69	17	67	65
	03/10/93	5.3	15	10	0.031	26.4	3.5	0.00	0.03	1.31	81	94	371	17	349	153
	12/10/93	3.8	15	10	0.031	26.4	3.5	0.00	0.03	1.29	70	93	376	17	353	153
	16/10/93	6.4	16	10	0.031	26.4	3.5	0.00	0.04	1.47	92	95	354	18	333	148
	31/01/02	6.2	20	262	0.031	26.4	3.5	0.02	0.06	2.91	47	35	27	21	28	35
	27/02/02	6.1	20	200	0.031	26.4	3.5	0.02	0.06	2.81	49	37	30	21	30	38
	01/03/02	6.7	24	150	0.031	26.4	3.5	0.01	0.08	5.19	56	40	35	25	35	42
Maputo	28/04/82	2.8	13	25	0.022	40	3.6	0.00	0.02	0.96	30	43	391	16	369	106
	15/07/82	1.5	6	8	0.022	40	3.6	0.00	0.01	0.20	40	44	2576	18	2413	263
	06/04/82	2.9	10	180	0.022	40	3.6	0.02	0.01	0.57	25	28	77	13	74	47
	19/04/82	3.3	12	120	0.022	40	3.6	0.01	0.02	0.82	27	31	96	14	92	53
	02/05/84	3.4	13	70	0.022	40	3.6	0.01	0.02	1.20	28	34	120	15	115	66
	17/05/84	3.3	14	50	0.022	40	3.6	0.00	0.03	1.25	28	37	169	16	160	75
	29/05/84	2.8	12	40	0.022	40	3.6	0.00	0.02	0.95	32	37	231	15	218	88
	02/08/84	2.8	11	49	0.022	40	3.6	0.00	0.02	0.77	28	36	212	14	201	83
Thames	07/04/49	5.3	14	40	0.026	58.5	7.1	0.00	0.01	0.60	101	109	1005	22	944	491
Corantijn	02/07/65	2.0	11	1995	0.026	69	6.5	0.12	0.01	0.38	50	53	36	15	36	76
	16/08/65	2.2	12	680	0.026	69	6.5	0.04	0.01	0.45	71	71	81	17	79	121
	08/12/78	1.8	10	115	0.026	69	6.5	0.01	0.01	0.55	84	92	298	16	281	311
	14/12/78	2.3	12	130	0.026	69	6.5	0.01	0.01	0.83	91	92	213	16	202	269
	20/12/78	1.6	9	220	0.026	69	6.5	0.02	0.01	0.49	88	73	158	14	151	238
Sinnamary	12/11/93	2.6	10	148	0.031	3.5	3.8	0.19	0.01	0.71	10	12	13	11	14	18
	27/04/94	2.9	12	108	0.031	3.5	3.8	0.11	0.02	1.19	10	13	15	13	16	20
	02/11/94	2.7	11	106	0.031	3.5	3.8	0.12	0.02	0.78	16	13	16	12	17	20
	03/11/94	2.9	12	106	0.031	3.5	3.8	0.11	0.02	1.02	15.5	13	16	13	17	20
Delaware	23/08/32	1.7	8	120	0.026	255	6.6	0.00	0.00	0.22	146	136	2122	24	1989	633
	04/10/32	1.7	8	72	0.026	255	6.6	0.00	0.00	0.22	159	146	3533	26	3310	816

be in a state of 90% equilibrium if $T_K < 0.1T_Q$, where T_Q is the time scale for the fresh water flow depletion. The second way of deriving a system response time scale is by using the time scale T_S needed to attain a new equilibrium condition, yielding (5.39). These equations are made dimensionless by comparing them to the flushing time scale T_f: (5.41). Both T_S and T_K require an expression for $S(x)$. After the derivations made in Section 5.5, this expression is available.

Savenije (1992b), taking $X = L/2$ performed the integration of these equations for integer values of $1/K$, which are not repeated here. If $1/K$ is not an integer number, the equations can only be solved numerically. As an example the analytical equations for K=0.5 are presented:

$$T_K = \frac{2\beta a A_0}{Q_f} \frac{\frac{L}{2a}(1+2\beta)-1}{\left(1-\beta\left(\exp\left(\frac{L}{2a}\right)-1\right)\right)^2} \text{ if } K = 0.5 \tag{5.75}$$

$$T_S = \frac{\beta(1+\beta)\, a A_0}{Q_f} \frac{\exp\left(\frac{L}{2a}\right) - \exp\left(-\frac{L}{2a}\right) - \frac{L}{a}}{\left(1-\beta\left(\exp\left(\frac{L}{2a}\right)-1\right)\right)^2} \text{ if } K = 0.5 \tag{5.76}$$

As L/a can be written as a function of β, using (5.48), these are functions of β and Q_f. Since β is also essentially function of Q_f, because D_0, is a function of Q_f, the time scales are primarily driven by the freshet. Also the expression for T_f of (5.41) can be written as a function of β.

$$T_f = \frac{A_0 a}{Q_f}\left(1-\exp\left(-\frac{L}{a}\right)\right) = \frac{A_0 a}{Q_f}\frac{1}{(1+\beta)} \tag{5.77}$$

Combination leads to the dimensionless time-scales:

$$\frac{T_K}{T_f} = 2\beta(1+\beta)\frac{\frac{L}{2a}(1+2\beta)-1}{\left(1-\beta\left(\exp\left(\frac{L}{2a}\right)-1\right)\right)^2};\ \text{if } K = 0.5 \tag{5.78}$$

$$\frac{T_S}{T_f} = \beta(1+\beta)^2\frac{exp\left(\frac{L}{2a}\right) - exp\left(-\frac{L}{2a}\right) - \frac{L}{a}}{\left(1-\beta\left(\exp\left(\frac{L}{2a}\right)-1\right)\right)^2};\ \text{if } K = 0.5 \tag{5.79}$$

Table 5.6: System response time in the dry season, in relation to water particle travel time Tf and hydrological time scale.

Estuaries	K	h (m)	a (km)	A_0' (m^2)	Q_0 (m^3/s)	L (km)	L/a	β	T_f (days)	T_K/T_f (days)	T_S/T_f (days)	T_K (days)	T_S (days)	T_Q (days)
Mae Klong	0.30	5.2	102	1400	30	26	0.25	3.44	12	0.55	0.12	7	1	reg
Solo	0.60	9.2	226	2070	10	35	0.15	5.97	78	0.63	0.19	49	15	reg
Lalang	0.65	10.6	217	2550	50	65	0.30	2.86	33	0.58	0.19	19	6	
Limpopo	0.50	7.0	130	1400	5	60	0.46	1.70	156	0.53	0.16	82	26	45
Tha Chin	0.35	5.3	87	1380	10	70	0.80	0.81	77	0.43	0.13	33	10	
Chao Phya	0.75	7.2	109	4300	30	50	0.46	1.72	67	0.53	0.21	35	14	
Incomati	0.15	3.0	42	1520	1	50	1.19	0.44	514	0.36	0.07	185	36	36
Pungue	0.30	5.3	20	28000	20	70	3.50	0.03	314	0.09	0.08	28	25	226
Maputo	0.38	3.6	16	6460	10	40	2.50	0.09	110	0.16	0.11	18	12	103
Thames	0.20	7.1	23	58500	20	90	3.91	0.02	763	0.08	0.06	61	46	50
Corantijn	0.21	6.5	64	34600	500	50	0.78	0.84	28	0.43	0.09	12	3	58
Sinnamary	0.45	10.0	35	4000	100	16	0.46	1.73	6	0.60	0.19	4	1	
Gambia	0.60	8.7	121	27200	2	300	2.48	0.09	17450	0.15	0.13	2618	2269	42
Schelde	0.25	10.0	26	150000	90	110	5.23	0.01	494	0.06	0.06	30	30	124
Delaware	0.22	6.6	41	255000	300	140	3.41	0.03	390	0.1	0.07	39	27	101

Because L/a is a sole function of β, these equations can be written as sole functions of β as well. In Table 5.6 the values of T_S, T_K and T_f have been presented and compared, for the various estuaries under a minimum flow Q_0, together with values of T_Q, where available. The values of T_K and T_S indicate the same pattern. It can be seen that in several cases $T_K < T_Q$ (Pungue, Maputo, Corantijn, Schelde and Delaware) but that in other cases $T_K > T_Q$ (Limpopo, Incomati, Thames and Gambia). The value of T_S is larger than T_Q only in the Gambia, and in the Incomati they are equal. Of these estuaries, the Gambia is clearly in unsteady state, the Incomati, the Limpopo and Thames are on the limit. For the Limpopo and Incomati, unsteady

state occurs only during the lowest minimum flow. Since both the values of T_K and T_S are inversely proportional to the root of Q_f, a modest increase in the discharge would bring about equilibrium (see Savenije 1992a). In applying the steady state model to the lowest flow situation, where equilibrium is not completely reached, we obtain a conservative estimate of the actual salt intrusion length, which is not so bad. Moreover, the Thames, the Limpopo and the Incomati have minimum flows which are regulated as a result of reservoir release and upstream withdrawal. Therefore, the time scale of regulated flow is much longer during minimum flow than the time scale of the natural recession curve. So the use of the steady state model in these estuaries is acceptable, even during low flow.

Hence, of all estuaries studied, the only estuary where the steady state model cannot be applied is The Gambia. This estuary will be used to demonstrate the unsteady state model.

5.6.2 Unsteady state dispersion

It has been mentioned that the steady state dispersion coefficient D_{SS} is not necessarily the same as the unsteady state dispersion coefficient D. This is particularly important in estuaries where the system lags considerably behind the steady state situation, as is the case in the Gambia.

It should be born in mind that none of the expressions in use for the dispersion is completely correct, physically; even the one-dimensional dispersion equation itself lacks a full physical basis. All equations in use for $D(x)$ are (at least partially) empirical, whether they are considered constant, a function of $\partial S/\partial x$ Thatcher and Harleman (1972), or a function of $(\partial S/\partial x)^2$ (Chatwin and Allen, 1985). In Chapter 4 it has been shown that the method where D is proportional to S^K can safely be added to this list and that it has a wide range of applicability.

Depending on which method is used to determine the dispersion, the unsteady state model will react differently. If the dispersion is computed on the basis of $\partial S/\partial x$, $(\partial S/\partial x)^2$ or S^K, then, in a state of disequilibrium (unsteady state), the dispersion is different from the steady state dispersion, $D \neq D_{SS}$, simply because the salinity distribution is different. Such a method is a "status quo" method; it uses the dispersion that corresponds to the present salinity distribution, irrespective of whether the system is in equilibrium or not. Here "status quo" equation applied to the unsteady state would read:

$$\frac{D}{D_0} = \left(\frac{s}{S_0}\right)^K \tag{5.80}$$

If however, a steady state model for the dispersion is used, e.g. Van der Burgh's method where the gradient of the steady state dispersion is inversely proportional to the cross-sectional area, then the outcome is different. The use of the steady state equation leads to a simulation where the dispersion coefficient used corresponds with the ultimate state of equilibrium that would occur if the discharge were maintained constant over a sufficiently long period. The steady state dispersion reads:

$$\frac{D_{SS}}{D_0} = 1 - \beta\left(\exp\left(\frac{x}{a}\right) - 1\right) \tag{5.81}$$

If we use a steady state dispersion model to a situation of unsteady state, we implicitly assume that the main factors describing the dispersion are time-invariant (e.g. the geometry and key hydraulic parameters, such as channel roughness, the ratio E/H, the phase lag ε, or the tidal damping), or that (unlike the salinity itself) the dispersion reacts directly to a change in the river discharge (much like the mass balance which affects buoyancy). Particularly, if dispersion is mostly driven by residual circulation, which depends on tidal characteristics and geometry, then this would be an acceptable approach. If, however, the dispersion is mostly density-driven, depending on the salinity gradient, then the application of (5.80) to the unsteady state would be best. In reality, dispersion is a combination of both mechanisms, and hence a combination of (5.80) and (5.81) appears the best approach.

Consider the hypothetical case where the fresh water discharge is suddenly decreased from Q_0 to Q_1 and where the salinity distribution needs considerable time to adjust to the new situation. A "status quo" method which computes the dispersion on the basis of the instantaneous longitudinal salinity distribution would then, for some time, continue to use a dispersion coefficient that corresponds essentially to a situation where $Q = Q_0$. The "ultimate equilibrium" method,

however, would immediately after the decrease in the discharge start to use a dispersion that corresponds with $Q = Q_1$, which at the toe of the intrusion curve leads to more dispersion. Hence, the "status quo" method reacts considerably slower than the "ultimate equilibrium" method in adjusting itself to the new situation.

Application of the "status quo" (5.80), has the disadvantage that dispersion is blocked at the toe of the salt intrusion curve. Application of the "ultimate equilibrium" method, however, has the disadvantage of too much dispersion at the toe of the salt intrusion curve. Which of the two approaches is the best is difficult to say, and moreover irrelevant as neither of the methods is physically completely "correct".

The method followed here is a practical one based on experiences gained with the Gambia estuary. The best result was obtained with an intermediate method that interpolates between the "status quo" dispersion and the "ultimate equilibrium" dispersion. With this method the model gradually converges to the steady state situation. A weighting factor is used as a calibration coefficient. In the case of the Gambia, equal weights were given to the "status quo" and "ultimate equilibrium" dispersion.

A special situation occurs when the fresh water discharge at the estuary mouth becomes negative, as may be the case when the net evaporation from the estuary surface exceeds the fresh water inflow into the estuary. The equation for the boundary condition D_0^{HWS}, (5.70), then no longer applies. For that situation, the dispersion of the "ultimate equilibrium" is assumed to be constant. The value that best fits the measurements is found through calibration. This special situation is only important in estuaries where evaporation plays an important role, as is the case in the estuaries discussed in the following sections: the Gambia, the Saloum, and the Casamance.

5.6.3 Application of the unsteady state model

An unsteady state equation can be solved using a six-point implicit finite difference scheme as suggested by Fischer et al. (1979). The unsteady state model makes use of the unsteady state equation that involves rainfall and evaporation, (5.24), in combination with Van der Burgh's equation, (5.43). Combination of these equations yields:

$$r_S \frac{\partial s}{\partial t} - (1-K)\frac{Q_r}{A}\frac{\partial s}{\partial x} - (1-K)\, r_S \frac{P_n b}{\overline{h}}\frac{\partial s}{\partial x} + \frac{D}{a}\frac{\partial s}{\partial x} - D\frac{\partial^2 s}{\partial x^2} + r_S \frac{P_n}{h_0} s = 0 \tag{5.82}$$

This equation can be written as:

$$r_S \frac{\partial s}{\partial t} - q\frac{\partial s}{\partial x} - D\frac{\partial^2 s}{\partial x^2} + r_S \frac{P_n}{h_0} s = 0 \tag{5.83}$$

with

$$q = (1-K)\,\frac{Q_r + r_S B P_n b}{A} - \frac{D}{a} \tag{5.84}$$

In the six-point finite differences scheme, this equation is for each time-step converted into a tridiagonal matrix of x-dependent coefficients, which can be solved by a Gaussian elimination method, as described by (Carnahan et al., 1969, pp.440-442). Details are described in Savenije (1992a).

The model functions very efficiently and has been successfully applied in the Gambia (Risley et al., 1993; Savenije, 1988), the Schelde, the Saloum and the Casamance (Savenije and Pagés, 1992). The application in the Gambia is presented below. The application in the Saloum and Casamance are presented in the Section 5.7.

5.6.4 Application to the Gambia estuary

Table 5.1 indicates that evaporation is important in the salinity distribution along the Gambia estuary. The question however is how important the effect is in quantitative terms. In Fig. 5.9a the calibration of the unsteady state model without the influence of rainfall and evaporation, is shown against the longitudinal salinity distribution measured (thick lines) at different times during the hydrological year 1972/73 (Savenije, 1988). It should be observed that the measurements have been carried out somewhat haphazardly, not taking into account the time of day (HWS,

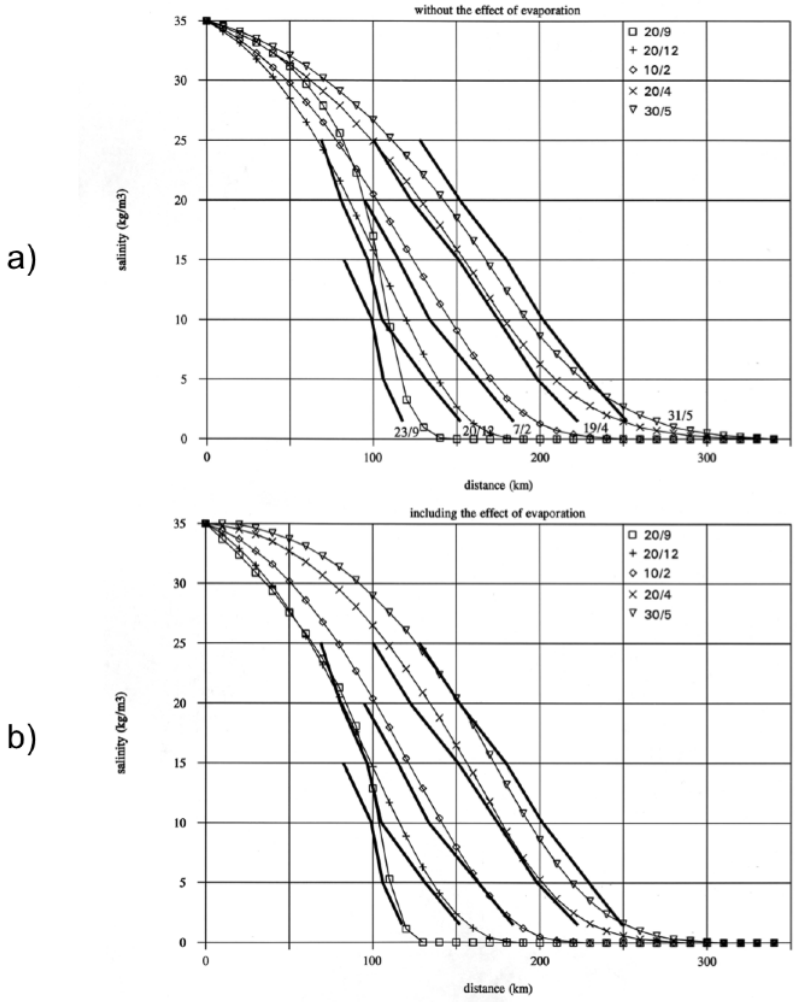

Figure 5.9: Computed and measured longitudinal salt intrusion distribution in the Gambia estuary, a) not taking into account net rainfall, b) taking into account net rainfall (after: Savenije, 1988).

LWS or TA) which may lead to a position error of about 5 km. However, it is clear from Fig. 5.9a that the maximum intrusion at the end of May in the central part of the salt intrusion curve is not reached, and that the minimum intrusion reached by the model at the end of September is too high.

The position of the toe of the salt intrusion curve (the point where $s \approx S_f$), however, is correctly modelled, which is illustrated by Fig. 5.10a. This figure follows the location of the toe of the salt intrusion curves (s=1 kg/m^3) with time. The problem faced, at that time, was to improve the fit of the longitudinal distribution, while not affecting the total salt intrusion length. The solution to this problem was the incorporation of r, the net rainfall, which is the difference between rainfall and evaporation. The toe of the curve is not directly affected by r either through the third term of (5.25), since $\partial s/\partial x$=0 at the toe, or through the sixth term, since s=0 at the toe. It is only indirectly affected by an increase of the salinity in the central part of the estuary, which, through dispersion, propagates upstream. Fig. 5.10b shows the position of the toe of the salt intrusion if the effect of rainfall and evaporation is taken into account. Figs. 5.10a and 5.10b are essentially the same. The only apparent difference between the figures lies in the discharge

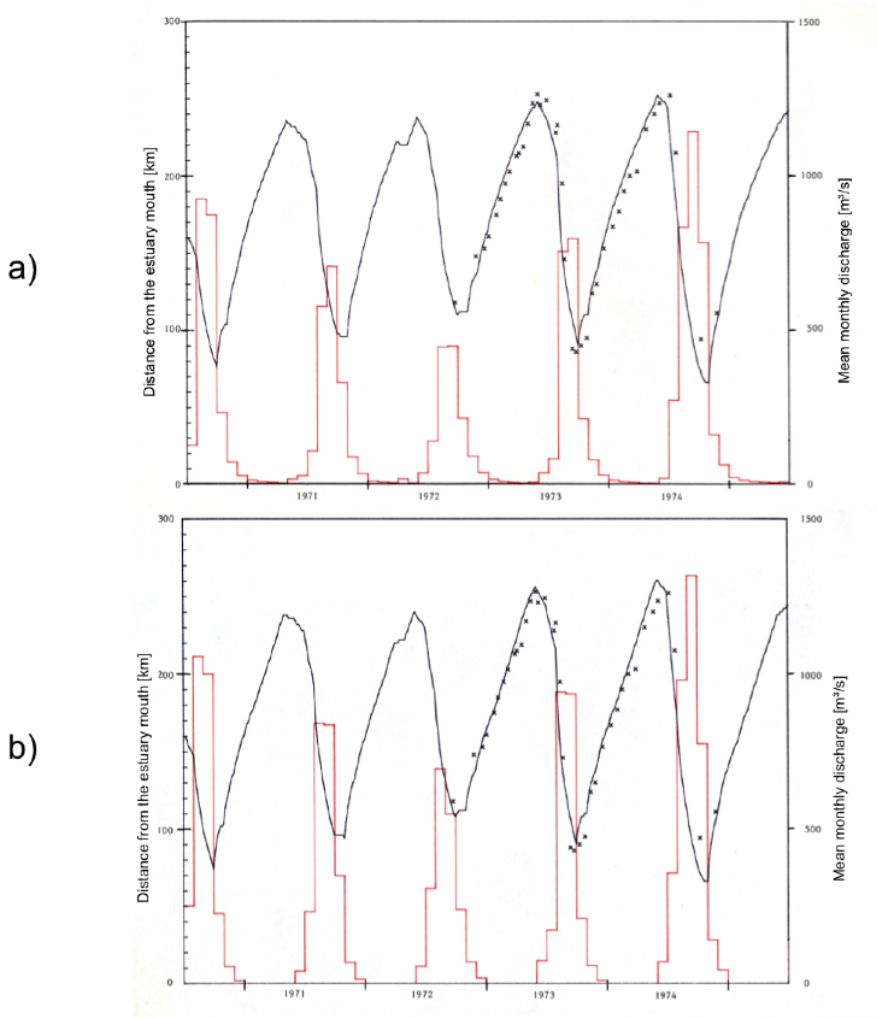

Figure 5.10: Computed and measured intrusion length and discharge to the sea in The Gambia estuary a) not taking into account net rainfall; b) taking into account net rainfall (after: Savenije, 1988).

of fresh water to the ocean.

Fig. 5.9b shows the longitudinal distribution after inclusion of the rainfall terms. The fit, although not perfect, is certainly better than in Fig. 5.9a. It can be seen that the upstream and downstream limits of the intrusion are essentially at the same position, but that the curves have become more concave in the dry season, as a result of excess evaporation, and less concave in the wet season, as a result of excess rainfall. The difference in runoff at the estuary mouth is considerable as a result of rainfall and evaporation, as can be concluded from comparing Figs. 5.10a and 5.10b.

The notion that evaporation played an important role in the Gambia estuary was strongly supported by Pagés and Citeau (1990) who stated that the Sahelian estuaries: Gambia, Sénégal, Casamance and Saloum, in that order, were all turning more and more saline due to the drought of the eighties. In the Sénégal the salinity was affected in much the same way as in the Gambia, but the Saloum and Casamance functioned as hypersaline estuaries.

5.7 Hypersaline estuaries

An estuary may become hypersaline if the salt flux F is not sufficient to evacuate the salt accumulation resulting from evaporation. The fresh water discharge of the Gambia is still too large for the estuary to become hypersaline, but the two estuaries bordering the Gambia to the North and to the South, the Saloum and the Casamance, are strongly hypersaline.

The Saloum has always been hypersaline. Measurements in the Saloum near a salt production farm go as far back as 1965 (Pagés and Citeau, 1990). The Casamance, however, although strongly influenced by evaporation, has only become hypersaline during the Sahelian drought, which started in the late 1970s. Around 1980, an ecological disaster took place in the Casamance. The fresh and brackish habitats turned hypersaline (up to 100 kg/m^3), blocking off migration routes for migrant species and stunting the growth of otherwise salt tolerant vegetation (Savenije and Pagés, 1992).

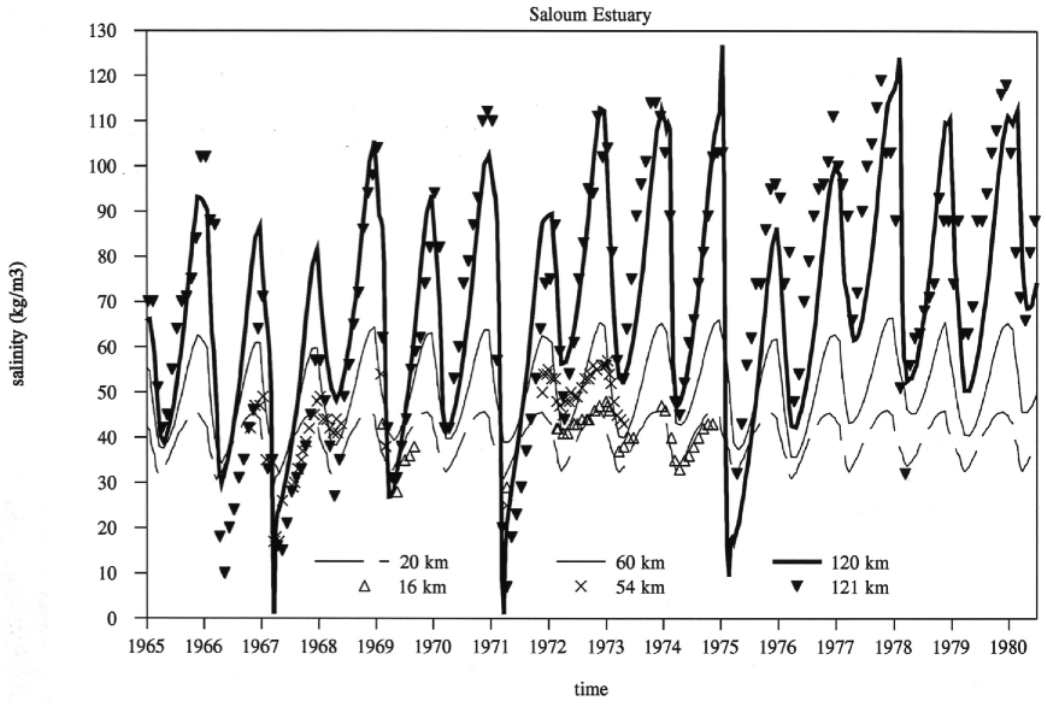

Figure 5.11: Computed and measured salinity variation along the Saloum estuary (after: Savenije and Pagés, 1992).

Fig. 5.11 shows model results of the Saloum against measurements at three locations along the estuary. It can be seen that pronounced hypersaline conditions have always existed due to the ephemeral character of the rivers entering the estuary. The fit of the model is not perfect. This is largely due to the lack of data on fresh water discharge into the estuary. A simple hydrological model had to be made on the basis of rainfall data to simulate inflow series. Moreover, hydrographic data on cross-section and depth were scarce. Since the effect of evaporation on salt accumulation, to a large extent, depends on the depth (see (5.25)), this lack of information strongly limits the accuracy of the model. In qualitative terms, however, the model is quite reliable, as can be judged from the longitudinal profiles presented in Fig. 5.12, where a comparison is made between measured and modelled salinities.

Figs. 5.13 and 5.14 show similar graphs for the Casamance estuary. In the Casamance it can indeed be seen that since the start of the Sahelian drought the environment has completely changed from a normal estuary into a hypersaline estuary. Until the year 1981, the estuary, at

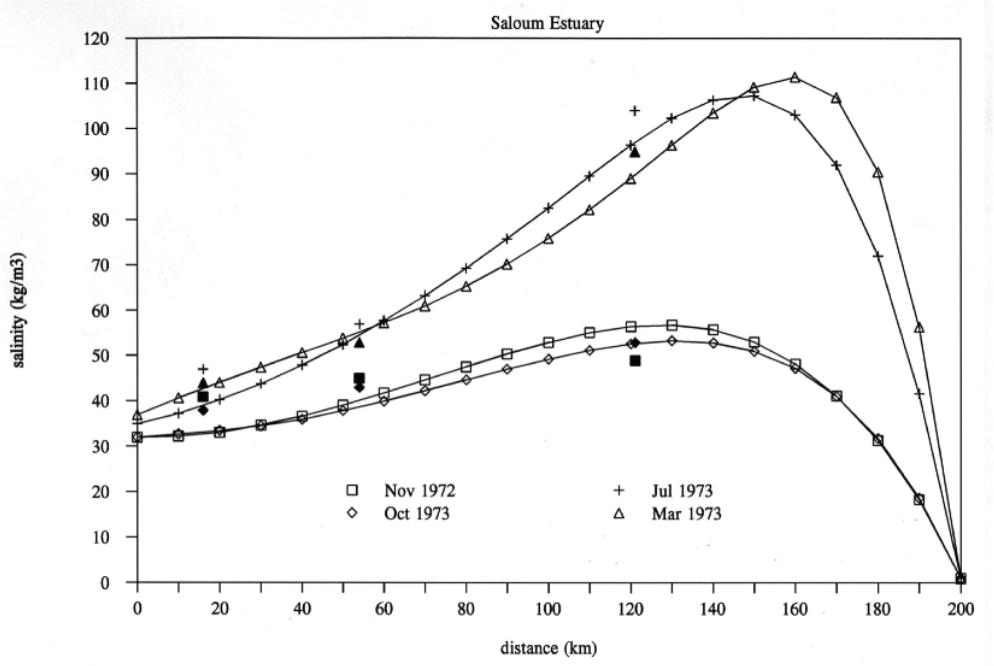

Figure 5.12: Computed and measured longitudinal distribution of the salinity along the Saloum estuary (after: Savenije and Pagés, 1992).

a distance of 180 km from the mouth, turned fresh annually. After that time serious salinization took place, which is dramatically illustrated by Fig. 5.14 in the longitudinal profile. The difference between the situations of 1978 and 1984 is striking.

Although data on fresh water inflow were available in the Casamance, the lack of reliable data on depths and cross-sections seriously hampered the calibration. Nevertheless, it appeared possible to apply the methodology described in this study to an extreme situation for which it had not been developed originally. Given the limited amount of data available, the model performs well.

5.8 Concluding remarks on the analytical salt intrusion model

In this chapter a predictive model for salt intrusion in well-mixed alluvial estuaries has been presented. In most cases the equation for steady state can be applied to the HWS situation, yielding a very simple equation to predict the intrusion length: (5.72). This equation is physically based in that it relates to the main driving mechanisms for salt intrusion: the gravitation circulation (determined by the Estuarine Richardson Number), and the residual circulation (determined mainly by E/a). Also in the unsteady state situation the method provides a useful tool, which is demonstrated by application in the Gambia and in hypersaline estuaries, such as the Saloum and the Casamance.

The strength of the method lies in its simplicity, while retaining its physical basis. The disadvantage of the method is that it requires a simplified topography. In cases where the topography is complex, one may have to rely on a two-dimensional model. But such models require large amounts of data. Even in case a more complex model is required, the one-dimensional model presented here can provide valuable information for the organisation of a hydrometric survey: with the one-dimensional model one can see which variables are most important and in which density of observation.

Hubert H. G. Savenije

The analytical model is especially powerful in combination with other models, such as morphological models, water quality models or ecological models that requiring knowledge on salinity distribution or density gradients. In estuaries, the mixing and transport of pollutants is driven by exactly the same equations as used in this chapter. As a result, the analytical model is an important tool to assess the spread and fate of pollutants in estuaries as well.

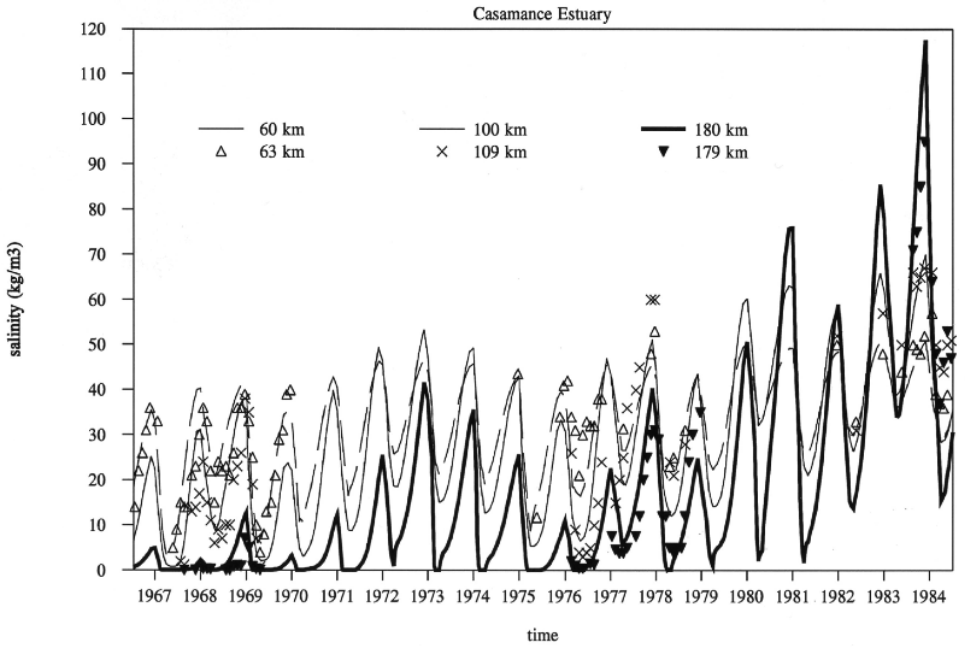

Figure 5.13: Computed and measured salinity variation along the Casamance estuary (after: Savenije and Pagés, 1992).

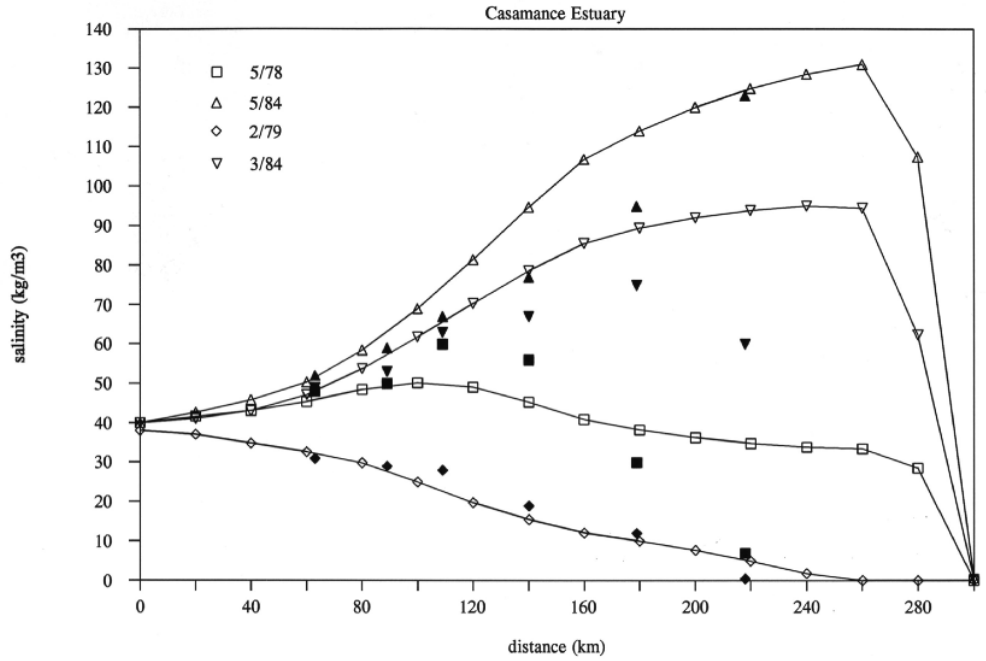

Figure 5.14: Computed and measured longitudinal salinity distribution along the Casamance estuary (after: Savenije and Pagés, 1992).

Bibliography

Abbott, M.R., 1960. Boundary layer effect in estuaries. Journal of Marine Research 18, 83 100.

Airy, G.B., 1845. Tides and waves, in: Al, E. (Ed.), Encyclopedia metropolitana. London. volume 5, pp. 241 396.

Beven, K., 1993. Prophecy, reality and uncertainty in distributed hydrological modeling. Advances in Water Resources 16, 41 51.

Blench, T., 1952. Regime theory for self-formed sediment-bearing channels. Transactions of the American Society of Civil Engineers 117, 383 400.

Bowden, K., 1967. Circulation and diffusion, in: Lauff, G. (Ed.), Estuaries: Physical Factors. Washington D.C.. volume AAAS Publ. No. 85, pp. 15 36.

Bowden, K.F., 1981. Turbulent mixing in estuaries. Ocean Management 6, 117 135.

Bretting, A.E., 1958. Stable channels, in: Acta Polytechnica Scandinavia, Copenhagen, Denmark.

Bruun, P., Gerritsen, F., 1960. Stability of coastal inlets. North Holland, Amsterdam.

Van der Burgh, P., 1972. Ontwikkeling van een methode voor het voorspellen van zoutverdelingen in estuaria, kanalen en zeeen. Rijkswaterstaat Rapport , 10 72.

Cai, H., Savenije, H.H.G., Yang, Q., Ou, S., Lei, Y., 2012a. Influence of river discharge and dredging on tidal wave propagation: Modaomen estuary case. Journal of Hydraulic Engineering 138, 885 896. Doi: 10.1061/(ASCE)HY.1943-7900.0000594.

Cai, H.Y., Savenije, H.H.G., Toffolon, M., 2012b. A new analytical framework for assessing the effect of sea-level rise and dredging on tidal damping in estuaries. Journal of Geophysical Research-Oceans 117, C09023. Doi:10.1029/2012JC008000.

Carnahan, B., Luther, H., Wilkes, J., 1969. Applied numerical methods. John Wiley & Sons, Inc., New York.

Cartwright, D.E., 1968. A unified analysis of tides and surges round north and east Britain. Philosophical Transactions of the Royal Society of London A263, 1–55.

Chatwin, P.C., Allen, C.M., 1985. Mathematical-models of dispersion in rivers and estuaries. Annual Review of Fluid Mechanics 17, 119–149.

D'Alpaos, A., Lanzoni, S., Marani, M., Fagherazzi, S., Rinaldo, A., 2005. Tidal network ontogeny: Channel initiation and early development. Journal of Geophysical Research-Earth Surface 110.

Davies, L., 1964. A morphogenic approach to the worlds' shorelines. Z. Geomorphol. 8, 127–142.

Dionne, J., 1963. Towards a more adequate definition of the st. lawrence estuary. Z. Geomorphol. 7, 36–44.

Dronkers, J., 1982. Conditions for gradient-type dispersive transport in one-dimensional, tidally averaged transport models. Estuarine Coastal and Shelf Science 14, 599–621.

Dronkers, J., Van Os, L., 1981. Predictive salinity modelling of the oosterschelde with hydraulic and mathematical models, in: Transport models for inland and coastal waters. Academic Press Inc., London, pp. 451–482.

Dronkers, J.J., 1964. Tidal computations in rivers and coastal waters. North-Holland Publishing Company, Amsterdam.

Dyer, K.R., 1973. Estuaries: a physical introduction. John Wiley & Sons Aberdeen, UK.

Dyer, K.R., 1974. The salt balance in stratified estuaries. Estuarine Coastal and Shelf Science 2, 273–281.

Dyer, K.R., 1997. (New revised issue) Estuaries: a physical introduction. John Wiley & Sons Aberdeen, UK.

Eaton, B.C., Church, M., 2007. Predicting downstream hydraulic geometry: A test of rational regime theory. Journal of Geophysical Research-Earth Surface 112.

Eaton, B.C., Millar, R.G., Davidson, S., 2010. Channel patterns: Braided, anabranching, and single-thread. Geomorphology 120, 353 364.

Engelund, F., Hansen, E., 1967. A monograph on sediment transport in alluvial streams, in: Teknisk Vorlag, Copenhagen, Denmark.

Fischer, H., List, E., Koh, R., Imberger, J., Brooks, N., 1979. Mixing in inland and coastal waters. Academic Press, New York.

Fischer, H.B., 1972. Mass transport mechanisms in partially mixed estuaries. Journal of Fluid Mech. 53, 671–687.

Fischer, H.B., 1974. Discussion of 'minimum length of salt intrusion in estuaries' by b.p. rigter, 1973. Journal of the Hydraulics Division-Asce 100, 708–713.

Friedrichs, C.T., Aubrey, D.G., 1994. Tidal propagation in strongly convergent channels. Journal of Geophysical Research-Oceans 99, 3321 3336.

Graas, S., 2001. Verloop van het getijverschil over het Schelde-estuarium. Master's thesis. TU Delft.

Green, G., 1837. On the motion of waves in a variable canal of small depth and width. Trans. Cambridge Philos. Soc. 6, 457–462.

Hansen, D., 1965. Currents and mixing in the columbia river estuary, in: Ocean Science and Ocean Engineering, pp. 943–955. Trans. Joint Conf. Mar. Tech. Soc. Am. Soc. Limnol. Oceanogr.,C.

Hansen, D.V., Rattray, M., 1965. Gravitational circulation in straits and estuaries. J. Mar. Res. 23, 104–122.

Harleman, D.R.F., 1966. Tidal dynamics in estuaries, in: Ippen, A.T. (Ed.), Estuary and coastline hydrodynamics. McGraw Hill, New York, USA. chapter 10, Part II: Real Estuaries, pp. 522–545.

Harleman, D.R.F. andThatcher, M., 1974. Longitudinal dispersion and unsteady salinity intrusion in estuaries. La Houille Blanche 1/2, 25 81.

Hayes, M.O., 1975. Morphology of sand accumulation in estuaries, in: Cronin, L.E. (Ed.), Estuarine research. Academic Press, New York, USA. chapter Vol II, pp. 3–22.

Holley, E., Harleman, D., Fischer, H., 1970. Dispersion in homogeneous estuary flow. J. Hyd. Div. Proc. ACSE 96, 1691–1709.

Horrevoets, A.C., Savenije, H.H.G., Schuurman, J.N., Graas, S., 2004. The, influence of river discharge on tidal damping in alluvial estuaries. Journal of Hydrology 294, 213–228.

Hunt, J., 1964. Tidal oscillations in estuaries. Geo. J. Roy. Ast. Soc. 8.

Ippen, A.T., 1966a. Estuary and coastline hydrodynamics. McGraw Hill, New York, USA.

Ippen, A.T., 1966b. Tidal dynamics in estuaries, in: Ippen, A.T. (Ed.), Estuary and coastline hydrodynamics. McGraw Hill, New York, USA. chapter 10, part I: Estuaries of rectangular cross-sections, pp. 493–521.

Ippen, A.T., Harleman, D.R.F., 1961. One-dimensional analysis of salinity intrusion in estuaries, in: Tech. Bull. Comm. tid. Hydraul., U.S. Army, p. 5.

Ippen, A.T., Harleman, D.R.F., 1966. Tidal dynamics in estuaries, in: Ippen, A.T. (Ed.), Estuary and coastline hydrodynamics. McGraw Hill, New York, USA. chapter 10, pp. 493 545.

Jansen, P.P., VanBendegon, L., Van den Berg, J., De Vries, M., Zanen, A., 1979. Principles of river engineering, the non-tidal alluvial river. Pitman Publ., London.

Jay, D.A., 1991. Green law revisited - tidal long-wave propagation in channels with strong topography. Journal of Geophysical Research-Oceans 96, 20585 20598.

Jay, D.A., Geyer, W.R., Uncles, R.J., Vallino, J., Largier, J., Boynton, W.R., 1997. A review of recent developments in estuarine scalar flux estimation. Estuaries 20, 262 280.

Jay, D.A., Smith, J.D., 1990a. Circulation, density distribution and neap-spring transitions in the Columbia river estuary. Progress in Oceanography 25, 81 112.

Jay, D.A., Smith, J.D., 1990b. Residual circulation in shallow estuaries .2. weakly stratified and partially mixed, narrow estuaries. Journal of Geophysical Research-Oceans 95, 733 748.

Kennedy, R., 1894. The prevention of silting in irrigation canals, in: Minutes of the Proc., Inst. of Civ. Engrs., London.

Kent, R., 1958. Turbulent diffusion in a sectionally homogeneous estuary. Tech. Rep. Chesapeake Bay Inst. 16, Ref. 58 I.

Ketchum, B., 1951. The exchanges of fresh and salt water in tidal estuaries. Journal of Marine Research X 1, 18–38.

Kranenburg, C., 1986. A time scale for long-term salt intrusion in well-mixed estuaries. Journal of Physical Oceanography 16, 1329–1331.

Van de Kreeke, J., Zimmerman, J., 1990. Gravitational circulation in well-and partially-mixed estuaries. The Sea 9, 495–521.

Lacey, G., 1963. Discussion of simons & albertson (1963). ASCE, Transactions 128.

Lamb, 1932. Hydrodynamics. Cambridge University Press.

Lane, E., 1955. Design of stable channels. Transactions, ASCE 120, 1234–1260.

Langbein, W., 1963. The hydraulic geometry of a shallow estuary. Bull. Int. Ass. Scient. Hydrol. 8, 84–94.

Lanzoni, S., Seminara, G., 1998. On tide propagation in convergent estuaries. Journal of Geophysical Research-Oceans 103, 30793–30812.

Lanzoni, S., Seminara, G., 2002. Long-term evolution and morphodynamic equilibrium of tidal channels. Journal of Geophysical Research-Oceans 107.

Leopold, L., Maddock, T., 1953. The hydraulic geometry of stream channels and some physiographic implications, in: Professional Paper no. 252, U.S. Geological Survey. Washington D.C.

Leopold, L., Wolman, M., Miller, J., 1964. Fluvial processes in geomorphology, in: Freeman. San Francisco.

Li, C.Y., O'Donnell, J., 1997. Tidally driven residual circulation in shallow estuaries with lateral depth variation. Journal of Geophysical Research-Oceans 102, 27915–27929.

Lindley, E., 1919. Regime channels. Proc. Punjab Engrg. Cong. 7, 63–74.

Longuet-Higgins, M., 1969. On the transport of mass by time-varying ocean currents. Deep Sea Res. Oceanogr. Abstr. 16, 431 447.

Lorentz, H.A., 1926. Verslag Staatscommissie Zuiderzee (in Dutch). Algemene Landsdrukkerij, The Hague, Netherlands.

Mccarthy, R.K., 1993. Residual currents in tidally dominated, well-mixed estuaries. Tellus Series a-Dynamic Meteorology and Oceanography 45A, 325 340.

McDowell, D., O'Connor, B., 1977. Hydraulic behaviour of estuaries. Macmillan Press, London, UK.

Nguyen, A.D., Savenije, H.H.G., Pham, D.N., Tang, D.T., 2008a. Using salt intrusion measurements to determine the freshwater discharge distribution over the branches of a multi-channel estuary: The Mekong Delta case. Estuarine Coastal and Shelf Science 77, 433 445.

Nguyen, A.D., Savenije, H.H.G., van der Wegen, M., Roelvink, D., 2008b. New analytical equation for dispersion in estuaries with a distinct ebb-flood channel system. Estuarine Coastal and Shelf Science 79, 7–16.

Nichols, M., Biggs, R., 1985. Estuaries, in: Davis, R. (Ed.), Coastal Sedimentary Environments. Springer-Verlag, New York, pp. 77 186.

O'Brien, M., 1931. Estuary tidal prisms related to entrance areas. Civil Engineering .

O'Kane, J., 1980. Estuarine water quality management. Pitman Publishing Ltd., London, UK.

Okubo, A., 1967. The effect of shear in an oscillatory current on horizontal diffusion from an instantaneous source. Int.J.Sea Res. 6.

Pagés, J., Citeau, J., 1990. Rainfall and salinity of a Sahelian estuary between 1927 and 1987. Journal of Hydrology 113, 325–341.

Park, J.K., James, A., 1990. Mass flux estimation and mass-transport mechanism in estuaries. Limnology and Oceanography 35, 1301–1313.

Pethick, J., 1984. An introduction to coastal geomorphology. Edward Arnold Publ., London, UK.

Pillsbury, G., 1939. Tidal hydraulics. Corps of Engineers, Vicksburg, USA.

Pillsbury, G., 1956. Tidal hydraulics (second edition). Corps of Engineers, Vicksburg, USA.

Ponce, V.M., Simons, D.B., 1977. Shallow wave-propagation in open channel flow. Journal of the Hydraulics Division-Asce 103, 1461–1476.

Prandle, D., 1981. Salinity intrusion in estuaries. Journal of Physical Oceanography 11, 1311–1324.

Prandle, D., 1985. On salinity regimes and the vertical structure of residual flows in narrow tidal estuaries. Estuarine Coastal and Shelf Science 20, 615–635.

Prandle, D., 2003. Relationships between tidal dynamics and bathymetry in strongly convergent estuaries. Journal of Physical Oceanography 33, 2738–2750.

Preddy, W.S., 1954. The mixing and movement of water in the estuary of the Thames. Journal of the Marine Biological Association of the United Kingdom 33, 645–662.

Pritchard, D., 1967. What is an estuary: a physical viewpoint. In: Lauff, G.H. (Ed.), Estuaries. Estuaries. American Association of Advancement of Science, Publ. 83, Washington DC.

Rattray, M., Dworski, J.G., 1980. Comparison of methods for analysis of the transverse and vertical circulation contributions to the longitudinal advective salt flux in estuaries. Estuarine and Coastal Marine Science 11, 515–536.

Riggs, H., 1974. Flash flood potential from channel measurements. Symposium on Flash Floods IAHS Publ. 112, 52–56.

Rigter, B.P., 1973. Minimum length of salt intrusion in estuaries - reply. Journal of the Hydraulics Division-Asce 101, 765 771.

van Rijn, L.C., 2011. Analytical and numerical analysis of tides and salinities in estuaries; part I: tidal wave propagation in convergent estuaries. Ocean Dynamics 61, 1719–1741. Doi:10.1007/s10236-011-0453-0.

Risley, J.C., Guertin, D.P., Fogel, M.M., 1993. Salinity-intrusion forecasting system for Gambia river estuary. Journal of Water Resources Planning and Management-Asce 119, 339–352.

Rodriguez-Iturbe, I., Rinaldo, A., 1997. Fractal River Basins; Chance and Self-organisation. Cambridge University Press, London.

Rodriguez-Iturbe, I., Rinaldo, A., 2001. Fractal River Basins; Chance and Self-organisation. Cambridge University Press(first published 1997), London.

Savenije, H.H.G., 1986. A one-dimensional model for salinity intrusion in alluvial estuaries. Journal of Hydrology 85, 87–109.

Savenije, H.H.G., 1988. Influence of rain and evaporation on salt intrusion in estuaries. Journal of Hydraulic Engineering-Asce 114, 1509–1524.

Savenije, H.H.G., 1989. Salt intrusion model for high-water slack, low-water slack, and mean tide on spread sheet. Journal of Hydrology 107, 9 18.

Savenije, H.H.G., 1992a. Lagrangian solution of St Venants equations for alluvial estuary. Journal of Hydraulic Engineering-Asce 118, 1153–1163.

Savenije, H.H.G., 1992b. Rapid assessment technique for salt intrusion in alluvial estuaries. Ph.D. thesis. International Institute for Infrastructure, Hydraulics and Environment. Delft, The Netherlands.

Savenije, H.H.G., 1993a. Composition and driving mechanisms of longitudinal tidal average salinity dispersion in estuaries. Journal of Hydrology 144, 127 141.

Savenije, H.H.G., 1993b. Determination of estuary parameters on basis of Lagrangian analysis. Journal of Hydraulic Engineering-Asce 119, 628–642.

Savenije, H.H.G., 1993c. Predictive model for salt intrusion in estuaries. Journal of Hydrology 148, 203–218.

Savenije, H.H.G., 1998. Analytical expression for tidal damping in alluvial estuaries. Journal of Hydraulic Engineering-Asce 124, 615 618.

Savenije, H.H.G., 2001a. Equifinality, a blessing in disguise? Hydrological Processes 15, 2835–2838.

Savenije, H.H.G., 2001b. A simple analytical expression to describe tidal damping or amplification. Journal of Hydrology 243, 205–215.

Savenije, H.H.G., 2003. The width of a bankfull channel; lacey's formula explained. Journal of Hydrology 276, 176–183.

Savenije, H.H.G., 2005. Salinity and Tides in Alluvial Estuaries. Elsevier, New York.

Savenije, H.H.G., Pagés, J., 1992. Hypersalinity - a dramatic change in the hydrology of Sahelian estuaries. Journal of Hydrology 135, 157–174.

Savenije, H.H.G., Toffolon, M., Haas, J., Veling, E.J.M., 2008. Analytical description of tidal dynamics in convergent estuaries. Journal of Geophysical Research-Oceans 113, 1–18. Doi:10.1029/2007JC004408.

Savenije, H.H.G., Veling, E.J.M., 2005. Relation between tidal damping and wave celerity in estuaries. Journal of Geophysical Research-Oceans 110, 1–10. Doi:10.1029/2004JC002278.

Schijf, J.B., Schönfeld, J.C., 1953. Theoretical considerations on the motion of salt and fresh water, in: Proc. Minnesota Int. Hydrauli. Conf., Minneapolis, Minnesota. pp. 321–333.

Shaha, D.C., Cho, Y.K., 2011. Determination of spatially varying Van der Burgh's coefficient from estuarine parameter to describe salt transport in an estuary. Hydrology and Earth System Sciences 15, 1369–1377.

Simons, D., Albertson, M., 1960. Uniform water conveyance channels in alluvial material. Journal of Hydr. Dev. ASCE 86, 33–71.

Sivapalan, M., Bloschl, G., Zhang, L., Vertessy, R., 2003. Downward approach to hydrological prediction. Hydrological Processes 17, 2101–2111.

Smith, R., 1980. Buoyancy effects upon longitudinal dispersion in wide well-mixed estuaries. Philosophical Transactions of the Royal Society of London Series a-Mathematical Physical and Engineering Sciences 296, 467–496.

Sobey, R.J., 2001. Evaluation of numerical models of flood and tide propagation in channels. Journal of Hydraulic Engineering-Asce 127, 805–824.

Stacey, M.T., Burau, J.R., Monismith, S.G., 2001. Creation of residual flows in a partially stratified estuary. Journal of Geophysical Research-Oceans 106, 17013–17037.

Stevens, M.A., 1989. Width of straight alluvial channels. Journal of Hydraulic Engineering-Asce 115, 309–326.

Stevens, M.A., Nordin, C.F., 1987. Critique of the regime theory for alluvial channels. Journal of Hydraulic Engineering-Asce 113, 1359–1380.

Stigter, C., Siemons, J., 1967. Calculation of longitudinal salt distribution in estuaries as function of time. Delft Hydraulics Laboratory Publ. 52.

Stommel, H., 1953. Computation of pollution in a vertically mixed estuary. Sewage and Industrial Wastes 25, 1065–1071. Xs025 Times Cited:43 Cited References Count:4.

Thatcher, M.L., Harleman, D.R.F., 1972. A mathematical model for the prediction of unsteady salinity intrusion in estuaries, in: R.M. Parsons Laboratory Report, No. 144, MIT, Cambridge, Massachusetts. pp. 1–227.

Toffolon, M., Savenije, H.H.G., 2011. Revisiting linearized one-dimensional tidal propagation. Journal of Geophysical Research-Oceans 116. Doi:10.1029/2010JC006616.

Toffolon, M., Vignoli, G., Tubino, M., 2006. Relevant parameters and finite amplitude effects in estuarine hydrodynamics. Journal of Geophysical Research-Oceans 111, 1–17. Doi:10.1029/2005JC003104.

Turrell, W.R., Brown, J., Simpson, J.H., 1996. Salt intrusion and secondary flow in a shallow, well-mixed estuary. Estuarine Coastal and Shelf Science 42, 153–169.

Uncles, R.J., Stephens, J.A., 1996. Salt intrusion in the Tweed estuary. Estuarine Coastal and Shelf Science 43, 271–293.

Van Dam, G.C., Schönfeld, J.C., 1967. Experimental and theoretical work in the field of turbulent diffusion performed with regard to the netherlands' estuaries and coastal regions of the north sea, in: Paper presented at General Assembly of IUGG, Berne, Switserland.

Van Os, A., Abraham, G., 1990. Density currents and salt intrusion. Delft Hydraulics, International Institute for Hydraulic and Environmental Engineering Lecture Notes.

Van Rijn, L., 1990. Principles of fluid flow and surface waves in rivers, estuaries, seas and oceans. Aqua Publ., Amsterdam.

Vignoli, G., Toffolon, M., Tubino, M., 2003. Non-linear frictional residual effects on tide propagation, in: Proceedings of XXX IAHR Congress, Thessaloniki (Greece), 24–29 August 2003. pp. 291–298.

Van der Wegen, M., Wang, Z.B., Savenije, H.H.G., Roelvink, J.A., 2008. Long-term morphodynamic evolution and energy dissipation in a coastal plain, tidal embayment. Journal of Geophysical Research-Earth Surface 113. Doi:10.1029/2007JF000898.

West, J.R., Broyd, T.W., 1981. Dispersion coefficients in estuaries. Proceedings of the Institution of Civil Engineers Part 2-Research and Theory 71, 721 737.

West, J.R., Mangat, J.S., 1986. The determination and prediction of longitudinal dispersion coefficients in a narrow, shallow estuary. Estuarine Coastal and Shelf Science 22, 161–181.

Whitham, G., 1974. Linear and nonlinear waves. John Wiley and Sons, New York, USA.

Wolanski, E., 1986. An evaporation-driven salinity maximum zone in Australian tropical estuaries. Estuarine Coastal and Shelf Science 22, 415–424.

Wright, L.D., Coleman, J.M., Thom, B.G., 1973. Processes of channel development in a high-tide-range environment - Cambridge Gulf-Ord River delta, Western Australia. Journal of Geology 81, 15–41.

Wright, L.D., Coleman, J.M., Thom, B.G., 1975. Sediment transport and deposition in a macrotidal river channel, Ord river, Western Australia, in: Cronin, L.E. (Ed.), Estuarine Research. Academic Press, New York, USA, pp. 309 322.

Zhang, E.F., Savenije, H.H.G., Wu, H., Kong, Y.Z., Zhu, J.R., 2011. Analytical solution for salt intrusion in the Yangtze estuary, China. Estuarine Coastal and Shelf Science 91, 492–501. Doi:10.1016/j.ecss.2010.11.008.

Zimmerman, J., 1979. On the Euler-Lagrange transformation and the stokes' drift in the presence of oscillatory and residual currents. Deep Sea Research Part A. Oceanographic Research Papers 26, 505 – 520.